Cellular droplet microarray: a miniaturized technique for high-throughput screening of small molecules and proteins

Zur Erlangung des akademischen Grades eines

DOKTORS DER NATURWISSENSCHAFTEN

(Dr. rer. nat.)

von der KIT-Fakultät für Chemie und Biowissenschaften des

Karlsruher Instituts für Technologie (KIT)

genehmigte

DISSERTATION

von

M.Sc. Yanxi Liu

1. Referent: Prof. Dr. Pavel Levkin

2. Referent: Prof. Dr. Martin Bastmeyer

Tag der mündlichen Prüfung: 22.07.2021

Abstract

High-throughput screenings are of momentous importance and have been one of the cornerstones of current life science research, such as biology, biotechnology, biochemistry, computational science, medical chemistry, and pharmacology. Interests in high-throughput screenings among academia, medium and small biotech companies, governmental, and not-for-profit screening sites as well as contract research organizations dramatically increased because high-throughput screenings enable efficient analysis of large numbers of compounds in a short time. The increasing interests result in the rapid development of high-throughput screening technologies in combination with complementary technologies. The conventional high-throughput screenings have disadvantages including high costs, high waste, long cycle time, low productivity, and limited expandability to larger libraries. These disadvantages underline the importance of efforts towards the development of miniaturized and automated high-throughput screenings technologies. Droplet microarray is one of the miniaturized techniques which is developed by combining surface science, surface functionalization and biology. The high density of droplets on droplet microarray slides decreases the costs, waste, cycle time of the screening and increases the productivity and applicability to high-throughput screenings of larger chemical and biological libraries. Further development, evaluation, and improvement of the droplet microarray platform not only play an important role in progress of high-throughput screenings, but also hold tremendous potential in pharmacological research and stem cell research such as increasing gene delivery efficiency and facilitating undifferentiated stem cell culture.

Pharmacological priming (drug repurposing) has been regarded as an adjuvant strategy to improve non-viral gene delivery efficiency. Nevertheless, the broad applicability of pharmacological priming has not been well established due to the prohibitively high costs of reagents and operation, which explains the urge of miniaturized platform and drug repurposing approach. In addition to the urgent requirement in pharmacological field, in order to realize clinical potential, stem cell research also requires miniaturized techniques to investigate the influence of cell-surface interactions and small cell culture medium on stem cell behavior and the effects of additives, surface coatings, including surface adsorbed proteins on stem cell fate.

The goal for the <u>first</u> section of the dissertation was to search for small molecules (compounds) which hold transfection enhancing effect using droplet microarray platform,

which could help in gene delivery and gene therapy research. An investigation of the influence of 774 Food and Drug Administration‑approved drugs on transfection efficiency with different cell types in a miniaturized and high-throughput manner was performed using the droplet microarray platform. The screening of the library identified fourteen individual compounds that presented approximately 2-5-fold transfection efficiency enhancement. These hit compounds were then verified and studied at larger scale. The results indicate that the high-throughput and drug repurposing approach based on droplet microarray platform is robust and can be used to study and develop more effective non-viral gene delivery systems.

The goal for the <u>second</u> section of the dissertation was to evaluate the effect of surface properties and small volumes on pluripotency of human induced pluripotent stem cells (hiPSCs) utilizing the droplet microarray platform. Two artificial surfaces contained different chemical elements and their corresponding droplet microarray slides were investigated for cultivation and pluripotency of hiPSCs *in vitro*. The surfaces and droplet microarray slides were used to culture human induced pluripotent stem cells in 2 mL and 200 nL volumes. The results showed that hiPSCs exhibited high viability, expected morphology and pluripotency in 200 nL droplets on both type A and type B droplet microarray slides without Matrigel coating for 24 h of culture. This makes droplet microarrays a versatile and simple platform for short-term and xeno-free high-throughput screening of hiPSCs.

The goal for the <u>third</u> section of the dissertation was to identify chemically defined proteins which could further improve hiPSCs culture and maintain pluripotency of stem cells using droplet microarray platform and also in standard microtiter plates. It is feasible to do protein coating, cell cultivation and immunofluorescence staining in a miniaturized and parallel manner on droplet microarray slides, resulting in reduction of consumables and experimental error. Thus, droplet microarray platform was used to screen eleven proteins and their related binary and ternary combinations (in total 231 diverse groups) for their capability of maintaining pluripotency of hiPSCs. Ten groups of ternary protein combinations were identified, which could support self-renewal and proliferation of hiPSCs better than on Matrigel-coated surfaces. The most effective protein combinations from the primary screening were further validated in long-term (five weeks) culture. Additionally, embryoid body formation from the hiPSCs cultured on selected protein coatings, followed by differentiation into three germ layers was achieved.

In summary, droplet microarray platform was utilized as a miniaturized and rapid screening platform to answer several biological questions. Firstly, 776 drug compounds were screened in nanoscale which is cost-, time- and labor-saving. Fourteen compounds showed approximately 2-5-fold increase of transfection efficiency. Secondly, chemical components of cell culture surface and small volumes (200 nL) of cell culture medium were found to contribute to the maintenance of pluripotency of hiPSCs. Thirdly, ten groups of ternary protein combinations were identified to show support of undifferentiated culture of hiPSCs. Two of them were further evaluated to achieve long-term undifferentiated culture of hiPSCs, followed by their differentiation into three-germ layers. A summary and an outlook are presented at the end of the dissertation.

Zusammenfassung

Das Hochdurchsatz-Screening ist von großer Bedeutung und bildet einen der Eckpfeiler der aktuellen Life-Science-Research wie Biologie, Biotechnologie, Biochemie, Computerwissenschaft, medizinische Chemie und Pharmakologie. Das Interesse an einem Screening mit hohem Durchsatz unter akademischen, mittleren und kleinen Biotech-Unternehmen, staatlichen und gemeinnützigen Screening-Standorten, sowie Auftragsforschungsorganisationen wurde spürbar erhöht, da Hochdurchsatz-Screenings eine effiziente Analyse von einer Vielzahl von Stoffen in kürzester Zeit ermöglicht. Das steigende Interesse an dieser Methode führte zu einer schnellen Entwicklung von Screening-Technologien mit hohem Durchsatz in Kombination mit komplementären Technologien. Die Nachteile herkömmlicher Hochdurchsatz-Screenings beinhalten hohe Kosten und Materialverschwendung, lange Zykluszeiten, geringe Produktivität und die begrenzte Ausbaufähigkeit der existierenden Stoffbibliotheken. Die genannten Nachteile verdeutlichen die Wichtigkeit der Bemühungen zur Entwicklung von verbesserten miniaturisierten und automatisierten Hochdurchsatz-Screening Methoden. Droplet Microarray (DMA) ist eine dieser miniaturisierten Plattformen, welche durch die Vereinigung von Oberflächenchemie, Oberflächenfunktionalisierung und Biologie erschaffen wurde. Die hohe Tröpfchendichte auf DMA senkt die Kosten, Materialverschwendung, Zykluszeit des Screenings und erhöht die Effizienz des Verfahrens, während sie effektiv die Verwendung größerer chemischer und biologischer Bibliotheken unterstützt. Die weitere Entwicklung, Auswertung und Verbesserung der DMAs spielt nicht nur für den Fortschritt der Hochdurchsatz-Screenings eine wichtige Rolle, sondern beherbergt auch unermessliches Potential in pharmalogischen Bereichen und der Stammzellenforschung, in welcher es die Wirksamkeit von Gentransfers und das Kultivieren von undifferenzierten Stammzellen erleichtert.

Pharmakologisches Priming (Drug Repurposing) wurde als adjuvante Strategie zur Verbesserung der Effizienz nicht-viraler Genübertragung angesehen. Dennoch ist die facettenreiche Anwendung des pharmakologischen Priming aufgrund der unerschwinglich hohen Kosten für Reagenzien und die Durchführung der Methode unweit verbreitet, was den aufkommenden Drang nach miniaturisierten Plattformen und Drug Repurposing erklärt. Abgesehen von der Dringlichkeit im pharmakologischen Bereich, um klinisches Potenzial zu realisieren, benötigt die Stammzellenforschung auch miniaturisierte Methoden um den Einfluss von Zelloberflächeninteraktionen und Zellkulturmedium auf das Verhalten von Stammzellen

und die Effekte von Zusatzstoffen, und Oberflächenbeschichtungen einschließlich oberflächenabsorbierter Proteine auf Stammzellen zu beobachten.

Das Ziel für den <u>ersten</u> Teil der Dissertation war es nach kleinen Molekülen (Stoffen) auf DMAs zu suchen, welche transfektionsverstärkende Effekte beinhalten, um eine mögliche Verbesserung in den Bereichen Gentransfer- und Therapie zu bieten. Eine Untersuchung der Einflüsse von 774 Food and Drug Administration (FDA)-zugelassenen Wirkstoffen auf die Transfektionseffizienz mit verschiedenen Zelltypen in miniaturisierter- und hochdurchsatzweise wurde mit Hilfe der DMAs veranlasst. Das Screening der FDA-zugelassenen Arzneimittelbibliothek identifizierte 14 einzelne Verbindungen, die eine zwei- bis fünffache Verbesserung der Transfektion aufwiesen. Diese Treffer wurden verifiziert und in großem Maßstab untersucht. Die Ergebnisse deuten darauf hin, dass der auf DMA basierende Ansatz für das Drug Repurposing beständig ist und zur Untersuchung und Entwicklung wirksamerer nicht-viraler Genübertragungssysteme verwendet werden könnte.

Das Ziel des <u>zweiten</u> Abschnitts der Dissertation war es, den Einfluss von Oberflächeneigenschaften und sinkendem Volumen auf die Pluripotenz von human induzierten pluripotenten Stammzellen (hiPSCs) zu bestimmen. Zwei künstliche Oberflächen mit unterschiedlichen chemischen Elementen und deren dazugehörigen DMAs wurden für die Kultivierung und Pluripotenz von hiPSCs *in vitro* untersucht. Die Oberflächen und DMAs wurden genutzt, um human induzierten pluripotenten Stammzellen in 2 ml und 200 nL-Volumen zu kultivieren. Die Ergebnisse zeigten, dass hiPSCs eine hohe Lebensfähigkeit, sowie die erwartete Morphologie und Pluripotenz in 200 nL Tröpfchen auf Typ A und Typ B DMAs ohne Matrigelbeschichtung nach 24 h Kultivierung aufwiesen. Dies beweist, dass DMAs eine vielseitige und simple Plattform für kurzzeitige und xeno-freie Hochdurchsatz-Screenings von hiPSCs sind.

Als Ziel für den <u>dritten</u> Teil der Dissertation wurde das Identifizieren von chemisch definierten Proteinen, welche das Kultivieren und Aufrechterhalten der Plutipotenz von hiPSCs Zellen auf DMAs, sowie Mikrotiterplatten weiter verbessern könnten, angesetzt. Es ist möglich eine Proteinbeschichtung, Zellkultur und Immunfluoreszenzfärbung auf miniaturisierter Ebene parallel mit Hilfe von DMAs durchzuführen, was zu einer Reduzierung von Versuchsfehlern und Verbrauchsmaterialien führt. Auf Grund dessen wurden DMAs als Basis zur Überprüfung von elf verschiedenen Proteinen und deren verwandten binären und ternären Kombinationen (insgesamt 231 verschiedene Gruppen) auf ihre Fähigkeit zur Erhaltung der Pluripotenz von

hiPSCs genutzt. Aus diesem Raster wurden zehn Gruppen von ternären Proteinkombinationen identifiziert, welche die Proliferation und das Self-Renewal besser unterstützen könnten als mit Matrigel beschichtete Oberflächen. Die effizientesten Proteinkombinationen des primären Screenings wurden weiterhin in einer Langzeitkultur (fünf Wochen) verifiziert. Zusätzlich wurde die Formation von embryonalen Körperchen der auf den ausgewählten Proteinbeschichtungen kultivierten Zellen erzielt und es folgte die Differenzierung der hiPSCs in drei Keimblätter.

Zusammengefasst, wurden DMAs als miniaturisierte Schnellscreening-Plattform verwendet, um mehrere biologische Fragen zu beantworten. Als erstes wurden 776 Wirkstoffe auf Nanoebene untersucht und somit kosten-, zeit- und arbeitssparend verwertet. Vierzehn Stoffe wiesen eine zwei- bis fünffache Verbesserung der Transfektionstechniken auf. Als zweites wurden chemische Komponente von Zellkulturoberflächen und kleinen Volumina (200nl) von Zellkulturmedium gefunden, die zur Erhaltung der Pluripotenz von hiPSCs beitragen. Als letztes wurden zehn Gruppen von ternären Proteinkombinationen identifiziert, welche das Kultivieren von undifferenzierten hiPSCs unterstützen. Zwei von ihnen wurden weiter untersucht, um eine Langzeitkultur von undifferenzierten hiPSCs zu erzielen, gefolgt von ihrer Differenzierung in drei Keimblätter. Eine Zusammenfassung und eine Aussicht auf die Zukunft befinden sich am Ende der Dissertation.

Table of contents

List of Figures

List of Tables

List of Abbreviations

µM	Micro Molar
AD	Alzheimer's disease
AFM	Atomic force microscope
ALS	Amyotrophic lateral sclerosis
BSA	Bovine serum albumin
BSG	Basigin
CAR	Coxsackie and adenovirus receptor
CHO-K1	Chinese hamster ovary cell clone K1
CRISPR-Cas9	Clustered regularly interspaced short palindromic repeats-associated protein 9
DAPI	4',6-diamidino-2-phenylindole
DAG1	Dystroglycan
DMA	Droplet Microarray
DMEM	Dulbecco's Modified Eagle Medium
EB	Embryoid body
ECM	Extracellular matrix
EDX	Energy-dispersive X-ray spectroscopy
EpCAM	Epithelial cell adhesion molecule
EphA1	Ephrin type-A receptor 1
EphB4	Ephrin type-B receptor 4
FBS	Fetal calf serum
FDA	U.S. Food and Drug Administration
FGF-2	Basic fibroblast growth factor

FN	Fibronectin
GFP	Green fluorescent protein
HA	Hyaluronic acid
HEK293T	Human embryonic kidney293 cells - SV40 large T antigen
hESCs	Human embryonic stem cells
hiPSCs	Human induced pluripotent stem cells
hPSCs	Human pluripotent stem cells
HTS	High-throughput screening
JAM1	Junctional adhesion molecule A
LN	Laminin
LPLD	Lipoprotein lipases deficiency
mESCs	Mouse embryonic stem cells
MG	Matrigel™
Oct4	Octamer-binding transcription factor 4
PBS	Phosphate-buffered saline
PD	Parkinson's disease
PFA	Paraformaldehyde
PI	Propidium iodide
qPCR	Quantitative polymerase chain reaction
rpm	Round per minute
RT	Room temperature
SEM	Scanning electron microscope
siRNA	Small interfaces RNA
Sox2	Sex determining region Y-box 2

SSEA4   Stage-specific embryonic antigen 4

TA DMAs   Type A droplet microarray slides

TB DMAs   Type B droplet microarray slides

TGF-β   Transforming growth factor beta

TRA-1-60   Tumor-related antigen-1-60

TRA-1-81   Tumor-related antigen-1-81

VN   Vitronectin

XPS   X-ray photoelectron spectroscopy

1 Introduction

1.1 Gene delivery

1.1.1 Gene delivery and its applications

Gene delivery is the procedure that deliberately introduces naked or purified nucleic acids into eukaryotic cells to produce genetically modified cells (Kim & Eberwine, 2010). According to the long-term effects on a cell, there are two types of gene delivery. One is called transient transfection, in which DNAs or RNAs are transiently maintained in the nucleus and only expressed for a limited period of time (Stepanenko & Heng, 2017). The other one is named stable transfection, in which DNAs or RNAs are integrated into the genome of the host cells and sustain transfer gene expression even after host cells replicate. The transient or stable transfection is ordinarily dependent on the nature of the induced nucleic acids (Recillas-Targa, 2006).

The main purpose of gene delivery is to investigate gene/protein functions and regulations by enhancing, inhibiting, or knocking-out specific gene expression in host cells. Over the last few decades, due to development of molecular biology together with other related fields such as materials science and high-throughput screening techniques, gene delivery received large interest and has been widely applied in gene therapy (Dunbar *et al.*, 2018), induced pluripotent stem cells (Okita *et al.*, 2008; Yu *et al.*, 2009), small interference RNA (siRNA) based therapeutics (Setten *et al.*, 2019), and protein production in eukaryotic cells for therapeutic purpose (Hacker & Balasubramanian, 2016; Priola *et al.*, 2016; Ye *et al.*, 2010).

Gene therapy, which can be most simply defined as genetic modification for cells of patients to produce a therapeutic effect (Kaji & Leiden, 2001). There are many types of genetic modifications that can be made to the cells, including knockouts (DNA sequence deletions), knockins (DNA sequence insertions), and replacements (replacement of DNA sequences with exogenous sequences) (Lanigan *et al.*, 2020). Based on these categories and approaches, gene therapy can be used for monogenic diseases and complex disorders and infectious diseases (Shahryari *et al.*, 2019; Wang

& Gao, 2014). The first gene therapy product that has obtained marketing authorization from European Commission (EC) is Alipogene tiparvovec (marketed as Glybera), is a gene therapy drug for Lipoprotein Lipases Deficiency (LPLD). It is a recombinant AAV (rAAV) vector for treating LPLD by replacing with a functional LPL gene (Yla-Herttuala, 2012). Except for Glybera, there are many other gene therapy products that are worldwide on the market. Table 1 summarized so-far approved gene therapy products and their therapeutic indications and target tissues. Over the last decades, considerable efforts in gene therapy field were put and a huge progress was achieved. However, only a few of them were translated into the clinic. Nearly 300 gene therapy product candidates are currently under investigation at different stages and could expand diverse applications in the coming future.

Table 1. Gene therapy products on the market

Product name	Therapeutic indication and target tissue	Key publication
Defitelio (Defibrotide)	Hepatic sinusoidal obstruction syndrome/veno-occlusive disease with multi-organ dysfunction	(Richardson *et al.*, 1998; Richardson *et al.*, 2016; Richardson *et al.*, 2010)
Exondys 51 (Eteplirsen)	Treatment of duchenne muscular dystrophy -Striated muscles	(Geary *et al.*, 2015; Kinali *et al.*, 2009)
Gendicine (rAd-p53)	Head and neck squamous cell carcinoma	(Li *et al.*, 2015; Zhang *et al.*, 2018)
Glybera (Alipogene tiparvovec)	Familial lipoprotein lipases deficiency, leg muscle	(Bryant *et al.*, 2013; Ferreira *et al.*, 2014)
Imlygic (Talimogen laherparepvec)	Multiple solid tumors (melanoma, pancreatic cancer)	(Hu *et al.*, 2006; Senzer *et al.*, 2009)

Luxturna (Voretigene neparvovec)	Inherited retinal dystrophies, retinal pigment epithelial cells	(Russell *et al.*, 2017; Utz *et al.*, 2018)
Kynamro (Mipomersen)	Treatment of homozygous familial hypercholesterolemia - Liver, hepatocytes	(Santos *et al.*, 2015)
Macugen (Pegaptanib)	Treatment of neovascular age-related macular degeneration -eye	(Gragoudas *et al.*, 2004; Parodi *et al.*, 2018)
Neovasculgen (Pl-VEGF165)	Atherosclerotic peripheral arterial disease, including critical limb Ischemia, intramuscular transfer	(Deev *et al.*, 2017; Deev *et al.*, 2015)
Oncorine (rAd5-H101)	Patients with last stage refractory nasopharyngeal, cancer (head and neck cancer), NSCLC lung cancer, liver cancer, malignant pleural and peritoneal effusion and pancreatic cancer	(Nemunaitis *et al.*, 2000; Xia *et al.*, 2004)
Patisiran (Onpattro)	Familial amyloid polyneuropathy -Liver, peripheral nerves heart, kidney, gastrointestinal tract	(Adams *et al.*, 2018; Adams *et al.*, 2017)
Rexin-G (Mx-dnG1)	metastatic solid tumors (pancreatic cancer, Breast cancer, Osteosarcoma, Sarcoma)	(Chawla *et al.*, 2010; Gordon & Hall, 2010)

Spinraza (Nusinersen)	Treatment of spinal muscular atrophy/motor neurons and central nervous system	(Finkel *et al.*, 2016)
Vitravene (Fomivirsen)	Treatment of cytomegalovirus retinitis -eye	(Amin *et al.*, 2000; Goldberg *et al.*, 2005)
Zolgensma (Onasemnogene abeparvovec)	Pediatric individuals less than 2 years of age diagnosed with SMA having bi-allelic mutations in SMN1 gene	(Al-Zaidy *et al.*, 2019; Dabbous *et al.*, 2019; Waldrop & Kolb, 2019)

1.1.2 Gene delivery methods

The gene delivery methods are broadly classified into three types: biological, chemical, and physical (Figure 1). The choice of different methods depends on cell types and purposes since each method has its advantages and disadvantages. The ideal method for gene delivery should have high cell viability and delivery efficiency, biocompatible, labor-saving, economical, and reproducible.
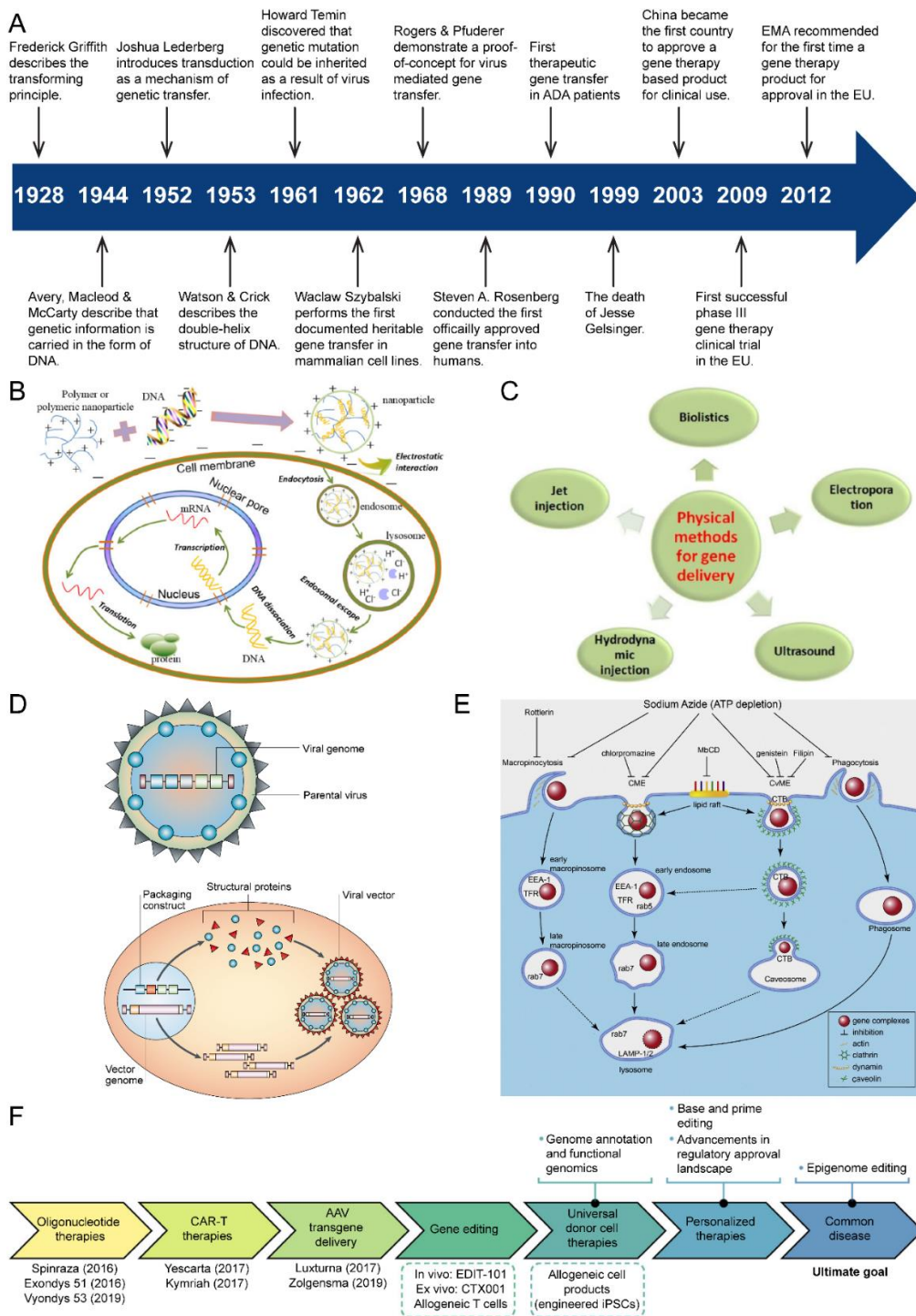
Figure 1. Gene delivery development and methods. (A) Important milestones for gene therapy. Modified from (Wirth et al., 2013). (B) Schematic illustration of polymer-based gene delivery. Modified from (Jin et al., 2014). (C) Physical methods for gene delivery. Modified from (Jin et al., 2014). (D) Schematic diagram of a generic viral vector and a packing construct is introduced into a packaging cell line. Modified from (Thomas et al., 2003). (E) Uptake mechanisms of non-viral gene delivery. Modified

from (Xiang et al., 2012). (F) Timeline depicting milestones (in colored arrows) towards gene therapies for common disease. Modified from (Bulaklak & Gersbach, 2020).

The most commonly used biological method for gene delivery is based on viral vectors, also known as transduction (Pfeifer & Verma, 2001). Viruses could easily target host cells and then navigate to cell nuclear to express the transfer gene due to the viral nature of them. By replacing part of the genome of a virus with a therapeutic gene, viral vector could integrate its DNA to host cell genome and sustainably express gene. Adenovirus (Lee *et al.*, 2017), adeno-associated virus (Daya & Berns, 2008), cytomegalovirus (van den Pol *et al.*, 1999), herpes simplex virus (Mata *et al.*, 2002), lentivirus (Cockrell & Kafri, 2007), pox virus (Moroziewicz & Kaufman, 2005), retrovirus (Yi *et al.*, 2011), and vaccinia virus (Yang *et al.*, 2018) are the most commonly used viral vectors. Nevertheless, concerns still remain for application of viral vectors, including immunogenicity (Woods *et al.*, 2003), the possibility of reverting to a wild-type or co-purify with replication-competent virions (Pack *et al.*, 2005), limited space to keep infectivity of foreign genes (Kim & Eberwine, 2010), target specificity, and high-costs of manufacturing. Therefore, the focus of developing safer and more economic viral vectors for gene delivery has been a major focus.

Chemical transfection methods are the currently most widely used gene delivery methods because they have improved safety, high gene compacity, stability, enormous flexibility, and easy to be altered to a large scale (Patil *et al.*, 2019). These advantages make them were the first methods used to introduce foreign genes into mammalian cells (Schenborn & Goiffon, 2000). In general, positively charged chemical materials electrostatically bind to negatively charged DNAs or RNAs to form transfection complex, protect transfer genes and mediate cellular entry, followed by translocate into cell nuclei and express transfer genes. The commonly used chemical transfection methods include calcium phosphate, dendrimer-based vectors, lipid-based vectors, nanoparticles, polymeric vectors, and polypeptide vectors. In 1973, calcium phosphate was firstly applied to introduce adenovirus DNA into mammalian cells (Graham & van der Eb, 1973). However, calcium phosphate transfections do not always work, resulting in variable transfection efficiency by cell type or conditions (Kim & Eberwine, 2010; Kingston *et al.*, 2003). Poly(amidoamine) (PAMAM) dendrimers have become the most widely utilized dendrimer-based vectors due to the ease of synthesis and the availability of commerciality (Dufes *et al.*, 2005; Haensler & Szoka, 1993). Except for

PAMAM, other dendrimer-based vectors, poly(propylenimine) dendrimers (PPI), poly(L-lysine) dendrimers, phosphorus-containing dendrimers, carbosilane dendrimers, are also well developed and established to achieve high transfection efficiency and low cytotoxicity. Liposome-based vector was one of the earliest approaches used to introduce transfer gene into host cells. These cationic lipids usually comprise three structural domains: a cationic headgroup, a hydrophobic portion and a linker between these two domains (Kim *et al.*, 2011; Li & Szoka, 2007). The first cationic lipid N-(1-(2,3-dioleyloxy)propyl)-N,N,N-trimethylammonium (DOTMA) was established in 1987, after that, similar cationic lipids such as 1,2-dioleoyl-3-trimethylammonium-propane (DOTAP), dimethyldioctadecylammonium bromide (DDAB), and cetyltrimethylammonium bromide (CTAB) have been developed and applied in gene transfection for various types of cells (Felgner *et al.*, 1987; Mintzer & Simanek, 2009; Niculescu-Duvaz *et al.*, 2003). Nanoparticle-based vectors is defined by low immunogenicity and a low production cost, as well as ease of synthesis when compared to other non-viral delivery systems (Encabo-Berzosa *et al.*, 2017). Nanoparticles, including quantum dots (Srinivasan *et al.*, 2006), gold nanoparticles (Williams *et al.*, 1991), silica nanoparticles (Kneuer *et al.*, 2000), carbon nanotubes (Klumpp *et al.*, 2006), lipid-based nanoparticles (Matsui *et al.*, 2007; Montana *et al.*, 2007), and polymeric hydrogel (Mok & Park, 2006) are some of non-viral gene transfection vectors that have been applied in transfer gene delivery. Polymer-based vectors can be of natural or synthetic origin. In 1975, polylysine (PLL) was found the ability to condense DNA and it was subsequently applied *in vitro* and *in vivo* gene transfer (Wu & Wu, 1987, 1988). Other examples of cationic polymers include polyethylenimine (PEI) (Ding *et al.*, 2014), polymethacrylate (Cherng *et al.*, 1996), β-cyclodextrin (Szejtli, 1998), chitosan (Borchard, 2001), poly(glycoamidoamine) (Liu *et al.*, 2004), schizophyllan (Mizu *et al.*, 2004), dextran (Rigby, 1969), linear poly(amido-amine) (PAA) (Richardson *et al.*, 2001), poly(4-hydroxy-L-proline ester) (Putnam & Langer, 1999), poly[α-(4-aminobutyl)-L-glycolic acid] (PAGA) (Lim *et al.*, 1999), poly(amino-ester) (PAE) (Green *et al.*, 2006), and phosphorus-containing polymers (Luten *et al.*, 2003; Wang *et al.*, 2002). Polypeptide vectors is another distinct approach to deliver transfer gene into cells with high efficiency and cell specificity. These peptides can deliver DNAs or RNAs into cells by making use of the readily plasma membrane crossing ability of short sequences of basic amino acid residues, such as trans-activating

transcriptional activators (TAT)-based peptides (Astriab-Fisher *et al.*, 2000; Torchilin *et al.*, 2003), antennapedia homeodomain peptide (Huang *et al.*, 2006; Joliot *et al.*, 1991), MPG peptide (Majidi *et al.*, 2016; Morris *et al.*, 1999), and transportan peptide (Kilk *et al.*, 2005). Except for the previously mentioned methods, as the research on non-viral vectors is progressing, more and more materials are being investigated to search for the promising effects towards high transfection efficiency and low cytotoxicity, such as graphene-based vectors and small molecules (Imani *et al.*, 2018; Kozisek *et al.*, 2020; Liu *et al.*, 2020). Compared to viral vector-based gene delivery, the transfection efficiencies of chemical methods are highly dependent on ratio between DNAs/RNAs and chemicals, cell membrane charge, their cellular uptake pathways, resulting in the probable low transfection efficiencies. Furthermore, the transfection efficiencies of chemical methods vary depending on cell types. Nevertheless, these methods possess merits of low cytotoxicity, no mutagenesis, no size limitation on the packaged DNAs or RNAs.

The physical gene delivery methods involve biolistic particle delivery, electroporation, laser-based transfection, magnetic field (magnetofection), microinjection, and ultrasound (sonoporation). Biolistic particle delivery relies on gold nanoparticles that conjugate with nucleic acids (O'Brien & Lummis, 2006). The conjugates are shot into recipient cells at high velocity. This is a fast and straightforward method, but the downsides are the high cell mortality rate and the high costs of expensive instruments. Electroporation and microinjection are two classical approaches pf physical transfection methods which are able to deliver DNAs or RNAs (Shi *et al.*, 2018; Zhang & Yu, 2008). However, these two methods are harsh on cells, often cause cell death, demand skill, and are very labor-intensive. Laser-mediated transfection (also known as optoporation or phototransfection) uses a pulse laser to irradiate cell membranes to form a transient pore (Barrett *et al.*, 2006). Once the pore on the membrane formed, the transfer gene could readily enter cells due to the osmotic difference between cell culture medium and cytosol. Magnetofection utilizes magnetic particles and magnetic fields to transfer gene into host cells. It can be combined with other transfection methods or vectors to achieve raised reporter gene expression (Scherer *et al.*, 2002). Sonoporation is a technique designed to enhance cell permeability through the use of ultrasound. The gene vectors are mixed with ultrasound contrast agents and the targeted gene could be transferred by selective insonation of a

predefined area (Miller *et al.*, 2002). Physical transfection methods provide appropriate options for cells that have been traditionally difficult to transfect. However, they need special expensive instruments and experimental skill, which make them very laborious. Furthermore, the nucleic acids are very vulnerable during the procedure.

Transfection methods are evolving rapidly to achieve higher transfection efficiency and lower cytotoxicity. From biological methods to physical methods, each method has its own pros and cons. The gene delivery method selection is strongly dependent on the experimental objectives.

1.1.3 Small molecules (drugs or compounds) for gene delivery

The primary method to improve transfection is chemical modification of existing gene delivery vectors based on the emerged structure-property trends (Gao *et al.*, 2018; Gao *et al.*, 2016; Madkhali *et al.*, 2019; Yao *et al.*, 2015). The methods aim to navigate a series of obstacles, such as complexation or condensation of DNAs or RNAs and transfection vectors (conditions including concentrations of DNAs or RNAs, pH, type of buffer, and B/P ratio, as well as sizes) (Mintzer & Simanek, 2009), serum stability (forming large aggregates resulting in ineffective gene delivery (Lai & van Zanten, 2001); adsorption of serum albumin and other negatively charged proteins lead to rapid clearance (Dash *et al.*, 1999), cellular uptake and endosome escape (most of the transfection complex internalized by cells via various endocytic routes (Mislick & Baldeschwieler, 1996; Molas *et al.*, 2003) and then trapped into endosome), cell nuclear localization, and transcriptional and translational regulation (Wiethoff & Middaugh, 2003). Although these methods have advantages in terms of non-immunogenicity of vectors, most of these approaches suffer from poor efficiency of delivery and transient expression of the gene. In addition, one of the drawbacks of these approaches is the diminished specificity of these materials (Putnam, 2006). An alternative adjuvant strategy is pharmacological priming (drug repurposing), by which conjugation with gene delivery vectors and nucleic acids can be achieved and further accomplish relevant gene delivery efficiency and transfer gene expression. Priming refers to exposing cells to small molecules (drugs or chemical compounds) before, during, or after the transfection in order to improve some aspects of the gene transfer. By pharmacological priming, the transfection efficiency enhancement and transfer gene expression can be

achieved through direct modulation of barriers mentioned above, or indirect through modulation cellular response to transfection in terms of toxicity and related gene expression (Nguyen *et al.*, 2016).

In 1983, Luthman et al. reported that exposure to chloroquine increased the proportion of transfected mouse cells to approximately 40% (Luthman & Magnusson, 1983). Chloroquine has been demonstrated to contribute to endosome escape and avoid lysosomal degradation (Figure 2A) (Cheng *et al.*, 2006). Glucocorticoid priming has been displayed to enhance viral and nonviral gene delivery for multiple cell types (Bernasconi *et al.*, 1997; Braun *et al.*, 1999). Abby M Kelly et al. showed that priming human mesenchymal stem cells (hMSCs), a typically difficult to transfect cell type, with dexamethasone increased 10- to 15- fold luciferase activity and the proportion of hMSCs expression transgenic enhanced green fluorescent protein (EGFP) by about three-fold (Kelly *et al.*, 2016). Neomycin is an aminoglycoside antibiotic which could stabilize multiplex nucleic acid structures (Arya *et al.*, 2001; Arya *et al.*, 2003), making it an enhancer for transfection efficiency of both reporter plasmids and oligonucleotides and resulting in a significant increase in transfer gene expression (Figure 2B) (Napoli *et al.*, 2005). Nocodazole, as an antineoplastic agent by interfering with the polymerization of microtubules (Vasquez *et al.*, 1997), could increase transfection efficiency of various gene delivery vectors (Figure 2C) (Hasegawa *et al.*, 2001; Li *et al.*, 2009; Wang & MacDonald, 2004). While broad applicability of transfection priming to various gene delivery vectors, nucleic acids, and cell types has not been established, a next step is utilizing this strategy to define other small molecules (drugs or chemical compounds) which might have priming effects.
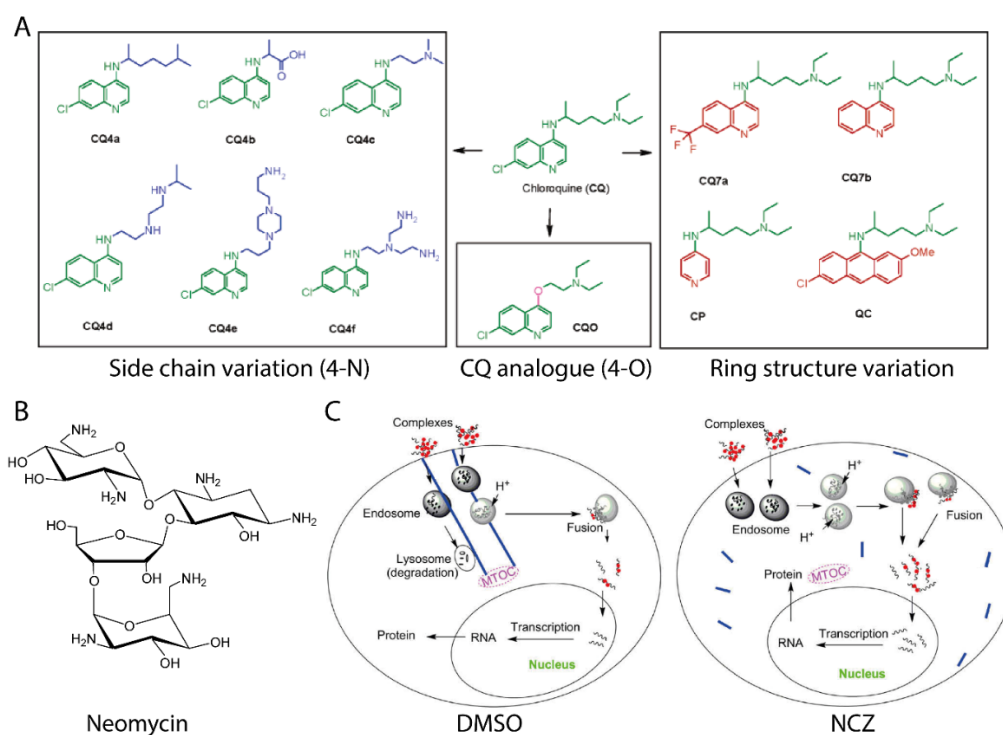
Figure 2. Small molecules enhance transfection efficiency. (A) Chloroquine is used as transfer gene expression enhancers in non-viral gene delivery. Modified from (Cheng *et al.*, 2006). (B) Neomycin is used as the transfection enhancer for cationic lipid-mediated transfection of DNA. Modified from (Napoli *et al.*, 2005). (C) Nocodazole (NCZ) improves the transfection efficiency of gold nanoparticles mediated gene delivery. Modified from (Li *et al.*, 2009).

1.2 Human induced pluripotent stem cells (hiPSCs)

1.2.1 HiPSCs and their potential in research

In the last decades, multitudinous technological breakthroughs were made and have driven basic, translational, and clinical advances in stem cell research fields, among which induced pluripotent stem cells (iPSCs) technology is the major milestone (Figure 3) (Omole & Fakoya, 2018). Four transcription factors — OCT4, SOX2, KLF4, and MYC — also known as "Yamanaka factors", were introduced into somatic cells (such as fibroblasts) and converted somatic cells into iPSCs (Takahashi & Yamanaka, 2006). In 2007, two research groups reported the successful generation of hiPSCs from human fibroblasts (Takahashi *et al.*, 2007; Yu *et al.*, 2007). In 2012, Shinya Yamanaka and John Gurdon were co-recipients of the Nobel Prize for Physiology or Medicine due to their discovery in reprogramming mature cells to a pluripotent state. Like human

embryonic stem cells (hESCs), hiPSCs have the capacity to self-renewal and differentiate into specialized cells in the human body, making them holding tremendous potential for regenerative and transplant medicine (Dakhore *et al.*, 2018), disease modeling (Figure 3B) (Spitalieri *et al.*, 2018), drug discovery and toxic screening (Cota-Coronado *et al.*, 2019), personalized theranostics (Figure 3C), and human developmental biology (Nelson *et al.*, 2010; Nishikawa *et al.*, 2008).
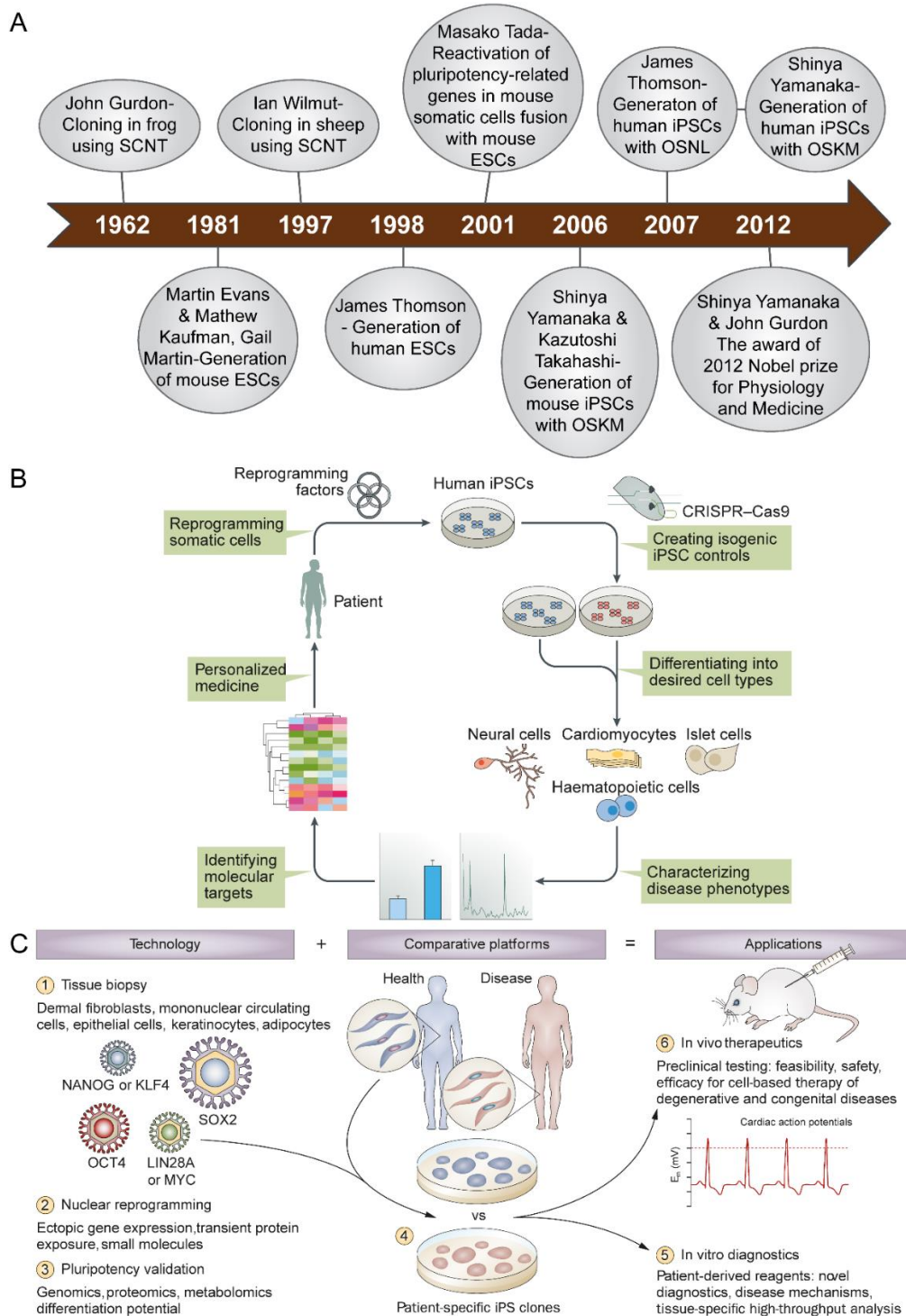
Figure 3. Development of iPSCs and their applications. (A) Timeline of the development of iPSCs. Modified from (Omole & Fakoya, 2018). The application of iPSCs in (B) disease modelling and (C) personalized theranostics. Modified from (Shi *et al.*, 2017) and (Nelson *et al.*, 2010), respectively.

The hiPSCs technology offers a unique opportunity for autologous transplantation. In regenerative medicine, tissues generated by hiPSCs could be transplanted to the site of injured or degenerated tissues and then repair the injury or degeneration. HiPSCs

have been applied in plenty of injuries, such as musculoskeletal injury (Tan *et al.*, 2012), spinal cord injury (Nori *et al.*, 2011), and liver damage (Liu *et al.*, 2011). Other than injuries, disease can also be treated with hiPSCs. In 2007, Hanna et al. treated sickle cell anemia (SCA) with iPSCs generated from autologous skin (Hanna *et al.*, 2007). The iPSCs were differentiated into hematopoietic progenitor cells and subsequently transplanted into mice models, resulting in rescue and correction of disease phenotype. Kazuki et al. reprogrammed fibroblasts from Duchenne muscular dystrophy (DMD) patients and corrected them by human artificial chromosome (HAC) via microcell-mediated chromosome transfer (MMCT), which might open a more sophisticated method for DMD gene therapies (Kazuki *et al.*, 2010). HiPSCs can also be used for production of red blood cells (RBCs), which helps blood generation (Lim *et al.*, 2013). For many other tissue repairmen, hiPSCs could also help, such as cardiovascular cells for repairing of heart valves, vessels, and ischemic tissues (Ye *et al.*, 2014). Wernig et al. reported transplanting of iPSCs-derived dopaminergic neurons improved dopaminergic function and behavioral symptoms in a Parkinson's disease (PD) rat model. In 2014, the first clinical trial using hiPSCs was initiated by transplanting hiPSCs-derived retinal pigment epithelial (RPE) to treat macular degeneration (Kimbrel & Lanza, 2015). The advances in genome editing or genome engineering allow site-specific genetic changes, taking iPSCs based regenerative medicine to new heights. Researchers now can repair gene mutations in patient-derived iPSCs to generate genetically healthy hiPSCs, as well as introduce specific mutations into non-diseased iPSCs to generate genetically matched isogenic hiPSCs that simulate the real pathology of the diseases. Gene editing technologies like zinc-finger nucleases (ZFN) (Hockemeyer *et al.*, 2009), transcription activator-like effector nucleases (TALENS) (Hockemeyer *et al.*, 2011), clustered regularly interspaced short palindromic repeats-associated protein 9 (CRISPR-Cas9) systems (Cong *et al.*, 2013), and meganucleases (Silva *et al.*, 2011) make great contribution to this field.

To look for new therapeutic strategies for human disease, identifying the pathological mechanisms plays a major role. Thus, a recapitulative human disease model is needed instead of currently commonly used animal models such as mice. It is of more importance and meaning to develop *in vitro* and corresponding *in vivo* model in parallel. Human patient-derived primary cells are helpful for therapeutic studies of human diseases. However, the application of primary cells is limited by the lack of

expandable sources of primary cells from human patients and hard-to-access. The ability of hiPSCs to infinite self-renewal and differentiate into all cell types in the human body ensures them as disease models to identify diseases both *in vitro* and *in vivo*, such as accessing neurons and cardiomyocytes from hiPSCs. In addition, hiPSCs are favorable sources for personalized medicine since hiPSCs can be derived from the relevant patients themselves. There are many *in vitro* studies have demonstrated the feasibility of using hiPSCs technology to study genetically inherited and sporadic diseases (the causes of which have not been identified in the family history of the patients or genetic mutations). Neural disorder is one of the most widely studied disease modeling for hiPSCs. Amyotrophic lateral sclerosis (ALS) is a type of neural disorder which exhibits persistent death of motor neurons and usually can be diagnosed in the late stage of disease progression. The first ALS disease model from hiPSCs was generated in 2008 (Dimos *et al.*, 2008). Since then, the mutations of ALS have been studied using hiPSCs-based ALS disease models, including Tar DNA binding protein-43 (TDP-43) (Kabashi *et al.*, 2010), vesicle-associated membrane protein-associated protein B (VAPB) (Mitne-Neto *et al.*, 2011), and superoxide dismutase 1 (SOD1) (Haidet-Phillips *et al.*, 2011). The Alzheimer's disease (AD) is caused by the misfolding of amyloid-β (Aβ) and tau proteins (Karagiannis *et al.*, 2019). The study of AD therapeutics focused on Aβ protein, amyloid precursor protein (APP), and prensilin-1 and -2 (PS1 and PS2) (Payne *et al.*, 2015; Tong *et al.*, 2015). Israel et al. developed a hiPSCs model and showed significantly higher levels of Aβ, phosphorylated (P-) tau protein, and active glycogen synthase kinase-3β (GSK-3β) (Israel *et al.*, 2012). Based on hiPSCs-derived neurons, Yagi et al. demonstrated that γ-secretase inhibitors remedied abnormal Aβ levels and Moore et al. showed γ-secretase inhibition increased P-tau levels (Moore *et al.*, 2015; Yagi *et al.*, 2011). Apart from the above studies, genetic and epigenetic differences between cell lines also influence the study of AD diseases. Hence, isogenic cell lines generated from hiPSCs were evolved to investigate AD related proteins and genes (Woodruff *et al.*, 2013; Young *et al.*, 2015). Parkinson's disease (PD) is a common neurodegenerative disorder and characterized by a significant loss of dopaminergic neuron (Davie, 2008). HiPSCs based studies found that SNCA (Ryan *et al.*, 2013), LRRK2 (Liu *et al.*, 2012), and PINK1 gene mutations play important roles in PD diseases (Seibler *et al.*, 2011). The first nonneuronal disease modeling investigation using hiPSCs was done by Vallier

laboratory (Rashid *et al.*, 2010). They successfully demonstrated that cells generated from patients hiPSCs could recapitulate key pathological features of the hepatological diseases such as aggregation of misfolded α1-antitrypsin in the endoplasmic reticulum, deficient low-density lipoprotein (LDL) receptor–mediated cholesterol uptake, and elevated lipid and glycogen accumulation. Besides, the hiPSCs of patients were also used to investigate other hepatological diseases, such as Niemann-Pick disease type C (NPC) (Soga *et al.*, 2015), familial amyloidotic polyneuropathy (FAP) (Hoepfner *et al.*, 2017; Isono *et al.*, 2014), urea cycle disorders (Kim *et al.*, 2016; Yoshitoshi-Uebayashi *et al.*, 2017). Except for 2D diseases models, hiPSCs were also used to form 3D cystic or ductal organoid for disease investigation (Ogawa *et al.*, 2015; Sampaziotis *et al.*, 2015). The hiPSCs are also used to study hematological and immunological diseases. The first hiPSCs-based hematological model was reported in 2009 (Raya *et al.*, 2009), in which the fibroblasts from Fanconi anemia (FA) patient were reprogrammed to prepare the FA disorder model. Further, by transplantation of hiPSCs differentiated hematopoietic progenitors into a mouse model resulted in recovered human hemoglobin levels (Wang *et al.*, 2012). Besides, hiPSCs-based diseases are also being used to investigate Shwachman-Diamond syndrome (SDS) (Tulpule *et al.*, 2013), Juvenile myelomonocytic leukemia (JMML) (Gandre-Babbe *et al.*, 2013), and chronic infantile neurological cutaneous articular (CINCA) syndrome (Tanaka *et al.*, 2012). Last but not least, hiPSCs are used to investigate human cardiac diseases, in which mouse models might be misleading, including hypertrophic cardiomyopathy (HCM) (Han *et al.*, 2014; Lan *et al.*, 2013), dilated cardiomyopathy (DCM) (Sun *et al.*, 2012a), cardiac arrhythmias (Egashira *et al.*, 2012; Itzhaki *et al.*, 2011), timothy syndrome (Yazawa *et al.*, 2011), and LEOPARD syndrome (Carvajal-Vergara *et al.*, 2010). The patient hiPSCs have created specific cells that can be used as *in vitro* models for many diseases for which previously there were none (Karagiannis *et al.*, 2019). However, the variance in maturity and functionality of the acquired somatic cells still limits the application of hiPSCs technology for the study of disease.

Another important application of hiPSCs is drug discovery. Animal-derived cells fail to replicate the exact human physiological conditions and related phenotype. Also, animal models are not good enough since a chemical might work for one animal but not work for another animal. Last, a newly discovered therapeutic must be tested on human cells or human test models while some cell types are hard-to-access. These

reasons make iPSCs and their directing differentiated somatic cells good candidates for drug discovery and screening. The first report of a large-scale drug screening based on iPSCs uses neural crest precursors derived from familial dysautonomia (FD) patient. Researchers tested 6,912 small molecules and characterized 8 small molecules rescued FD responsible gene IKBKAP (Lee *et al.*, 2012). Burkhardt et al. reported drug screening on iPSCs generated from amyotrophic lateral sclerosis (ALS) patients (Burkhardt *et al.*, 2013). TAR DNA-binding protein (TDP43) aggregation in motor neurons was identified and used as a read out to select compounds that reduced TDP43 aggregation. A new molecular mechanism of fibrodysplasia ossifcans progressiva (FOP) was identified by an iPSCs model (Hino *et al.*, 2015). Based on the same model, a high-throughput screening was applied. In the screening, rapamycin was identified to prevent the ossification in mice (Hino *et al.*, 2017). The first drug that reached clinical trial for iPSCs studies was ezogabine, which is indicated for epilepsy. Studies using ALS patients derived iPSCs showed that ezogabine could protect the correcting motor neuron physiology through Kv7.2/3 class of potassium channels (McNeish *et al.*, 2015). Other examples such as bosutinib and statin were reported for promote survival of motor neurons (Imamura *et al.*, 2017) and promote bone growth in skeletal dysplasia (Yamashita *et al.*, 2014), respectively. Development of new drugs and candidates is expensive. The prediction of adverse and side effects at early stage will significantly lower the costs. However, the requirement of abundant and stable human samples makes development of new drugs problematic. The intrinsic properties of hiPSCs provide a superior option. In general, the toxicity screening targets are neurons, cardiomyocytes, and hepatocytes. A broad set of structurally diverse drugs are applied to predict drug induced arrhythmia, torsade de pointes (TdP), and QT prolongation (Guo *et al.*, 2013). Human iPSCs derived hepatic cells that expressed functional molecules such as cytochrome P450 3A4 (CYP3A4) could uptake indocyanine green and respond to known hepatotoxic drugs (Takayama *et al.*, 2012; Yamada *et al.*, 2002). Even though there are many advantages of iPSCs technology, challenges such as cell maturity and cellular heterogeneity still exist.

The decades development of iPSCs technology combined with other novel technologies makes us to have a better understanding the molecular mechanisms of iPSCs, diseases, treatments, and developmental biology. However, several issues remain to be addressed. The first issue is the differentiation efficiency variations (Inoue

et al., 2014). The second issue is the heterogeneity of "primed" and "naive" states of iPSCs, which lead to heterogeneous cell population and differentiation potential (Narsinh *et al.*, 2011). The third issue is the probable biomedical ethics for combination of iPSCs with 3D technology. For example, the relevant ethics for organoid technology have not been sufficiently addressed until now. The clinical applications of iPSCs have been achieved less than ten years after the first human iPSCs were reported. It can be expected that great and encouraging success will be achieved in the coming future.

1.2.2 Substrates for hiPSCs cultivation
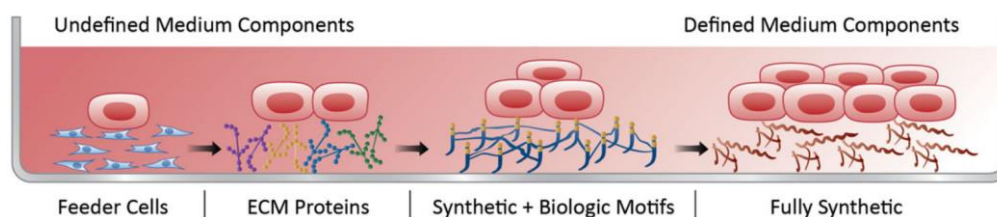
Figure 4. Evolution of hiPSCs cultivation. The illustration depicts the progression (left to right) from co-culture with feeder cells and serum-containing medium, to feeder-free culture in chemical-defined medium. Modified from (Villa-Diaz *et al.*, 2013).

Even though some research has cultured hiPSCs in suspension (Wang *et al.*, 2013; Zweigerdt *et al.*, 2011), hiPSCs are usually regarded as anchorage-dependent cells for which cell culture substrates are required for cell survival and proliferation *in vitro*. HiPSCs do not inherently attach on any general cell culture substrates, such as normal glass, plastics, or agars. Thus, there must be some surface functionalization or modification to promote adhesion (Hayashi & Furue, 2016). HiPSCs rely on various signaling pathways which are related to basic fibroblast growth factor (FGF-2), Activin/Nodal, and transforming growth factor beta (TGF-β) pathways for self-renewal (Vallier *et al.*, 2009). Besides, hiPSCs have a drastic loss of viability after enzymatic dissociation as single cells. Thus, hiPSCs are usually dissociated and passaged as colonies and aggregates (Ohgushi *et al.*, 2010; Watanabe *et al.*, 2007) .

Figure 4 shows the evolution of hiPSCs culture substrates. The early culture methods for hiPSCs were similar to the methods developed mouse embryonic stem cells (mESCs) (Evans & Kaufman, 1981), in which irradiated or mitomycin C-treated mouse embryonic fibroblasts (MEFs) or immortalized embryonic fibroblast lines (SNL or STO

cell lines) (Pan *et al.*, 2010; Yoshida *et al.*, 2009) were utilized as feeder cells in cell culture medium containing fetal calf serum (FCS) or serum replacement (SR) (Llames *et al.*, 2015). Feeder cells can support hiPSCs attachment and self-renewal by secretion of essential growth factors, cytokines, and extracellular matrices (ECM) such as FGF-2, TGF-β, activin A, laminin (LN), and vitronectin (Eiselleova *et al.*, 2008). However, the gamma-irradiation not only impedes cell proliferation but also influences general cell metabolization and subsequently alters the secretion of factors, cytokines and deposition of ECM (Villa-Diaz *et al.*, 2013). Moreover, the undefined environments or components of feeder cells, FCS, or SR make it difficult to identify which factors are indispensable for hiPSC culture and self-renewal. The feeder cells also have other troubles such as cellular cross-contamination, the lack of reproducibility, and time-consuming problems.

To overcome these problems, feeder-free culture approaches have been developed. Several commercially available feeder-free culture systems for hiPSCs have been displayed, including Matrigel (Corning Life Sciences, USA) (Gross *et al.*, 2013), Geltrex (Life Technologies, USA) (Ullah *et al.*, 2020), and Cultrex Basement Membrane Extract (Trevigen Inc, USA) (Fridman *et al.*, 2012). They are derived from Engelbreth-Holm-Swarm mouse sarcomas which contains numerous growth factors (such as TGF-β and FGF-2), proteins (~ 60% LN, ~ 30% collagen IV, entactin and the heparin sulfate proteoglycan perlecan), enzymes (such as matrix metalloproteinases (MMPs) (Gillette *et al.*, 2003), as well as other unknown components. However, the animal origin leads to problems related to immunogenicity, and microbial and viral contamination. In addition, Matrigel undergoes gelation at temperatures in the range of 22-37 ºC, resulting in variations in the mechanical and biochemical properties within a single batch and among batches. Therefore, a chemically well-defined, xenogenic-free cell culture environment is strongly required and should be applied to *in vitro* culture of hiPSCs.

In order to overcome problems coming from animal-derived materials and their mechanical and biochemical properties, the cell culture substrates must be carefully audited for animal-derived raw materials controls in compliance with regulations in applying to clinical and regenerative medicine. Thus, specific ECM proteins and synthetic substrates have been commonly investigated and used in recent years. LNs

are widely used ECM proteins for hiPSCs cultivation since they play important roles in structural organization of the basement membrane and the regulation of cell behavior (de la Loza *et al.*, 2017). LNs are heterotrimeric proteins that contain an α-chain, β-chain and a γ-chain, in which five, four, and three genetic variants were found, respectively. The LN subtypes are named according to their chain compositions (Aumailley *et al.*, 2005). For instance, LN-111 consists of α1, β1 and γ1 chains. There are at least sixteen isoforms of LN expressing in the human body (Yurchenco, 2011), including LNs-111, 121, 211, 213, 221, 331, 312, 321, 332, 411, 421, 422, 423, 511, 521, and 521 (Aumailley *et al.*, 2005; Macdonald *et al.*, 2010). Several studies investigated the role of LNs in hiPSCs attachment and self-renewal. A study showed that LN-511 could support long-term self-renewal of human pluripotent stem cells (hPSCs) (Rodin *et al.*, 2010). Another study showed that α-5 LN promotes hPSCs self-renewal in an autocrine and paracrine manner (Laperle *et al.*, 2015). LN-521 was also demonstrated to successfully maintain hPSCs self-renewal for long-term culture when combined with E-cadherin (Rodin *et al.*, 2014). Moreover, recombinant E8 fragments of LN-511 or LN 332 (LM-E8) were proven to sustain long-term self-renewal of hPSCs in defined xeno-free media (Miyazaki *et al.*, 2012). Other than LNs, some ECM proteins have been demonstrated to support the self-renewal of hPSCs. Vitronectin is a glycoprotein of the hemopexin family which is found abundantly in serum, the ECM, and bone (Schvartz *et al.*, 1999). Research have shown that vitronectin could support the self-renewal of hPSCs for long-term (Braam *et al.*, 2008; Rowland *et al.*, 2010). Chen et al. compared the wide type vitronectin (VTN-WT) with three variants which truncated at N-terminus (VTN-N), C-terminus (VTN-C) or both (VTN-NC) as coatings for hPSCs (Chen *et al.*, 2011a). VTN-N was found to better support the attachment and survival of hPSCs than VTN-WT. Fibronectin (FN) is an ECM glycoprotein which binds to integrins (Pankov & Yamada, 2002). It has been demonstrated to successfully support long-term self-renewal of hPSCs (Baxter *et al.*, 2009; Hughes *et al.*, 2011), although some results showed that it cannot maintain the pluripotency of hPSCs (Braam *et al.*, 2008; Xu *et al.*, 2001). This discrepancy might come from the differences of sources, differences in production process, or manipulating methods. To our knowledge, the systemically investigations of other single ECM proteins to long-term culture of hPSCs have not been reported. Other proteins, such as collagen, hyaluronic acid (HA), E-cadherin, are reported to successfully support hPSCs in an undifferentiated state

when combined with other materials or techniques. Lee et al. found that collagen type I could achieve 100% adhesion maintenance and suppress differentiation of hESCs when co-immobilized with Heparin-catechol (HepC) (Lee *et al.*, 2016). One study showed when encapsulated in 3D HA hydrogels, hESCs maintained their undifferentiated state and fully differentiation capacity (Gerecht *et al.*, 2007). E-cadherin is a Ca^{2+}-dependent cell-cell adhesion molecule. It was reported that the pluripotency of hPSCs could be maintained for a long-term on the surface coated with a fusion protein consisting of the E-cadherin extracellular domain and the IgG Fc domain (E-cad-Fc) (Nagaoka *et al.*, 2010).

However, the expensive manufacturing cost of natural and recombinant proteins under good manufacturing practices (GMPs), large-scale purification and production of functional proteins is laborious, costly and time consuming. Thus, the synthetic materials that can be easily modified have been designed and developed for undifferentiated hPSCs culture. Poly(2-(methacryloyloxy) ethyl dimethyl-(3-sulfopropyl) ammonium hydroxide) (PMEDSAH) was the first fully synthesized polymer that reported to support long-term culture of hESCs (Qian *et al.*, 2014). The self-renewal influence factors for hESCs, such as hydrophilicity, thickness, and surface charge, can be adjusted by altering the polymerization mode and the reaction time. PMEDSAH showed a similar gene expression pattern after 20 passages when compared with Matrigel. In another study, 16 polymers out of 90 polymers showed similar capability to Matrigel in short-term culture of hPSCs and maintaining pluripotency of hPSCs (Brafman *et al.*, 2010). Among these 16 polymers, a synthetic polymer poly (methyl vinyl ether-alt-maleic anhydride) (PMVE-alt-MA) was demonstrated to support long-term attachment, proliferation and self-renewal of hPSCs. In addition to the physical properties, such as stiffness, topography, and surface charge, the biochemical properties of the cellular microenvironment also of importance in stem cell culture. The cell-matrix interactions can be tuned on synthetic materials by combining with cell-adhesion motifs. Peptides that bind to integrin receptors have been developed and investigated on synthetic materials to maintain cell proliferation and support long-term self-renewal. One of the most ubiquitously utilized peptide is the FN-derived three amino acids peptide Arg-Gly-Asp (RGD), which could bind to αvβ3 and αvβ5 integrins (Mondal *et al.*, 2013). Based on RGD peptide, one study reported to covalently tethered RGD peptide to poly (acrylamide-*co*-propargyl acrylamide) (PAPA) brushes could

achieve scalable, stable, and long-term culture of hPSCs (Lambshead *et al.*, 2018). The cyclo (Arg-Gly-Asp-D-Phe-Lys) (cRGDfK) was identified the most effective peptide for hPSCs culture when compared with other peptides originated from LN, fibronectin, and vitronectin. In another study, several hydrogels with varying RGD concentrations were identified to show similar pluripotency maintenance capability of hESCs to Matrigel (Nguyen *et al.*, 2017). Except for RGD peptide, other peptide derived from ECM proteins have also been studied. A peptide (Ac-KGGPQVTRGDVFTMP sequence), which is derived from an active domain of VN, was covalently tethered to the poly (oligo (ethylene glycol) methacrylate (OEGMA-*co*-HEMA) polymer brushes modified surface. The synthetic substrate supports long-term proliferation and self-renewal of hiPSCs (Deng *et al.*, 2013). In another study, a VN derived peptide (KGGPQVTRGDVFTMP) was grafted on poly (vinyl alcohol-*co*-itaconic acid) (PVA-IA) hydrogel to investigate the effect of substrate stiffness on pluripotency and proliferation fates of hPSCs (Higuchi *et al.*, 2015). The hPSCs cultured on the hydrogel surface maintained their pluripotency for over 20 passages in xeno-free conditions. Other studies showed that proteoglycan-binding peptides, which can interact with glycosaminoglycans on the cell surfaces, are effective for supporting self-renewal of hPSCs (Klim *et al.*, 2010; Musah *et al.*, 2012). Except for FN- and VN-derived peptides modification, the synthetic materials have also been used to mimic the role of proteoglycans to support stem cells culture. Chang et al. reported poly (sodium 4-styrenesulfonate) (PSS) copolymerizing with polyacrylmide (PAM) at certain ratios and the obtained hydrogel (PAM$_6$-*co*-PSS$_2$) could support long-term self-renewal of hPSCs (Chang *et al.*, 2013). Apart from 2D stem cell culture, 3D cell culture holds benefits including rapid cell growth, prevention of large cell aggregates formation, isolation of cells from shear forces, and sufficient porosity for nutrient diffusion. For instance, Lei et al. reported a hydrogel-based 3D cell culture system for expansion and differentiation of hPSCs (Lei & Schaffer, 2013). One study synthesized poly(ethylene glycol) (PEG)-based hydrogels formed by light-triggered thiol–ene 'click' chemistry with specific receptor-binding peptides for investigating their influence on iPSC viability and differentiation, in which YIGSR and PHSRNG$_{10}$RGDS were identified to effective for iPSCs proliferation and clustering in 3D (Ovadia *et al.*, 2018). In another study, Caiazzo et al. reported MMP-degradable, RGD-functionalized PEG hydrogels increasing the reprogramming efficiency of human fibroblasts into hiPSCs by 2.5-fold

compared with a conventional 2D culture and supporting homogeneous hiPSCs colony formation (Caiazzo *et al.*, 2016).

1.3 High-throughput screening (HTS)

1.3.1 HTS and its applications

The concept of high-throughput screening (HTS) firstly appeared in the mid-1980s and has evolved over the last decades to serve the needs in biological and pharmaceutical research (Figure 5). It is the process by which multitudinous compounds or drugs can be tested in an automated fashion (Broach & Thorner, 1996). Now HTS is one of the cornerstones of modern drug discovery sitting at the interfaces between pharmacology, biology, computational science, and medicinal chemistry. The ultimate goal of HTS is to generate "hits" or "leads" which are crucial in determining the later potential of success and feeding into the drug discovery and development in therapeutics setting or being applied to address biological questions in the basic research (Table 2) (An & Tolliday, 2010; Bleicher *et al.*, 2003). The rapid progress of chemistry and biology in late 1980s to mid-1990s drives a significant advancement in HTS. The potential of combinatorial chemistry and genomic targets makes HTS technologies to evaluate numerous new candidates in pharmaceutical industries. As a result, speedy promotions raise HTS technologies in an automated and miniaturized manner (Hertzberg & Pope, 2000). Decade from 1991 to 2001 witnessed a huge technological revolution due to the human genome project first published a 90% complete sequence of all three billion base pairs in the human genome (Lander *et al.*, 2001). The world's pharmaceutic companies raced to identify new drugs and novel drug targets. In recent years, interest in HTS among academic, medium and small biotech companies, governmental, and not-for-profit screening sites as well as contract research organizations (CROs) have been dramatically increased, resulting in the rapid development of HTS technologies in combination with complementary technologies such as computational science and combinatorial chemistry (Wildey *et al.*, 2017).
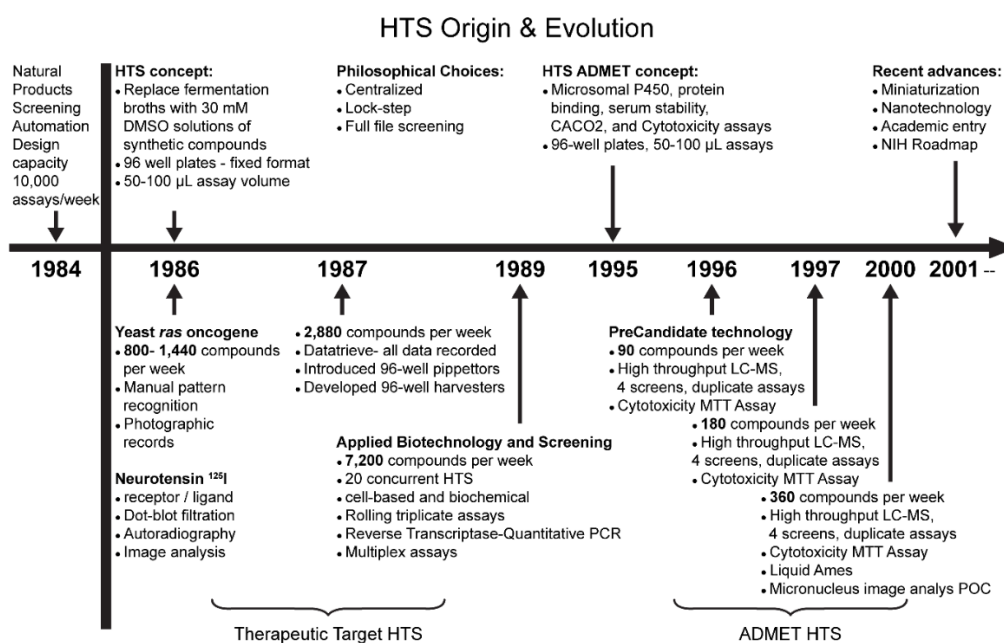
Figure 5. The origin and evolution of HTS. Modified from (Pereira & Williams, 2007).

Table 2. Terminology in HTS

Terms	Definitions
Assay	Precisely defined and efficiently designed experiment measuring the effect of a substance on a biochemical or cellular process of interest
High-throughput screening (HTS)	Iterative testing of different substances in a common assay. Screen is generally considered high throughput for >10,000 wells per day. Ultra HTS (uHTS) is reserved for >100,000 wells per day
Active	Biochemical activity at 1 concentration, 1 well
Confirmed active	Retest of active in replicate
Hit	Artifacts removed by deselection assays, typically single point
Confirmed hit	Dose–response curve, basic structure confirmation, and purity tested by LCMS
Lead	Member of a series of compounds for which a chemical optimization plan can be foreseen

| False positive | HTS "active" that is not active at the target |
| False negative | A compound with activity toward the target biology that is not identified in HTS. |

The HTS is a time-limited but intensive process which is influenced by two most critical elements—assays and the quality of the compound collection. Appropriate design of the assay is essential to perform a successful HTS. One of the main challenges in the evolution of HTS is to develop assays which can be performed at a high-throughput, statistical robustness, and reproducibility with the budgetary constraints. For this reason, there is a trend for decreasing the assay volumes and increasing the density, which is more time-saving and requires less consumption of consumables. The other critical element is the management of compound collections. Many sets of guidelines and recommendations have been developed over the last decades to reach a high quality HTS library (Lipinski *et al.*, 1997). Christopher A. Lipinski formulated a rule, which is called Lipinski's rule of five or Pfizer's rule of five, to evaluate the drugability of chemical compounds. The rule states as a molecule with a molecular mass less than 500 Da, no more than 5 hydrogen bond donors, no more than 10 hydrogen bond acceptors, and an octanol–water partition coefficient (log *P*) not greater than 5. The physicochemical characteristics of components in the HTSs library, such as molecular weight, solubility, and aggregation as well as predicted characteristics are of key importance for the quality of the HTS library. Except the characteristics of the library, the storage format, purity/integrity, and retrieval flexibility are also highly relevant to the outcome of HTS. Dimethyl sulfoxide (DMSO) is a widely used solvent for most libraries due to its ability to solve most small molecules at millimolar concentrations. Peptides libraries need other solvents. The libraries are normally stored at -20 ℃ to -80 ℃. The storage format has been developed from 96-well plates to the current 384-well plates and sealed microtubes. The quality control of commercially available libraries is usually performed by liquid chromatography-mass spectrometry to ensure the purity and stability of the compounds.

HTS enables investigation of very large numbers of molecules in miniaturized *in vitro* assays to identify molecules which are capable of addressing related questions,

making it widely acceptable and being applied in several fields. HTS is originally developed for pharmaceutical industry, it is one of the major steps in drug discovery. In 2007, US National Research Council (NRC) reported on *Toxicity Testing in the 21st Century*, which emphasized the importance of new technologies like HTS in the toxicity testing field. Based on this report, toxicity tests utilizing HTS technology have been widely conducted (Krewski *et al.*, 2020). These efforts provide a new foundation for much more rapid risk assessments and subsequent risk decision-making. HTS can be widely used in biochemical assays and cell-based assays, including enzymatic activity assessment (Burns *et al.*, 2006), biocatalysts screening (nitrilases) (Xue *et al.*, 2016), ligand-binding assessment (Fang, 2012), ion channels (Yu *et al.*, 2016) and protein-protein interactions (Voter *et al.*, 2016). In 2001, Regelin et al. developed a 96-well plates-based and a pipetting robot equipped HTS method to characterize transfection efficiency and cytotoxicity of diverse cationic lipids in various adherent cell types, including melanoma cancer cell MEXF462NL, colon carcinoma cell HT-29, kidney carcinoma cell RXF944L, bronchial epithelial cell line 16HBE-140⁻, endothelial cells HUVEC, Chinese hamster ovary cell (CHO), and monkey kidney derived COS-7 cells (Regelin *et al.*, 2001). He et al. reported an experimental-computational pipeline for HTS of drug combination effects in cancer cells. When integrating HTS with advanced synergy scoring tools, reliable detection of synergistic drug interactions within a specific window of concentrations can be achieved (He *et al.*, 2018). In another study, a cell-based HTS of a library of 12,816 chemical compounds was reported to identify miRNA pathway modulators in human HeLa cells and mouse NIH 3T3 cells (Brustikova *et al.*, 2018). The primary HTS experiments were followed by 11 dose-responsive validation experiments with 248 compounds selected from the primary HTS experiments. The results identified 163 putative miRNA inhibitors, providing a comprehensive reporter collection for future application of small compound modulators of miRNA pathways. A 96-well plates-based HTS that screened totally 10,011 small molecule compounds was reported to determine the efficacy in recombinant protein expression (Chang *et al.*, 2020). Two histone deacetylase inhibitors, apicidin and M-344, were found to increase the expression of recombinant protein, suggesting the increasing effect was mediated by promoting histone acetylation. The HTS has experienced decades of progress and is now being more and more mature in biochemical and pharmaceutical fields (Figure 6). When combined with artificial

intelligence (AI), HTS is expected to make the hunt for new biological targets, drugs and molecules faster, cheaper, and more effective.
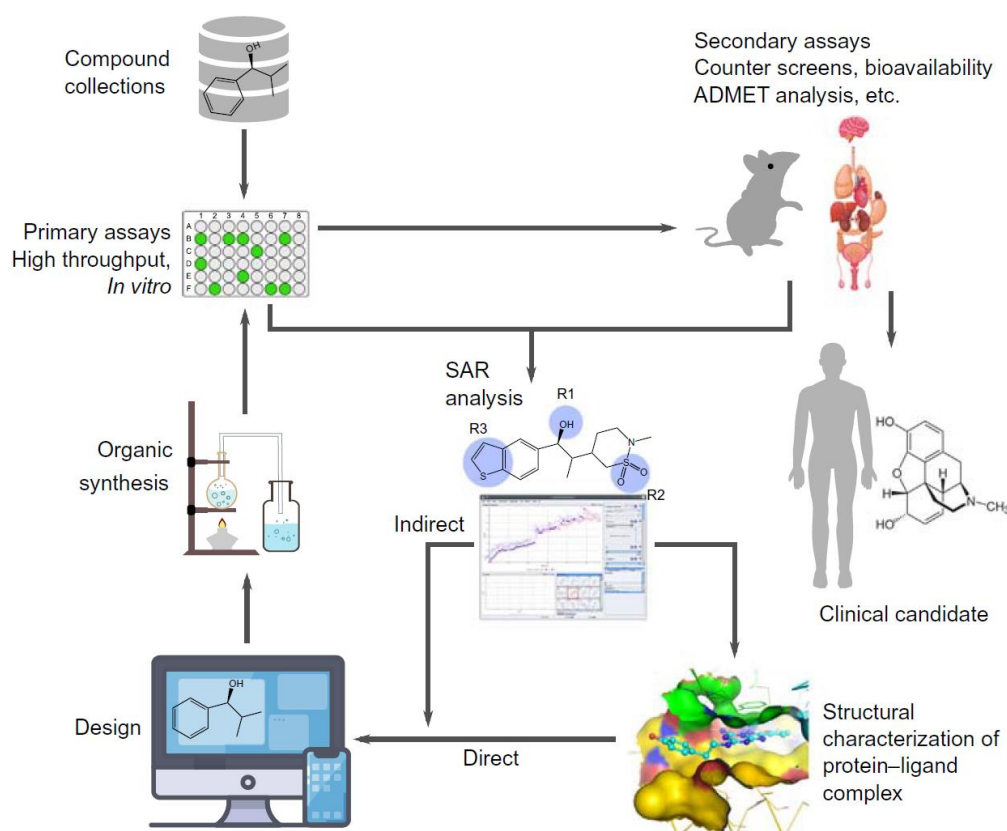
Figure 6. Major steps in drug discovery, including primary HTS in vitro, secondary screening, structure-activity relationship (SAR) and in silico studies. In the secondary screening, counter screenings and ADMET studies (adsorption, distribution, metabolism, excretion, and toxicity) need to be conducted. After these processes, the selected compounds have now passed all preclinical tests and then are transferred to clinical trials. Modified from (Chan *et al.*, 2019).

1.3.2 Current platforms and technologies for HTS

The microtiter plate based HTS platform has been increased from 96-well plates, to the currently standard 384-well plates, 1536-well plates, 3456-well plates and even higher well densities (ultra HTS (uHTS)). The throughput and efficiency have been improved accompanied with the well density increase. Boettcher and Mayr compared the impact of density for 1 million compound library screening with a commercially available protease assay. If the protease assay was done in 96-well plates, it requires 11,364 96-well plates. Increasing density to 384- and 1536-well plates could reduce the costs about threefold and sixfold, respectively. This comparison indicated the

importance and necessity of miniaturization. The density of microtiter plates could be increased up to 3456-well plates. However, the corresponding liquid handling instruments and robotics are expensive and requires in-depth effort.

Droplet-based microfluidic technology has been developed rapidly over the past decades and it currently offers multiple applications in scientific research. Two immiscible phases were used for droplets generation, including continuous phase and dispersed phase. In life science, droplet-based microfluidic technology is widely used for screening cellular responses, biomimetic microenvironments, and biomaterials production. Droplet-based microfluidic technology demonstrates considerable advantages, including reduced sample consumption, enhanced reaction speed, and increased reliability and reproducibility. This makes it a popular platform in HTS. Compared to 96-well plates, droplet microfluidic platforms reduce costs to 200-fold and reaction time from 2 h to 2.5 min (Courtney *et al.*, 2017). However, there are some drawbacks of droplet-based microfluidics, including difficulty to add different compounds into droplets, challenges to culture cells inside such droplets immersed into oils, and difficulty to add solutions into droplets multiple times.

A study done by Wang et al. demonstrated a multilayer pneumatic pump based microfluidic array for cell cytotoxicity screening with BALB/3T3, HeLa, and bovine endothelial cells against a panel of five toxins (digitonin, saponin, $CoCl_2$, $NiCl_2$, acrolein), which was comparable to microtiter plates (Wang *et al.*, 2007). Chung et al. developed a microfluidic platform for high-throughput capture and imaging of thousands of single cells (Chung *et al.*, 2011). This technique could be integrated with other methods such as single cell printing to extend the application of droplet-based microfluidic technology and single cell-based analysis. Another study showed a HTS of a drug library for its cytotoxicity against U937 cells based on a microfluidic technology-based single cell HTS platform (Brouzes *et al.*, 2009). Except for 2D cells, microfluidic technology has also been developed for 3D cell culture. Lee et al. developed a miniaturized 3D cell-culture array by encapsulating human MCF-7 cells in 20 nL collagen or alginate gels (Lee *et al.*, 2008). The cells on the 3D cell culture array exhibited similar drug response when compared to conventional 96-well plates assay, indicating the feasibility of a near 2000-fold miniaturization for 3D cell cytotoxicity HTS. In a separate study, Park et al. utilized a 3D cytotoxicity assay using an injection

molded plastic array culture (CACI-IMPACT) device to assess the killing ability of cytotoxic lymphocytes in a 3D cultured tumor cells in a high-throughput manner (Park *et al.*, 2019).

Bioprinting is a technique by which droplets can be printed on various surfaces to fabricate complex arrays on the microscope glass slides. There are three main types of modalities of bioprinting, including laser- (Koch *et al.*, 2010), droplet (Xu *et al.*, 2010), and extrusion-based bioprinting (Ozbolat & Hospodiuk, 2016). The mild and mark-less patterning and small dot size (below 100 μm) makes this technology suitable for HTS (Suntivich *et al.*, 2014). The other advantage of bioprinting is that it could boost rapid bioprinting through multiple nozzles in a highly reproducible manner (Xu *et al.*, 2011). Matsusaki et al. developed human 3D‑tissue structures on 440 micro-arrays by integration of hierarchical cell manipulation and automatic inkjet printing techniques (Matsusaki *et al.*, 2013). The assays of liver functions (albumin secretion, cytochrome-P450 (CYP450) enzyme secretion and CYP450 metabolism activities) were conducted in a high-throughput way. Bioprinting has also been applied in cancer research. Demirci's group demonstrated a high-throughput automated cell printing system to bioprint 3D coculture tumor tissue models (Xu *et al.*, 2011). In this study, human ovarian cancer (OVCAR-5) cells and fibroblasts were printed on Matrigel via a dual-ejector system focusing on the same point, resulting in the multicellular acini generation in a high-throughput and reproducible manner. This development provides a tool for high-throughput drug screening against 3D tumor models.

Microarray based HTS has been widely used in drug screening, gene expression and protein analysis. One study created a microarray of 2,100 individual cell-based assays on a standard microscope glass slide format (Kwon *et al.*, 2011). Then this microarray device was used to screen a small library of compounds for the apoptosis and necrosis inducing ability in human breast cancer MCF-7 cells. The use of hanging droplet method on the underside of cell culture plate lids is a typical method to generate 3D cellular spheroids. This method can also be used in microarrays. In a separate study, Beachley et al. developed 2D and 3D tissue ECM arrays for screening biological responses of human stem, cancer, and immune cells to tissue-specific scaffold microenvironments (Beachley *et al.*, 2015). The matrix production, adhesion and proliferation, and morphological changes of cells after culture were investigated and

analyzed in a HT way. Recently, researchers developed a stretchable high-throughput (HT) 3D cell microarray platform by printing cell-laden gelatin methacrylate (GelMA) on an elastic substrate (Sakthivel *et al.*, 2020). Then this platform was used to analyze cell mechano-responses in a high-throughput manner. Our lab also reported the generation of single-spheroid-microarrays by hanging droplet method on droplet microarray platform and the application in high-throughput screening of 3D cancer spheroids or microtumors (Popova *et al.*, 2019). Details of the droplet microarray platform are discussed in section 1.4.

1.3.3 High-throughput screening of transfection enhancers

Many methods can be used to improve transfection efficiency, including but not limited to viral vector-based gene delivery, non-viral vector-based gene delivery, and microinjection (discussed in section 1.1.2). Several studies about high-throughput transfection were reported (Figure 7), including using acoustic dispensing technology (Colin *et al.*, 2019), high-throughput microfluidic platform (Woodruff & Maerkl, 2016), and reverse transfection arrays (Erfle *et al.*, 2007; Lehner & Fraser, 2004). However, some of them suffered from relative low transfection efficiency and high toxicity. An alternative approach to improve transfection efficiency is pharmacological priming (drug repurposing). Priming is a pharmacological modulation of transfection efficiency and transfer gene, in which the cells were treated with chemical compounds before, during, or after mixing with transfection mixture in order to improve some aspects of the transfection process. Drugs such as dexamethasone and chloroquine have been demonstrated to enhance non-viral gene delivery (Cheng *et al.*, 2006; Kelly *et al.*, 2016). While broad applicability of priming has not been well established, the next step is to search for other compounds which have priming effects. With a broad set of compounds need to be tested for the priming effects, a HTS method for identifying transfection enhancers is necessary. In one study, the NIH Clinical Collection (NCC) compounds library was screened to identify clinical compounds that prime polyethylenimine (PEI) transfection (Nguyen *et al.*, 2016). By microscope image analysis and microplate measurements, the transfection efficiency changes were determined. Then the compounds were clustered by Tanimoto coefficients in ChemMine Tools. Among the compounds showing priming effects, antioxidants, GABBA receptor modulators, and

glucocorticoids were identified. In a separate study, a library of 31,413 small molecules was screened to identify compounds that increase antibody titers after transfection of a HEK293 cell line (Meyer *et al.*, 2017). The determined top two small molecule hits showed significant increasing of antibody expression, which might be due to their capacity to arrest cells in cell cycle G2/M phase with a decrease in growth and nutrient consumption and elevated nuclear plasmid DNA copy numbers and mRNA levels. Another HTS of over 700 clinically approved drugs was done to determine the prime effects on non-viral gene delivery to adipose-derived human mesenchymal stem cells (Kozisek *et al.*, 2020). A glucocorticoid, clobetasol propionate, was identified to increase transfer gene production 18-fold over the unprimed transfection.
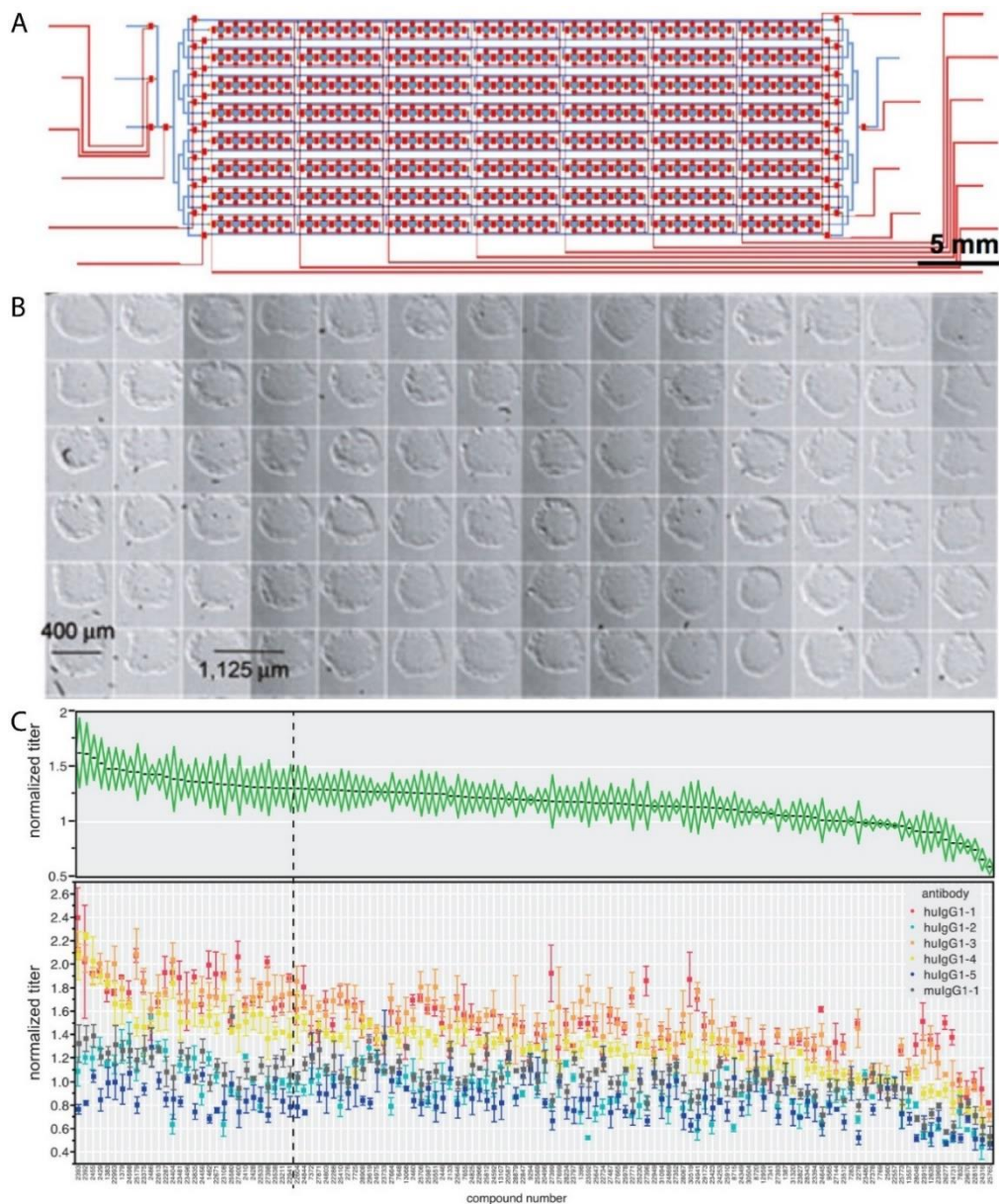
Figure 7. Examples of HTS of transfection enhancers. (A) Schematic of a high-throughput microfluidic platform for mammalian cell transfection. Modified from (Woodruff & Maerkl, 2016). (B) A bright field image showing the layout of a siRNA array for high-throughput transfection screening. Modified from (Erfle et al., 2007). (C) The results of HTS of transfection and protein expression enhancers. Modified from (Meyer et al., 2017).

1.3.4 HTS screening of substrates for hiPSCs

The optimization of defined substrates for hiPSCs proliferation and self-renewal is of vital importance for medical applications of hiPSCs. Most attempts to understand the role of the substrates were based on a trial-and-error manner and not sufficient to address the complement of the factors that may regulate hiPSCs proliferation and self-renewal, as well as fail to recapitulate the complexity of the uninvestigated platform. Back in 2009, Brafman et al. utilized an arrayed cellular microenvironments (ACMEs) technology to screen ECM proteins (human collagen I, collagen III, collagen IV, collagen V, FN, and LN) and other signaling molecules (bFGF, BMP-4, retinoic acid, and Wnt3a) that may regulate hESCs state (Figure 8A) (Brafman *et al.*, 2009). Among all the combinations, one substrate which composed of human collagen I, collagen IV, fibronectin and LN was identified as the hit. The hit was further verified by the capacity to sustain long-term culture of three hESC cell lines in an undifferentiated state. The same group then applied the same technology to conduct a high-throughput screening of the effects of multiple extracellular components on hPSCs (Figure 8B) (Brafman *et al.*, 2012). Mei and co-workers leveraged microfabrication technology to develop a polymer microarray platform to screen a variety of tunable properties of polymers for clonal growth of hPSCs (Figure 8C) (Mei *et al.*, 2010). Materials properties including wettability, surface topography, surface chemistry, and indentation elastic modulus were investigated for determining the relationships between materials properties and biological performance on the high-throughput polymer arrays. From the screening, a polymer with high acrylate content, a moderate wettability and a VN coating was identified to promote colony formation of hESCs. In another study, HTS microarray was utilized to discover novel polymers for hPSCs culture (Figure 8D) (Celiz *et al.*, 2015). In the screening, 4,356 individual assays were conducted on the glass slide and three generations of screening were performed. The monomer N-(4-hydroxyphenyl) methacrylamide) (HPhMA) was found to support cell adhesion both as homopolymer

and as a copolymer. The hit polymer, poly(HPhMA-*co*-HEMA), was validated by the long-term culture of hPSCs and differentiation into three germ layers. This study provides a cost-effective HTS method for identifying substrates suitable for hPSCs expansion omitting undefined and xenogenic matrix. High-throughput protein and biomaterial array were used to explore substrates for hPSCs expansion as discussed above. However, these studies are either conducted with non-chemically-defined media or requiring precoating with proteins or serum. Therefore, Ireland et al. developed a matrix microarray to investigate the combinatorial effects of ECM compositions (fibronectin, vitronectin, LN-521, and collagen IV) and substrate stiffness with elastic moduli ranging from ~ 1 to 60 kPa on hPSCs culture (Ireland *et al.*, 2020). As a result, three novel culture substrates were identified to support hPSCs proliferation and self-renewal better than the current hPSCs culture substrates.
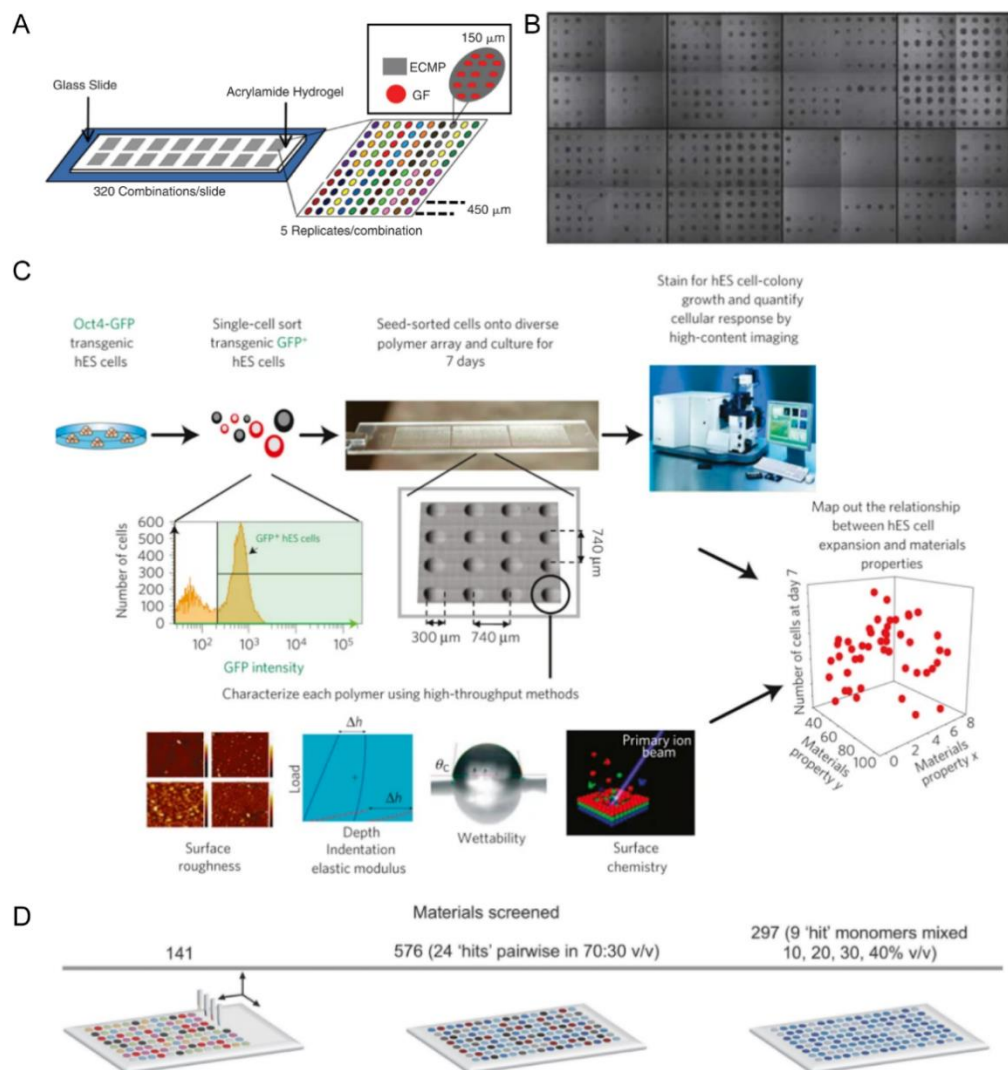
Figure 8. Examples of substrates for culturing hiPSCs. (A) HTS of combinations of extracellular matrix proteins and signaling molecules for the culture of HPSCs. Modified from (Brafman *et al.*, 2009). (B) Phase contrast images of HTS arrayed cellular microenvironments for identifying culture conditions of HPSCs. Modified from (Brafman *et al.*, 2012). (C) Schematic diagram of a HTS of biomaterials for clonal growth of HPSCs. Modified from (Mei *et al.*, 2010). (D) An illustration of a HTS of polymer for HPSC attachment. Modified from (Celiz *et al.*, 2015).

1.3.5 Challenges of current methods of HTS

HTS technology holds promise in analyzing thousands of samples in a single chip through systemic variations of different parameters. Compared to trail-to-error basis of testing molecules on after the other, HTS provide rapid, precise, and reproducible results with less reagents and biological samples. However, certain challenges remain in different applications of the HTS technique. The first challenge is the translatability of the HTS results. The HTS at the molecular level should be translated into possible tissue-, organ-, and organism-level before going to clinics, which is still challenging on current HTS platforms. Reducing the translating perturbations could help shorten this process. With the current technology limitations, orthogonal assays should be better developed to ensure the hits from a screen is more translatable. The second challenge is the formats differences between the library storage formats and the HTS platforms. The method to convert the libraries from their storge format to HTS platform in a time-saving and labor-efficient way is still developing. For instance, the library was stored in 96-well plates format while the HTS platform was developed on 384-well plates or with other formats. It is labor-intensive to transfer these libraries from the 96-well plates to the HTS platform. The automated instruments could help the transfer of libraries from the storage platform to the HTS platform. However, the corresponding liquid handling instruments and robotics are expensive and requires in-depth effort. The last challenge is the changes of the screened materials. The properties of materials temporally changed once after other factors were introduced. Thus, it is of importance to combine HTS platforms with real-time detection techniques and analysis systems to better understand the dynamic interactions between screened materials and HTS targets.

1.4 Droplet microarray (DMA) technology

1.4.1 Fabrication of DMA

Droplet microarray substrates can be fabricated by bioprinting, microfluidic technology, soft-lithography, and surface patterning. Here I focused on the hydrophilic-hydrophobic patterned substrates commonly used in our lab which is fabricated via surface modification and surface patterning. Feng et al. reported a fast and initiator-free approach to fabricate superhydrophilic-superhydrophobic micropatterns via sequential thiol-yne click chemistry (Feng *et al.*, 2014). The normal optical glass slide was coated with a 2.5 μm-thin porous polymer layer of poly(2-hydroxyethyl methacrylate-*co*-ethylene dimethacrylate) (HEMA-EDMA) for the subsequent modification (Geyer *et al.*, 2011). Then the hydrophobic alkyne polymer layer could be sequentially modified with 1*H*,1*H*,2*H*,2*H*-perfluorodecanethiol and cysteamine hydrochloride to introduce superhydrophobic and superhydrophilic surfaces with the help of a photomask, respectively. Based on this technique, the fabrication of droplet microarrays hold superhydrophilic spots separated by superhydrophobic barriers could be easily achieved. Through a straightforward discontinuous dewetting technique (Jackman *et al.*, 1998), droplet microarrays (DMAs) with isolated pico- to microliter-sized aqueous droplets with defined geometry and volume could be created in one step (Ueda *et al.*, 2012). Immersing DMA slide into aqueous solution and pulling it out or rolling a bulk aqueous droplet across the DMA slide leads to spontaneously formation of droplets in defined geometry and size. The geometry and size of superhydrophobic spots and superhydrophilic barriers can be precisely controlled by a photomask (Geyer *et al.*, 2011), resulting in the adjustable density and volumes of droplet arrays. Arrays of square superhydrophilic spots with side lengths of 1,000, 500, and 350 μm with 80, 9, and 3 nL volumes were successfully fabricated, of which the consumption were 600, 5,000, and 15,000 times less than that of 384-well plates, respectively (Popova *et al.*, 2016). Thus, DMA technology holds tremendous potential as a useful platform in further biological and chemical applications.

1.4.2 Advantages of DMA technology

The DMA platform possesses certain advantages and is an ideal miniaturized platform for a broad set of assays. The advantages include: 1) Rapid array formation. Due to wettability of differences between superhydrophobic and superhydrophilic surfaces, aqueous liquid can be trapped in each individual superhydrophilic spots, resulting in defined array formats. Besides, the liquid could also be dispensed on DMA slides by non-contact dispenser. The dispenser makes the multiple times addition of liquid to different locations possible. 2) No cross-contamination among spots on DMA slides. The superhydrophilic spots on DMA are divided by superhydrophobic borders. Thus, no additional devices or surfactants are required, leading to a relative clean environment compared to droplet-based microfluidic technology. As a result, there is no cross-talk among spots on the DMA slides. 3) Defined location. The array format brings the defined localization of each spot on DMA slides, making it suitable for simple indexing and time-lapse measurements at the same position. 4) Getting rid of physical walls. Microtiter plates are conventional platforms for high-throughput screening and other applications with the physical wells to prevent cross-contamination between wells. Large numbers of samples or solutions need to be added into each well of microtiter plates, such as 96-, 384-, and 1536-well plates. Liquid handling instruments and robotics could be adjusted to add samples and solutions into these wells in parallel. However, it is time- and labor-intensive to pipette chemicals or other substances into open wells due to the high costs and complexity of the instrumental setup. Liquid handling robotics are designed to solve this problem while introduce new problems such as high costs and complicated setups. Absence of physical wells makes DMA extremely easier and more rapid to change the components in spots on DMA slides with a rolling droplet method and with a liquid dispenser. 5) Adjustability. The density of arrays and the sizes of each individual spot can be adjusted by using various photomasks according to the purpose of the experiments, leading to wide applications of DMA to diverse objects. 6) Less manipulation. Compared to conventional microtiter plates (96-, 384-, and 1536-well plates), less steps are required for handling liquid into each individual spot on DMA than handling liquid into each well of the well plates due to the absence of physical wells. For instance, adding liquid into each well of a 384-well plate needs 384 times pipetting. While adding liquid into 384 spots on DMA slides just needs one pipetting of a bulk droplet, which is much more time- and labor-effective.

Besides, a parallel liquid dispensing using a liquid dispenser takes 40 seconds to dispense liquid into 672 spots on DMA slides. 7) High-throughput. The high density of arrays makes the DMA as a high-throughput even ultrahigh-throughput platform. Arrays of square superhydrophilic spots with side lengths of 1,000, 500, and 350 μm result in 588, 2178, and 4563 spots on a normal optical glass slide, respectively. The lower limit of patterning with a photomask is 20 μm, which means the higher density of arrays can be fabricated on DMA if necessary. 8) Miniaturization. The more spots are on the DMA slides, the smaller or more miniaturized are the DMAs. 9) Low cost. The lower volumes indicate the less consumption of cells, reagents and other consumables related to the experiments. As an example, a high-throughput screening of 774 FDA-approved drugs on DMA leads to around 2500-fold costs saving compared to experiments conducted in 384 - well plates. 10) Controllable neighboring spots merging. Since there are no physical walls on DMA, the neighboring spots can be merged by controlling the liquid volumes adding into the spots. 11) Wide compatibility. On the one hand, as a high-throughput screening platform, DMA has a wide compatibility with biological samples (cells, 3D spheroids, and zebra fish embryos), chemical samples (solvents, chemical compounds), and material samples (hydrogel, organols). On the other hand, the wide compatibility of DMA indicates the feasibility of DMA to broader applications in biology, chemistry, medical science, and material science. 12) Combination with other technologies. To precisely index one position and do a high-throughput screening on DMA, supplementary instruments or technologies are required. For example, high-throughput screening microscope is well established for the DMA format with easy setups. Another example is high-throughput printer. With the printer, the samples can be added on DMA by printing instead of pipetting, making the whole process on DMA pipetting-free and semi-automated.

1.4.3 Applications of DMA platform

Due to the advantages of DMAs, wide applications have been performed in biology, chemistry, and material science (Figure 9). Neto et al. developed a method for rapid fabrication of alginate hydrogel particles with defined sizes and shapes. Cells can be encapsulated into hydrogel particles with almost no toxicity. Based on this technology, magnetic hydrogel particles can be constructed for modular tissue engineering and

shape-coded hydrogel of distinct cell types (Neto *et al.*, 2016). Ueda et al. utilized DMA as a high-throughput screening platform to optimize reverse transfection parameters that affect transfection efficiency and cytotoxicity, indicating the feasibility of DNA as cell microarrays for optimizing reverse transfection conditions before performing further cell screenings (Ueda *et al.*, 2016). This study clearly demonstrates the potential of the DMA platform for miniaturization of biochemical and cellular HTS. By adjusting the cell density and seeding time, single cell array could also be obtained based on DMA (Jogia *et al.*, 2016). Around 100% cell viability of single cells and comparable single cell doubling time with that of cells in conventional culture can be observed, indicating DMA as a suitable platform for further single cell analysis. Tronser et al. used DMA to investigate the development, differentiation, and maintenance of stemness of mouse embryonic stem cells (Tronser *et al.*, 2017). Except for 2D cell culture, DMA is applied in 3D cell structure field. Tronser et al. reported rapid and facile one step embryoid body formation on DMA slides by a hanging droplet method. A dense array of homogenous and single embryoid bodies can be obtained and further utilized to screen 774-FDA approved compounds (Tronser *et al.*, 2018). In a separate study, Popova et al. established a miniaturized single-spheroid-microarray of 3D spheroids based on DMAs through a hanging droplet method and displayed a methodology for 3D cancer spheroids or microtumor screening (Popova *et al.*, 2019). On the basis of this achievement, Cui et al. precisely controlled the assembly of multi-spheroids by programmable droplet merging on DMA slides (Cui *et al.*, 2021). This study provides a method for miniaturized and high-throughput construction of complex 3D multicellular structures on DMA and can be further applied in various biological process. Furthermore, single zebra fish embryos array was developed on DMA and further applied for fluorescently labeled peptoids screening and toxicity screening via a sandwiching method (Popova *et al.*, 2018). In addition to the applications in cell biology, DMA platform has also been used in microbiology. Lei et al. developed a rapid method to generate bacteria droplets arrays and used them for antibacterial screening (Lei *et al.*, 2020a). A novel simple colorimetric readout method was established, indicating the great potential of rapid bacteria array formation and high-throughput drug screening on DMA. In 2007, Bruchmann et al. established homogeneous biofilm microcluster arrays with 2D geometries on DMA (Bruchmann *et al.*, 2017). The method is based on hydrophilic spots with geometries separated by "slippery" lubricant-infused

porous surface (SLIPS). Critical parameters influencing minimal adhesive regions for biofilm attachment and minimal SLIPS dimensions to avoid biofilm formation were studied. Lei et al. further investigated interconnected networks of bacteria on SLIPS based on DMA (Lei *et al.*, 2019). The study showed the network was formed by a "biofilm bridges" mechanism. In the following work, the precise control of geometry and flow through bacterial bridges were investigated in details (Lei *et al.*, 2020b). A study given by Oudeng et al. further extended the application of DMA to simultaneous detection of multiple HIV retroviral nucleic acids (Oudeng *et al.*, 2020). In this study, a Förster resonance energy transfer (FRET) sensing microarray was developed by modifying fluorescent dye-labeled oligomer probes MoS_2 nanosheets on DMA. The limit of detection is 50 pM.

Apart from the application in biology, DMA platform has also been investigated in chemistry and materials science. Rosenfeld et al. developed a solid-phase combinatorial synthesis method on DMAs and created an exemplary chemical library by this method (Rosenfeld *et al.*, 2019). Cell screening was done after the small molecules were released on DMA via UV irradiation. The same author subsequently reported the miniaturized high-throughput synthesis and screening of responsive hydrogels on DMA (Rosenfeld *et al.*, 2020). Unique hydrogels were constructed in nanoliter-sized droplets on DMA which allows encapsulation of cells and varies in hydrogel height and width. Another solid-phase synthesis study on DMA was given by Brehm et al., in which a 588-compound library of bisamides was established via a four-component Ugi-reaction (Brehm *et al.*, 2020). Interestingly, Benz et al. married chemistry with biology by combining on-chip solution based combinatorial synthesis and cellular screening (Benz *et al.*, 2019). In this study, a "chemBIOS" platform was developed and used for 75 parallel, three-component reactions to synthesize a library of lipidoids. The lipidoids were further applied in on-chip cell screening. The "chemBIOS" platform was further optimized for on-chip characterization and in-situ reaction monitoring in the ultraviolet, visible (on-chip UV-Vis spectroscopy and optical microscopy) and infrared (on-chip IR spectroscopy) regions, indicating the new avenues in high-throughput synthesis and drug discovery (Benz *et al.*, 2020). Although significant progress has been done on DMA platform, further applications in other directions are still of interest and importance, such as HTSs of nano coatings for diverse chemical and biological

applications, organ-on-a-chip screening on DMAs, and other popular research fields in life science.
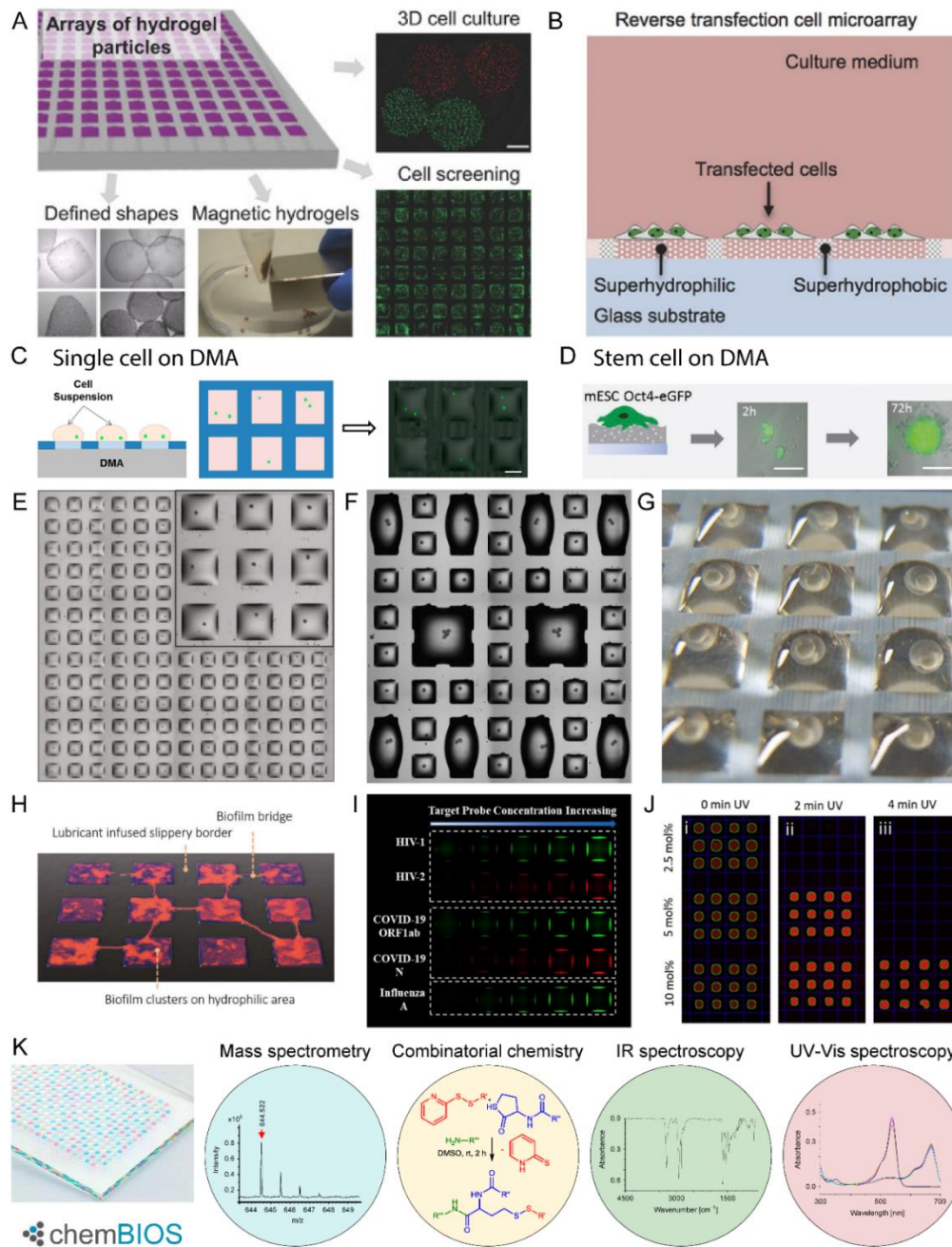
Figure 9. Applications of DMA. The DMA platform has been used for (A) magnetic hydrogel particles (modified from (Neto *et al.*, 2016)), (B) reverse transfection optimization (modified from (Ueda *et al.*, 2016)), (C) single cell analysis (modified from (Jogia *et al.*, 2016)), (D) feeder-free mouse embryonic stem cell culture and screening (modified from (Tronser *et al.*, 2017)), (E) 3D tumor spheroids formation and screening (modified from (Popova *et al.*, 2019)), (F) controlled multi-spheroids assembly (modified from (Cui *et al.*, 2021)), (G) fish embryos toxicity screening (modified from (Popova *et al.*, 2018)), (H) biofilm bridges based network forming (modified from (Lei *et al.*, 2019)), (I) multiple HIV retroviral

nucleic acids detection (modified from (Oudeng *et al.*, 2020)), (J) miniaturized high-throughput synthesis and screening of responsive hydrogels (modified from (Rosenfeld *et al.*, 2020)) and (K) combined high-throughput and high-content platform for unified on-chip synthesis, characterization and biological screening (modified from (Benz *et al.*, 2020)).

1.5 Objective

Large numbers of small molecule compounds or proteins have to be often screened with live cells in order to investigate their influence on therapeutically relevant cell types or, for example, to investigate the effect on cell transfection (so called, pharmacological transfection priming). However, the current *in vitro* high-throughput or ultra high-throughput screening methods are usually hindered by the prohibitively high costs associated with large volumes of reagents, tedious work flows and man-power required for the screenings using microtiter plates (usually 96- and 384-well plates) (Becker *et al.*, 2018). These problems limit the number of screenings performed and lead to the speed reduction of discovery of novel biologically active entities. These problems urgently require novel high-throughput screening platforms that can not only enable high-throughput screening of small molecules, but also be accessible for the screening of proteins or other biomolecules. Therefore, a miniaturized and biocompatible high-throughput screening droplet microarray platform has been investigated. Thus, this dissertation was focused on utilizing miniaturized droplet microarray platform to answer several fundamentally and practically important biological questions.

The first objective of this Ph.D. work was to investigate the influence of 774 Food and Drug Administration approved drugs on transfection efficiency using the droplet microarray platform. To screen candidates for cells with different characteristics CHO-K1 and Jurkat cells were used due to their difficult to transfect property and HEK293T cells were used because of their propensity for transfection. To analyze and characterize the potential transfection enhancer candidates, the drug compounds which could potentially enhance transfection efficiency and/or increase the numbers of green fluorescent protein expressing cells were identified. The next objective was to validate the potential transfection enhancer candidates in larger scale (384- and 96-well plates).

Since droplet microarray platform is a novel miniaturized screening platform, the effect of the droplet microarray platform on the culture of human induced pluripotent stem cells (hiPSCs) needs to be firstly evaluated. Therefore, the <u>second</u> objective of this Ph.D. work was to investigate the influence of surface properties and small cell culture volumes on the cell behavior of hiPSCs. To characterize the surface properties, water contact angle goniometry, energy-dispersive X-ray spectroscopy, scanning electron microscopy, atomic force microscopy, and X-ray photoelectron spectroscope measurements were conducted. To investigate the influence of small volumes, the cell morphology, viability, and pluripotency of hiPCS cultured on a large area (2.5 cm $\times$ 7.5 cm) covered with 2 mL of culture media and in confined 200-nL droplets on droplet microarray platform without Matrigel coating were compared.

The <u>third</u> objective of this Ph.D. work was to utilize droplet microarray platform to assess the ability of proteins to maintain undifferentiated *in vitro* culture of hiPSCs. To establish the protein screening protocol, the cell printing parameters, cell viability, and pluripotency were investigated. To determine the quality of screening, a screening window coefficient, Z-factor, was employed. To identify hits, the primary screening was employed on the basis of ability to maintain pluripotency compared to Matrigel. The next objective was to validate the proteins identified in the primary screening. The developed approach could be further expanded to investigate more complicate interactions of cells with their ambient environment.

2 Materials and Methods

2.1 Materials

2.1.1 Chemicals

Table 3. List of involved chemicals

Name	Company	Catalog number
1H, 1H, 2H, 2H-perfluorodecanethiol	Sigma-Aldrich (Munich, Germany)	660493-25G
2-mercaptoethanol	Alfa Aesar (Massachusetts, USA)	A15890.30
Dimethyl sulfoxide (DMSO)	Carl Roth (Karlsruhe, Germany)	A994.1
Triton X-100	Alfa Aesar (Massachusetts, USA)	A16046.AE
Shandon™ Immu-Mount™	Thermo Fisher Scientific (Massachusetts, USA)	9990402
ScreenFect®A transfection reagent	Screenfect GmbH (Eggenstein-Leopoldshafen, Germany)	S-3001
SCREEN-WELL® FDA Approved Drug Library V2	Enzo Life Sciences Inc. (New York, USA)	BML-2843 Version 1.2
Paraformaldehyde (PFA)	Carl Roth (Karlsruhe, Germany)	0335.1

2.1.2 Media, buffers, and solutions

Table 4. List of used media, buffers, and solutions

Name	Company	Catalog number
Doxycycline	Sigma-Aldrich (Munich, Germany)	D9891

DMEM	Gibco Life Technologies GmbH (Darmstadt Germany)	11965092
DMEM/F12 (1:1) medium	PAN-Biotech GmbH (Aidenbach, Germany)	P04-41450
FBS	Gibco Life Technologies GmbH (Darmstadt Germany)	10270106
Ham's F12	Biowest (Nuaillé, France)	L0136
Matrigel® Matrix (hESC-qualified)	Corning (New York, USA)	354277
mTeSR™ Plus	STEMCELL Technologies (Vancouver, Canada)	#05825
Normocin™	InvivoGen (California, USA)	ant-nr-1
PBS with Calcium/Magnesium	Thermo Fisher Scientific (Massachusetts, USA)	10010023
PBS without Calcium/Magnesium	Thermo Fisher Scientific (Massachusetts, USA)	14040117
Penicillin/Streptomycin (Pen/Strep)	Gibco Life Technologies GmbH (Darmstadt Germany)	15140122
ReLeSR™	STEMCELL Technologies (Vancouver, Canada)	# 05872
RPMI-1640	Gibco Life Technologies GmbH (Darmstadt Germany)	21875034
Trypsin-EDTA, 0.25%	Thermo Fisher Scientific (Massachusetts, USA)	25200056
Y-27632	STEMCELL Technologies (Vancouver, Canada)	# 72302

2.1.3 Cell stains and antibodies

Table 5. List of cell stains and antibodies

Name	Company	Catalog number

4',6-diamidino-2-phenylindole (DAPI)	Thermo Fisher Scientific Inc. (Massachusetts, USA)	D3571
Anti-β-Tubulin III Rabbit antibody	Sigma-Aldrich (Munich, Germany)	T2200
Anti-Brachyury Goat antibody	R&D Systems (Minneapolis, USA)	AF2085
Anti-E Cadherin Rabbit antibody	Abcam (Cambridge, UK)	ab15148
Anti-HNF-3β (FoxA2) goat antibody	R&D Systems (Minneapolis, USA)	AF2400
Anti-Nanog Rabbit mAb	Cell Signaling Technology (Massachusetts, USA)	4903
Anti-Oct-4A Rabbit mAb	Cell Signaling Technology (Massachusetts, USA)	2840
Anti-SSEA4 Mouse mAb	Cell Signaling Technology (Massachusetts, USA)	4755
Anti-Sox2 Rabbit mAb	Cell Signaling Technology (Massachusetts, USA)	5049
Anti-TRA-1-60(S) Mouse mAb	Cell Signaling Technology (Massachusetts, USA)	4746
Anti-TRA-1-81 Mouse mAb	Cell Signaling Technology (Massachusetts, USA)	4745
Calcein AM	Invitrogen (California, USA)	C3099
Goat Anti-Rabbit IgG H&L (Alexa Fluor® 488)	Abcam (Cambridge, UK)	ab150077
Goat Anti-Mouse IgG H&L (Alexa Fluor® 594)	Abcam (Cambridge, UK)	ab150116
Hoechst 33342	Thermo Fisher Scientific Inc. (Massachusetts, USA)	H3570
Phalloidin–Atto 565	Sigma-Aldrich (Munich, Germany)	94072
Propidium iodide (PI)	Invitrogen (California, USA)	P1304MP

| Rabbit Anti-Goat IgG H&L (Alexa Fluor® 488) | Abcam (Cambridge, UK) | ab150141 |

2.1.4 Cells

Table 6. List of involved cells

Name	Description	Source	Media
CHO-K1	Chinese hamster ovary (CHO) cells	Screenfect GmbH (Eggenstein-Leopoldshafen, Germany)	Ham's F12 + 10% FBS
Jurkat	Human T-cell lymphocyte cells	ATCC (Massachusetts, USA)	RPMI-1640 + 10% heat inactivated FBS + 1% Pen/Strep
HEK293T	Human embryonic kidney 293T cells	Screenfect GmbH (Eggenstein-Leopoldshafen, Germany)	DMEM + 10% FBS + 1% Pen/Strep
hiPSCs	Human induced pluripotent stem cells	Prof. Dr. Martin Bastmeyer, KIT	mTeSR™ Plus complete medium

2.1.5 Apparatus

Table 7. List of used apparatus

Name	Company
Atomic force microscope	Bruker (Billerica, USA)
CO_2 incubator CB260	Binder GmbH (Tuttlingen, Germany)
Drop shape analyzer DSA25E	Krüss GmbH (Hamburg, Germany)

ENVAIR ECO Air	ENVAIR Deutschland GmbH (Emmendingen, Germany)
Heraeus BB15 CO_2 Incubator	Thermo Fisher Scientific (Massachusetts, USA)
Heraeus Labofuge 400R Centrifuge	Thermo Fisher Scientific (Massachusetts, USA)
I-DOT One Noncontact dispenser	Dispendix GmbH (Stuttgart, Germany)
Keyence fluorescence microscope BZ-X810	Keyence (Osaka, Japan)
Keyence fluorescence microscope BZ-9000	Keyence (Osaka, Japan)
Leica TCS SPE confocal laser scanning microscope	Leica Microsystems CMS GmbH (Mannheim, Germany)
MiniSpin Plus	Eppendorf AG (Hamburg, Germany)
Nanodrop 2000	Thermo Fisher Scientific (Massachusetts, USA)
Olympus IX81 inverted motorized microscope	Olympus (Tokyo, Japan)
Scanning electron microscope	Leica (Hillsboro, USA)
sciFLEXARRAYER S11 dispenser	Scienion AG (Berlin, Germany)
StepOnePlus Real-Time PCR System	Thermo Fisher Scientific (Massachusetts, USA)
X-ray photoelectron spectroscopy	Shimadzu (Kyoto, Japan)
Zeiss LSM 800 confocal laser scanning microscope	Carl Zeiss AG (Oberkochen, Germany)

2.1.6 Kits and primers

Table 8. List of kits and primers

Name	Company	Catalog number

1 kb DNA Ladder	New England Biolabs (Massachusetts, USA)	N3232S
GoTaq® qPCR Master Mix	Promega (Wisconsin, USA)	A6001
Plasmid Maxi kits	QIAGEN (Hilden, Germany)	12162
Primers	Integrated DNA Technologies GmbH (Munich, Germany)	—
RNeasy® Mini Kit (50)	QIAGEN (Hilden, Germany)	74104
SuperScript IV First-Strand Synthesis System for RT-PCR	Invitrogen (California, USA)	18080051
SYBR Safe DNA Gel Stain	Invitrogen (California, USA)	S33102
Taq PCR Master Mix Kit	QIAGEN (Hilden, Germany)	201443

2.1.7 Consumables

Table 9. List of consumables

Name	Company	Catalog number
Corning® Thermowell GOLD PCR tubes	Corning (New York, USA)	3475
DMA slides	Aquarray (Eggenstein-Leopoldshafen, Germany)	G-np-Custom-0001, G-np-Custom-0002, G-np-602, G-np-102
CELLSTAR® Cell culture dishes	Greiner Bio-One International GmbH (Kremsmünster, Österreich)	664160
CELLSTAR® Cell culture flasks	Greiner Bio-One International GmbH (Kremsmünster, Österreich)	690160, 658170
CELLSTAR® Cell culture plates	Greiner Bio-One International GmbH (Kremsmünster, Österreich)	650160, 665180, 657160

CisNovo serological pipets	CisNovo (New York, USA)	P8050, P8100, P8250
Eppendorf Conical Tubes®	Eppendorf AG (Hamburg, Germany)	0030125.150, 0030123.344
FrameStar® 96 Well Semi-Skirted PCR Plate, ABI® Style	4titude (Surrey, UK)	4ti-0910/C
Nexterion® Coverslip Glass D	SCHOTT Nexterion AG (Jena, Germany)	1472315
Nunc™ Rectangular Dishes (4 wells)	Thermo Fisher Scientific (Massachusetts, USA)	267071
qPCR Seal	4titude (Surrey, UK)	4ti-0560
VWR® Tissue culture plates	VWR (Pennsylvania, USA)	10814-226

2.1.8 Proteins

Table 10. List of proteins

Name	Company	Catalog number
Basigin	Sino Biological Europe GmbH (Eschborn, Germany)	10186-H08H
Coxsackie and adenovirus receptor (CAR)	Sino Biological Europe GmbH (Eschborn, Germany)	10799-H08H
Dystroglycan (DAG1)	Sino Biological Europe GmbH (Eschborn, Germany)	14421-H08H
E-cadherin	Sino Biological Europe GmbH (Eschborn, Germany)	10204-H08H
Epithelial cell adhesion molecule (EpCAM)	Sino Biological Europe GmbH (Eschborn, Germany)	10694-H08H
Ephrin type-A receptor 1 (EphA1)	Sino Biological Europe GmbH	15789-H08H

	(Eschborn, Germany)	
Ephrin type-B receptor 4 (EphB4)	Sino Biological Europe GmbH (Eschborn, Germany)	10235-H08H
Hyaluronic acid (HA)	Abcam (Cambridge, UK)	ab143634
Junctional adhesion molecule A (JAM-1)	Sino Biological Europe GmbH (Eschborn, Germany)	10198-H08H
Laminin 521	STEMCELL Technologies (Vancouver, Canada)	#77003
Thy-1	Sino Biological Europe GmbH (Eschborn, Germany)	16897-H08H

2.1.9 Primers for qPCR

Table 11. List of primers for amplification in qPCR

Gene	Forward primer sequence (from 5' to 3')	Reverse primer sequence (from 5' to 3')
GAPDH	CTCTGCTCCTCCTGTTCGAC	ACGACCAAATCCGTTGACTC
Nanog	GTCTCGTATTTGCTGCATCGTA	AGCTAATTTCCTTCTCCACCCC
Oct4	CAAAACCCGGAGGAGTCCC	AAAGCGGCAGATGGTCGTTT
SOX2	GACAGTTACGCGCACATGAA	TAGGTCTGCGAGCTGGTCAT

2.2 Cell culture

Unless otherwise stated, all the cell culture and experiments were conducted under standard condition in a 5% CO_2 and 37 °C atmosphere. Mycoplasma negative cells were used for the experiments. The involved media, cells, and consumables were listed in Table 2, 4, and 7.

2.2.1 Routine culture of CHO-K1, HEK293T, and Jurkat cells

CHO-K1 cells were routinely grown in Ham's F12 medium supplemented with 10% FBS at 37 °C in 5% CO_2. Jurkat human T-cell lymphocyte cells were maintained in RPMI-1640 cell culture medium supplemented with 10% heat inactivated FBS and 1% Pen/Strep at 37 °C in a 5% CO_2 incubator. HEK293T cells were grown in DMEM medium supplemented with 10% FBS and 1% Pen/Strep. For passaging adherent CHO-K1 and HEK-293T cells, cells were firstly washed with 37 °C water bath pre-warmed PBS. Then PBS was removed and cells were incubated with 0.25% trypsin-EDTA at 37 °C for 1 min. Afterwards, the cells were resuspended in fresh medium and centrifuged at 1200 rpm for 3 min. Cells were passaged as 1:3 ratio for routine culture. For Jurkat cell passaging, cells were collected and centrifuged prior to resuspended into fresh medium and split as 1:3 ratio.

2.2.2 Conventional routine culture of hiPSCs

The tissue culture six-well plates were coated with 1 mL/well 1% (v/v) Matrigel in DMEM/F12 medium at RT for 1 h. Then the DMEM/F12 was aspirated and freshly prepared mTeSR plus medium supplemented with 1 μg/mL doxycycline and 50 μg/mL Normocin was added. Undifferentiated hiPSCs were maintained on tissue culture treated six well plates coated with Matrigel. The hiPSCs were passaged every 4 – 5 days through transferring mechanically dissociated clusters into fresh Matrigel coated six-well plates using a sterile Pasteur pipette. Cells were mechanically cleaned daily and the prewarmed mTeSR plus medium was changed daily.

2.2.3 The cultivation of cells on DMAs

The DMA glass slides were sterilized by immersing into 70% ethanol for 30 min and being air-dried on the clean bench before using. For HEK293T and CHO-K1 cells printing, cells were trypsinized and resuspended in complete medium till determined concentrations. As for Jurkat cells printing, cells were resuspended in fresh medium and diluted to determined concentrations. The volume of 100 nL of cell suspension was printed by I-DOT One Noncontact dispenser onto 1 mm DMA spots. Cells were further

grown at 37 °C in a 5% CO_2 incubator. The experiments were repeated three times to decrease experimental error.

For cultivation of hiPSCs on DMAs, the sterile 1 mm DMAs were precoated with 60 nL 1% (v/v) Matrigel in mTeSR plus medium per spot at RT for 1 h. Usually around 20 colonies per well of hiPSCs in a six-well plate were used for small clusters dissociation and further printed on DMAs. HiPSCs were dissociated by the detaching reagent ReLeSR according to the manufacturer's instructions. Briefly, the cells were washed with prewarmed DMEM/F12 medium three times prior to incubating with ReLeSR for 5-8 min and resuspending cells in fresh complete mTeSR plus medium. Then cells were printed onto each spot of DMAs with I-DOT One Noncontact dispenser. The hiPSCs on DMAs were incubated at 37 °C, 5% CO_2 atmosphere. The experiments were repeated three times to decrease experimental error.

2.3 Small molecules library screening

2.3.1 Small molecules library

The SCREEN-WELL® FDA-approved drug library V2, containing 774 small molecule drugs, was provided as 10 mM stock solutions in DMSO and arrayed in a total eleven 96-well plates, leaving the first and last columns in each plate for controls. Each drug solution in these microplates was diluted with sterile Milli-Q water to produce 10 and 100 μM prediluted plates. The prediluted drug plates were sealed and stored at –80 °C.

2.3.2 GFP plasmid DNA preparation

To easily visualize the results of gene transfection, a plasmid encoding for green fluorescent protein (pGFP) was used as a reporter gene. Highly purified covalently closed circular plasmid DNA was obtained by plasmid purification maxi kits from Qiagen according to the instructions from manufacturer. Briefly, bacteria were centrifuged at 4°C for 15 min with the speed of 6000 × g. Then the bacteria were resuspended in 10 mL buffer P1 prior to adding 10 mL buffer P2 and incubating 5 min

at RT. Buffer P3 was then added and the bacteria were incubated on ice for 20 min. Centrifuging the bacteria at 4°C for 30 min with the speed of $20{,}000 \times g$. The Qiagen-tip was equilibrated with buffer QBT followed by supernatant from centrifugation was added into the column and entered the resin by gravity. The Qiagen-tip was further washed with buffer QC. The DNA were then eluted with buffer QF and precipitated by adding isopropanol. Centrifugation was applied at 4°C for 30 min with the speed of $20{,}000 \times g$. The DNA pellet was then washed at RT with 70% ethanol and dried. Then the air-dried pellet was dissolved in TE buffer. The final concentration of DNA was 0.5–2.0 µg/µL and the A_{260}/A_{280} value was above 1.8. Prepared plasmid DNA was stored at -20 °C for further using.

2.3.3 Printing

The small molecule drugs in the library were preprinted onto individual spot on DMAs with three volumes using a sciFLEXARRAYER S11. The evaporation of drug droplets was fast since the tiny volumes (2 nL of 10 µM drug dilution for 1 µM group, 20 nL of 10 µM drug dilution for 10 µM group, and 6 nL of 100 µM drug dilution for 30 µM group). Due to the different volumes printed on DMAs, to keep all the condition the same, the drugs were dried in a desiccator under 50 mbar vacuum overnight. The cells with and without transfection reagents were then printed onto DMA by I-DOT One Noncontact dispenser. The dispenser is equipped with a powerful humidifier and a hygrometer. Once the humidity reached 70% at 25 °C, it started printing cells. When the printing was done, the printed DMAs were placed into a 10 cm diameter petri dish with 3 mL PBS and a wet humidifying pads in the upper lid to prevent evaporation during the following 24 h incubation in the 37 °C incubator.

2.3.4 Cell viability staining

The CHO-K1, Jurkat, and HEK293T cells were cultured on DMA as described above for 24 h. Live/dead staining and microscopic imaging were performed to evaluate cell viability. The Hoechst 33342 (working concentration: 10 µg/mL) and propidium iodide (PI, working concentration: 0.67 µg/mL) were used to visualize cell nuclei and dead cells, respectively. Hoechst 33342 could bind DNA of all cells, so it was used to

stain all the cells. PI cannot pass through intact cell membranes but readily passes through damaged membranes and binds with DNA, which indicates dead cells in red fluorescence (Chen *et al.*, 2011b). The Hoechst 33342 and PI positive cell numbers were analyzed by Image J (https://imagej.nih.gov/ij/). Cell viability was calculated as the following equation: cell viability (%) = 1 – (PI‑positive cell numbers/Hoechst positive cell numbers) × 100.

2.3.5 *In vitro* transfection screening

A one-step transfection method was applied for *in vitro* transfection in this part. The FDA-approved drugs were firstly printed or seeded on DMAs or in well plates prior to being vacuum dried overnight. Then, 20 μL transfection mixture was prepared as showed in Table 12 for different platforms (500 μm DMAs, 1 mm DMAs, and 384-well plates) and incubated at RT for 20 min to allow the transfection complex formation. The transfection mixture was next mixed with fresh cell suspension and printed or added on DMAs or in well plates followed by 24 h incubation in a standard cell culture incubator. Then cells were stained by Hoechst 33342 and PI, and cell viability was also calculated as described previously. The transfection efficiency was calculated as the following equation: transfection efficiency (%) = (GFP positive cell numbers/Hoechst 33342 positive cell numbers) × 100.

Table 12. *In vitro* transfection parameters on 500 μm DMA, 1 mm DMA, and in 384-well plates

	ScreenFect®A in 10 μL ScreenFect dilution buffer (μL)	GFP plasmid DNA in 10 μL ScreenFect dilution buffer (ng)	Cell/mL	Volume per spot/well
500 μm DMA	0.3	300	2×10^6	20 nL
1 mm DMA	0.15	150	1.25×10^6	100 nL

384-well plate	0.0017	17	7.13×10^4	20 µL

2.3.6 Screening workflow

For the primary screening, the 774 FDA-approved small molecule drugs were obtained in 10 mM stock solution of DMSO and diluted with sterile water to produce 10 and 100 µM plates. Then, the drugs were printed on sterile DMA patterned with 2187 square spots and 500 µm side length (section 2.3.3). Then the printed DMAs were vacuum dried in a desiccator overnight. The positive control (drug-free) was set as GFP plasmid DNA transfection efficiency without any drug but in the presence of equivalent DMSO. The negative controls were set as blank cells, cells with transfection reagent but without GFP plasmid DNA, and cells with GFP plasmid DNA but without transfection reagent. The fourteen hits from primary screening was selected and further validated on 1 mm side length DMAs and 384-well plates.

2.4 Proteins screening

2.4.1 DMA surface characterization

2.4.1.1 Water contact angle (WCA)

The WCAs of surfaces were characterized using Drop Shape Analyzer DSA 25 goniometer (Krüss) under ambient conditions (25 °C). A water droplet of 8 µL was deposited on the substrate and the water contact angle was measured within five seconds. The measurements were repeated for three times and the standard derivation is less than 2º.

2.4.1.2 Scanning electron microscope (SEM) and Energy-dispersive X-ray spectroscopy (EDX)

The morphology and elemental analysis of surfaces were determined by SEM and EDX. Specimen were analyzed with a LEO 1530 scanning electron microscope from Leica (Hillsboro, USA) with an accelerating voltage of 5-10 kV. For SEM analysis the specimens were sputtered with an ~ 5 nm thin layer of gold. For EDX a NORAN System SIX from Thermo Scientific (Waltham, USA) was used.

2.4.1.3 Atomic force microscope (AFM)

The roughness of surfaces was investigated by AFM using a Dimension Icon with ScanAsyst from Bruker (Billerica, USA). Cantilevers with a resonance frequency of 325 kHz from Olympus (Shinjuku, Japan) were used. The amplitude setpoint, the proportional gain and the integral gain were adjusted for an optimal overlap of the trace and retrace profile. The scan rate was held constant at 1 Hz. Data analysis was performed with the software Gwyddion V. 2.56 (GPL). The scanned surface dimensions were 10×10 µm and three different spots were examined for each surface. The R_a values were calculated over the entire surface areas. Values are given as an average with standard deviation (n=3).

2.4.1.3 X-ray photoelectron spectroscopy (XPS)

The chemical composition (C1s, Si2p, O1s, F1s, and S2p) of two surfaces was measured by XPS. XPS spectra were recorded on an Axis Ultra DLD from Shimadzu (Kyoto, Japan) utilizing monochromatized Al Kα radiation. The survey scan and the high-resolution scans were operated at an analyzer pass energy of 160.0 eV and 40.0 eV, respectively. The binding energy (BE) scale was referenced by setting the peak maximum in the C1s spectrum to 284.6 eV.

2.4.2 Cell viability staining

The cell viability of hiPSCs were assessed by a live/dead staining. Calcein AM is a fluorogenic esterase substrate that is hydrolyzed to a green-fluorescent product

(Calcein). Thus, green fluorescence is an indicator of cells with intact membrane to retain esterase products, which visualizes live cells in green fluorescence (Alisson-Silva *et al.*, 2014). PI cannot pass through intact cell membranes but readily passes through damaged membranes and binds with DNA, which indicates dead cells in red fluorescence. The final concentration of 0.5 µg/mL were used for both Calcein AM and PI. Fluorescent images were taken by Keyence BZ‑9000 and Olympus IX81 microscope. The area of Calcein AM and PI positive were analyzed by Image J (https://imagej.nih.gov/ij/). The cell viability was calculated as Calcein AM positive area to the sum of Calcein AM and PI positive area.

2.4.3 Immunofluorescence staining

The hiPSCs cultured on different surfaces and DMAs were fixed *in situ* with 3.7% (v/v) PFA for 15 min at RT and further permeabilized for another 15 min with 0.1% (v/v) Trinton X-100 in PBS (-/-). Then the cells were incubated with 1% (v/v) BSA at 37 ℃ for 1 h to block non-specific binding. The primary antibodies rabbit anti-Oct-4A (1:200), rabbit anti-Sox2 (1:200), rabbit anti-Nanog (1:200), mouse anti-SSEA4 (1:200), mouse anti-TRA-1-60(S) (1:200), mouse anti-TRA-A-81 (1:200), rabbit anti-E-cadherin (1: 400), anti-Brachyury (1:200), anti-FOXA2/HNF-3β (1:200), and anti-β-Tubulin3 (1:300) were used for staining at 4 ℃ overnight. Secondary antibodies goat anti-rabbit Alexa Fluor 488, goat anti-mouse Alexa Fluor 594, and rabbit anti-goat Alexa Flour 488 were diluted 1:500 and incubated 2 h at 37 °C before 1.43 µM DAPI was used to counterstain cell nuclei for 15 min at 37 °C. All the staining was observed under confocal microscopes. The same procedure was applied for phalloidin staining except the antibodies were replaced by Alexa Fluor™ 568 Phalloidin staining solution.

2.4.4 qPCR analysis for pluripotency genes

The hiPSCs were seeded and cultured on different surfaces (PA and ME, cells cultured on Matrigel was used as control) and DMAs (PA-DMA and ME-DMA) for 24 h. Cell were then detached by cell scrapers after 24 h incubation prior to RNA of different sample groups were isolated using the RNeasy® Mini Kit. The quantities and purities of extracted RNA were evaluated via Nanodrop 2000 spectrophotometer. Total

RNA (1 μg) was reverse-transcribed into template cDNA by reverse transcription using the SuperScript III First-Strand Synthesis System for RT-PCR kit according to manufacturer's instruction. Briefly, 1 μL Random Hexamers (50 ng/ μL), 1 μL dNTP mix (10 mM), a certain amount of RNA and nuclease-free water were mixed to a final volume of 10 μL in EP tubes and incubated for 5 min at 65°C. Then the tubes were placed on ice for 2 min. The cDNA Synthesis Mix was prepared as follows: 2 μL 10× RT buffer, 4 μL 25 mM $MgCl_2$, 2 μL 0.1 M DTT, 1 μL RNaseOUT (40U/ μL) and 1 μL SuperScript$^®$ III RT (200U/ μL) in the indicated order. Then 10 μL cDNA Synthesis Mix was added to each RNA/primer sample. Samples were incubated for 10 min at 25 °C, 50 min at 50 °C, 5 min at 85 °C, and then place on ice to add 1 μL RNase H prior to incubate at 37 °C for 20 min. Then the samples were kept at –20 °C for further process and longer storage. To confirm the cDNA synthesis and check primers, a control PCR was performed with 10 μL Taq PCR Master Mix 2×, 1 μL forward primer, 1 μL reverse primer, 2 μL cDNA and 6 μL nuclease free water (95 °C 3 min, cycle 35 [95 °C 30 s, 54 °C 30 s, 72 °C 90s], 72 °C 5 min and 10 °C ∞) followed by a 1.5% agarose gel electrophoresis (90 V, 400 mA, 75 min) and the gel was stained with SYBR Safe DNA Gel Stain (1:10000). Quantitative real-time PCR with 10 μL GoTaq$^®$ qPCR Master Mix, 1 μL forward primer, 1 μL reverse primer, 1 μL cDNA and 7 μL nuclease free water was performed using StepOnePlus Real-Time PCR system. The target genes and associated primers were listed in Table 9. Real-time data was analyzed as described (Pfaffl, 2001). The profiles of gene expression in hiPSCs were quantified with TaqMan Gene Expression Assays for each target gene. The expression level of target genes was determined by the comparative C_t method and normalized to GAPDH gene expression. The relative expressions of each marker in hiPSCs cultured on different surfaces and DMAs were normalized to that in hiPSCs cultured on Matrigel.

2.4.5 Proteins screening control investigation

DMA pre-coated with Matrigel was set as positive control and DMA without Matrigel pre-coating was set as negative control. The hiPSCs were printed on two control DMAs and incubated for 24 h. Then the Nanog expression of two control hiPSCs were obtained by IF staining according to the method described in 2.4.3. Then the staining was imaged by Olympus IX81 inverted motorized microscope with 10×

magnification. The statistical analysis of mean fluorescence intensity was performed using MATLAB R2018a (The MathWorks, USA). The fluorescence images were taken and then images borders were cropped, then a segmentation using 95th percentile of pixel brightness values as threshold was done. Found structures were optimized using morphological operators (opening (r=7), hole-filling). All remaining objects were quantified by their area and their brightness above background (set a minimum brightness in the image). The robustness and feasibility of the screening was evaluated prior to the screening by calculation of the Z-factor (Z') between positive and negative controls according to the following equations:

$$z' = 1 - \frac{(3\sigma_{c+} + 3\sigma_{c-})}{|\mu_{c+} - \mu_{c-}|}$$

where σ = standard deviation (SD) of brightness, μ = mean of brightness, c+ = positive control, and c- = negative control.

2.4.6 Proteins screening

Eleven individual proteins and their binary and ternary combinations (listed in Table 13 and 14) were applied for the protein screening for pluripotency maintaining of hiPSCs. The proteins were each diluted to 10, 20, and 30 μg/mL and combined in PBS to reach the final concentration of each individual component was 10 μg/mL. Then the protein solutions were spotted 60 nL/spot on DMAs. The printed DMAs were then placed in sealed 10 cm diameter petri dishes for 2 h at RT to allow the proteins coating. The hiPSCs were printed onto DMAs and cultured for 24 h, followed by IF staining for Nanog expression (as an indicator of hiPSCs pluripotency). The images of IF staining were acquired and analyzed to compare the Nanog expression. The screening threshold was set as mean ± 3SD. The 'hit' proteins which showed higher Nanog expression (larger than mean + 3SD of Matrigel group) were then selected and further validated by cell attachment efficiency, long-term maintenance of pluripotency marker expression and three germ layers (ectoderm, mesoderm, and endoderm) differentiation ability.

Table 13. Eleven proteins used for macromolecule screening

	Proteins
A	Thy-1
B	EphB4
C	EphA1
D	E-cadherin
E	CAR
F	JAM1
G	EpCAM
H	BSG
I	DAG1
J	HA
K	Laminin 521

Table 14. Single proteins and binary and ternary proteins combinations used in the primary screening. The final concentration of proteins is 10 μg/mL.

No.	CP	No.	CP	No.	CP	No.	CP	No.	CP	No.	CP	No.	CP	No.	CP
1	A	30	BK	59	GJ	88	ADI	117	BCI	146	BIK	175	CJK	204	EGJ
2	B	31	CD	60	GK	89	ADJ	118	BCJ	147	BJK	176	DEF	205	EGK
3	C	32	CE	61	HI	90	ADK	119	BCK	148	CDE	177	DEG	206	EHI
4	D	33	CF	62	HJ	91	AEF	120	BDE	149	CDF	178	DEH	207	EHJ
5	E	34	CG	63	HK	92	AEG	121	BDF	150	CDG	179	DEI	208	EHK

6	F	35	CH	64	IJ	93	AEH	122	BDG	151	CDH	180	DEJ	209	EIJ
7	G	36	CI	65	IK	94	AEI	123	BDH	152	CDI	181	DEK	210	EIK
8	H	37	CJ	66	JK	95	AEJ	124	BDI	153	CDJ	182	DFG	211	EJK
9	I	38	CK	67	ABC	96	AEK	125	BDJ	154	CDK	183	DFH	212	FGH
10	J	39	DE	68	ABD	97	AFG	126	BDK	155	CEF	184	DFI	213	FGI
11	K	40	DF	69	ABE	98	AFH	127	BEF	156	CEG	185	DFJ	214	FGJ
12	AB	41	DG	70	ABF	99	AFI	128	BEG	157	CEH	186	DFK	215	FGK
13	AC	42	DH	71	ABG	100	AFJ	129	BEH	158	CEI	187	DGH	216	FHI
14	AD	43	DI	72	ABH	101	AFK	130	BEI	159	CEJ	188	DGI	217	FHJ
15	AE	44	DJ	73	ABI	102	AGH	131	BEJ	160	CEK	189	DGJ	218	FHK
16	AF	45	DK	74	ABJ	103	AGI	132	BEK	161	CFG	190	DGK	219	FIJ
17	AG	46	EF	75	ABK	104	AGJ	133	BFG	162	CFH	191	DHI	220	FIK
18	AH	47	EG	76	ACD	105	AGK	134	BFH	163	CFI	192	DHJ	221	FJK
19	AI	48	EH	77	ACE	106	AHI	135	BFI	164	CFJ	193	DHK	222	GHI
20	AJ	49	EI	78	ACF	107	AHJ	136	BFJ	165	CFK	194	DIJ	223	GHJ
21	AK	50	EJ	79	ACG	108	AHK	137	BFK	166	CGH	195	DIK	224	GHK
22	BC	51	EK	80	ACH	109	AIJ	138	BGH	167	CGI	196	DJK	225	GIJ
23	BD	52	FG	81	ACI	110	AIK	139	BGI	168	CGJ	197	EFG	226	GIK
24	BE	53	FH	82	ACJ	111	AJK	140	BGJ	169	CGK	198	EFH	227	GJK
25	BF	54	FI	83	ACK	112	BCD	141	BGK	170	CHI	199	EFI	228	HIJ
26	BG	55	FJ	84	ADE	113	BCE	142	BHI	171	CHJ	200	EFJ	229	HIK
27	BH	56	FK	85	ADF	114	BCF	143	BHJ	172	CHK	201	EFK	230	HJK
28	BI	57	GH	86	ADG	115	BCG	144	BHK	173	CIJ	202	EGH	231	IJK
29	BJ	58	GI	87	ADH	116	BCH	145	BIJ	174	CIK	203	EGI		

2.4.7 Hits validation

2.4.7.1 Colony attachment efficiency on hits coatings

The solutions of hit proteins were added to wells of 12-well plates to coat the plates at RT for 2 h with the concentration of 10 μg/mL. The protein solutions were aspirated and hiPSCs were then detached by ReLeSR and added into each well. Cell attachment

were visually scored by counting attached colony numbers in seven random selected fields in each technically repeated well at 24, 48, 72, and 96 h. Experiments were repeated three times. The average of the attached colony numbers of protein groups were compared with that of Matrigel to assess the colony attachment ability of 'hit' proteins from the screening.

2.4.7.2 Long-term hiPSC culture on hits coatings

The 12-well plates were coated with 'hit' proteins according to the method described in 2.4.7.1. HiPSCs were mechanically dissociated and 10-20 colonies were transferred to the pre-coated plates. Then the cells were manually cleaned together with daily medium change. The cells were passaged every 3-5 days under the same conditions for five passages. HiPSCs culture on Matrigel-coated plates were used as a control. The morphology of hiPSCs at each passage was acquired by an inverted microscope and pluripotency at each passage was investigated by Nanog expression IF staining.

2.4.7.3 Differentiation into three germ layers of hiPSCs cultured on hits coatings

To induce embryoid body (EB) formation, hiPSCs colonies were dissociated and collected after five passages on 'hit' protein coatings. Then cells were seeded as 25 µL/drop on the lid of a 10 cm petri dish. The lid was then inverted to close the petri dish with 10 mL PBS below in the petri dish. The hanging droplets contained petri dish was then placed for 48 h to let the formation of EBs. The formed EBs were then transferred onto Matrigel coated well-plates and cultured in DMEM medium supplemented with 15% FBS and 1% Pen/Strep for additional 14 days to induce spontaneous differentiation into three-germ layers (endoderm, mesoderm, and ectoderm). Then IF staining experiments were conducted as described in 2.4.3 with anti-Brachyury (mesoderm), anti-FOXA2/HNF-3β (endoderm), and anti-β-Tubulin3 (ectoderm) antibodies.

2.5 Image acquisition and analysis

Images were taken by Keyence fluorescence microscope BZ-X810, Keyence fluorescence microscope BZ-9000, Leica TCS SPE confocal laser scanning microscope,

and Zeiss LSM 800 confocal laser scanning microscope. For screening, the automated Olympus IX81 inverted motorized microscope was involved. Exposure times were kept identical in all experiments for different channels and for microscopes used at different time points. For small molecule screening in the first part, the cells were stained with Hoechst 33342 and PI. The Hoechst 33342 and PI positive cell numbers were analyzed by Image J (https://imagej.nih.gov/ij/). Cell viability was calculated as the following equation: cell viability (%) = [1 − (PI positive cell numbers/Hoechst positive cell numbers)] × 100. The transfection efficiency was calculated as the following equation: transfection efficiency (%) = (GFP positive cell numbers/Hoechst 33342 positive cell numbers) × 100. The screening threshold of transfection efficiency was set as mean ± 3SD. The transfection efficiency higher than mean + 3SD of control were regarded as hit compounds and further validated in a larger scale using the same calculation method. For macromolecule screening, the cells were stained with Calcein AM and PI. The area of Calcein AM and PI positive were analyzed by Image J (https://imagej.nih.gov/ij/). The cell viability was calculated as Calcein AM positive area to the sum of Calcein AM and PI positive area. The Nanog expression by IF staining was used as the read-out for protein screening. Then the staining was imaged by Olympus IX81 inverted motorized microscope with 10× magnification. The statistical analysis of mean fluorescence intensity was performed using MATLAB R2018a (The MathWorks, USA). The fluorescence images were taken and then images borders were cropped, then a segmentation using 95th percentile of pixel brightness values as threshold was done. Found structures were optimized using morphological operators (opening (r=7), hole-filling). All remaining objects were quantified by their area and their brightness above background (set a minimum brightness in the image). Threshold of the screening was set as mean ± 3SD. The Nanog expression which was higher than that for mean + 3SD of Matrigel group was regarded as hit. Then hit proteins were further validated by long-term culture and three specific germ layers differentiation.

2.6 Statistical analysis

All the experiments were conducted with three technical repeats and biological repeats and used for statistical analysis. The data were presented as mean ± standard deviation (SD) or mean ± standard error of the mean (SEM). Comparisons were

conducted via two-tailed unpaired student's t-test, unless otherwise specified. A significant difference was defined as $*P < 0.05$.

3 Results and discussion

3.1 High-throughput screening of cell transfection enhancers using miniaturized droplet microarray[1]

3.1.1 Cell culture on DMA and workflow of the screening

Droplet microarray (DMA) slide is a glass slide (75 mm × 25 mm × 1mm) patterned with an array of hydrophilic (static water contact angle ~22.6º) spots assigned by superhydrophobic (static water contact angle ~156.5º) borders based on nanostructured substrate (Figure 10A and 10B). The layout of the DMA was described in Figure 10. The DMA slides divided into three fields (left field, central field, and right field; Figure 10B) were used in this project, which containing 588 (1 mm side length of square spots) and 2,187 (500 μm side length of square spots) individual spots, respectively (Figure 10C). Due to the precise patterned square spots and stable borders, homogeneous cellular microarrays can be created by printing cell suspensions directly into each individual spot using a non-contact cell printer and further incubated cells for determined time periods. The fluorescence images of GFP expressing cells, Hoechst 33342 staining cells and PI staining cells were taken and further applied for cell toxicity and transfection efficiency analysis.

Figure 11A displays a 588 spots DMA with 100 nL water per spot to visualize the DMA format. The cells could be printed on DMA and further incubated for 24 h (Figure 11B). Except cell culture, transfection could also be done and observed on DMA (Figure 11C, green dots represented GFP expressing cells). Beyond that, DMA platform was also accessible for cultivation and transfecting cells in different characteristics, such as adherent HEK293T cells (Figure 11D), CHO-K1 cells (Figure 11E) and suspension Jurkat cells (Figure 11F).

---

[1] **Liu, Y., Tronser, T., Peravali, R., Reischl, M., & Levkin, P. A.** (2020). High-Throughput Screening of Cell Transfection Enhancers Using Miniaturized Droplet Microarrays. *Advanced biosystems*, *4*(3), 1900257.
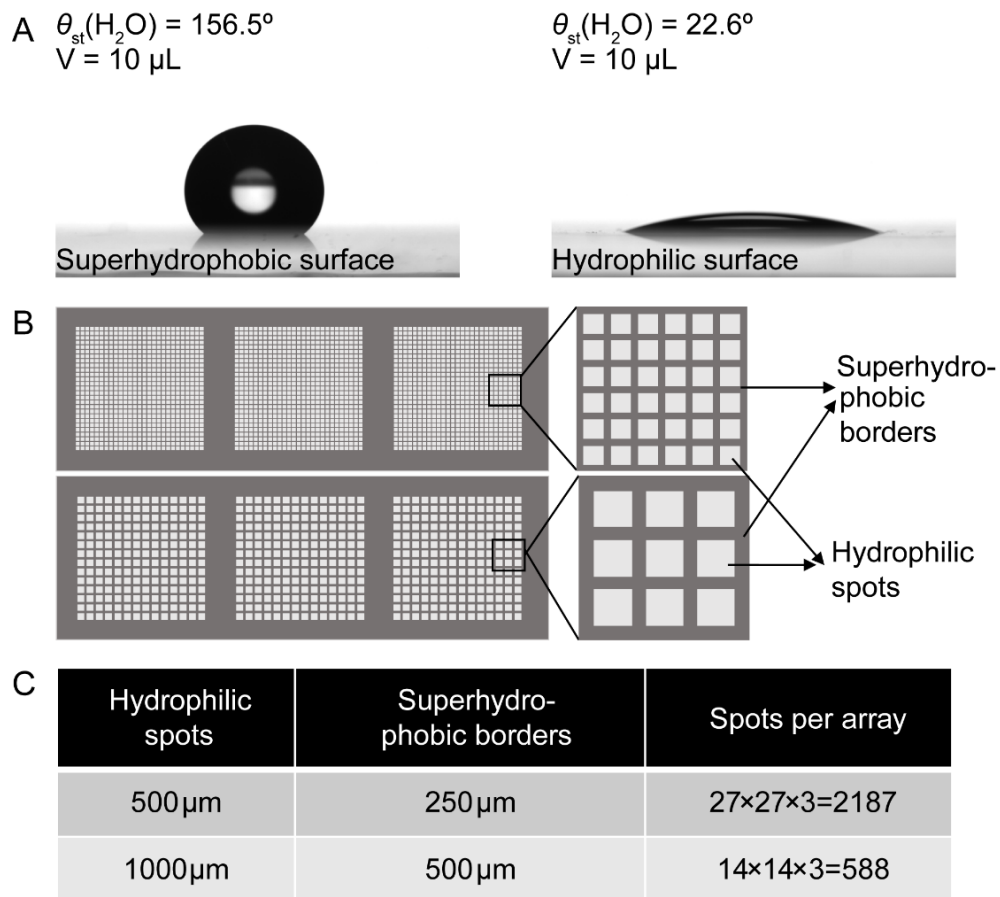
A $\theta_{st}(H_2O) = 156.5°$
   $V = 10 \mu L$

$\theta_{st}(H_2O) = 22.6°$
$V = 10 \mu L$

Superhydrophobic surface

Hydrophilic surface

B

Superhydro-phobic borders

Hydrophilic spots

C

Hydrophilic spots	Superhydro-phobic borders	Spots per array
500 μm	250 μm	27×27×3=2187
1000 μm	500 μm	14×14×3=588

Figure 10. Schematic illustration of DMA. (A) Photographs of water droplets on hydrophobic surface (static water contact angle ~ 156.5°) and hydrophilic surface (static water contact angle ~ 22.6°) with corresponding statistic water contact angles. Droplet volume: 10 μL. (B) A schematic of 500 μm and 1 mm DMA showing the superhydrophobic borders and hydrophilic spots. (C) A table showing the sizes of hydrophilic spots and corresponding superhydrophobic borders of 500 μm DMA and 1 mm DMA.
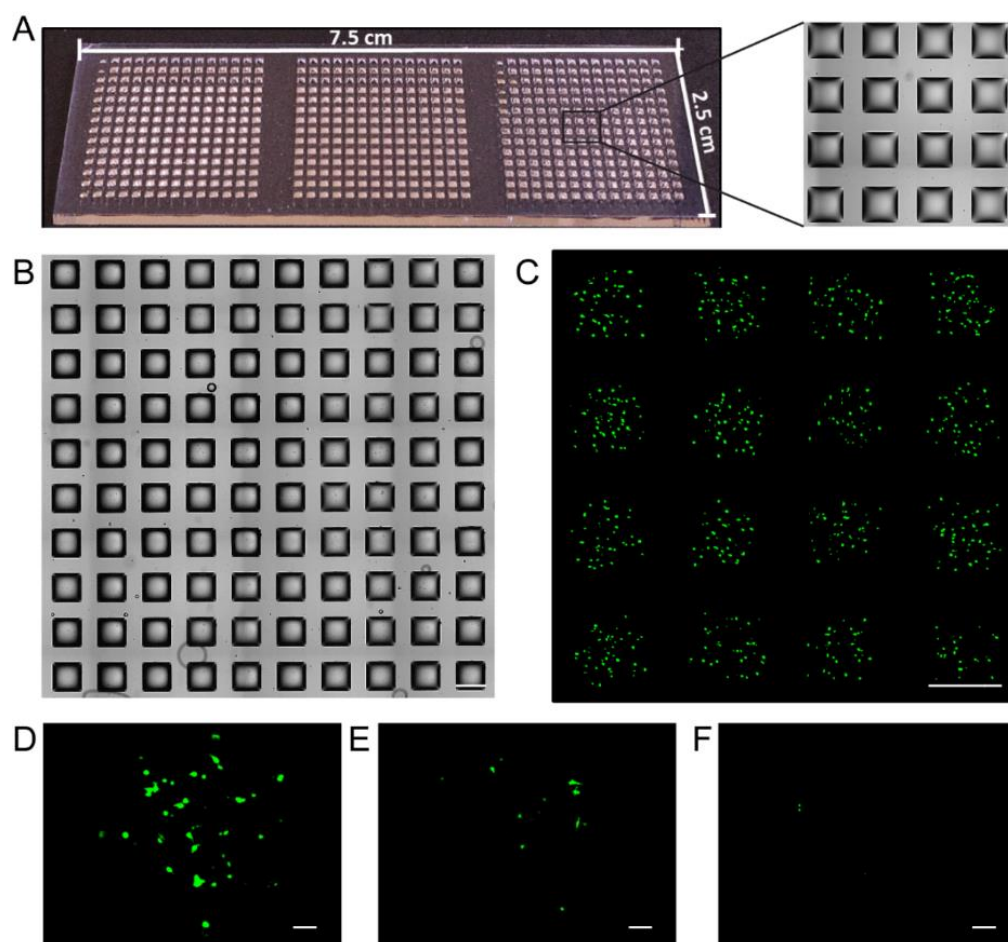
Figure 11. DMA slides and GFP plasmid DNA transfection on DMA. (A) Representative image of DMA glass slide (7.5 × 2.5 cm) patterned with 588 square spots. The side length of each square spot is 1 mm. The distance between centers of two neighboring spots is 1.5 mm. (B) DIC images showed the cells after 24 h incubation on DMA slides. Scale bar: 1 mm. (C) Representative image of GFP plasmid DNA transfection in spots of DMA after 24 h. Scale bar: 1 mm. Green fluorescence came from GFP. Fluorescent images of GFP plasmid DNA transfection results of (D) HEK293T cells, (E) CHO-K1 cells, and (F) Jurkat cells. Scale bar: 1 μm.

In order to identify compound candidates that can potentially enhance transfection efficiency and/or increase GFP expression cell numbers, I developed an HTS assay that can rapidly screen numerous compounds. As for cell systems, I chose CHO-K1, Jurkat, and HEK293T cells. CHO-K1 is one of the most important cell lines for the production of biotherapeutic protein and antibodies, but they are typically difficult to transfection (Kadlecova *et al.*, 2012; Ye *et al.*, 2010). Jurkat cells are an immortalized line of human T lymphocyte which are widely used due to their relevance to blood cells. However, they are hard to transfect due to a low proteoglycans content in their cellular membranes (Palchetti *et al.*, 2017; Riedl *et al.*, 2018; Zhao *et al.*, 2012). And HEK293T cells are a

standard cell line used by many scientists because of their propensity for transfection (Jager *et al.*, 2013).

A schematic diagram of the HTS workflow is depicted in Figure 12A and 12B. Firstly, the stock solution of 774 FDA-approved drugs were diluted to three concentrations 1, 10, and 30 µM, and then 20 nL of each drug was printed on 500 µm DMA slides with three replicates.

The remaining amount of dimethyl sulfoxide (DMSO) after drug printing was toxic for cells. To remove DMSO from the DMA and to make all the conditions the same during printing, the DMA slides were dried in a vacuum desiccator overnight. Complexes of GFP plasmid DNA and ScreenFect®A transfection reagent were prepared and then mixed with cells (Figure A 1). Then the mixture was printed into each spot and incubated with drugs at three concentrations along with a drug-free control (DMSO). And the same three controls were located at each square field inside of each slide. Besides, the outer two rows and columns were subtracted because of the edge effect. After 24 h incubation, cells were fixed, and the GFP expressed cells were imaged by an automated fluorescence microscope and the number of GFP-positive cells was quantified. Then the relative transfection enhancement was calculated as a ratio of the mean number of GFP positive cells for each drug over the mean number of GFP positive cells of drug‑free control. In order to investigate the printing procedure, cell distribution of cells after printing on three fields of DMAs were analyzed. The cells were printed and stained with Hoechst 33342 on DMA. Then the total numbers of cells in each spot were calculated by ImageJ software and further analyzed by Poisson function (Figure A 2). The primary screening was done on 500 µM DMA of 774 FDA approved drugs, and then the secondary screening of fourteen selected hits was done on 1 mm DMA. The further confirmation and validation of the screening was conducted in conventional 384- and 96-well plates.
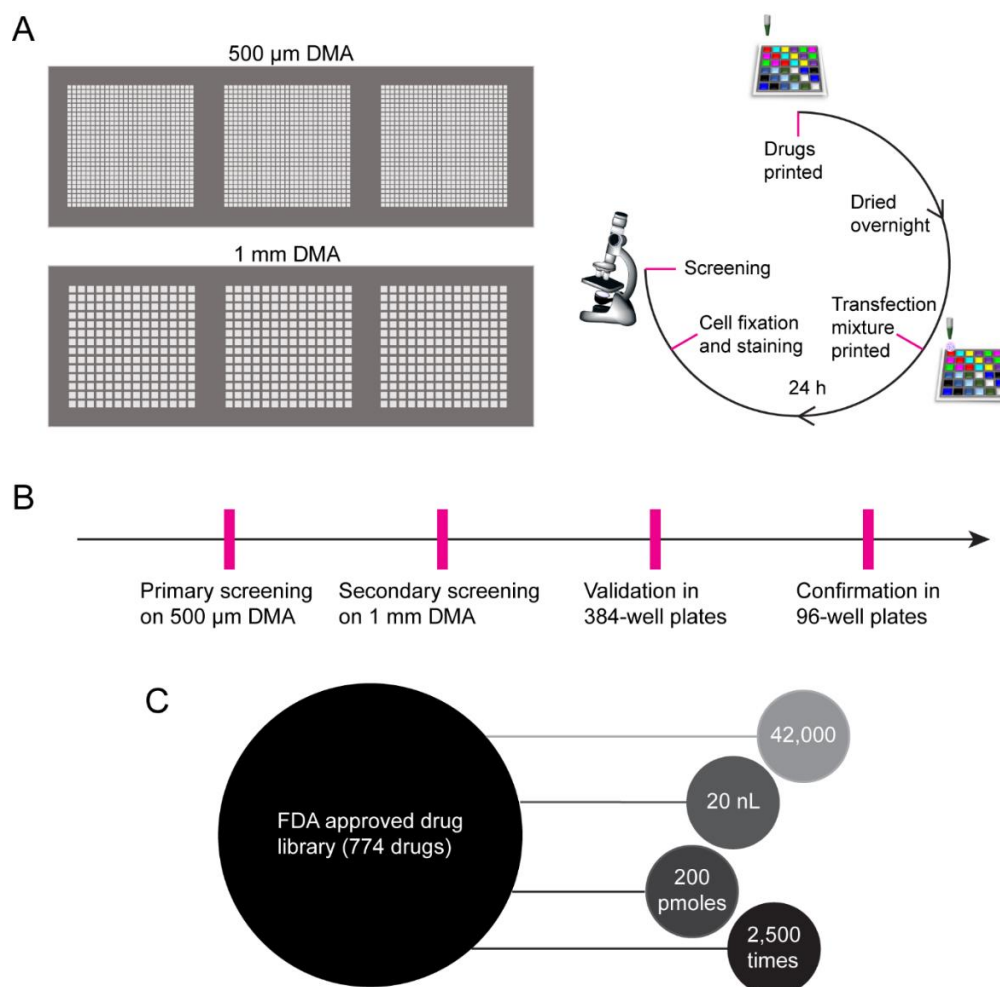
Figure 12. The workflow of *in vitro* transfection screening. (A) The illustration of 500 μm DMA and 1 mm DMA. 500 μm and 1 mm indicated the side length of square spots. There were 729 individual spots for one field on DMA slide, resulted in totally 2,187 individual spots. For 1 mm DMA, there were 588 individual spots for one field on DMA and in total 588 individual spots could be obtained. In the primary screening which were done on 500 μm DMA, 774 FDA approved drugs were printed and dried in the vacuum desiccator overnight. Cells mixed with transfection mixture (ScreenFect®A transfection reagent and GFP plasmid DNA in dilution buffer) at RT for 20 min and printed into each spot, prior to incubating for 24 h. Then cells were fixed and automated imaged by screening fluorescence microscope. Three concentrations were used for the primary screening of transfection enhancers (1, 10 and 30 μM). Fourteen 'hit' compounds were chosen from the primary screening and validated on 1 mm DMA and in 384-well plates. The experiments were done in the same way as on 500 μm DMA, except for wider ranges of drug concentrations, which were 1, 5, 10, 20, 30, and 40 μM. For the drug-free control, the transfection mixture was printed on blank DMAs. (B) Illustration of whole pipeline of the screening. The primary screening was done on 500 μm DMA and the secondary screening was done on 1 mm DMA with wider drug concentration range. Then the 'hit' compounds were further validated and confirmed in conventional 384- and 96-well plates. (C) The screening of 774-FDA approved drugs in three concentrations with three replicates resulted in a total of 41,796 individual experiments. In the primary

screening, the volume of each individual spot was 20 nL, resulted in total only 0.84 mL consumption of cell suspension and 200 pmoles of drugs, which was 2,500 times less that if the same experiment would have to be conducted in 384-well plates.

3.1.2 High-throughput screening results of transfection enhancers

Heatmaps in Figure 13 displayed the results of primary screening of CHO-K1 cells transfection. The blue cells of the heatmap represent spots with less GFP positive cells than that in the drug-free control spots (white cell), while the red color represents experiments with more GFP positive cells than that in the drug-free controls. For CHO-K1 cells, there were 425 compounds which showed transfection enhancement, while 349 compounds showed transfection decrease at the concentration of 1 μM when compared to drug-free controls. As for 10 μM, 624 compounds showed transfection enhancement while 150 compounds showed transfection decrease. At 30 μM concentration, the numbers of the transfection enhancement and transfection decrease were 233 and 541, respectively. The transfection enhancement demonstrated a concentration-dependent manner and at the concentration of 10 μM, the most drugs showed transfection enhancement compared to the concentration of 1 and 30 μM. It might be that the drugs have various influence on the cellular endocytosis, intracellular delivery and localization of the transfection complex, resulting in a different expression of GFP followed by different transfection efficiency. Furthermore, a principal component analysis (PCA) based multiobjective optimization procedure was also utilized for double verification of the screening results to get rid of false signals and for the dimensionality reduction, whose efficacy was demonstrated by solving up to 50-objective optimization problems. In the PCA score plot (Figure 13B), each number represented one drug and significantly different behaviors of transfection under different drugs can be observed. The GFP expressed cell numbers vary in the presence of drugs, resulted in drugs that were distinct from the transfection under control conditions. The outliers (hit compounds) got from the PCA analysis are almost the same as identified using the above algorithm.
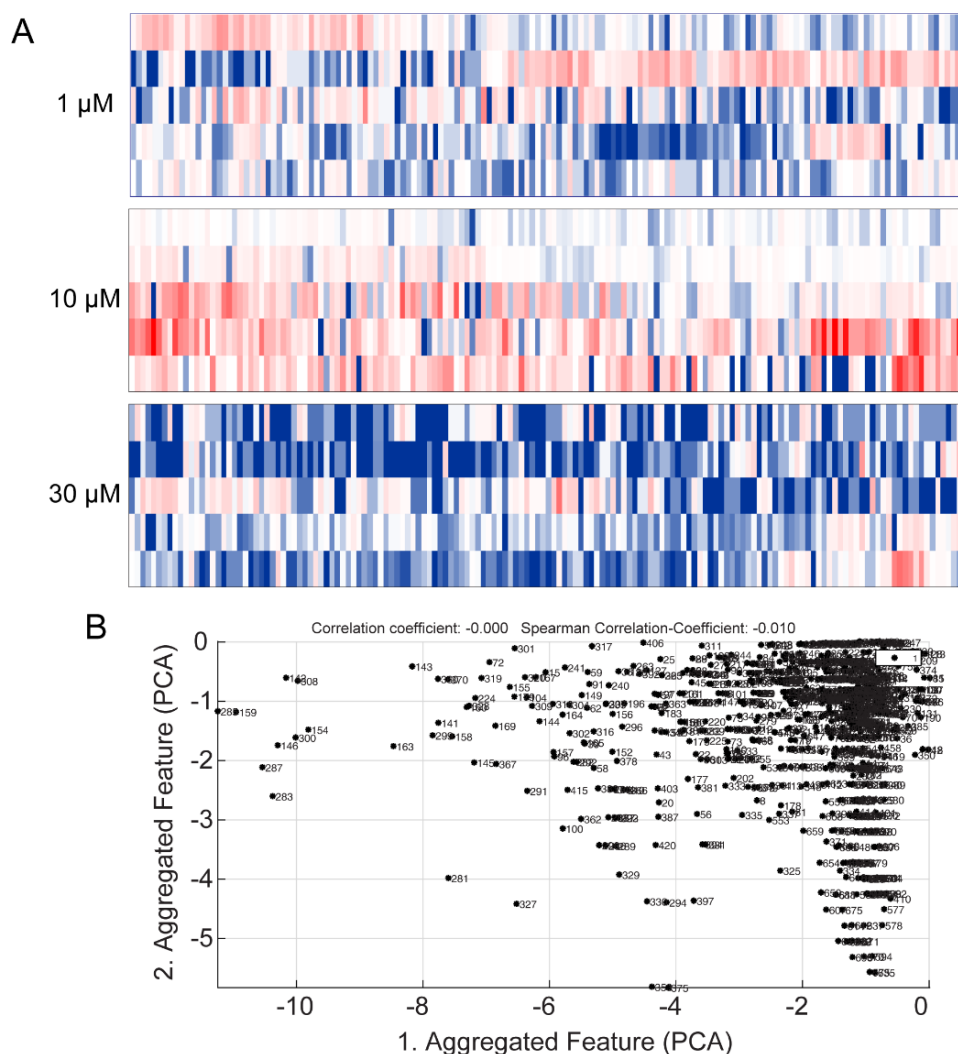
Figure 13. Impact of FDA-approved drugs on transfection efficiency of CHO-K1 cells. (A) Heatmaps showed the impact of FDA-approved drugs on CHO-K1 cells at three concentrations (1, 10, and 30 μM). The heatmaps were generated according to the quantified relative transfection efficiency data, which was obtained from in total 20,898 individual experiments (three technical repeats and three biological repeats). The three heatmaps were sorted altogether by enhancement level of gene transfection compared to positive (drug-free) control. The blue patch and red patch represented a decrease and increase compared to drug-free control (white patch at the upper left corner), respectively. (B) Principal component analysis (PCA) graph showed overview of impact of FDA-approved drugs on transfection efficiency of CHO-K1 cells. Numbers accompanied with each dot represented drugs in the FDA-approved library.

Primary hits (hit compounds) were identified as drugs that increased the number of GFP positive cells in comparison to the drug‑free mean by at least three standard deviations. Thus, at 1 μM concentration, 19 hits were identified, as well as 78 hits at 10 μM concentration and 18 hits at 30 μM concentration (Figure 14). Seven compounds (auranofin, captopril, carbidopa, oxacillin sodium salt monohydrate, oxiconazole

nitrate, piroxicam, and tranylcypromine hemisulfate) showed repeatable transfection enhancement at different concentrations. There are more hits at 10 μM than at 1 μM, it might be the stimuli from the drugs at low concentration increases the cell division activity which could lead to the negative results. There are more hits at 10 μM concentration than at 30 μM, which can be explained by increased toxicity at the highest concentration used and, thus lower overall cell number per experiment.

The same primary screening was also conducted with Jurkat human T‑cell lymphocyte cells, which has traditionally proven to be very difficult to transfect due to a low proteoglycans content in the cellular membranes and a reduced attachment of the transfection complex to the surface of cells (Basiouni *et al.*, 2012; Riedl *et al.*, 2018). The results of the primary screening of Jurkat cells showed significantly less positive hits in comparison to the transfection of CHO‑K1 cells (Figure A 3 and Table A 1). For Jurkat cells, there were 244 compounds which showed transfection enhancement while 530 compounds showed transfection decrease at the concentration of 1 μM when compared to the drug‑free controls. As for 10 μM, 325 compounds showed transfection enhancement while 449 compounds showed transfection decrease. At 30 μM, the numbers of the transfection enhancement and transfection decrease were 192 and 582, respectively. Due to the difficult transfection characteristic of Jurkat cells, less transfection enhancement compounds could be found compared to CHO‑K1 cells. When the threshold of the primary screening was set as mean + 3SD, no hits were identified at 1 μM concentration. But 2 hits at 10 μM concentration and 1 hit at 30 μM concentration were identified. The higher overall transfected cell number demonstrates six‑to eight-fold relative transfection enhancement of the two hits compared to the drug‑free controls in the primary screening.
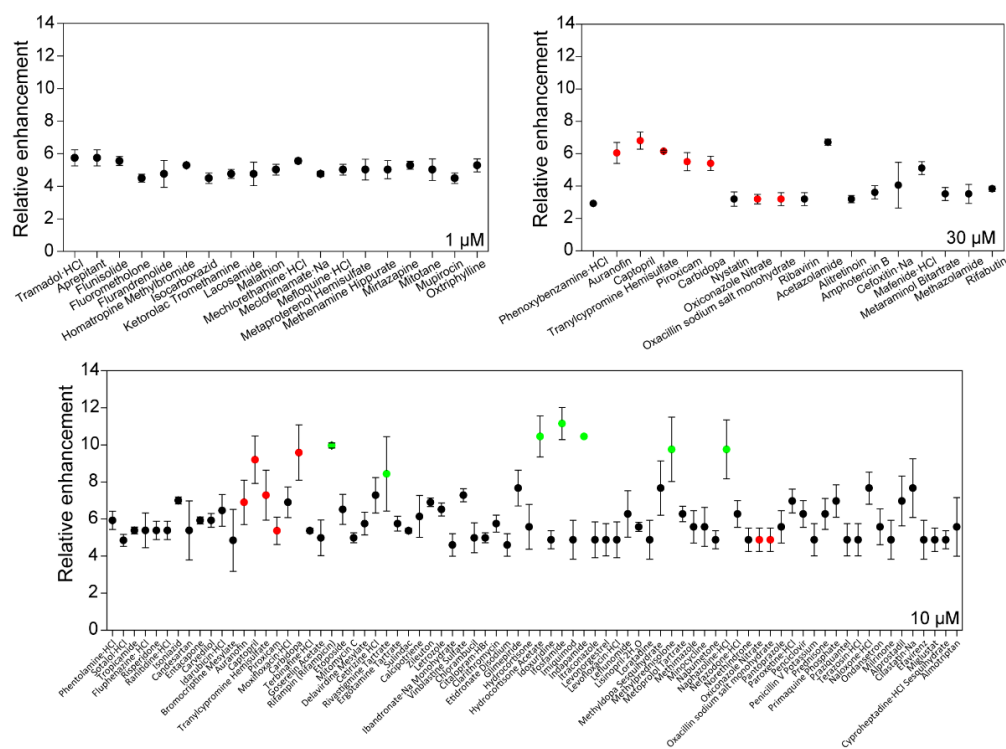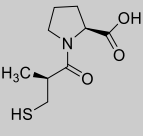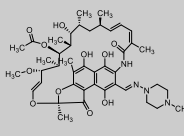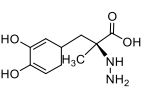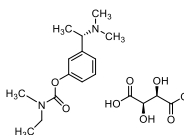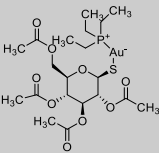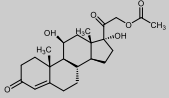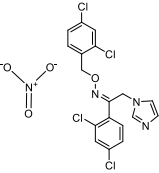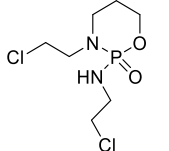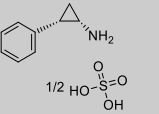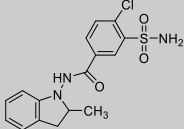
Figure 14. Hit compounds identified as transfection enhancers in the primary screening of CHO-K1 cells. The scatter graph in the upper left panel showed the 19 out of 774 drugs in the FDA-approved drug library at 1 μM concentration as transfection enhancer for in vitro CHO-K1 cells transfection. The scatter graphs in the lower panel and upper right panel displayed 78 hit compounds and 18 hit compounds out of 774 drugs in the FDA-approved drug library at 10 and 30 μM concentrations as transfection enhancers, respectively. The red dots in the scatter graph indicated the compounds (auranofin, captopril, tranylcypromine hemisulfate, piroxicam, carbidopa, oxacillin sodium salt mon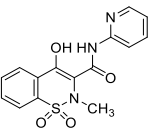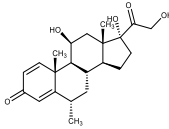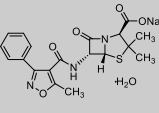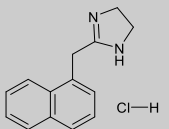ohydrate, and oxiconazole nitrate) which showed repeatable positive enhancement at different concentrations and the green dots in the scatter graph indicated the compounds (rifampin, rivastigmine tartrate, hydrocortisone acetate, ifosfamide, indapamide, methylprednisolone, and naphazoline·HCl) which showed strong enhancement effect at one concentration. Data were presented as mean ± SD of three biological experiments with three technical repeats each time.

In the primary screening, I assumed that the numbers of cells printed onto each individual spot are the same. Nevertheless, cells precipitate during printing due to the printing pressure and gravity, resulting in the variability of cell numbers among spots (Figure A 2). For this reason, the hits from primary screening were further validated. Fourteen hit compounds that showed a strong enhancement effect at one concentration or showed repeatable positive enhancement at different concentrations were selected for the secondary screening to validate the observed effects (Figure A 4 and Table 15). The validation experiment was performed on 1 mm DMA at concentrations ranging from 1 to 40 μM. To further test whether the transfection hit compounds contribute to

transfection efficiency enhancement, I introduced HEK293T, a well-known easy to transfect cell type (Wu *et al.*, 2002), to test the hits from the primary screening as well. ach drug was evaluated by three parameters: 1) number of GFP expressing cells, 2) dead cell number (stained by PI), and 3) total cell numbers (stained by Hoechst 33 342). The transfection efficiency and cell viability of influence of each drug on CHO-K1 cells transfection were displayed in Figure 15. The secondary screening showed obvious and reproducible dose-dependent effects of the drugs on transfection efficiency of CHO-K1 cells. Transfection efficiencies increased between 1.8-fold to 5.1-fold compared to drug-free control. However, 12 out of 14 hit compounds showed considerable transfection efficiency at higher drug concentrations (30 and 40 μM) due to the high toxicity towards cells. In the case of piroxicam and tranylcypromine hemisulfate, the transfection enhancement was observed even at higher concentrations. Some drugs (ifosfamide, methylprednisolone, and oxacillin sodium salt monohydrate) showed the same trend in the primary screening and the secondary screening. All fourteen compounds also demonstrated a dose-dependent negative effect on cell viability of CHO-K1 cells. The hit compounds validation on Jurkat cells (Figure A 5) and HEK293T cells (Figure A 6) were also conducted. The results of HEK293T that is a well-known easy to cultivate and transfer cell type, showed the same transfection enhancement trend as CHO-K1 cells with higher transfection efficiency (increasing between 1.2-fold and 3.5-fold when compared to drug-free control). In the case of Jurkat cells, no significant transfection enhancement was observed at all concentrations tested, probably due to the overall too low transfection efficiency.

Table 15. Fourteen hit compounds selected from the primary screening for secondary screening

Compound	Therapeutic effect	Structure	Compound	Therapeutic effect	Structure
Captopril	Inhibitor of angiotensin converting enzyme (ACE)		Rifampin (Rifampicin)	Inhibitor of DNA-dependent RNA polymerase	
Carbidopa	Inhibitor of DOPA decarboxylase		Rivastigmine tartrate	Inhibitor of parasympathomi metic and cholinesterase	

Auranofin	Inhibitor of kappaB kinase and thioredoxin reductase		Hydrocortisone acetate	Anti-inflammatory or immune-suppressive drug	
Oxiconazole nitrate	Antibiotic used in resistant staphylococci infections		Ifosfamide	Alkylating agent and immune-suppressive agent	
Tranylcypromine hemisulfate	Inhibitor of monoamine oxidase (MAO)		Indapamide	Antihypertensive and diuretic agent	
Piroxicam	Nonsteroidal Antiinflammatory agent (NSAID)		Methylprednisolone	Anti-inflammatory and immune-suppressive agent	
Oxacillin sodium salt monohydrate	Penicillin beta-lactam antibiotic		Naphazoline·HCl	Sympathomimetic alpha adrenergic agonist	

76
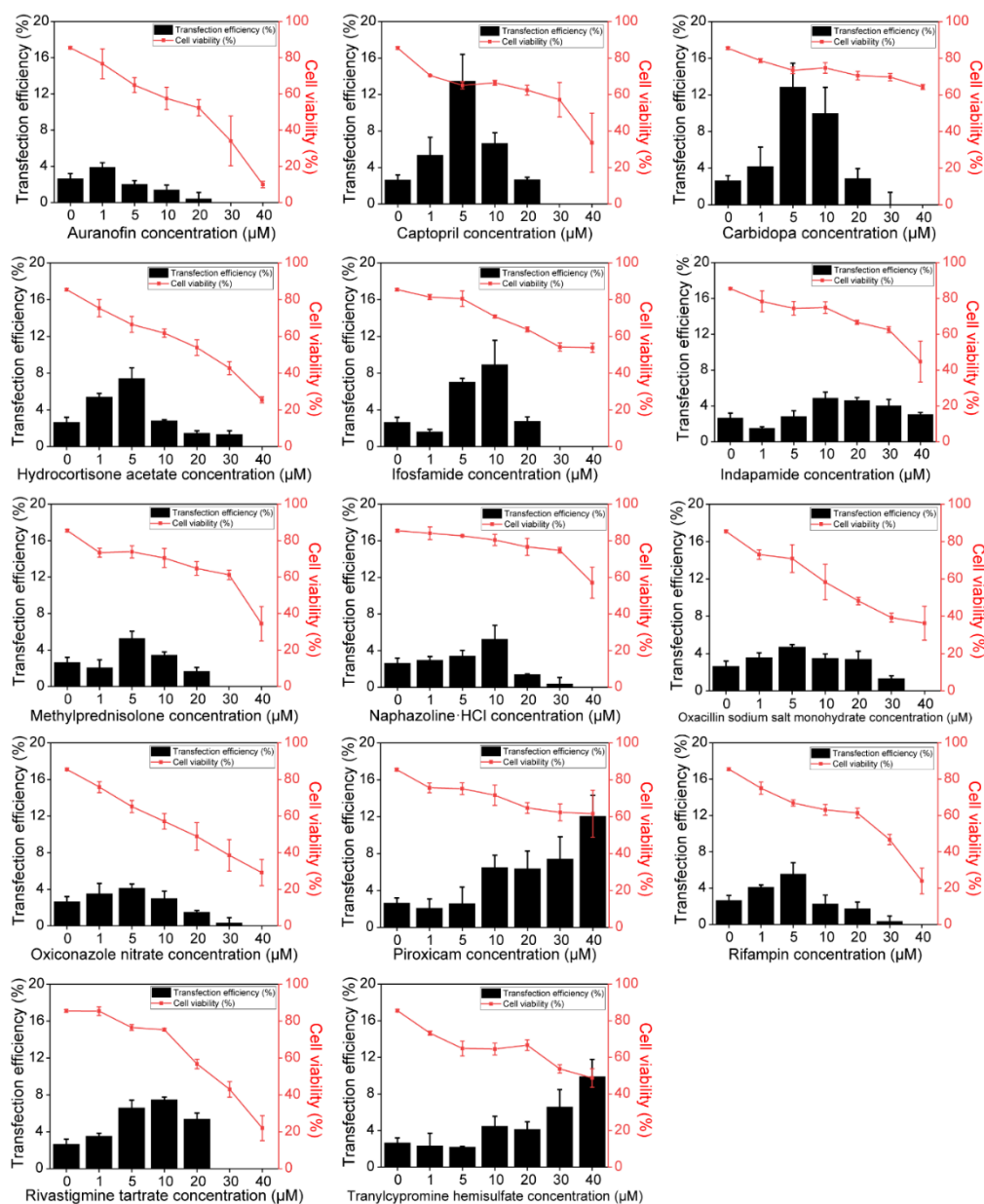
Figure 15. Secondary screening results of impact of fourteen hit compounds on CHO-K1 cells transfection efficiency. Fourteen hit compounds (auranofin, captopril, carbidopa, hydrocortisone acetate, ifosfamide, indapamide, oxacillin sodium salt monohydrate, methylprednisolone, naphazoline·HCl, rifampin, oxiconazole nitrate, piroxicam, tranylcypromine hemisulfate, and rivastigmine tartrate) were printed onto 1 mm DMA and dried in vacuum desiccator overnight. Then 100 nL transfection mixture (transfection reagent, GFP plasmid DNA and CHO-K1 cells) were printed and incubated at 37 °C for 24 h before quantification. The final treatment concentrations of each compound were set as 0, 1, 5, 10, 20, 30, and 40 μM. Cells were then stained with 10 μg/mL Hoechst 33342 and 0.67 μg/mL PI to visualize all cell nuclei and dead cells, respectively. The GFP expressing cell numbers, PI positive cell numbers and Hoechst positive cell numbers were counted by ImageJ software. Cell viability was calculated as the following equation: cell viability (%) = 1 − (PI‑positive cell numbers/Hoechst positive cell numbers) × 100. The transfection efficiency was calculated as the

following equation: transfection efficiency (%) = (GFP positive cell numbers/Hoechst positive cell numbers) × 100.

3.1.3 Validation of hit compounds from screening

In order to further validate the obtained results, I compared the transfection efficiency of hits at their most effective concentrations on DMA (Table A 2) on both DMA slides and conventional 384-well plates of CHO-K1 cells (Figure 16) and HEK293T cells (Figure A 7). In general, the transfection efficiency of the individual wells in 384-well plates was less variable than that on the individual spots on DMA, which could be attributed to the 11.35-fold less cells in each droplet of the DMA in comparison with the plate format (100 nL volume with 100 cells per spot vs 20 µL volume with 1135 cells per well). The average transfection efficiency showed no significant differences between the two platforms, which confirmed validity of the results from the primary and secondary screening and the possibility to translate obtained results into larger, more commonly used formats, such as microtiter plates.
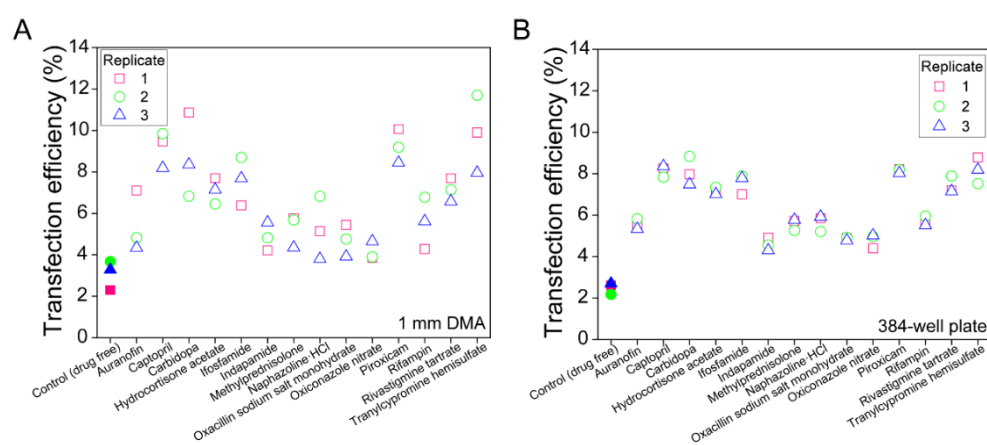
Figure 16. Fourteen hit compounds transfection enhancement comparison on two platforms. The impact fourteen compounds under the most effective concentration for CHO-K1 cells transfection on (A) 1 mm DMA slide and (B) 384-well plates. Experiments were done with three replicates on two platforms. Transfection efficiency in every spot on DMA or well in well plates were displayed separately. The three different shapes demonstrated three individual replicates (replicate 1-square, replicate 2-circle, and replicate 3-triangle). The most effective concentration of each compound was used (Table A2).

DMA and conventional microtiter plates are two different *in vitro* cell culture systems in terms of the cell cultivation and experiment parameters, which might be

diverse due to the discrepancy in formats, edge‑effects, evaporation, and area to volume ratio. The transfection parameters are also supposed to be different. Therefore, I selected four hits (hydrocortisone acetate, naphazoline·HCl, oxacillin sodium salt monohydrate, and piroxicam) after validation and further evaluated the transfection efficiency in an optimal condition of transfection in 96‑well plates. First, the transfection optimization in the presence or absence of the drugs was conducted (Figure A 8A-E) using transfection reagent amounts from 0.1 to 0.4 µL/96‑well plate well and from 50 to 100 ng per well of plasmid DNA. As shown in Figure A 8, the highest transfection efficiency was achieved at 0.4 µL transfection reagent with 100 ng DNA per well with or without the drugs. Thus, these conditions were chosen for the following experiments. The transfection efficiency and cell viability were evaluated with these four drugs and compared with the drug‑free control. As shown in Figure A 8F, naphazoline·HCl, oxacillin sodium salt monohydrate, and piroxicam could increase the transfection efficiency from 30.3% ± 1.6% (drug‑free control) to 36.3% ± 0.9%, 38.8% ± 1.1%, 33.9% ± 1.2%, respectively. It should be noted that the mechanisms behind the increase of transfection efficiency caused by these molecules are still unknown and need further investigation. The transfection enhancement may be caused by the influence of these drugs on the expression of particular genes involved in the cellular uptake processes, endosomal escape, or other mechanisms (Lehmann *et al.*, 1997; Yoshimura & Oka, 1990). The results of this study demonstrate the great potential of the DMA platform in miniaturized high‑throughput screenings of small molecules such as drugs, high‑throughput cell transfection experiments, and search for new biologically active molecules.

Biological development has shifted toward identifying leads that most effectively fulfill the therapeutic and experimental request in a miniaturized and automated way. The development demands the ability to rapidly screen numerous molecules in parallel at micro- and nanoscale volumes. The significant screening results can expand the diversity of these molecules and consequently improve the prospect of selected molecules with the desired characteristics. With the aim of improving transfection efficiency, I selected pharmacological priming as a rapid strategy to achieve this goal. Pharmacological priming (drug repurposing) is a pharmacological modulation of

transfection efficiency, in which the cells were treated with chemical compounds before, during, or after mixing with the transfection mixture in order to improve some aspects of gene transfection process. Except for the pharmacological priming, adding small molecule compounds to the cell culture media is the other possibly simple and effective method to improve transfection efficiency. However, in order to identify such transfection-enhancing molecules, thousands of small molecules must be tested. Current high-throughput screening (HTS) technologies based on microtiter plates cannot be used in such screenings due to prohibitively high costs associated with large volumes of reagent and the man-power required.

The main idea of the screening was established by comparing cells treated with biologically active compounds, versus untreated but transfected cells, where the GFP expression was different between each condition in CHO-K1, Jurkat, and HEK293T cells. Our study indicated that compounds from diverse drug indications could be screened for transfection enhancers in the context investigating biological mechanisms of transfection. By exposing to biological active compounds to enhance non-viral transfection, the genomic targets might be modulated in the cell processes involved in transfection, including mitochondrial dysfunction, oxidative stress, cell division, cell cycle, and cell death. It indicates that apart from overcoming the primary barriers to transfection, overall cellular response or process need to be modulated to achieve higher transfection efficiency and more sustained gene expression.

3.2 Miniaturized droplet microarray platform enables maintenance of human induced pluripotent stem cell pluripotency

3.2.1 DMAs for culture of hiPSCs

DMAs consist of an array of hydrophilic spots (1-mm side length) on a superhydrophobic background (Figure 17). In this study, I optimized and adapted the DMA platform for culturing and screening hiPSC in 200-nL droplets. To fully characterize the phenotype and behavior of hiPSC cultured on the DMA platform, I investigated the morphology, viability and pluripotency of cells cultured on TA and TB DMAs (Figure 17). To distinguish the influence of surface properties and small nanoliter volumes on these characteristics, I investigated and compared the phenotypes of hiPSCs cultured on a large area (2.5 cm × 7.5 cm) of hydrophilic surface covered with 2 mL of culture media (TA and TB surfaces) and in confined 200-nL droplets formed on these two surfaces (TA and TB DMAs). Both TA and TB DMAs were prepared on a standard microscope glass slide by introducing superhydrophobic borders on TA and TB surfaces. Since hiPSCs are known to be sensitive to surface cues, such as hydrophilicity, topography, and roughness, I first characterized the two types of surfaces (Cui *et al.*, 2020; Ross *et al.*, 2012).
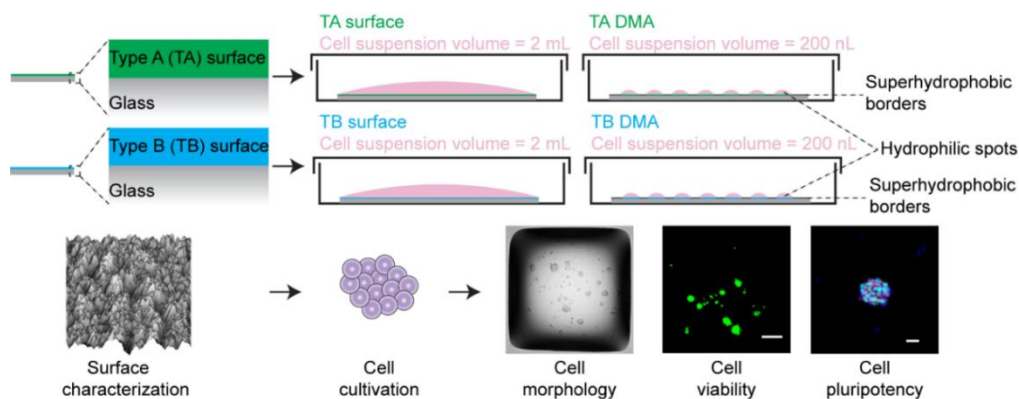
Figure 17. Schematic representation of the investigated substrates and overview of the studies. Illustration of TA and TB surfaces and their corresponding DMAs (TA DMA and TB DMA) containing superhydrophobic borders and hydrophilic spots (1-mm side length). The two surfaces were characterized. The hiPSCs were seeded and cultivated on TA and TB surfaces in 2 mL cell culture medium and on TA and TB DMAs in 200 nL cell culture medium droplets confined to square hydrophilic

spots (1-mm side length). Morphology, viability, and pluripotency of hiPSCs cultured on TA and TB surfaces, as well as TA and TB DMAs, were investigated.

3.2.2 Surface characterization

Two types of surfaces were characterized by water contact angle (WCA) goniometry, energy-dispersive X-ray spectroscopy (EDX), scanning electron microscopy (SEM), atomic force microscopy (AFM), and X-ray photoelectron spectroscopy (XPS). The hydrophilic areas of the TA and TB surfaces exhibited similarly low water contact angles of $15.5° \pm 2.0°$ and $14.1° \pm 0.1°$, respectively, thus confirming the hydrophilic properties of the surfaces (Figure 18A). EDX spectra showed the following elements present on the hydrophilic surfaces (Figure 18B): a sulfur (S) peak was uniquely detected on the TA surface and a fluorine (F) peak was uniquely detected on the TB surface, whereas neither of the surfaces showed any additional characteristic elements apart from those of glass (e.g. Si, O, Na, Mg, and K). The surface morphology and roughness were characterized by SEM and AFM (Figure 18C and 18D). Both the TA and TB surfaces exhibited a homogenously rough morphology at the nanoscale. Surface roughness (R_a) determined from the AFM height profiles further confirmed the topological similarity of the TA and TB surfaces (60 nm $\pm$ 19 nm and 57 nm $\pm$ 15 nm, respectively: n = 3). XPS was employed to investigate the surface chemistry in more detail. The survey scan XPS spectra displayed the differences in the chemical elements of the TA and TB surfaces (Figure 18E and 18F). For the survey scan of the TA surface, only C, Si, and O were detected, although the presence of sulfur was confirmed by the occurrence of a characteristic S 2p doublet at 163.3 eV in the narrow scan. A shoulder leaning to higher energies (approximately 286 eV) in the C 1s narrow scan indicated the presence of C-O species on the TA surface, as expected for adventitious carbon (Figure 18E). A fluorine peak was observed in survey scan XPS spectra of the TB surface (Figure 18F). A C 1s scan of the TB surface then revealed binding energies at 293.6 and 291.3 eV, which are indicative of $-CF_3$ and $-CH_2$ bonds, respectively. A shoulder toward higher energies (approximately 286 eV) might stem from oxidized carbon species or adventitious carbon. In the narrow scan of F 1s, a peak at 688.7 eV was detected, which is characteristic of organic fluoro-compounds. The Si 2p and O 1s narrow scans of both the TA and TB surfaces were practically identical and indicative of the silicon dioxide present in the coating (Figure A 9A and A 9C). To ensure

reproducibility and homogeneity of the surface functionalization, three high-resolution scans were conducted on different spots of the surfaces (Figure A 9B and A 9D). To trace sulfur, 10 scans were conducted without scanning other energies (except for a C 1s scan as a reference) to avoid photochemical destruction of sulfur-carbon bonds (Figure A 9B). In conclusion, both the TA and TB surfaces possessed almost identical characteristics in terms of hydrophilicity and morphology, but differed in their chemical environment.

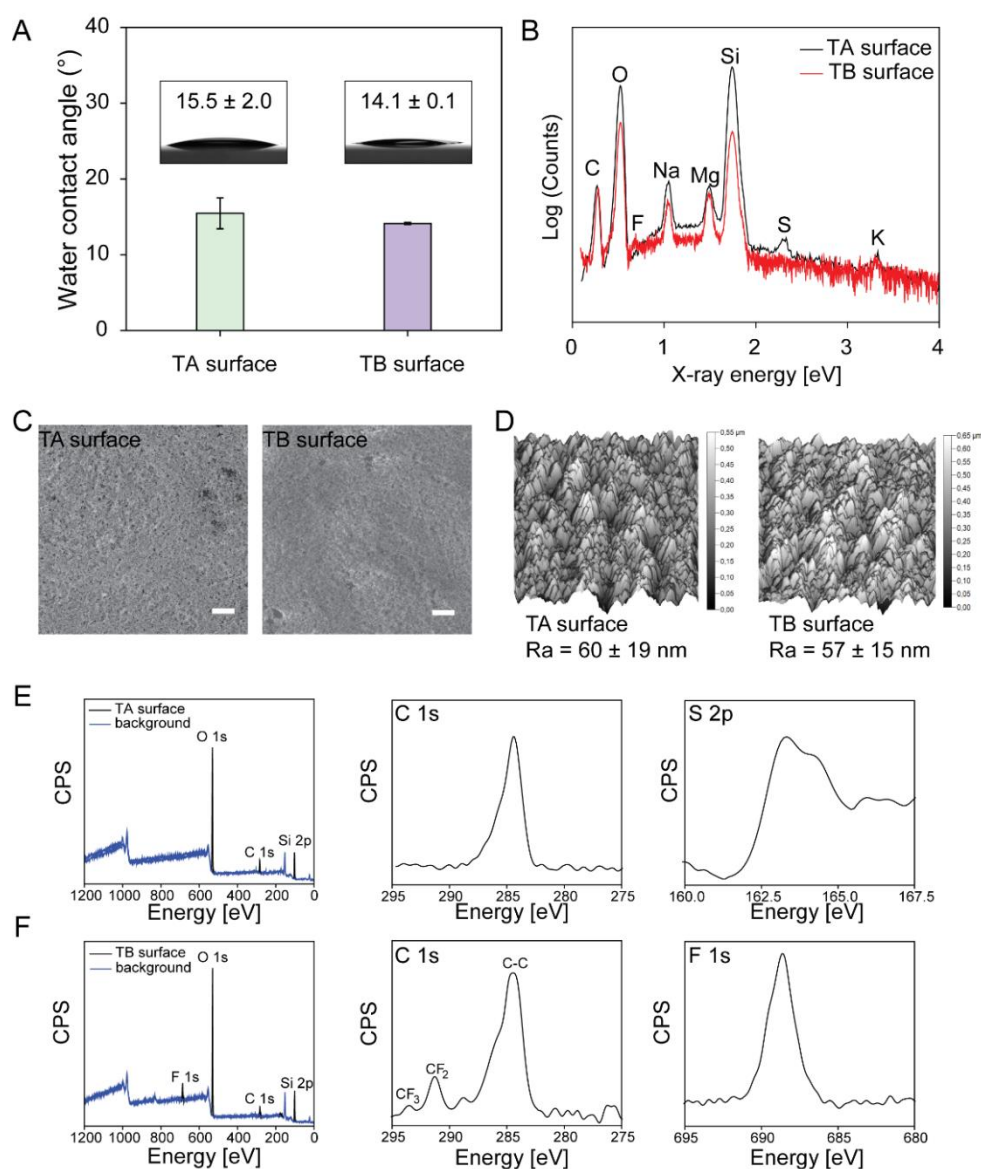**Figure 18. Characterization of TA and TB surfaces**. (A) Water contact angles of the TA and TB surfaces measured with 8 μL water droplets under ambient conditions (25 °C). Data represent the mean ± standard deviation (n = 3 replicates). (B) EDX (energy-dispersive X-ray) spectra of the TA and TB surfaces. The surfaces were coated with carbon to ensure conductivity. A sulfur peak and a fluorine peak

were observed on the TA surface and TB surface, respectively. The surface topography was characterized by (C) scanning electron microscopy (SEM) and (D) atomic force microscopy (AFM). Surface roughness (R_a) was determined from the AFM height profiles (n = 3). (E) Survey scan X-ray photoelectron spectroscopy (XPS) spectra of the TA surface, and XPS spectra of C 1s and S 2p on the TA surface. (F) Survey scan XPS spectra of the TB surface, and XPS spectra of C 1s and F 1s on the TB surface. Scale bar: 2 μm.

3.2.3 Culturing and characterization of hiPSCs on TA and TB DMA

HiPSCs are commonly maintained in different culturing vessels, including flasks, petri dishes and multi-well plates, in volumes ranging from one to dozens of mL on a MG layer. MG promotes the attachment and proliferation of hiPSCs *in vitro*. In this study, I investigated the feasibility of culturing hiPSC in 200-nL droplets on DMAs coated with (MG$^+$) and without (MG$^-$) Matrigel (1% v/v) while preserving all important characteristics of these cells such as morphology, viability and the most important factor – pluripotency.

HiPSCs are very sensitive to environmental stresses, such as compression and shear, which can occur during dispensing of cells and cause dissociation-induced cell death (Goetzke *et al.*, 2018; Ohgushi *et al.*, 2010). Therefore, I first compared the viability of hiPSCs dispensed onto DMAs using different printing settings, such as the pressure applied during dispensing of cells and reagents with the non-contact low volume dispenser used in this study (Figure 19). A live/dead staining method was used to assess the viability of hiPSCs on MG$^-$ TA DMA and MG$^-$ TB DMA after dispensing with distinct printing pressures of 75, 150, and 300 mbar·ms after 24 h of culture. For this, a solution containing calcein AM (0.5 μg/mL) and propidium iodide (PI, 0.5 μg/mL) was dispensed directly onto the droplets containing cells to stain and dead cells, respectively. Cell viability was calculated as the ratio of the calcein AM-positive area to the sum of the calcein AM- and PI-positive areas. The viability of cells cultured for 24 h and dispensed under pressures of 150 and 300 mbar·ms was comparable, while the viability of cells dispensed under 75 mbar·ms was approximately 28% lower. This might be because single cells are more commonly dispensed than aggregates of cells under lower printing pressure, and single hiPSCs are more prone to cell death. The viabilities of hiPSCs cultured on TA DMA for 24 h were 43.74% ± 9.90%, 70.73% ± 6.25% and 72.52% ± 7.51% for printing pressure of 75, 150 and 300 mbar·ms,

respectively (Figure 19A and 19B). The viabilities of cells cultured on TB DMA under these three conditions were 40.50% ± 9.47%, 70.43% ± 6.91%, and 71.70% ± 7.63%, respectively (Figure 19C and 19D). There were no significant differences in the viability of hiPSCs cultivated on MG⁻ TA and MG⁻ TB DMAs under the same conditions. These observations suggest that the DMA printing pressure has an impact on viability of hiPSCs. Therefore, I used a printing pressure of 150 mbar·ms and cultivation time of 24 h for all further experiments.
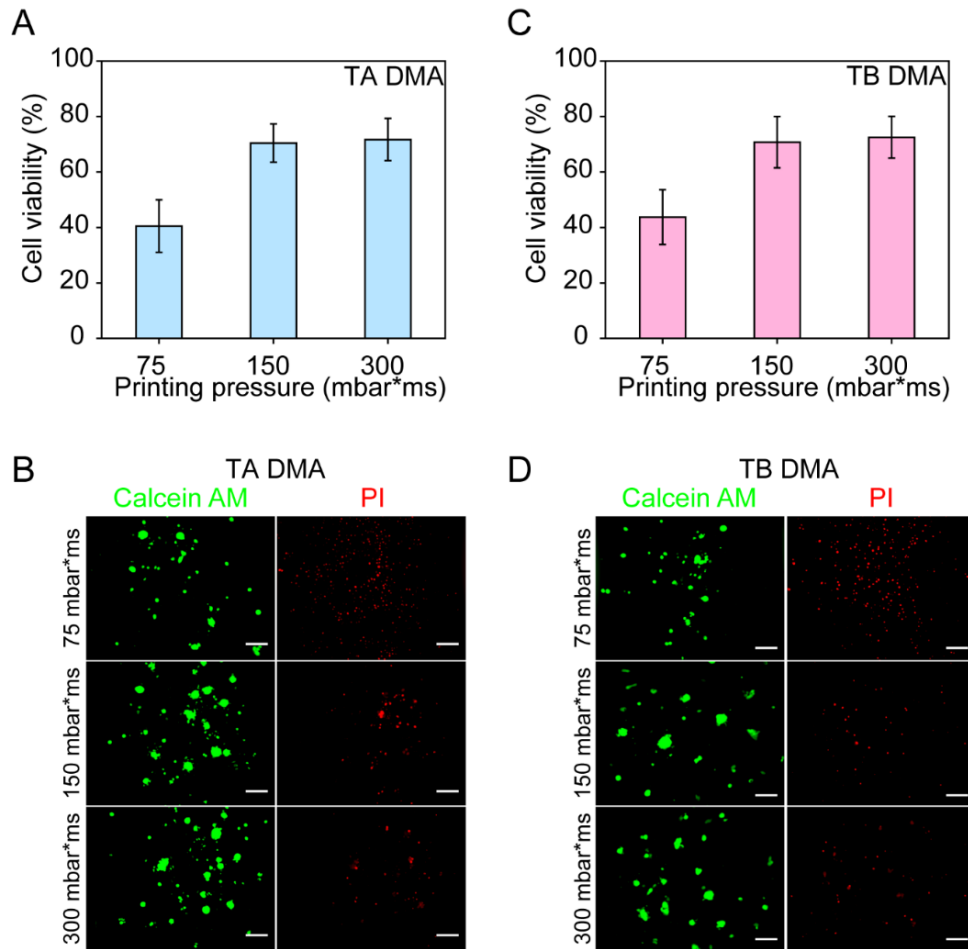
Figure 19. Comparison of viability of hiPSCs on TA DMA and TB DMA with different printing pressures. HiPSCs were cultured in mTeSR plus medium for several passages prior to being detached by ReLeSR™ and printed into DMA spots. In each individual spot, 200 nL of hiPSCs cell suspension was printed. After 24 h of culture, calcein AM and PI were then printed for live/dead staining. The cell viability was calculated as the ratio of the calcein AM-positive area to the sum of the calcein AM- and PI-positive areas. (A) The viability of hiPSCs printed on TA DMA under pressures of 75, 150, and 300 mbar·ms and cultured for 24 h (n = 3 biological replicates). (B) Representative fluorescence images of hiPSCs seeded onto TA DMA under 75, 150, and 300 mbar·ms printing pressure and cultured for 24 h. (C) The viability of hiPSCs printed onto TB DMA under pressures of 75, 150, and 300 mbar·ms and

cultured for 24 h (n = 3 biological replicates). (D) Representative fluorescence images of hiPSCs seeded onto TB DMA under 75, 150, and 300 mbar·ms printing pressure and cultured for 24 h. Data represent the mean ± SD. Scale bar: 100 μm.

HiPSC cultured *in vitro* typically grow in tightly packed colonies, which distinguishes them from somatic cells (Kato *et al.*, 2016; Singh *et al.*, 2013). Therefore, the morphology of hiPSC colonies is considered to be an important factor that indicates the pluripotency hiPSCs *in vitro*. HiPSCs cultured *in vitro* are usually passaged as multi-cellular clusters since single cells are more prone to cell death whereas colonies are quickly re-established by cell clusters (Liu *et al.*, 2019). I investigated the morphology of hiPSCs cultivated on MG^+ and MG^- TA DMA and MG^- TB DMAs (Figure 20A and 20B). HiPSCs exhibited typical morphology of tightly compacted, well-defined colonies consisting of round cells with large nuclei and a high nucleo-cytoplasmic ratio on both MG^+ and MG^- DMAs (Figure 20A and 20B) (Courtot *et al.*, 2014; Kato *et al.*, 2016). These observations indicated the feasibility of utilizing the DMA platform for hiPSC culture. The morphology of hiPSCs grown on surfaces (MG^+ 2 mL, MG^- TA 2 mL, and MG^- TB 2 mL) were also investigated (Figure A 11). Bright field images of 10 spots were acquired in three independent experiments (Figure A 12 and A 13). I compared the viability of hiPSCs on MG^+ and MG^- TA DMA and MG^- TB DMA after 24 h of culture. The viability of hiPSCs ranged from 70% to 76% (Figure 20C and 20E) and live hiPSCs were abundant on DMAs (Figure 20D and 20F Our results showed that there were no significant differences in the viability of hiPSCs cultured on both MG^+ and MG^- DMAs, which indicated that MG coating is not crucial for culturing hiPSCs on DMAs for 24 h.
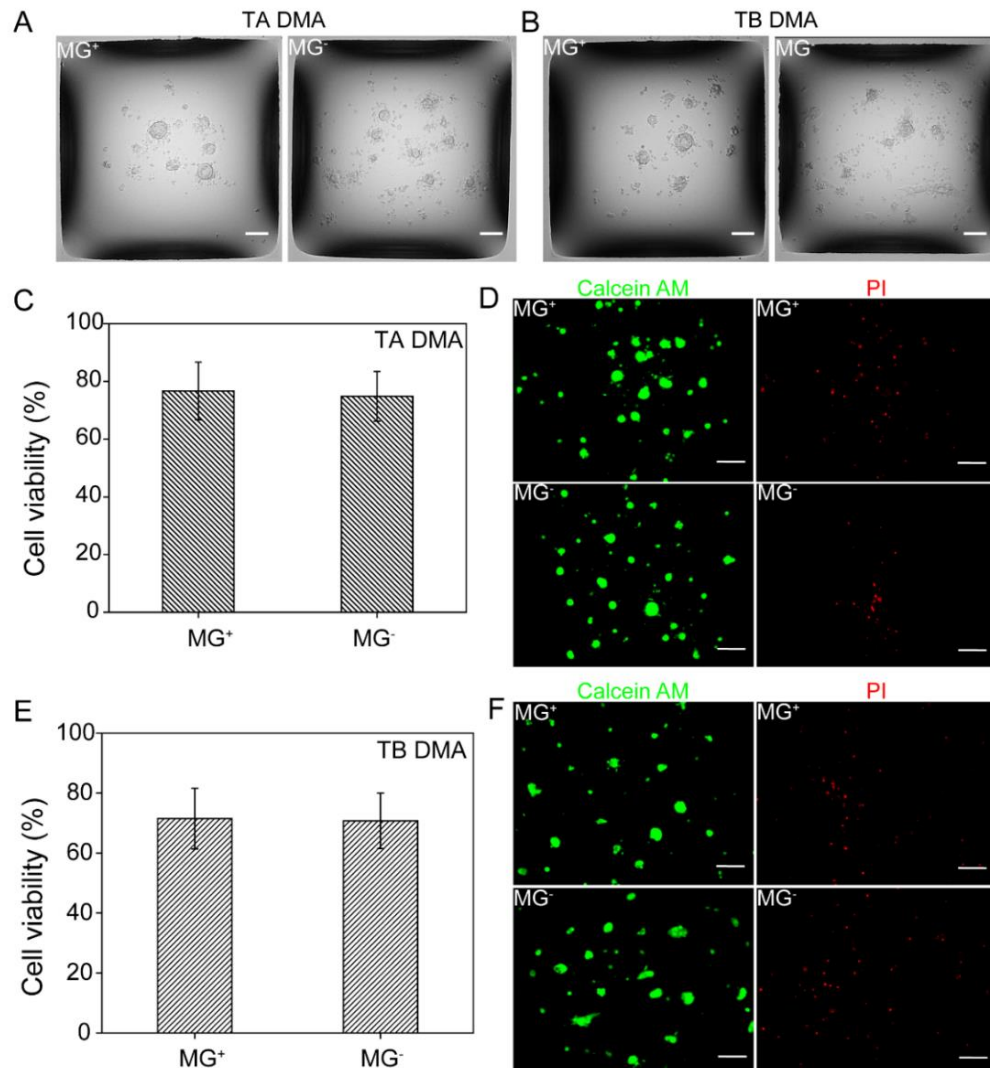
Figure 20. Morphology and viability of hiPSCs on TA and TB DMA with and without MG coating (MG$^+$ and MG$^-$). (A) Morphology of hiPSCs cultivated on MG$^+$ and MG$^-$ TA DMA. (B) Morphology of hiPSCs cultivated on MG$^+$ and MG$^-$ TB DMA. (C) Comparison of viability of hiPSCs cultivated on MG$^+$ and MG$^-$ TA DMA for 24 h. The cell viability was determined as the ratio of the calcein AM-positive area to the sum of the calcein AM- and PI-positive areas (n = 3 biological replicates). (D) Representative fluorescence images of live (green, calcein AM-positive) and dead (red, PI-positive) hiPSCs cultured on MG$^+$ and MG$^-$ TA DMA. (E) Comparison of viability of hiPSCs cultivated on MG$^+$ and MG$^-$ TB DMA for 24 h. The cell viability was determined as the ratio of the calcein AM-positive area to the sum of the calcein AM- and PI-positive areas (n = 3 biological replicates). (F) Representative fluorescence images of live (green, calcein AM-positive) and dead (red, PI-positive) hiPSCs cultured on MG$^+$ and MG$^-$ TB DMA. Data represent the mean ± SD. Scale bar: 100 μm.

The pluripotency of hiPSCs cultured *in vitro* is the most crucial and defining characteristic of these cells since it represents the ability of a cell to differentiate into any cell type. To maintain hiPSCs in the pluripotent state, several research groups have

reported new cell culture substrates with the potential for use as MG substitutes. HiPSCs cultured on these substrates have similar gene expression patterns and a comparable level of pluripotency to cells grown on MG (Brafman *et al.*, 2010; Caiazzo *et al.*, 2016; Musah *et al.*, 2012). However, spontaneous differentiation of hiPSCs into random/multiple lineages during *in vitro* culture is still common. Thus, the search for a coating with well-defined composition that is xeno-free to replace the commonly used MG and facilitate the generation of a reproducible culturing environment for hiPSCs is still ongoing.

Therefore, as a next step, I characterized and compared the pluripotency of hiPSC cultured on MG^+ and MG^- TA and TB DMAs, as well as on MG^+ and MG^- TA and TB DMA surfaces (Figure 17). HiPSC pluripotency is precisely regulated by a core set of transcription factors, including *Nanog*, *Oct4*, and *Sox2* (Boyer *et al.*, 2005; Wang *et al.*, 2006). However, Nanog is at the heart of the gene regulatory network and fluctuations in its expression have been linked to cell fate decisions such as self-renewal (*Nanog* high) and differentiation (*Nanog* low), making it a critical factor for maintaining pluripotency (Blinka & Rao, 2017; Navarro *et al.*, 2012). I therefore assessed the impact of cultivation environment on pluripotency of hiPSCs by immunofluorescence (IF) staining and qPCR analysis of Nanog protein and gene expression, respectively. I compared Nanog expression in hiPSC cultured on MG^- TA and TB DMAs (200 nL cell culture medium), as well as MG^- TA and TB surfaces (2 mL cell culture medium) (Figure 21A) using Nanog expression in hiPSCs cultured on a MG^+ standard tissue culture plate ("MG^+ 2 mL") and a MG^+ DMA ("MG^+ 200 nL") as controls (Figure 21A). Relative Nanog protein expression, calculated as the mean fluorescence intensity of Nanog IF staining and further normalized with the MG^+ 2 mL group varied in hiPSCs cultured on different substrates (Figure 21B). Generally, higher Nanog expression was observed in hiPSCs cultivated on DMAs (MG^+ 200 nL, MG^- TA 200 nL, and MG^- TB 200 nL) compared with that in hiPSCs cultivated on surfaces (MG^+ 2 mL, MG^- TA 2 mL, and MG^- TB 2 mL) (Figure 21A and 21B). Nanog expression in hiPSCs cultivated on MG^+ 200 nL was 1.67 ± 0.23-fold higher than that in MG^+ 2mL. Furthermore, Nanog expression levels in hiPSCs cultivated on MG^- TA 200 nL and MG^- TB 200 nL were 1.77 ± 0.35 and 1.69 ± 0.53 times higher than that on MG^- TA 2 mL and MG^- TB 2 mL, respectively. Compared to the Nanog expression on MG^- TA 200 nL and MG- TB 200 nL, the Nanog expression levels on MG^+ 200 nL were 1.78 ± 0.24-fold and 1.56 ± 0.21-

fold higher, respectively. The same trend was observed for MG$^-$ TA 2 mL and MG$^-$ TB 2 mL, for which Nanog expression levels were 45% and 40% lower than for MG$^+$ 2 mL, respectively. This trend was also observed in the qPCR analysis. HiPSCs grown on DMAs in 200-nL droplets (MG$^+$ 200 nL, MG$^-$ TA 200 nL, and MG$^-$ TB 200 nL) generally displayed higher *Nanog* gene expression than that in cells grown on surfaces in a 2-mL volume (MG$^+$ 2 mL, MG$^-$ TA 2 mL, and MG$^-$ TB 2 mL) (Figure 21C The Nanog expression of hiPSCs grown on MG$^+$ 200 nL was 3.36 ± 0.3 times higher than that of hiPSCs grown on MG$^+$ 2 mL. *Nanog* expression levels of hiPSCs grown on MG$^-$ TA 200 nL and MG$^-$ TB 200 nL were 5.74 ± 0.45-fold and 6.87 ± 0.96-fold higher than those of hiPSCs grown on MG$^-$ TA 2 mL and MG$^-$ TB 2 mL, respectively. However, similar *Nanog* expression levels were observed in hiPSCs grown on MG$^-$ TA 2 mL and MG$^-$ TB 2 mL, which were 76% and 66% lower than that in cells grown on MG$^+$ 2 mL, respectively. I also analyzed the expression levels of the pluripotency markers genes, *Oct4* and *Sox2* (Figure A 14). The results showed a similar trend in the expression of these genes compared to that of *Nanog*, with higher levels of pluripotency gene expression in cells cultured on DMAs (200 nL) compared with that in cells cultured on surfaces (2 mL). Our results showing that hiPSCs grown on different surfaces express different levels of Nanog indicates that the maintenance of pluripotency on DMAs is influenced by both surface properties and confined nanoliter culturing volumes. In general, the pluripotency of hiPSCs cultured on DMAs in 200 nL droplets was higher than that of cells cultured on the same surfaces but in larger 2 mL volumes. Although Nanog expression was higher in cells cultured on MG$^+$ 200 nL and MG$^+$ 2 mL compared to MG$^-$ conditions, the pluripotency of hiPSCs cultured on MG$^-$ DMAs was maintained for 24 h, indicating that it is feasible to use DMAs without MG coating to successfully culture and screen hiPSCs *in vitro*.
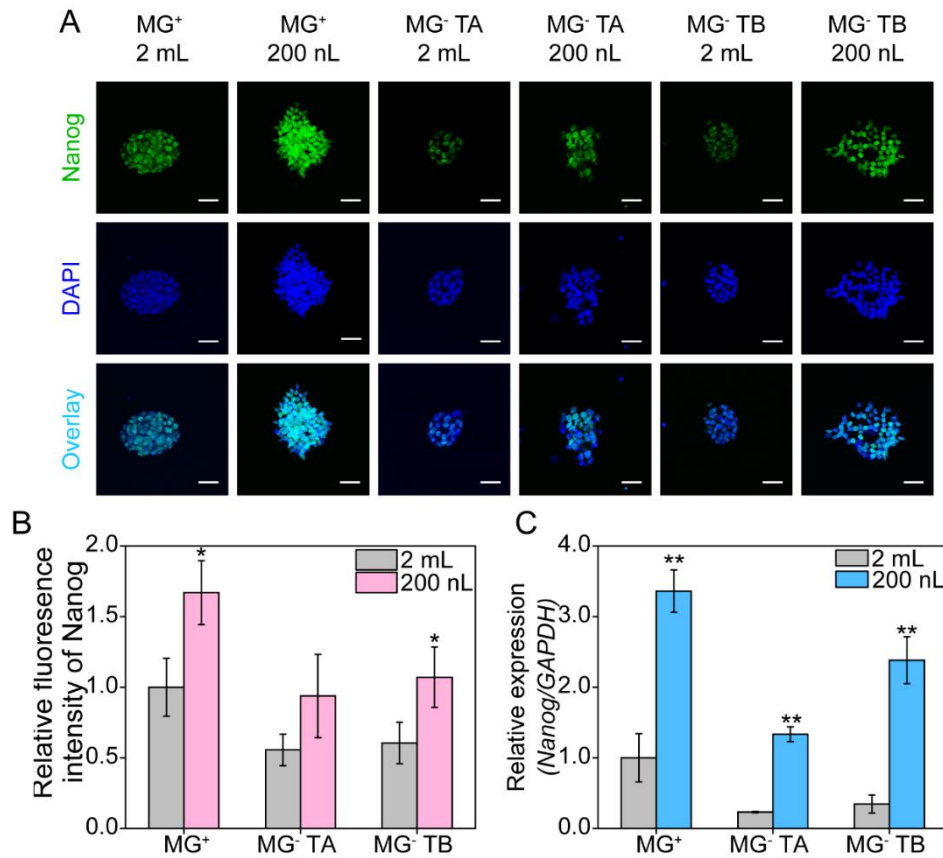
Figure 21. Comparison of hiPSCs pluripotency for cells cultivated on different surfaces and in different volumes. (A) Immunofluorescence (IF) staining of hiPSCs cultivated on MG^+ surface (MG^+ 2 mL), MG^+ DMA (MG^+ 200 nL), MG^- TA surface (MG^- TA 2 mL), MG^- TB surface (MG^- TB 2 mL), MG^- TA DMA (MG^- TA 200 nL), MG^- TB DMA (MG^- TA 200 nL). Cells were stained with DAPI (blue) and Nanog (green) (n = 3 biological replicates). Scale bar: 20 μm. (B) Mean fluorescence intensity of Nanog IF staining was measured by ImageJ. Three images of each experimental group were randomly selected and analyzed. (C) Expression of the pluripotency specific gene *Nanog* was investigated by qPCR analysis of RNA isolated from cells cultured on different surfaces and volumes (n = 3 biological replicates). All gene expression data were normalized with the reference gene *GAPDH* and represented as mean ± SEM. *$P < 0.05$, significant differences between the 2 mL and 200 nL groups. **$P < 0.01$.

In this study, I evaluated the DMA platform for culturing of hiPSC in 200-nL droplets for the first time. I investigated the impact of the printing process on the survival of hiPSCs on DMAs. I analyzed the viability, morphology and pluripotency of hiPSC cultured on MG TA and MG TB DMAs, and compared these with the properties

of cells cultured on MG⁻ TA and MG⁻ TB surfaces and on MG. I demonstrated that hiPSCs cultured on TA and TB surfaces and TA and TB DMAs had typical colony morphology and cell survival in the presence and absence of MG. Based on our results, I conclude that hiPSCs exhibit high viability as well as expected morphology and pluripotency when cultured for 24 h in 200-nL droplets on both TA and TB DMAs without MG coating.

I observed that hiPSCs cultured in nanoliter droplets exhibited higher Nanog protein and gene expression and better maintained pluripotency compared to hiPSCs cultured on the same surfaces in 2 mL volumes. This observation may be accounted for by mechanical cues, which might contribute to the maintenance of pluripotency in a small volume (200 nL). It is known that multiple biophysical cues, such as mechanical forces, shear stress, strain forces, and other forces from the adjacent environment of cells, can influence the maintenance of hiPSC pluripotency (Ireland & Simmons, 2015; Keung *et al.*, 2010; Sun *et al.*, 2012b). Strain forces and frictional forces are generated intracellularly by cell-cell and cell-surface interactions, respectively. Shear stress, which is applied externally by shear or tension on the cells, is sensed by mechanically gated ion channels, changes in ligand-receptor binding, and deformation of the cytoskeleton. The cytoskeleton generates and transfers forces from membrane proteins to intracellular structures, such as the nucleus, via suitable cell signaling pathways. HiPSCs are anchorage-dependent cells expressing integrins; therefore, these cells sense and respond to biophysical cues via integrin signaling pathways (Vitillo & Kimber, 2017). It has also been reported that plasma membrane tension can activate integrin adhesion receptors in the absence of ligand binding, suggesting that integrins can function as mechano-sensors independently of their role in cell adhesion (Ferraris *et al.*, 2014; Petridou & Skourides, 2016). Therefore, it is possible that hiPSCs cells cultured on DMAs in nanoliter droplets sense mechanical stimuli from the adjacent environment resulting in activation of integrins without any coating (such as MG or ECM proteins) followed by adjustment of downstream signaling pathways to maintain hiPSCs pluripotency.

There is an urgent need for well-defined, xeno-free *in vitro* systems for culturing of hiPSCs. In this study, I demonstrated that it is possible to maintain hiPSCs in their pluripotent state during culture on DMAs for 24 h without any additional coating.

DMAs can be precisely adjusted in terms of surface topography and chemical modification, as well as cell culture volumes, making it a well-defined and also animal source-free platform that is suitable for culturing hiPSCs *in vitro*.

HiPSCs have become a focus of research because of their potential in regenerative medicine and use as a model for early toxicity and efficacy screening. In this field, there is still a high demand for cost- and labor-effective platforms for hiPSCs because existing screening methods are usually hampered by the need for large quantities of cells and the high cost of reagents. In addition to well-defined culturing conditions, DMAs enable cultivation of hiPSC in nanoliter volumes in hundreds of parallel wells, making it an ideal platform for HTS applications.

To exploit the benefits of hiPSCs fully, further studies utilizing the advantages of DMAs are required. Examples are: 1) the generation of well-defined substrates for xeno-free hiPSC culture with maintained pluripotency; 2) analysis of the effects of small molecules or their combinations on signaling pathways, such as the Wnt signaling pathway, to induce or hinder hiPSCs differentiation; and 3) screening of small molecules favoring pluripotency of naïve hiPSCs.

3.3 Rapid high throughput combinatorial screening of protein coatings on miniaturized droplet microarray identifies novel cell culture substrates to maintain pluripotency of hiPSCs

3.3.1 DMA and workflow of the screening

The layout of DMA and the screening workflow of proteins are described in Figure 22. The DMA is a 2.5×7.5 cm glass slide with a 14×48 array of hydrophilic spots with complementary superhydrophobic borders, resulting in 672 independent 1×1 mm square spots separated by 500 µm borders. Eleven single proteins were screened (Thy-1, ephrin type-B receptor 4 [EphB4], ephrin type-A receptor 1 [EphA1], E-cadherin, coxsackie and adenovirus receptor [CAR], junctional adhesion molecule A [JAM1], epithelial cell adhesion molecule [EpCAM], basigin [BSG], dystroglycan [DAG1], hyaluronic acid [HA], and laminin 521 [LN521]), as well as their binary and ternary combinations (231 experimental groups in total) (Table 16). Proteins in a 60-nL solution were dispensed onto individual spots of the DMA using a non-contact liquid dispenser (Figure A 15A). To reduce experimental error, each protein or combination was printed in six replicates. Then, hiPSCs were printed with 200 nL per spot and further cultured on DMA slides for 24 h (Figure A 15B). Cells were stained for Nanog (an indicator of pluripotency) by immunofluorescence staining, followed by automated imaging (Navarro *et al.*, 2012). The first screen was used to identify hits on the basis of their ability to maintain pluripotency compared to Matrigel, which was used as a positive control. Selected hits were then validated for their ability to maintain the pluripotency markers Nanog, TRA-1-81, Oct-4A, SSEA4 Sox2, and TRA-1-60 in long-term hiPSC culture (5 weeks). Finally, the ability of cultured cells to differentiate into three germ layers (ectoderm, mesoderm, and endoderm) was tested.
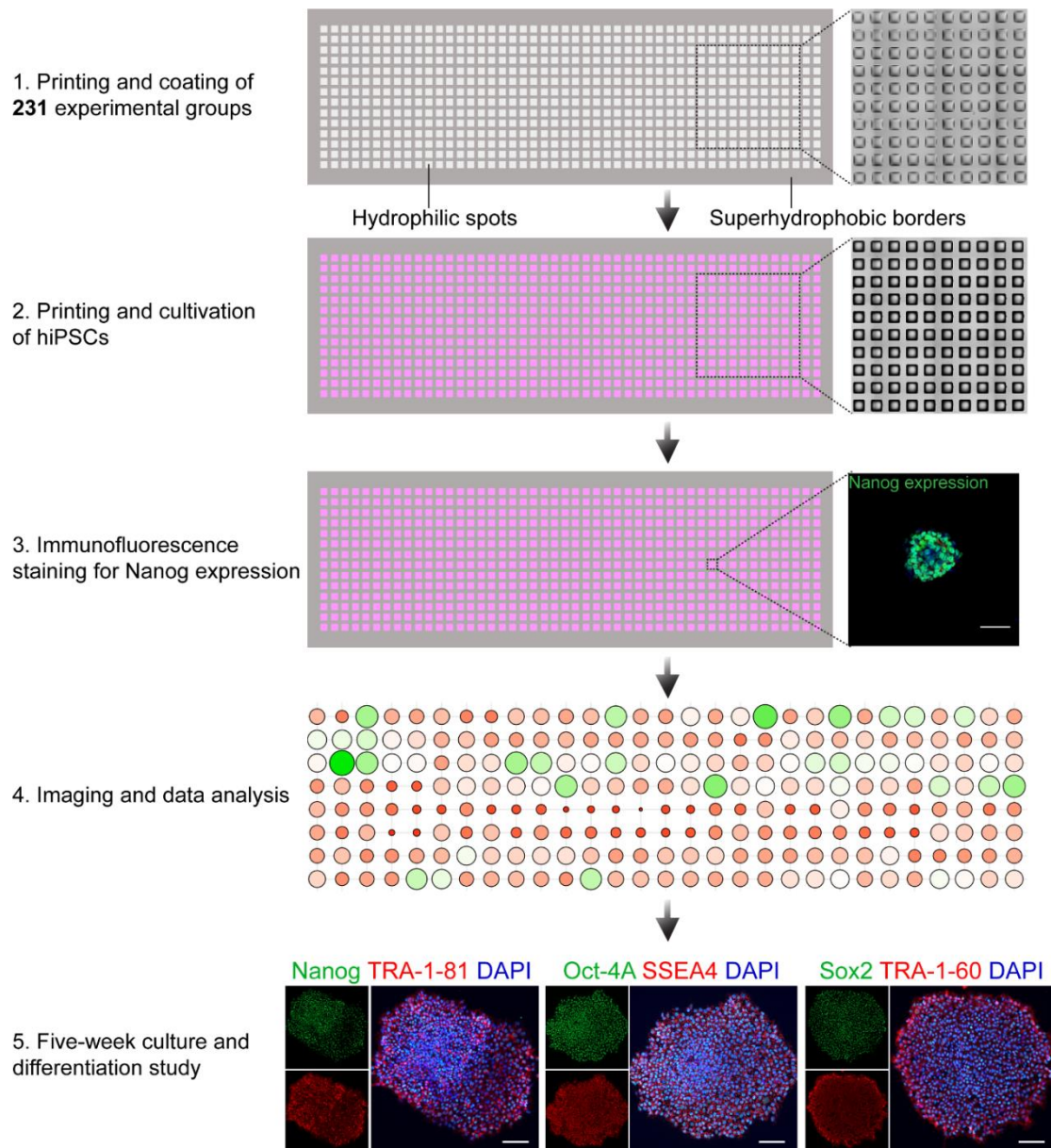
Figure 22. Schematic representation of screening workflow. Printing: 60 nL of protein solution (final concentration of each protein of 10 µg/mL) was printed onto each pre-determined spot and incubated at room temperature for 2 h. Cultivation: hiPSCs were then dispensed in a volume of 200 nL and cultured for 24 h before immunofluorescence staining for Nanog expression. Image analysis: mean fluorescence intensity of immunofluorescence staining was quantified. The primary high-throughput screening was done with 11 single proteins, 55 binary combinations and 165 ternary combinations; a total of 231 screening groups. Validation: hits were selected and further validated by immunofluorescence staining of pluripotency markers (Nanog, TRA-1-81, Oct-4A, SSEA4 Sox2, and TRA-1-60) in hiPSCs cultured for 5 weeks on selected substrates. This was followed by differentiation of these cells into three germ layers, validated by immunofluorescence staining for germ layer markers (FOXA2, endoderm; brachyury, mesoderm; and β-Tubulin3, ectoderm).

3.3.2 Establishing a screening protocol

HiPSCs are very sensitive to environmental stimuli, such as compression and shearing forces. They are also prone to cell death after dissociation (Ohgushi *et al.*, 2010). In regular expansion and HTS of hiPSCs, cell survival is crucial; cell toxicity is a major cause of failure in drug discovery and development (Beers *et al.*, 2012). First, I compared the viability of hiPSCs cultured on DMA after either manual seeding or non-contact printing (Figure A 16). The viability of cells seeded manually or by non-contact liquid dispenser after 24 h were $69.43 \pm 5.90\%$ and $58.28 \pm 1.90\%$, respectively.

I next assessed whether the Matrigel-coated DMA could support undifferentiated hiPSCs, using immunofluorescence staining for the pluripotency markers Sox2, Oct-4A, Nanog, TRA-1-60, SSEA4, and TRA-1-81. Typical immunofluorescence staining procedures involve washing steps, which often result in cell loss. Thus, we assessed the changes in cell numbers before and after immunofluorescence staining. As shown in Figure A 17, around 50% of hiPSCs were left in DMA spots after immunofluorescence staining. Average numbers of hiPSC colonies after immunofluorescence staining were also investigated; there were approximately seven colonies in one DMA spot, with no significant difference between colony numbers remaining among three biological repeats (Figure A 18). These results indicated the feasibility and reproducibility of the established protocol for immunofluorescence staining on DMA. Immunofluorescence staining results (Figure 23A indicated that expression of pluripotency markers in hiPSCs grown on DMAs was similar to that in cells cultured in multi-well plates (Figure A 19), demonstrating that hiPSCs cultured on DMAs retained their pluripotency and ability to self-renew. Next, I used phalloidin staining to visualize the typical cytoskeletal arrangement of hiPSCs colonies; for hiPSCs cultured on DMAs, F-actin cytoskeletal organization was observed (Figure A 20).

Taking together, my results demonstrated that hiPSCs cultured on DMAs show the same characteristics (expression of pluripotency markers and morphology) as cells cultured on state-of-the-art platforms, thus the DMA platform could be used for culturing and screening undifferentiated hiPSCs.

As a next step, the feasibility and robustness of utilizing the DMA platform for HTS of hiPSCs was assessed. Matrigel coating (MG$^+$) was set as positive control and no Matrigel coating (MG$^-$) was set as negative control. The morphology of hiPSCs in

positive and negative controls are shown in Figure 23B. The positive control group demonstrated typical hiPSC morphology, with compacted cells and distinct edges. In the negative control group, hiPSCs displayed poor aggregation with no distinct edges and compacted cells.

Nanog, Oct4, and Sox2 are the core transcription factors regulating pluripotency of stem cells. While the expression of Oct4 and Sox2 is relatively uniform, stem cells fluctuate between high Nanog expression and high pluripotency and low Nanog expression with low pluripotency Hence, Nanog expression detected by immunofluorescence staining was selected to be the read-out for primary screening. Thus, in the immunofluorescence images, higher mean fluorescence intensity of cells indicates higher self-renewal than in lower mean fluorescence intensities. Figure 23C show a significant difference in mean fluorescence intensity for Nanog expression in positive and negative controls.

Then, I employed the screening window coefficient, Z-factor (Z'), to evaluate the quality of the primary HTS assay (Zhang *et al.*, 1999). I calculated the Z' for the assay from three biological replicates as the following formula:

$$Z' = 1 - \frac{(3\sigma_{c+} + 3\sigma_{c-})}{|\mu_{c+} - \mu_{c-}|}$$

in which σc+ represents standard deviation (SD) of the positive control, σc- represents SD of the negative control, μc+ and μc- indicate the means of positive control and negative control signals, respectively. The value of Z' was 0.64 (Figure 23D), indicating an excellent assay according to classification of screening assay quality (Zhang *et al.*, 1999).

Along with various transcription factors, E-cadherin is important for establishing and maintaining stem cell pluripotency and their ability to self-renew via cell–cell adhesions (Narva *et al.*, 2017). Hence, E-cadherin is widely used as a marker for undifferentiated stem cells (Watanabe *et al.*, 2007). Therefore, I investigated E-cadherin expression in hiPSCs in both the positive and negative controls (Figure 23E). High E-cadherin expression was observed in positive controls, while low-to-no E-cadherin expression was observed in negative controls. The mean E-cadherin

fluorescence intensity of negative controls was 17.01 ± 7.84% of that of positive controls (Figure A 21).

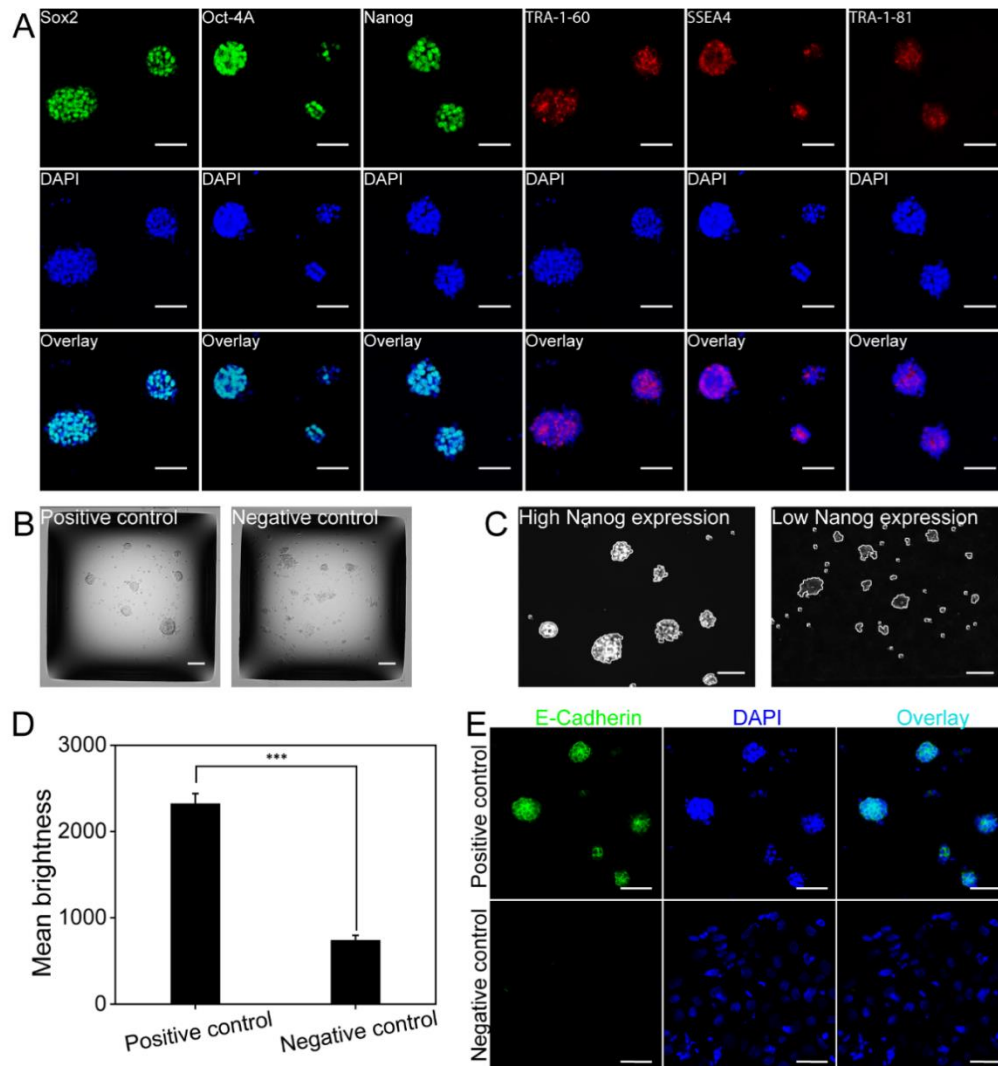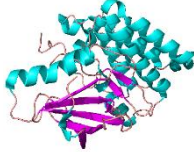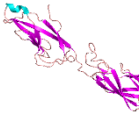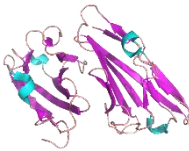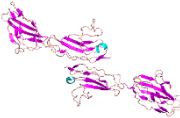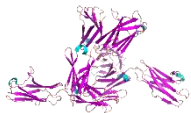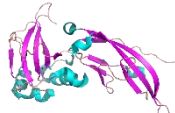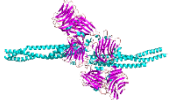**Figure 23. Validation of screening protocol**. (A) Representative confocal laser scanning microscope (CLSM) images of hiPSCs cultivated on DMA coated with Matrigel stained for six pluripotency markers: Sox2, Oct-4A, Nanog, green fluorescence; TRA-1-60, SSEA4, TRA-1-81, red fluorescence. Three independent experiments were conducted (n = 3), obtaining comparable results. DAPI was used to counterstain nuclei. Scale bar: 50 μm. (B) Bright-field images of hiPSCs cultivated on positive (Matrigel, MG⁺) and negative (no Matrigel, MG⁻) controls. Scale bar: 100 μm. (C) Nanog expression level was used as a read out for the primary screening. Immunofluorescence staining was carried out on DMA followed by automated microscopy. Scale bar: 50 μm. (D) Quantification of mean fluorescence intensity of hiPSCs cultured on positive and negative controls and stained for the pluripotency marker Nanog. The graph shows a large separation band between signal detected from positive and negative controls (Z′ value is between 0.5 and 1, corresponding to a high-quality screening assay). (E) Representative CLSM images of E-cadherin expression in hiPSCs cultured on positive and negative control coatings. E-cadherin mediates cell–cell interactions and contributes to stem cell colony formation and pluripotency.

Thus, on the positive control coating, undifferentiated hiPSCs show high expression of E-cadherin, while differentiated hiPSCs on the negative control coating show low-to-no E-cadherin expression. DAPI was used to counterstain nuclei. Scale bar: 50 μm.

Table 16. The list of proteins used in this study with their corresponding structures and PDB codes

Proteins	Descriptions	Structures	PDB codes
Thy-1 (CD90)	Glycophosphatidylinositol (GPI) anchored conserved cell surface protein, combinatorial surface marker for stem cells		Modeling by SWISS-MODEL with ProMod3 3.0.0
Ephrin type-B receptor 4 (EphB4)	Membrane-bound protein, binding and activation of Eph/ephrin intracellular signaling pathways, involved in the regulation of cell adhesion and migration		6fnm (Troster *et al.*, 2018)
Ephrin type-A receptor 1 (EphA1)	Membrane-bound protein, binding and activation of Eph/ephrin intracellular signaling pathways, regulates cell proliferation		3hil (Walker, 2009)
E-cadherin	Calcium-dependent cell-cell adhesion glycoprotein composed of five extracellular cadherin repeats, a transmembrane region, and a highly conserved cytoplasmic tail		2O72 (Parisini *et al.*, 2007)
Coxsackie and adenovirus receptor (CAR)	Transmembrane bound protein with two Ig-like extracellular domains, a transmembrane domain, a cytoplasmic domain and two N-linked glycosylation sites, may function as a cell adhesion molecule		1f5w (van Raaij *et al.*, 2001)
Junctional adhesion molecule A (JAM1)	Junctional adhesion molecule transmembrane protein family member, receptor of CAR		1nbq (Prota *et al.*, 2003)
Epithelial cell adhesion molecule (EpCAM)	Transmembrane glycoprotein involved in cell signaling, migration, proliferation and differentiation, plays a role in embryonic stem cells proliferation and differentiation		4mzv (Pavsic *et al.*, 2014)

Basigin (BSG)	Member of the immunoglobulin superfamily, plays fundamental roles in intercellular recognition involved in various immunologic phenomena, differentiation, and development		3b5h (Yu *et al.*, 2008)
Dystroglycan (DAG1)	Transmembrane linkage between the extracellular matrix and the cytoskeleton, involved in a number of processes including laminin and basement membrane assembly		5llk (Covaceuszach *et al.*, 2017)
Hyaluronic acid	One of the chief components of the extracellular matrix, contributes to cell proliferation and migration		1poz (Teriete *et al.*, 2004)
Laminin 521	A component of the extracellular matrix, used to enhance pluripotent stem cell culture		5xau (Takizawa *et al.*, 2017)

Helix	Sheet	Loop

Table 17. Comparison of reagent, cell consumption, and estimated cost for the screening performed on DMAs, 384- and 96-well plates.

	DMA	384-well plates	96-well plates
Volume of proteins (mL)	~0.08	~13.9	~69.3
Amounts of proteins (μg)	~0.8	~139	~693
Numbers of cells	~2.8×10^5	~3.1×10^6	~6.9×10^6
Volumes of medium (mL)	~0.28	~27.7	~231.6
Estimated costs of proteins ($)	~170	~4000	~14300

3.3.3 Primary screening

For the primary screening, hiPSCs were cultured on coatings created from 231 protein groups (11 single proteins [Figure 24A], 55 binary combinations of proteins, and 165 ternary combinations of these proteins). The final concentration for each protein/group was 10 µg/mL, and culture took place over 24 hours. Cells were then subjected to immunofluorescence staining for the pluripotency marker Nanog, followed by automated fluorescent microscope imaging and image analysis. The main aim here was to search for proteins maintaining the pluripotency of hiPSCs (Table 13, 14, and 16).

In total, only 0.083 mL of protein solution (8.3 µg protein), $\sim 2.8 \times 10^5$ cells and ~0.28 mL of cell culture medium were required for the whole primary screening using a DMA. This resulted in decreased consumption of proteins and cell suspensions by 668 and 500-fold, respectively, versus HTS conducted in conventional 96-well plates. This approach therefore suggests considerably reduced costs are possible for hiPSC expansion and large-scale protein production (Table 17). The mean fluorescence intensity representing Nanog expression level in hiPSCs cultured on each protein coating was then analyzed and normalized against the intensity of cells cultured on positive control coatings (MG$^+$ spots). Figure 24B presents a schematic of the protein combinations used in the experiment (A–K), and a heat map representing the ratio of Nanog expression of hiPSCs grown on different experimental protein groups versus cells grown on a positive control coating. In the heat map, red indicates lower Nanog expression (cells are less pluripotent) and green represents higher Nanog expression (cells are more pluripotent) compared with its expression level in cells cultured on the positive control coating (MG$^+$). The threshold of mean + 3 SD (1.00 + 0.57) compared with positive control (MG$^+$) was established to identify positive hits showing significantly increased Nanog expression in hiPSCs (Malo *et al.*, 2006). The 10 top protein groups were identified (Figure 24C and 24D, a detailed description of these is presented in Figure A 22. In Figure 24C, the green, red, and violet columns indicate relative Nanog expression level in hiPSCs cultured on positive (MG$^+$) and negative (MG$^-$) control coatings, and hits in the primary screening, respectively. The fold changes of experimental groups versus MG ranged from 0.22 (red) to 2.18 (green). Two protein groups that promoted the highest increase in Nanog expression in hiPSCs were

BIK and GHK, with fold changes of 2.18 ± 0.32 and 2.00 ± 0.22, respectively (Figure 24B and 24D).

EphB4 (B) belongs to Eph receptor tyrosine kinase, which promiscuously binds transmembrane ephrin-B family ligands residing on adjacent cells and mediates cell–cell interactions (Liu *et al.*, 2017). EphB4 contributes to tumor malignancy and regulates the development of various tumors. EphB4 can also promote the self-renewal and proliferation of human neural stem cells. However, little is known about the role of EphB4 in the maintenance of pluripotency in hiPSCs. DAG1 (I) is a heavily glycosylated protein that is strongly expressed in hiPSCs (Sugawara *et al.*, 2019). It can interact not only with laminin to mediate cell–ECM interactions, but also participates in direct out–in signaling, together with integrins. Thus, it might contribute to the adhesion of hiPSCs to culture substrates. EpCAM (G) is a transmembrane glycoprotein, which mediates cell–cell interactions via cadherins linking the cytoskeleton. It is a surface marker on undifferentiated hESCs (Ng *et al.*, 2010). Reducing EpCAM expression decreased the proliferation of hESCs and expression of other pluripotency markers. EpCAM might regulate the pluripotency of hiPSCs. BSG (H) is a member of the immunoglobulin superfamily, which is involved in reproduction, neural function, inflammation and tumor invasion (Muramatsu & Miyauchi, 2003). It is a cell surface marker that is consistently upregulated in early and late passages of hiPSCs (Pripuzova *et al.*, 2015). Thus, I hypothesized that BSG might be involved in maintaining the pluripotency of hiPSCs. Laminins (LNs) are well-known ECM proteins, which contribute to ECM structure and have effects on cell adhesion, differentiation, migration, and other cell behaviors (Domogatskaya *et al.*, 2012). LN 511 enables self-renewal of mouse ESCs, and its E8 fragment efficiently supports the adhesion and expansion of hiPSCs (Miyazaki *et al.*, 2013). Besides, α-5 LN was shown to promote self-renewal of hiPSCs (Laperle *et al.*, 2015). Furthermore, α-5 LN promotes the self-renewal of hiPSCs. Hence, I selected LN 521 as a candidate for maintaining the pluripotency of hiPSCs.

Results of our primary screening showed that single proteins did not promote significantly higher Nanog expression in hiPSCs than the MG coating. However, protein combinations, especially ternary protein groups, promoted significantly higher

pluripotency marker expression in hiPSCs than cells cultured on the MG coating (Figure 24D).
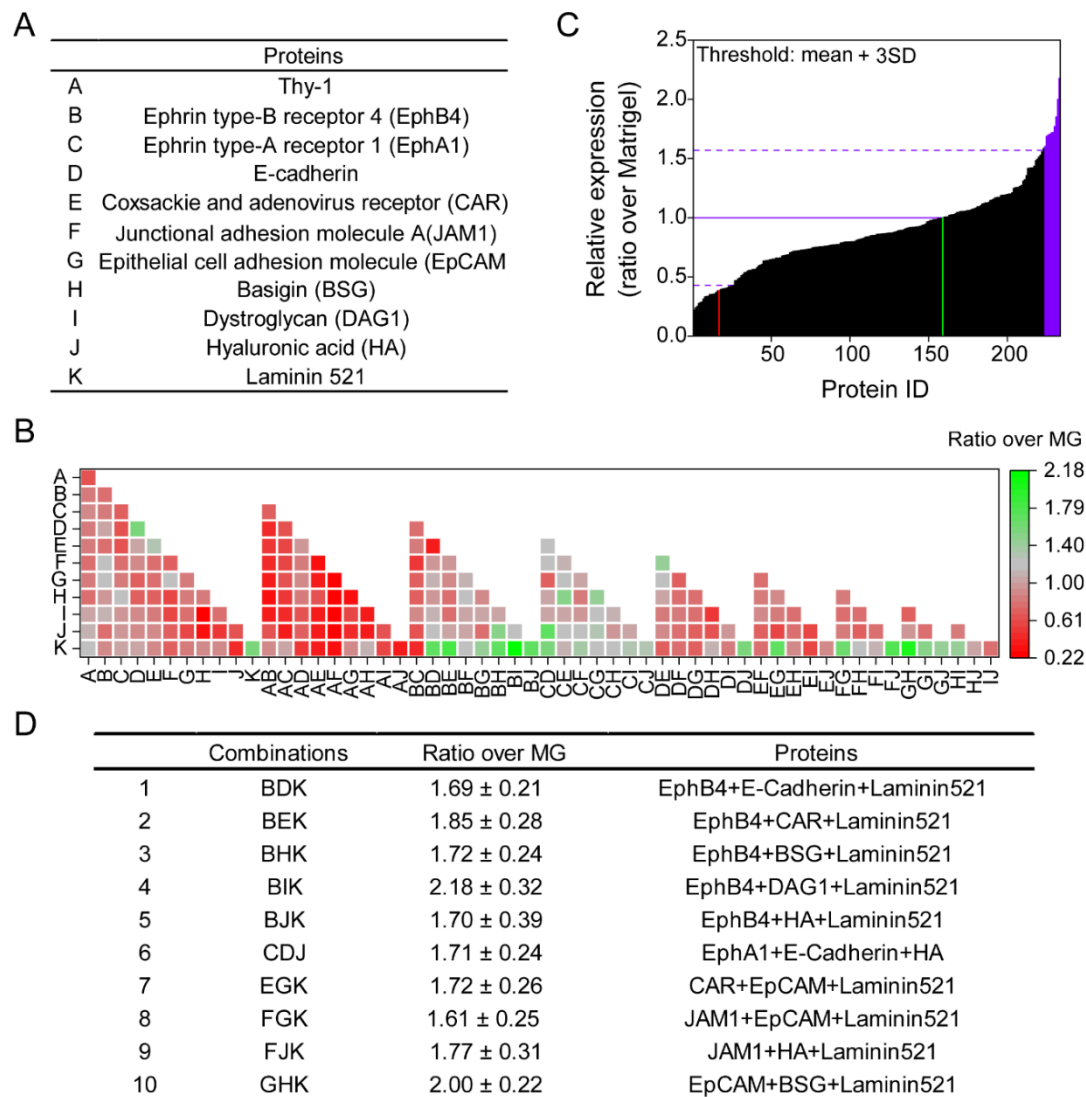
Figure 24. Results of primary screening. (A) List of proteins and their corresponding letter codes used in the screening. (B) Heat map demonstrating the fold change of Nanog expression in hiPSCs cultured on coatings containing single proteins and protein combinations. Six replicates were used for each independent array experiment. The mean fluorescent intensity of Nanog expression of each independent group was normalized against expression level of Nanog in cells cultured on Matrigel (MG) coating (positive control). Green indicates high Nanog expression level (higher capacity for self-renewal) and red indicates low Nanog expression (lower capacity for self-renewal) than marker expression levels in cells cultured on a positive control (MG⁺) coating. (C) Graph showing relative Nanog expression of all tested protein groups in the screening. The threshold for protein coating promoting significant change in Nanog expression was set as mean + 3 SD. Red column indicates negative control (non-coated, MG⁻),

green column indicates positive control (MG-coated, MG⁺), and violet columns show positive hits. (D) The list of top 10 positive hits identified in the primary screening.

3.3.4 Validation of hits from primary screening

To identify the most effective proteins for the maintenance of pluripotency of hiPSCs in longer term *in vitro* culture, two protein combinations (BIK and GHK) were selected for further validation. BIK and GHK were coated onto 12-well plates at room temperature for 2 h, then the solution was aspirated before adding hiPSCs. These two protein combinations could facilitate attachment of hiPSCs in *in vitro* culture for up to 4 days – similar to MG (Figure 25A). On day 1, compared with MG (set as 100%), the attachment efficiencies of BIK and GHK were 94.76 ± 3.44% and 95.84 ± 9.78%, respectively. Over the following three days, BIK showed high attachment efficiency for day 2 (92.59 ± 6.00%), day 3 (84.15 ± 9.16%), and day 4 (79.13 ± 12.57%). GHK showed similar attachment efficiency for day 2 (91.14 ± 12.67%), day 3 (79.81 ± 6.84%), and day 4 (78.48 ± 1.91%). In comparison, non-coated well plates did not facilitate the attachment of hiPSCs. These results demonstrate that BIK and GHK can facilitate the attachment of hiPSCs in culture to a similar extent as Matrigel. Over five generations, hiPSCs cultured on BIK and GHK displayed typical hiPSC colony morphology (Figure A 23) and comparable levels of pluripotency marker (Nanog and TRA-1-81) expression to cells cultured on Matrigel (Figure 25B and A 24-26).

To further validate the pluripotency of hiPSCs grown on BIK and GHK coatings, the expression of pluripotency markers was investigated by immunofluorescence staining and quantitative PCR (qPCR) analysis over five generations. HiPSCs cultured on BIK and GHK-coated surfaces stained positive for Nanog, Oct-4A, Sox2, TRA-1-81, SSEA4, and TRA-1-60, similar to cells cultured on Matrigel (Figure 25C). This demonstrates that, like Matrigel, BIK and GHK coatings can also support the long-term expansion of hiPSCs and maintain their pluripotency.

To investigate the level of pluripotency marker expression at the generation level, qPCR analysis for *Nanog, Oct4, and Sox2* was conducted. The gene expression of target pluripotency genes (*Nanog, Oct4, and Sox2*) was normalized against the expression level of *GAPDH,* and expression levels of pluripotency genes in hiPSCs cultured on BIK and GHK coatings were further normalized against expression levels of these

genes in cells grown on Matrigel (Figure 25D In hiPSCs cultured on Matrigel, BIK and GHK coatings, gene expression levels of *Nanog*, *Oct4*, and *Sox2* were 1.00 ± 0.05, 1.00 ± 0.04, 1.00 ± 0.25; 1.04 ± 0.14, 0.99 ± 0.07, 1.01 ± 0.03; and 1.05 ± 0.14, 1.07 ± 0.22, and 1.05 ± 0.09, respectively (Figure 4D). The qPCR results demonstrated that hiPSCs cultured on BIK and GHK-coated surfaces expressed pluripotency marker genes at similar levels to those in cells cultured on Matrigel. Taken together, our results demonstrated that hiPSCs grown on BIK and GHK surfaces sufficiently support self-renewal and pluripotency of hiPSCs in feeder-free conditions.

A unique characteristic of hiPSCs is their ability to form an embryoid body (EB) and differentiate into three germ layers (pluripotency). Therefore, for cells cultured *in vitro* on BIK and GHK-coated surfaces, we investigated EB formation and the differentiation of three germ layers, according to a previously described method (Figure 25E) (Kurosawa, 2007). Briefly, hiPSCs grown on BIK and GHK-coated surfaces were dissociated after five generations and seeded in 20 µL hanging droplets on the lid of a Petri dish. Two days later, EBs were transferred onto gelatin-coated coverslips in 12-well plates to induce spontaneous differentiation into three germ layers (endoderm, mesoderm, and ectoderm) and cultured for 14 days. Then, the three germ layers were stained for specific markers (endoderm, FOXA2; mesoderm, brachyury; and ectoderm, β-Tubulin3). Cells originated from hiPSCs cultured on BIK and GHK-coated surfaces showed similar expression of three germ layer markers to those of cells obtained from Matrigel-coated surfaces (Figure 25F). Cells cultured on non-coated surface did not express the three germ layers markers. These results demonstrate that BIK and GHK coatings are sufficient and effective in maintaining pluripotency and the differentiation capacity of hiPSCs, as confirmed by estimating cell attachment, expression of pluripotency markers (*Nanog*, *Oct4*, and *Sox2*) in long-term culture over five generations, formation of EBs, and differentiation into three germ layers.
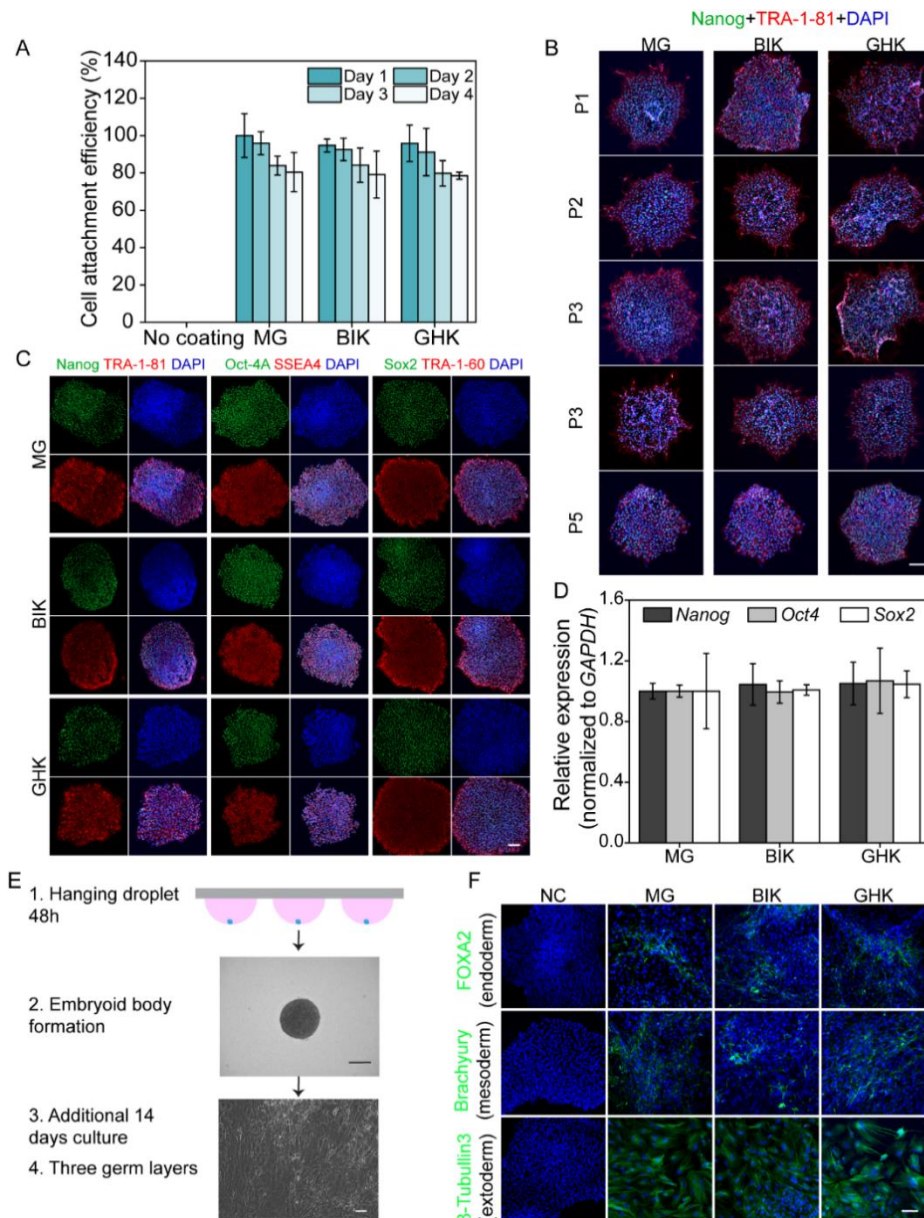
Figure 25. Validation of two hits from the primary screening by long-term culture and three germ layer differentiation. (A) Colony attachment efficiency of hiPSCs on non-coated 12-well plates, Matrigel (MG)-coated 12-well plates, and BIK and GHK-coated 12-well plates for 4 days. BIK and GHK were identified from the primary screening as showing higher Nanog expression. (B) Maintenance of pluripotency of hiPSCs on MG, BIK and GHK coatings for long-term culture (five generations, P1–P5) was estimated by immunofluorescence staining of Nanog (green) and TRA-1-81 (red). DAPI was used to counterstain nuclei. Scale bar: 50 μm. (C) Immunofluorescence images of hiPSCs cultured on MG, BIK and GHK coatings and stained for six pluripotency markers (Nanog, Oct-4A, Sox2, green fluorescence; TRA-1-81, SSEA4, TRA-1-60, red fluorescence). Scale bar: 50 μm. (D) qPCR profiling of pluripotency marker genes (*Nanog, Oct4, and Sox2*) of hiPSCs grown on MG, BIK and GHK-coated well plates for five generations (n=3, biological replicates). Gene expression data were normalized against a reference gene *GAPDH*. In hiPSCs cultured on BIK and GHK coatings, the gene expression

level was normalized against that of cells grown on MG. Data represented as mean ± SEM. (E) Schematic diagram of the differentiation of hiPSCs into three germ layers. (F) Immunofluorescence staining for markers of three germ layers FOXA2 (endoderm), brachyury (mesoderm), and β-Tubulin3 (ectoderm) in hiPSCs cultured on non-coated surface (NC), MG, BIK and GHK. Scale bar: 50 μm.

HiPSCs are subjected to cell culture substrates change since they do not attach to normal glass, plastic cell culture labware, plastics, or agars, which are conventionally used for general cell culture. It is well established that proliferation and maintenance of pluripotency of hiPSCs is mainly dependent on cell culture substrates and the early methods used for hiPSCs culture on feeder cells and Matrigel. However, the involvement of animal-derived materials has xenogenic, undefined, and possess significant safety concerns which hinder their potential and application in clinical. As a result, most studies have focused on developing well-defined and xeno-free synthesized and natural cell culture substrates for hiPSCs. Some of previously attempts to define optimal culture substrates for hiPSCs were made with stochastic combinations of a few proteins, which lacks of complexity. Thus, complex and systematic experiments are required to study the full extent of proteins and their interactions *in vitro*. However, one of the bottlenecks for these studies is lacking of complexity due to the high-costs for cell sources, proteins. Toward this end, I developed a combinatorial protein microarray platform to assess how protein composition influence cell behavior.

The majority of cell culture substrates screening focus on ECM proteins via cell-ECM interactions. However, surface proteins of hiPSCs, such as EpCAM, also participate in maintenance of pluripotency of hiPSCs via cell-cell interactions. Thus, I systematically screened eleven proteins in a combinatorial manner that my potentially influence pluripotency of hiPSCs. From the primary screening, I identified ten protein coatings that could maintain pluripotency of hiPSCs for 24 h. The eleven single proteins did not show higher pluripotency marker expression than that of combinations. These ten hits are all ternary combinations of proteins and for each group both ECM proteins and surface proteins are involved. Of all these ten hits, I selected two groups for validation. I then demonstrated these two coatings were able to maintain the pluripotency of hiPSCs grown on these substrates for long-term. Furthermore, the differentiation ability of hiPSCs were verified by three-germ layers differentiation. Several studies have utilized array-based systems to screen factors that might influence cell fate. However, these research require pre-coating or immersing into media which

might lead to crosstalk and cause false positive results. The combinatorial screening here distinguishes itself in three major ways. First of all, a combinatorial microarray of multiple proteins (ECM proteins and surface proteins) could be fabricated in a nanoscale volume while previous studies mainly focused on ECM proteins. The second is the coating of proteins instead of covalently linking. Previous study showed that cross-linking of Wnt3a protein produced an inactive protein (Brafman *et al.*, 2009). In this study, proteins were printed onto DMA spots and coated them without any further manipulation, which might maintain maximal biological activity of proteins. The third is the existence of superhydrophobic borders that prevents the diffusion of protein solutions, which prevent crosstalk among spots.

4 Summary and Outlook

4.1 Summary

It is hypothesized that by treating cells with small molecules, the transfection efficiency can be improved. However, in order to identify such transfection-enhancing molecules, thousands of molecules must be tested. Current high-throughput screening technologies based on microtiter plates are not suitable for such screenings due to the prohibitively high costs of reagents and operation. Therefore, in the first part of my thesis, I systematically screened the effect of 774 Food and Drug Administration-approved drugs and their concentrations on transfection efficiency in three different cell types on a miniaturized droplet microarray platform. Based on the primary screening, 14 hit compounds were selected and further evaluated and validated on the droplet microarray platform as well as both in 384- and 96-well plates. Several compounds (auranofin, carbidopa, captopril, hydrocortisone acetate, ifosfamide, indapamide, oxacillin sodium salt monohydrate, methylprednisolone, naphazoline·HCl, rifampin, oxiconazole nitrate, piroxicam, tranylcypromine hemisulfate, and rivastigmine tartrate) demonstrated up to fivefold increase of transfection efficiency, which can be important for further fundamental research projects such as gene therapy but also for the production of therapeutically relevant proteins. The results also demonstrate the power of the droplet microarray platform in miniaturized high-throughput experiments. In this study, I performed in total around 42,000 individual experiments using 20 nL droplets, which resulted in only 0.84 mL of total cell suspension and required only 200 pmoles of drugs (total 0.02 moles). This is 2,500 times smaller than if the same experiment would have to be performed in 384-well plates. Combining high-throughput droplet microarray platform and pharmacological priming (drug repurposing) approach may have valuable applications in biology, drug discovery and other related fields.

In vitro culture and expansion of human induced pluripotency stem cells (hiPSCs) is considered technically difficult since the self-renewal and differentiation of these cells is extremely sensitive and responsive to cell culture substrates. It has been shown that surface properties, such as topography, have an impact on hiPSC pluripotency, self-renewal and differentiation. Moreover, stemness has been reported to be dependent on droplet volumes. In the second part of my thesis, culturing of hiPSCs in 200-nL droplets

on droplet microarray platform was evaluated for the first time. I have investigated the impact of printing process on survival of hiPSCs on droplet microarray slides. The cell viability, morphology and pluripotency of hiPSCs cultured on type A and type B droplet microarrays without Matrigel coating were investigated. These results were compared with those of cells cultured on type A and type B surfaces without Matrigel coating and with Matrigel coating conditions. The results demonstrated that hiPSCs cultured on type A and type B droplet microarray slides had typical colony morphology and cell survival in the presence and absence of Matrigel. Based on the results, it can be concluded that hiPSCs exhibited high viability, expected morphology and pluripotency in 200-nL droplets on both type A and type B droplet microarray slides without Matrigel coating for 24 h of culture.

HiPSCs have been attractive hotspots for researchers because they hold the potential in regenerative medicine and could be used as a model for early toxicity and efficacy screening. In this field, there are still a great deal of demands for cost- and labor-effective platforms for hiPSCs because existing screening methods are usually hampered by the need of large quantity of cells and high costs of reagents. In addition to well-defined culturing conditions droplet microarray platform enables culturing of hiPSCs in nanoliter volumes in hundreds of parallel wells, making it an ideal platform for high-throughput screening applications of hiPSCs.

Animal derived materials are typically used for *in vitro* culture of hiPSCs, which hinders their clinical application. Proteins have emerged as powerful candidates for hiPSC culture. In the <u>third</u> part of my thesis, the droplet microarray platform was exploited for combinatorial protein screening in order to identify proteins that are able to maintain pluripotency of hiPSCs. With this screening, ten groups of ternary protein combinations, which can sufficiently support self-renewal and proliferation of hiPSCs better than Matrigel, were identified. Two of them were further validated for long-term (five weeks) culture of hiPSCs grown on these protein coatings. Additionally, embryoid body formation and differentiation of hiPSCs into three germ layers were achieved. The results demonstrated that droplet microarray platform and the high-throughput screening approach were efficient for hiPSCs-based high-throughput screening, which could be further expanded to investigate more complicated interactions of cells with their ambient environment. In addition, the identified protein coatings could carry the

potential for xeno-free expansion of hiPSCs, which hold tremendous potential for hiPSCs research ranging from fundamental biology to clinical applications.

4.2 Outlook

In the first part, I tested the cells treated with compounds after mixing with transfection mixture. Other possibilities exist to broaden the applications of pharmacological priming. First of all, the influence of cells treatment before and during mixing with transfection mixture can be investigated. By adding compounds at different stages (before, during, and after mixing with transfection mixture), researchers could compare difference of cellular processes of transfection. The second possibility is the testing various drug libraries. There are various types of compound libraries available, which could be further tested for specific drug repurposing. Except for these comprehensive libraries, specific libraries such as kinase inhibitor library, epigenetics compound library, and inhibitor library are also of great importance and being used in oncology, metabolism, and antivirus fields. By combing the miniaturized droplet microarray platform and these libraries, more biological questions can be answered and more drugs can be repurposed for other applications. The third possibility is the investigation of influence of small molecules on cell transfection barriers. As I mentioned before, cellular uptake, endosome escape, cell nuclear localization, and transcriptional and translational regulation are the main rate determining steps for transfection. Utilizing other technologies and methods could help us have a better understanding of the impact of small molecules on each step. For instance, a fluorescently labeled pDNA or nanoparticles could be primed with small molecules and then investigated the cellular uptake rate by flow cytometry or fluorescence microscopy, followed by endosome and cell nuclear colocalization assessment. As for protein expression, a wildly used method - luciferase assay – could be applied to identify the small molecules that increase the expression levels of recombinant proteins.

The derivation of mouse epiblast stem cells clarified that pluripotency contain two developmental stages. Specifically, mouse embryonic stem cells derived from preimplantation inner cell mass represent the "naive" stage and mouse epiblast stem cells derived from the post-implantation epiblast represent the "primed" stage (Nichols & Smith, 2009). Primed human induced pluripotent stem cells form flattened colonies,

whereas naïve Primed human induced pluripotent stem cells form dome-like 3D colonies. Conventional human induced pluripotent stem cells represent primed state. It will be interesting to test the effect of different proteins on induction and maintenance of pluripotency of naïve human induced pluripotent stem cells. Droplet microarray platform then can be used as a high-throughput screening platform for testing and screening molecules (small molecules and proteins) that induce and maintain pluripotency of naïve human induced pluripotent stem cells. The proteins I identified in the third part of my thesis could also be further tested for their influence on induction and maintenance of pluripotency of naïve human induced pluripotent stem cells.

Using the protein coatings markedly supports human induced pluripotent stem cells maintaining in an undifferentiated state. However, the use of these protein coatings is time, labor, and cost-consuming due to the pre-coating of these proteins required before cell seeding. Thus, there is increasing interest in coating-free culture or use of proteins as additives in solution for the culture of human induced pluripotent stem cells. Coating free means directly adding proteins to the cell suspension, thereby omitting the precoating procedure of cell culture vessels and might be adequate for subculture of hiPSCs. Recent case reported by Miyazaki et al. also supported that comparable efficacy at lower amount of the substrate than the precoating preparation of cell culture vessels (Miyazaki *et al.*, 2017). Thus, the proteins that I have identified could also have the potential to support long-term maintenance of hiPSCs in a more efficient, less costly, time- and labor-saving way. For testing this hypothesis, cell dissociating methods, protein concentrations (certain concentrations of proteins per unit area or certain concentrations of proteins per unit volume), cell culture time, and cell seeding density should be carefully investigated and verified.

Droplet microarray platform offers a miniaturized and high-throughput screening platform that can be used in various life science research fields such as anticancer screening, transfection enhancer screening, human induced pluripotent stem cells-based screening, embryoid body screening, and combinatorial materials screening. With the rapid change of world situation and the speedy development of technologies, more attractive and interesting applications of droplet microarray platform are anticipated to answer a wide range of biological questions.

The COVID-19 disease has spread worldwide, leading to an ongoing pandemic. The life of all the people including me is strongly influenced by this disease. There are four main diagnostic methods nowadays available for COVID-19, including nuclei acid test, chest CT scans, serological tests, and antigen test. Antigen test is fast but with low sensitivity and accuracy, while nuclei acid test, chest CT scans and serological test are more sensitive but they are time- and cost-consuming. Thus, a rapid and high-throughput detection platform with high accuracy and sensitivity is of importance for COVID-19 detection. Since our laboratory has already shown droplet microarray platform could achieve simultaneous detection of HIV-1 and HIV-2 nucleic acids with a limit of detection of 50 pM, I could hypothesize that droplet microarray platform might be used as a rapid, time- and cost-saving, and high-throughput detection platform for COVID19 detection. In addition, utilizing the same mechanism as pregnancy test kit (immune colloidal gold technique), rapid visual diagnosis can be easily achieved on droplet microarray platform. Antibodies labeled with colloidal gold particles might be possible to modified on spots of droplet microarray slides and testing samples could be further added to run the test in a nanoscale and rapid high-throughput manner. As for the readout, a document scanner could be used for scanning the color change of each individual spots and then an analyzing program should be further introduced to analyze it. However, since cell phone is an indispensable part of modern life, a more rapid and intelligent method is using the camera of the cell phone. Taking a picture by a cell phone of the test and then import this picture into a well-established cell phone application. By the automatic analysis function of the application, the results then could be presented in a direct and visual manner. For achieving this, more communication and collaboration must be done including computational science, artificial intelligence, biology, and materials science.

The second promising application of droplet microarray platform is 3D cellular culture. Two approaches of 3D cell culture have emerged over the last several decades: organoid technology and organ-on-a-chip technology. 3D cellular models offer greater predictivity of gene and protein expression, metabolic function, and physiological and functional readouts than 2D cell culture models. By deducing culture conditions of human induced pluripotent stem cells, multicellular organoids could be obtained. Current organ-on-a-chip approaches mainly rely on combining different differentiated cells to emulate the native tissue composition. Since I have successfully demonstrated

the culture of human induced pluripotent stem cells on droplet microarray platform, droplet microarray platform could be used as 3D cell culture platform by directed differentiation of human induced pluripotent stem cells and controlled assembly of cells to form organoid-on-a-chip and organ-on-a-chip with precise initial size, composition and spatial organization.

There are other attractive topics in the field of droplet microarray platform based on the research, such as combining human induced pluripotent stem cells with new and powerful genome editing and spatiotemporal control of gene expression (CRISPR/Cas9), chemically programmed tissue assembly, and 3D bioprinting. Integrated approaches including techniques mentioned above but not limited to them will provide crucial insight into further research in pharmacology, human development, disease, and other related fields.

5 Appendix

5.1 High-throughput screening of cell transfection enhancers using miniaturized droplet microarray
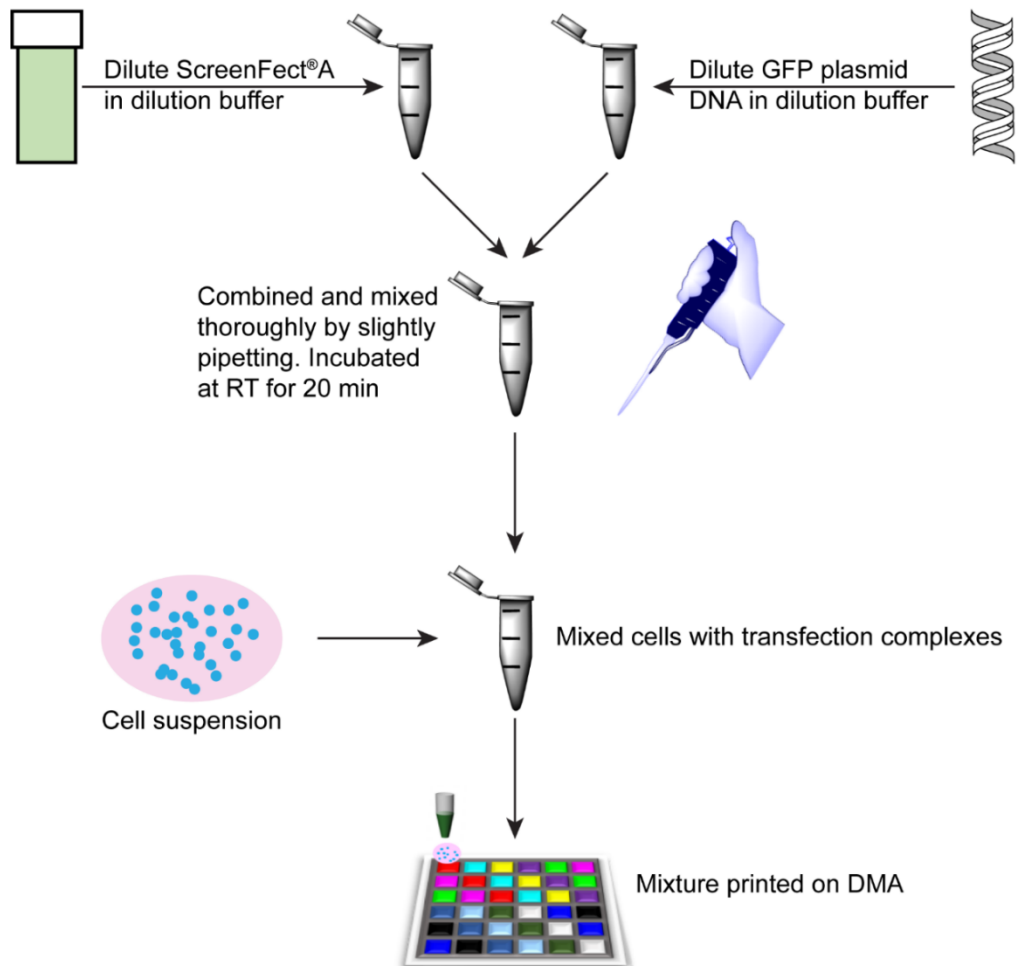

Figure A 1. Schematic showing the process of transfection mixture preparation and subsequently printed on DMA. Briefly, a certain amount of ScreenFect®A transfection reagent was diluted in 10 μL ScreenFect dilution buffer and a certain of GFP plasmid DNA was diluted in 10 μL ScreenFect dilution buffer, prior to combining and mixing them thoroughly by slight pipetting. The mixture was then incubated at RT for 20 min to allow the formation of transfection complex, followed by cell suspension introducing and mixing. Then the transfection mixture was printed onto each individual spot on DMA slides at the volume of 20 nL and 100 nL for 500 μm and 1mm DMA, respectively.
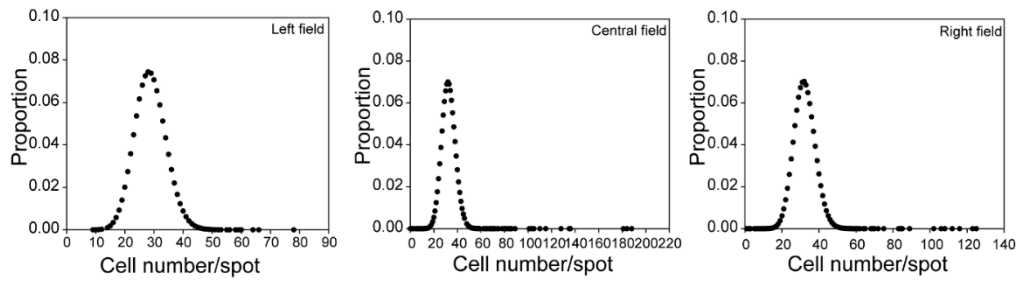
Figure A 2. Cell distribution after printing on three fields of DMA. The distribution of printed cells was plotted in Excel program by using Poisson function.
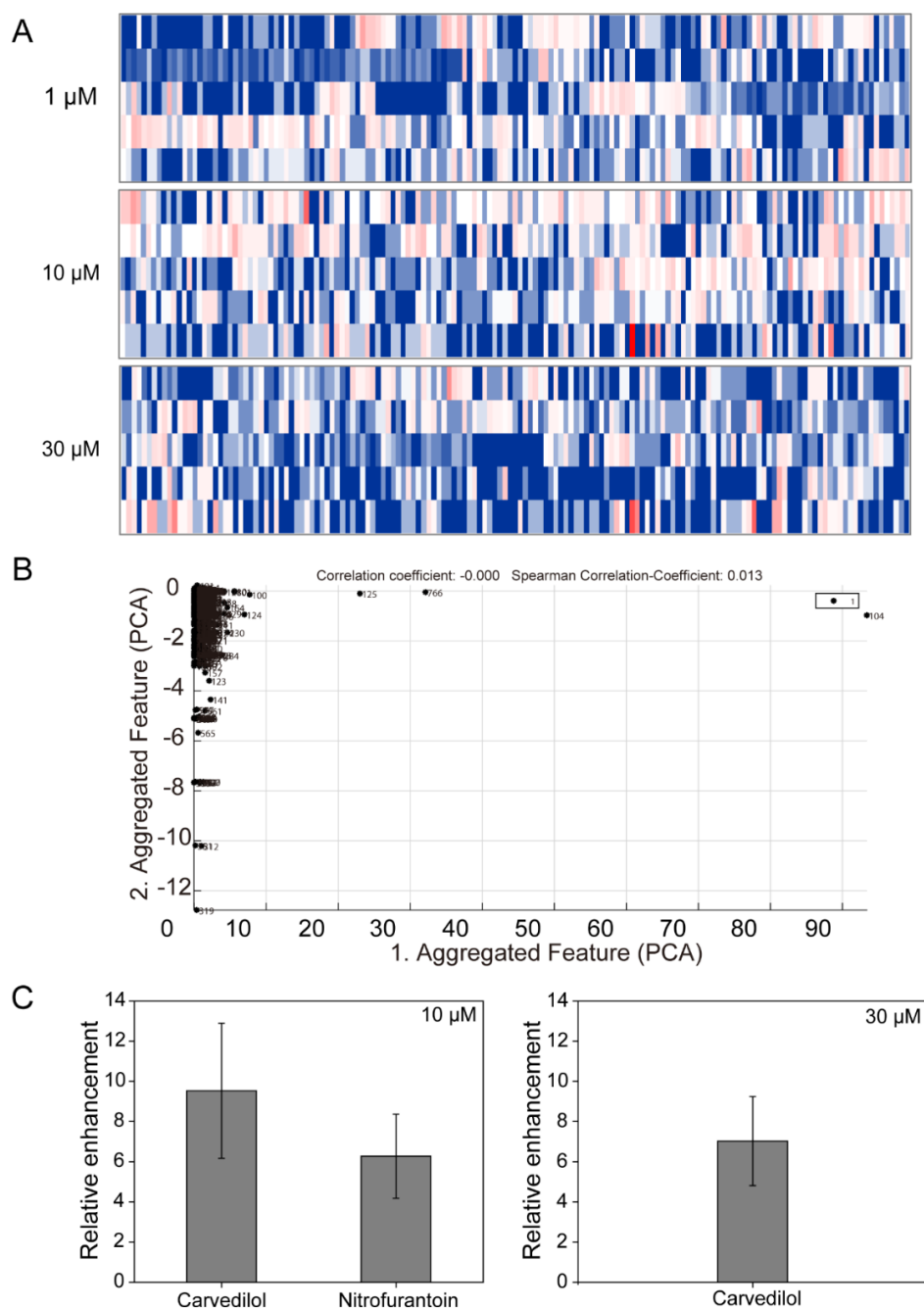
Figure A 3. Primary transfection enhancer screening results of Jurkat cells. Impact of FDA-approved drugs on transfection efficiency of CHO-K1 cells. (A) Heatmaps showed the impact of FDA-approved drugs on Jurkat cells at three concentrations (1, 10, and 30 µM). The heatmaps were generated according to the quantified relative transfection efficiency data, which was obtained from in total 20,898 individual experiments (three technical repeats and three biological repeats). The three heatmaps were sorted altogether by enhancement level of gene transfection compared to positive (drug-free) control. The blue patch and red patch represented a decrease and increase compared to drug-free control (white patch at the upper left corner), respectively. (B) Principal component analysis (PCA) graph showed

overview of impact of FDA-approved drugs on transfection efficiency of Jurkat cells. Numbers accompanied with each dot represented drugs in the FDA-approved library.
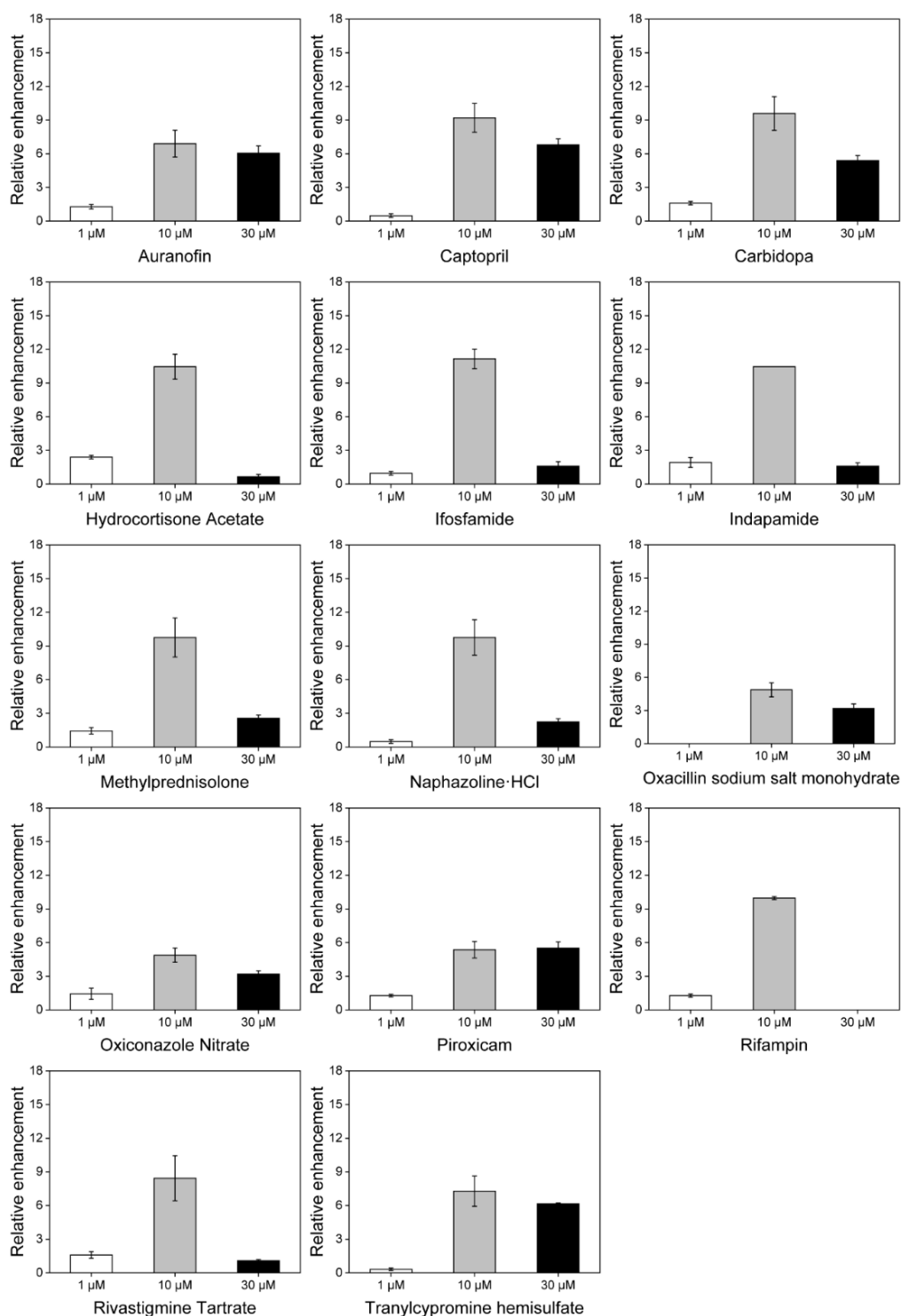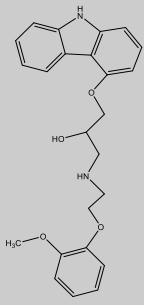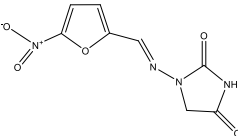

Figure A 4. Primary screening: fourteen hit compounds on CHO-K1 transfection. The relative transfection enhancement results of the 14 hit compounds at three concentrations (1, 10 and 30 µM) from the primary screening results of CHO-K1 cells. The relative transfection enhancement expressed as ratios

of GFP positive cell numbers for each drug over the mean GFP positive cell numbers of drug-free control. Data were presented as mean ± SD of three biological experiments with three technical repeats each time.

Table A 1. Hit compounds selected from primary screening of Jurkat cells. Two selected hits are selected for the secondary screening for Jurkat suspension cells and tabulated along with compound names, known therapeutic effects and structures.

Compound	Therapeutic effect	Structure
Carvedilol	Inhibitor of beta adrenoceptors	
Nitrofurantoin	Inhibitor of the citric acid cycle as well as synthesis of DNA, RNA, and protein	
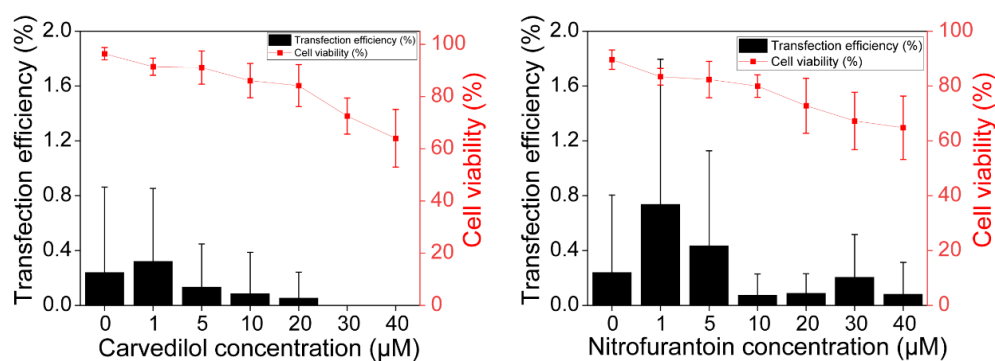
Figure A 5. Secondary screening results of impact of two hit compounds on Jurkat transfection. Jurkat cells were cultured in presence of respective compounds in concentrations varying from 1 to 40 µM on 1 mm DMA for 24 h. Cells were then stained with Hoechst 33342 (33.3 µg/mL) to visualize cell nucleus and PI (6.7 µg/mL) to distinguish dead cells. DMA was then placed in a petri cell culture incubator for 15 minutes. Images of spots were taken using the Olympus IX81 inverted motorized microscope. The number of GFP positive, Hoechst 33342 and PI positive cells were counted using ImageJ. Cell viability was calculated as following equation: Cell viability (%) = 1 - (PI positive cell numbers/Hoechst positive cell numbers) ×100. The transfection efficiency was calculated as the

following equation: Transfection efficiency (%) = (GFP positive cell numbers/Hoechst positive cell numbers) ×100. Data were presented as mean ± SD of three biological experiments with ten technical repeats each time.
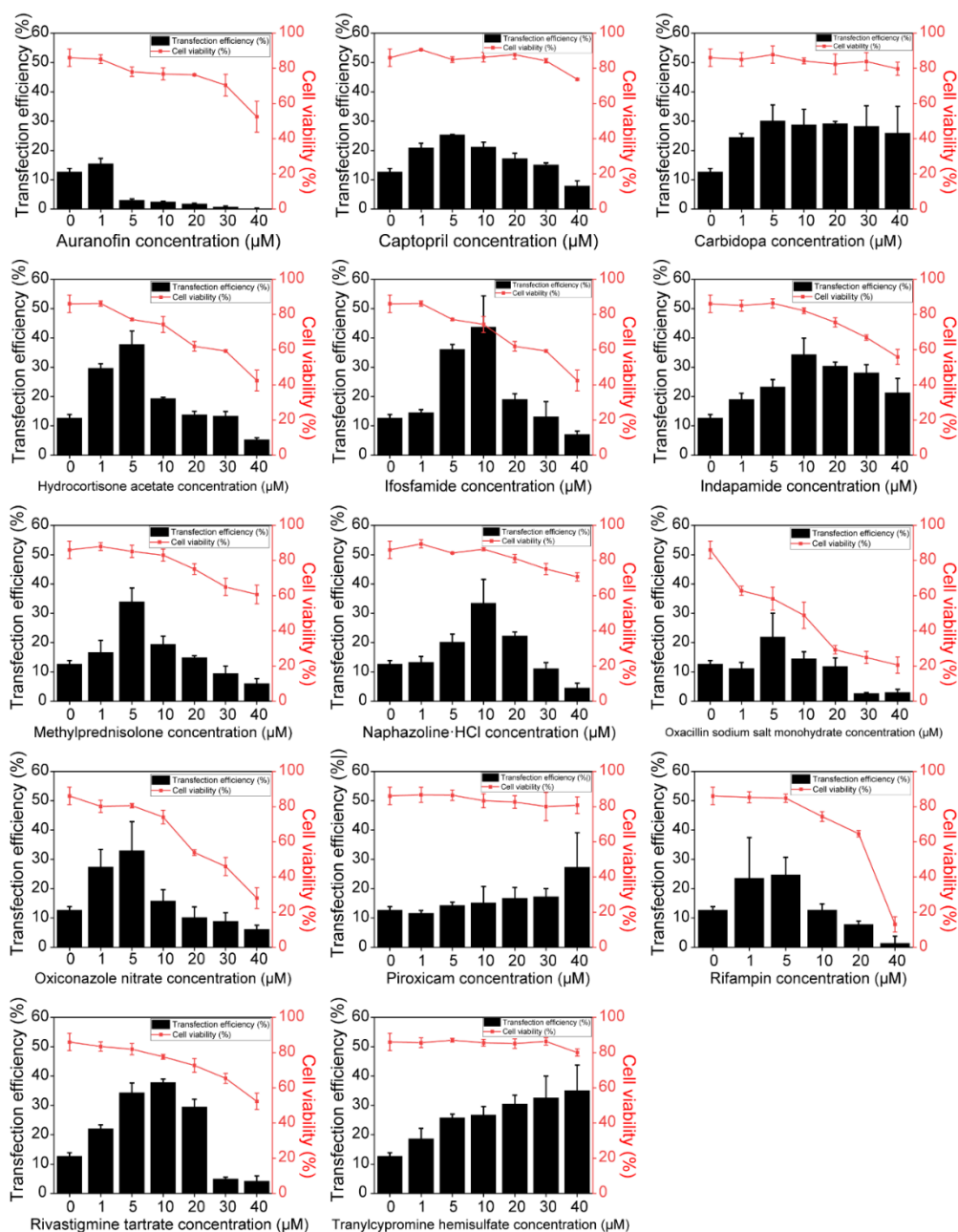
Figure A 6. Impact of fourteen hit compounds on HEK293T cell transfection on 1 mm DMA. Fourteen hit compounds (auranofin, captopril, carbidopa, hydrocortisone acetate, ifosfamide, indapamide, methylprednisolone, naphazoline·HCl, oxacillin sodium salt monohydrate, oxiconazole nitrate, piroxicam, rifampin, rivastigmine tartrate and tranylcypromine hemisulfate) were printed on DMA at diverse volumes. HEK293T cells were then cultured in the presence of each compounds in concentration varying from 1 to 40 µM on DMA for 24 h. Then the cells were stained by Hoechst 33342

and PI to visualize cell nuclear and dead cells, respectively. Graphs presented transfection efficiency and cell viability. Data were presented as mean ± SD of three biological experiments with ten technical repeats each time.

Table A 2. Most effective concentration of hit compounds in secondary screening on 1 mm DMA

Compound	Most effective concentration (µM)
Auranofin	1
Captopril	5
Carbidopa	5
Hydrocortisone acetate	5
Ifosfamide	10
Indapamide	10
Methylprednisolone	5
Naphazoline·HCl	10
Oxacillin sodium salt monohydrate	5
Oxiconazole nitrate	5
Piroxicam	40
Rifampin	5
Rivastigmine tartrate	10
Tranylcypromine hemisulfate	40
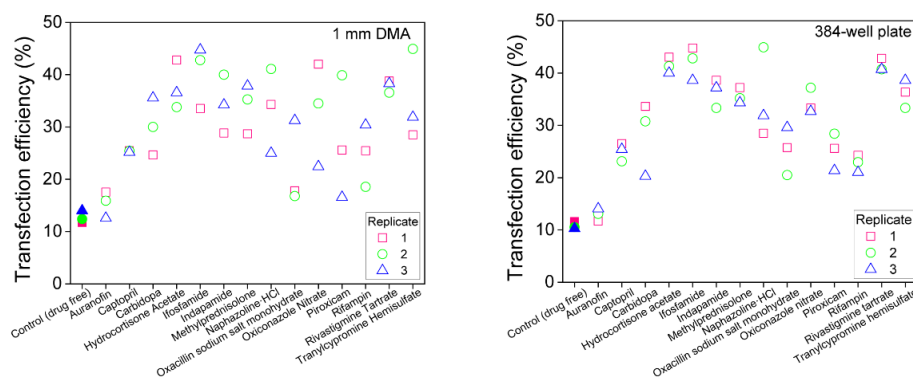
Figure A 7**. Impact of fourteen hit compounds on transfection of HEK293T cells on two platforms**. HEK293T cells were cultured in the presence of fourteen hit compounds under their most effective concentration (A) on DMA and (B) in 384-well plates in all three analyzed replicates. Transfection efficiency in every image taken/per spot (per well) is shown separately. The different shapes indicate individual replicates (replicate 1- square, replicate 2-circle and replicate 3- triangle). Optimal concentrations were used for each drug (see Table A2). The transfection complexes were prepared with 0.017 μL ScreenFect®A in 10 μL ScreenFect dilution buffer, followed by diluting a total of 17 ng GFP plasmid DNA in dilution buffer to a final volume of 10 μL (ratio of the ScreenFect®A-to-plasmid DNA is 1:1). Then 80 μL fresh cell suspension at a concentration of 7.13×104 cells/mL were added to complexes followed by mixing and seeding into each well at a volume of 20 μL/well. The volume used for DMA and 384-well plates were 100 nL and 20 μL, respectively. Data were presented as mean ± SD.
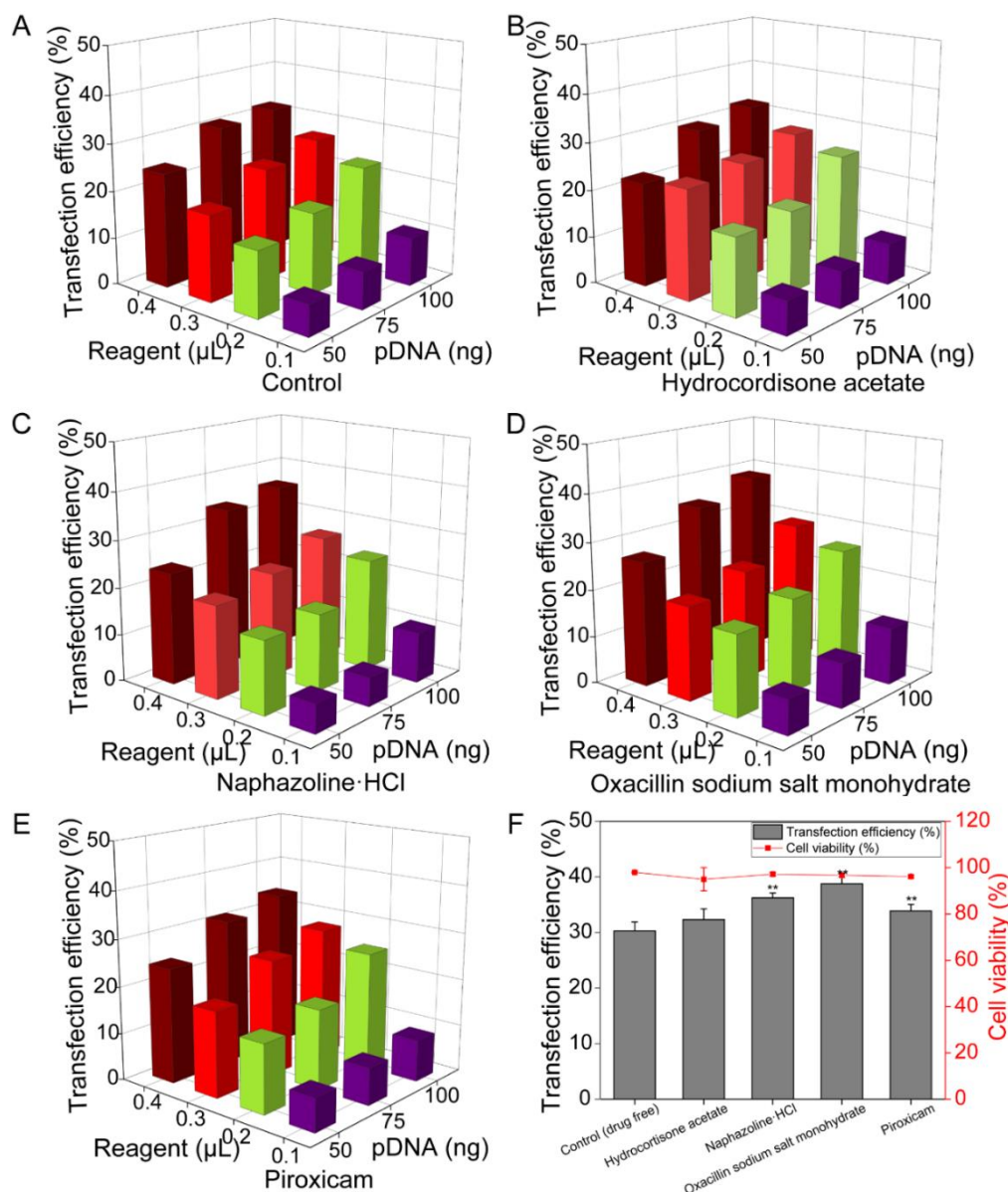
Figure A 8. Optimization for transfection of HEK293T cells with four selected hit compounds in 96-well plates. (A) Transfection optimization of HEK293T cells was conducted in 96-well plates in the absence of compounds. The transfection reagent volume and DNA amount were investigated. Transfection optimization of HEK293T cells in the presence of (B) hydrocortisone acetate at a working concentration of 5 µM, (C) naphazoline·HCl at a working concentration of 10 µM, (D) piroxicam at a working concentration of 40 µM, and oxacillin sodium salt monohydrate at a working concentration of 5 µM. (F) Overview of transfection efficiency under optimized conditions in the presence of compounds. Nine images of each well were taken and analyzed. Graphs showed the transfection efficiency and cell viability. Data were presented as mean ± SD. ** was defined as $P < 0.01$.

5.2 Miniaturized droplet microarray platform enables maintenance of human induced pluripotent stem cell pluripotency
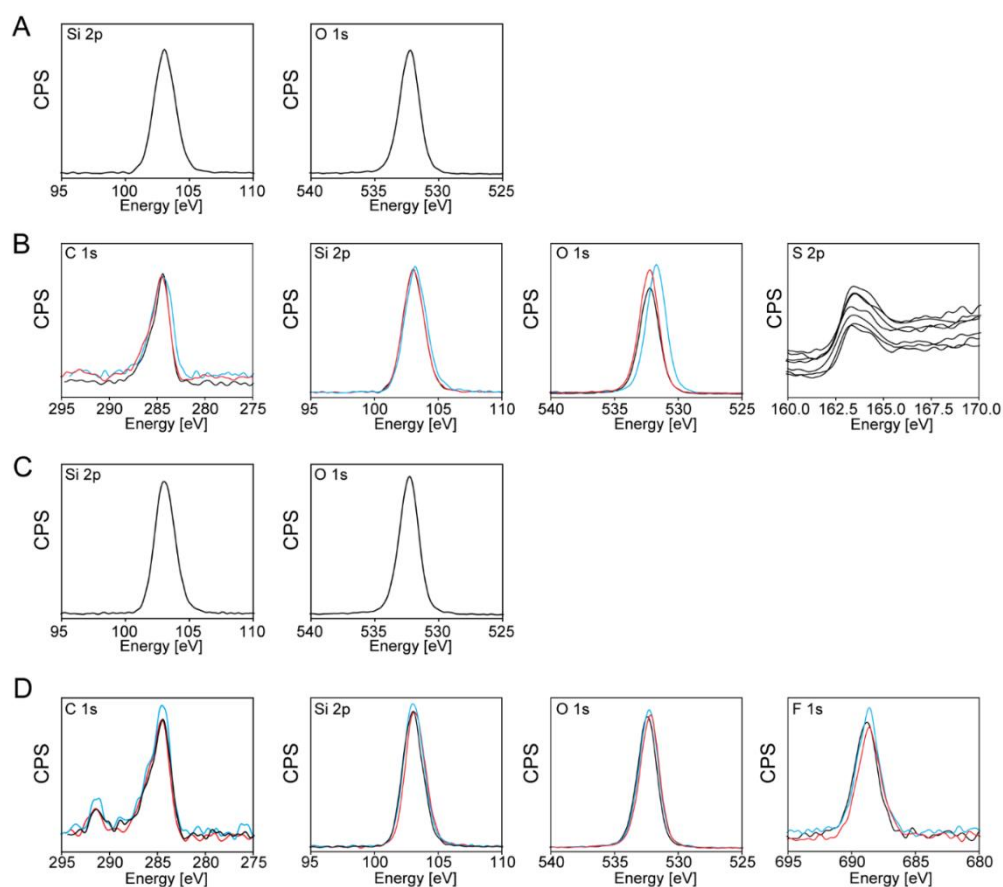
Figure A 9. Narrow XPS scan of TA and TB surfaces. (A) High-resolution XPS spectra of the Si 2p and O 1s peaks measured on the TA surface. (B) Three repetitive high-resolution scans of C 1s, Si 2p, O 1s, and F 1s peaks measured on the TA surface. Blue, red, and black curves indicate the three independent spots, respectively. (C) High-resolution XPS spectra of the Si 2p and O 1s peaks measured on the TB surface. (D) High-resolution scans of C 1s, Si 2p, O 1s, and S 2p peaks analyzed on the TB surface. Blue, red, and black curves indicate three individual spots of high-resolution scans, respectively. To trace sulfur, ten scans were conducted without scanning other energies except carbon in order to avoid removal of sulfur from the sample.
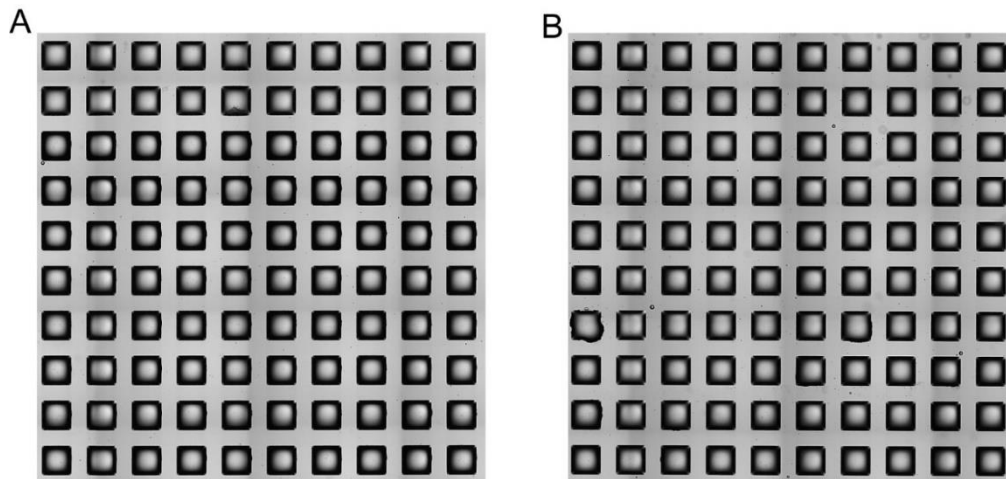
Figure A 10. Bright field images of hiPSCs printed on DMAs. The hiPSCs were printed with the volume of 200 nL/spot on (A) ME and (B) PA DMA. The side length of each square spot is 1 mm.
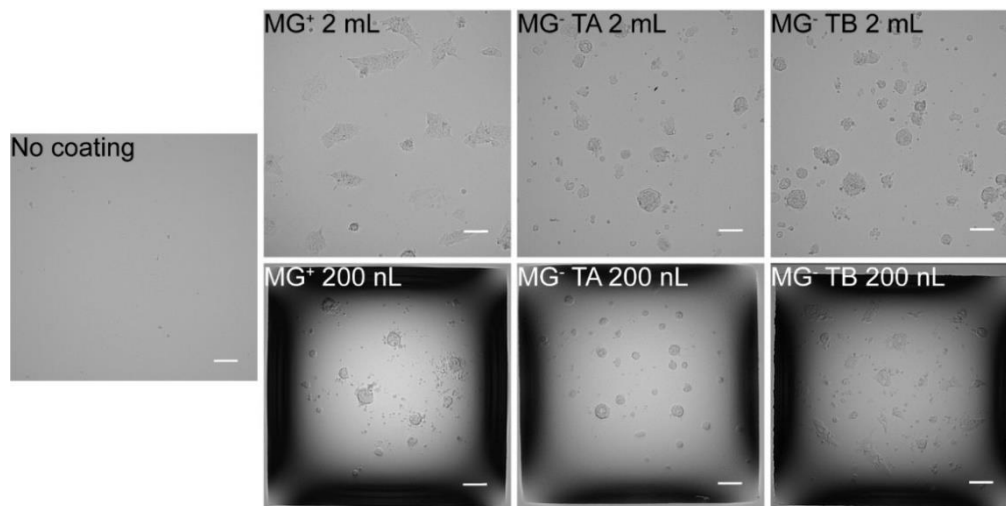
Figure A 11. Morphology of hiPSCs cultured on surfaces with big volumes (MG+ 2 mL, MG- TA 2 mL, and MG- TB 2 mL) and on DMAs with small volumes (MG+ 200 nL, MG- TA 200 nL, and MG- TB 200 nL). Scale bar: 100 μm.
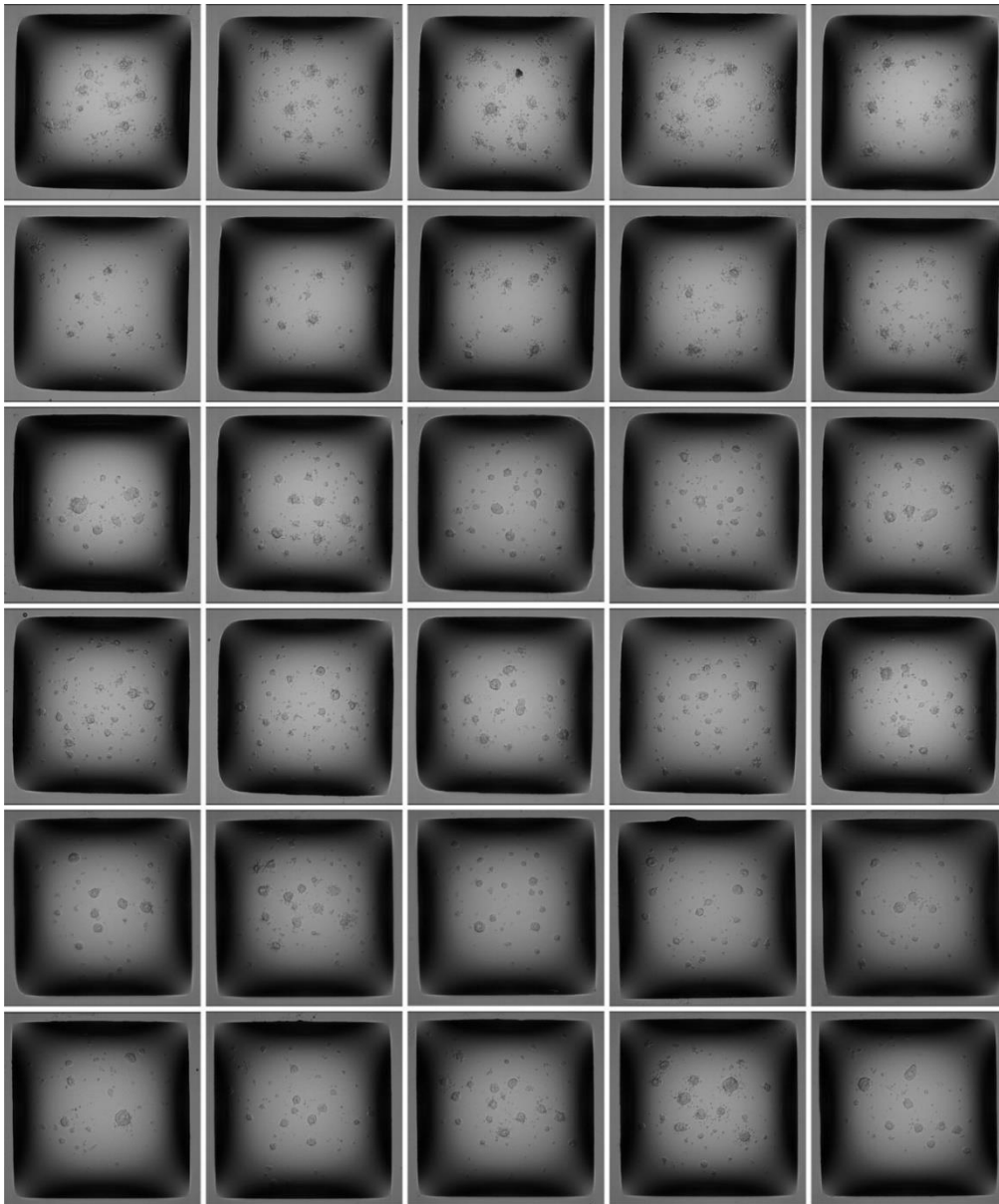
Figure A 12. Bright field images presenting hiPSCs morphology on TA DMA. Thirty bright field images were presented to show the statistic of cell morphology for hiPSCs cultivated for 24h on TA DMA. The size length of each square spot is 1 mm.
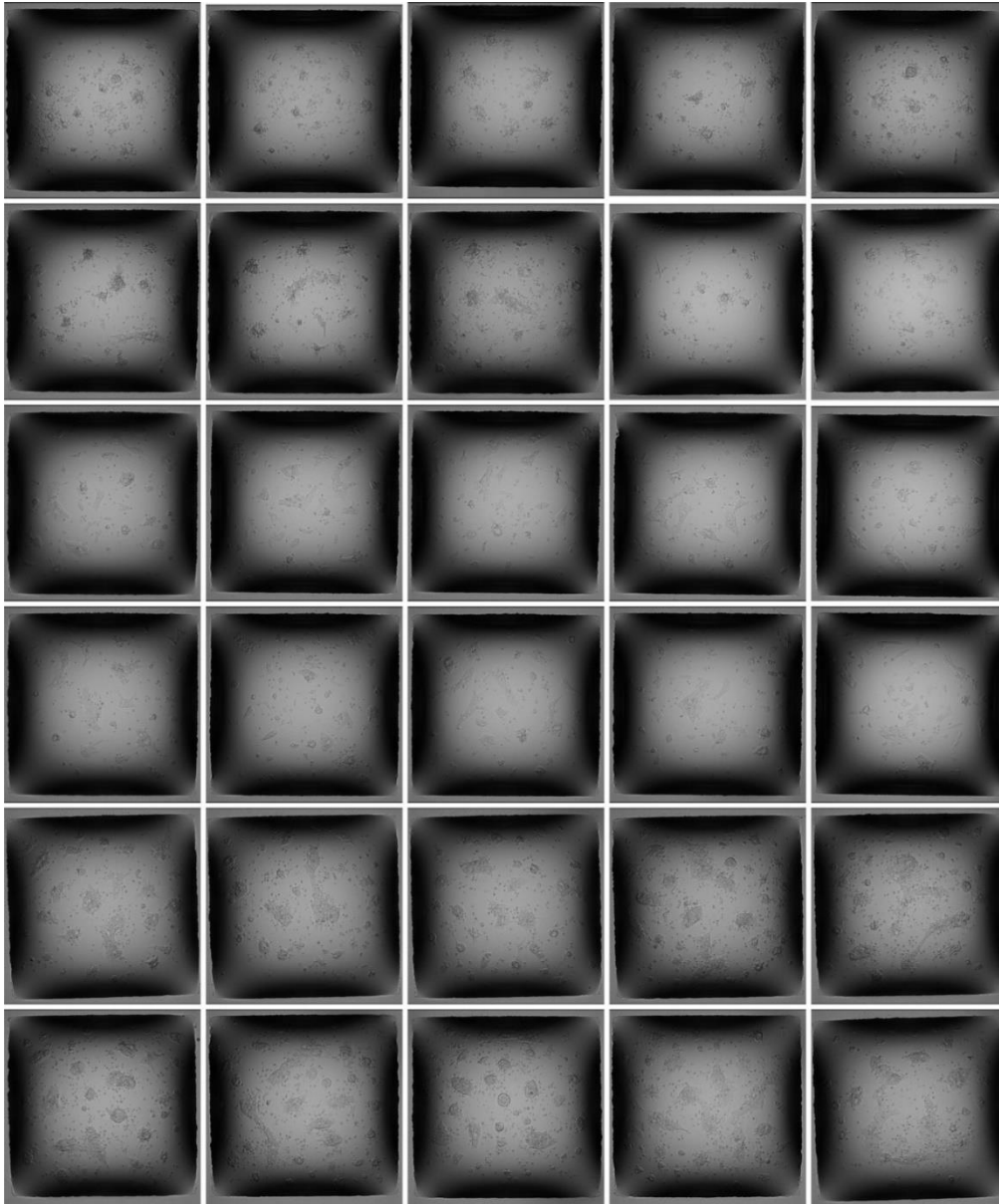
Figure A 13. Bright field images presenting hiPSCs morphology on TB DMA. Thirty bright field images were presented to show the statistic of cell morphology for hiPSCs cultivated for 24h on TB DMA. The size length of each square spot is 1 mm.
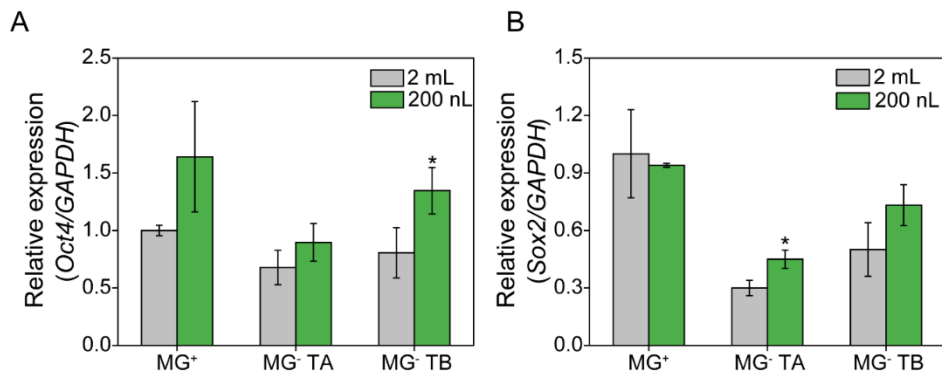
Figure A 14. Oct4 and Sox2 gene expression of HiPSCs cultivated on TA and TB surfaces and DMAs. Quantitative real-time PCR showed (A) *Oct4* and (B) *Sox2* pluripotency gene expression of hiPSCs grown on MG+ surface (MG+ 2 mL), MG+ DMA (MG+ 200 nL), MG- TA surface (MG- TA 2mL), MG- TB surface (MG- TB 2mL), MG- TA DMA (MG- TA 200 nL), MG- TB DMA (MG- TA 200 nL). All the data of gene expression were normalized with reference gene *GAPDH*. * indicates $p < 0.05$, which means significantly different between 2 mL and 200 nL groups.

5.3 Rapid high throughput combinatorial screening of protein coatings on miniaturized droplet microarray identifies novel cell culture substrates to maintain pluripotency of hiPSCs
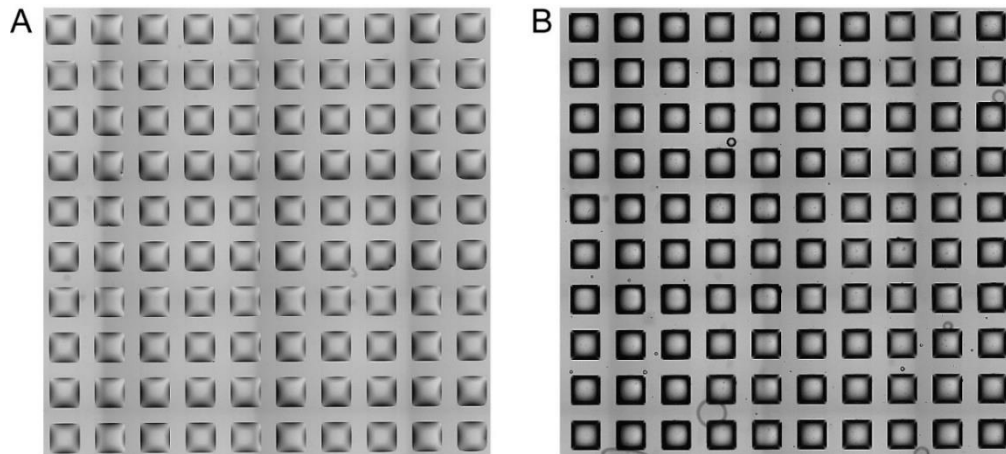
Figure A 15. Images of DMA with Matrigel and hiPSCs cells. Representative bright field images displayed (A) 1% Matrigel solution printed as 60 nL/spot on DMA and followed by (B) 200 nL/spot hiPSCs cell suspension was added. Each spot is a square with side length of 1 mm.
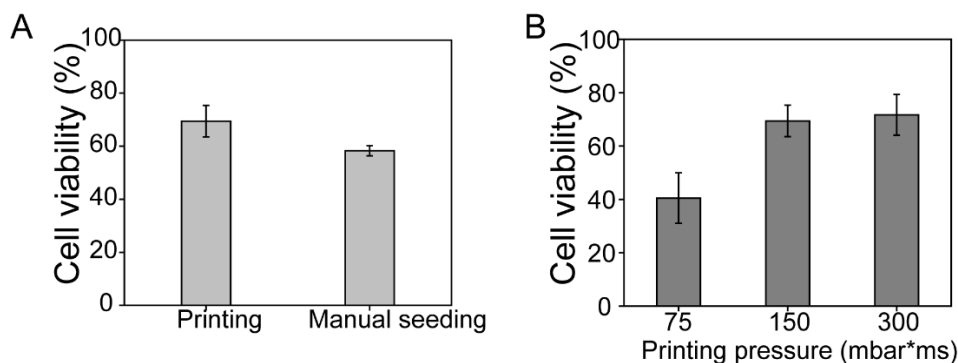
Figure A 16. Cell viability comparison (A) Cell viability comparison of cells seeded by non-contact printer and manual standing droplet seeding method and further cultured for 24 h. (B) The cell viability of hiPSCs printed by different printing pressure (75, 150, and 300 mbar*ms. The live cell coverage for printing and manual seeding were 69.43 ± 5.90 % and 58.28 ± 1.90 %, respectively. The cell viability of cells printed by 75, 150, and 300 mbar*ms after 24 h incubation were 40.50 ± 9.47 %, 69.43 ± 5.90 %, and 71.70 ± 7.63 %, respectively. The lower cell viability of 75 mbar*ms was due to the lower cell clusters numbers printed on droplets with a low printing pressure. No significant difference of the survival of cells printed by 150 and 300 mbar*ms was observed. Data represented as mean $\pm$ SD.
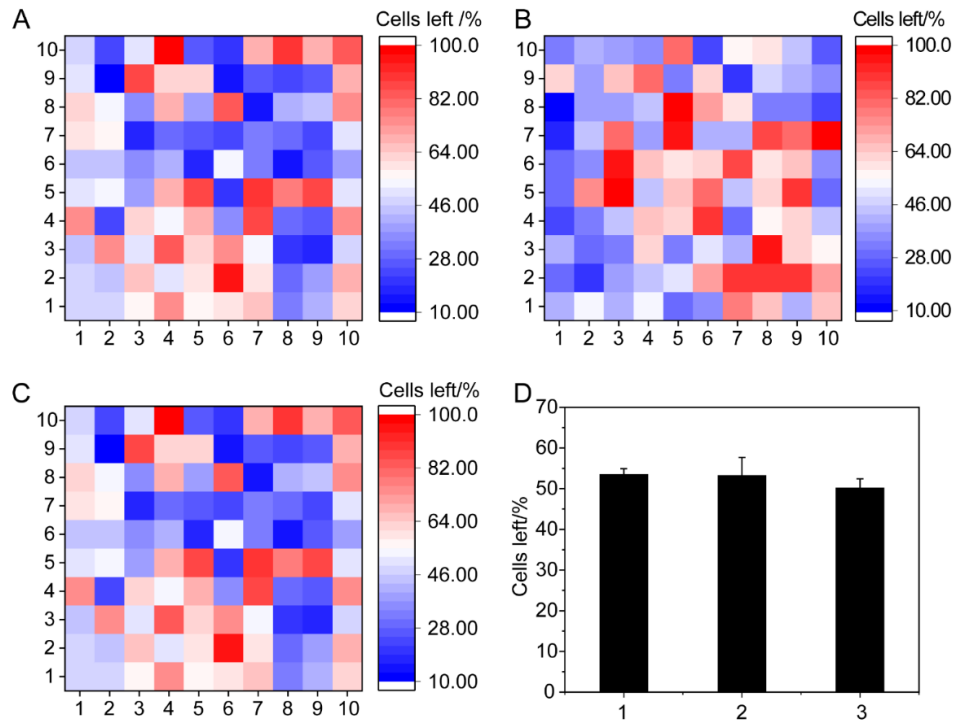
Figure A 17. Statistical analysis of hiPSC cells left after IF staining. (A-C) Statistical estimation of cells left after the whole IF staining procedure for three repeats. Each cell represented one single spot on DMA at corresponding position. (D) The graph showed the average cells left for each repeat. Around 50% hiPSCs were left after several times washing in IF staining and there was no significance among repeats.
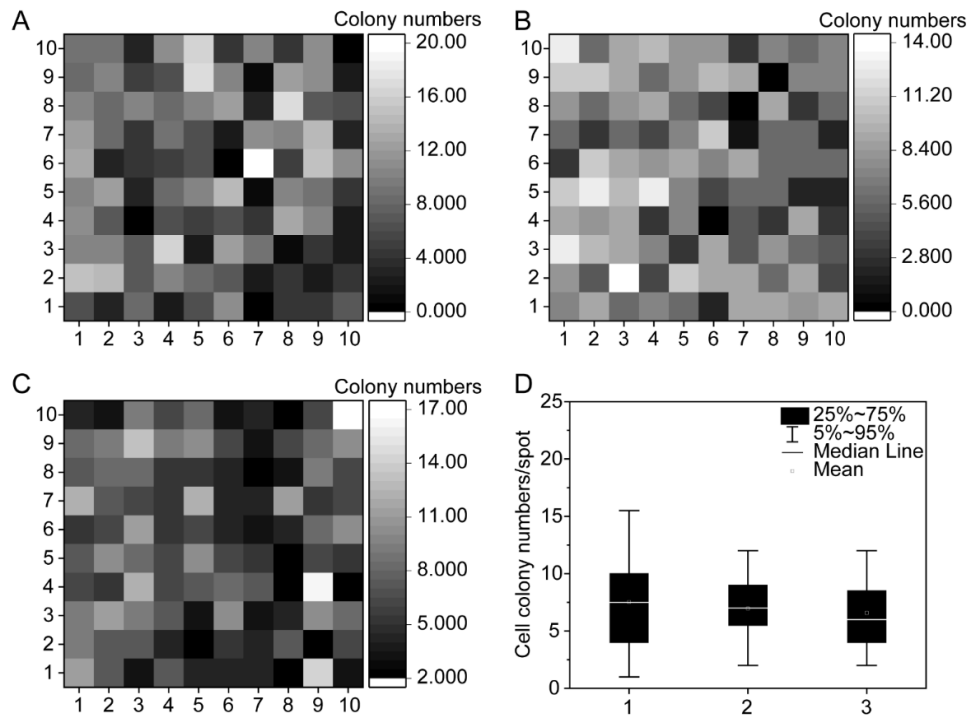
Figure A 18. Statistical analysis of hiPSC colonies left after IF staining. (A-C) Statistical estimation of hiPSCs colonies numbers after the whole IF staining procedure for three repeats. Each cell represented one single spot on DMA at corresponding position. (D) The graph showed the average hiPSCs colonies numbers for each repeat. Approximately seven hiPSCs colonies were left after several times washing in IF staining and there was no significance among repeats.
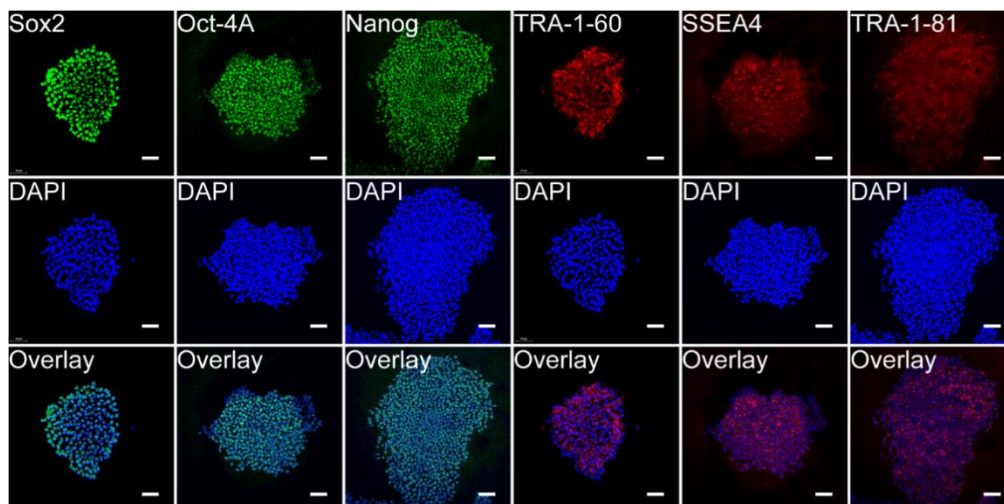
Figure A 19. Six pluripotency markers staining of hiPSCs on Matrigel coated well plates. Representative confocal laser scanning microscope (CLSM) images of hiPSCs cultivated on well plates coated with Matrigel stained for six pluripotency markers: Sox2, Oct-4A, Nanog, green fluorescence;

TRA-1-60, SSEA4, TRA-1-81, red fluorescence. Three independent experiments were conducted (n=3) obtaining comparable results. DAPI was used to counterstain nuclei. Scale bar: 50 μm.
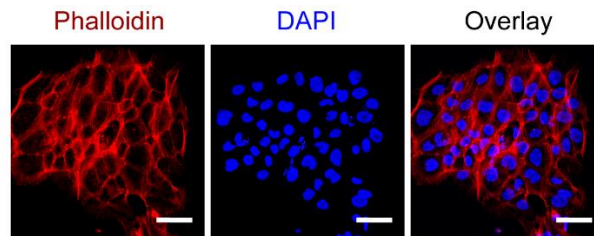
Figure A 20. The CLSM images of F-actin cytoskeletal organization (red). Cells seeded on MG coated DMA showed nicely spreading and well-organized actin stress fibers, indicating the feasibility of using DMA for hiPSCs cultivation. Scale bar: 50 μm.
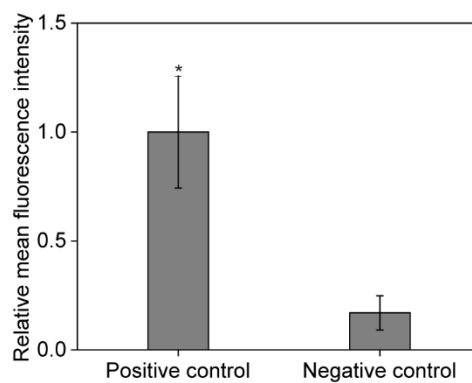
Figure A 21. Relative mean fluorescence intensity of E-cadherin expression for positive and negative controls. The mean fluorescence intensity were calculated from three-independent IF staining images for E-cadherin and normalized with positive control.
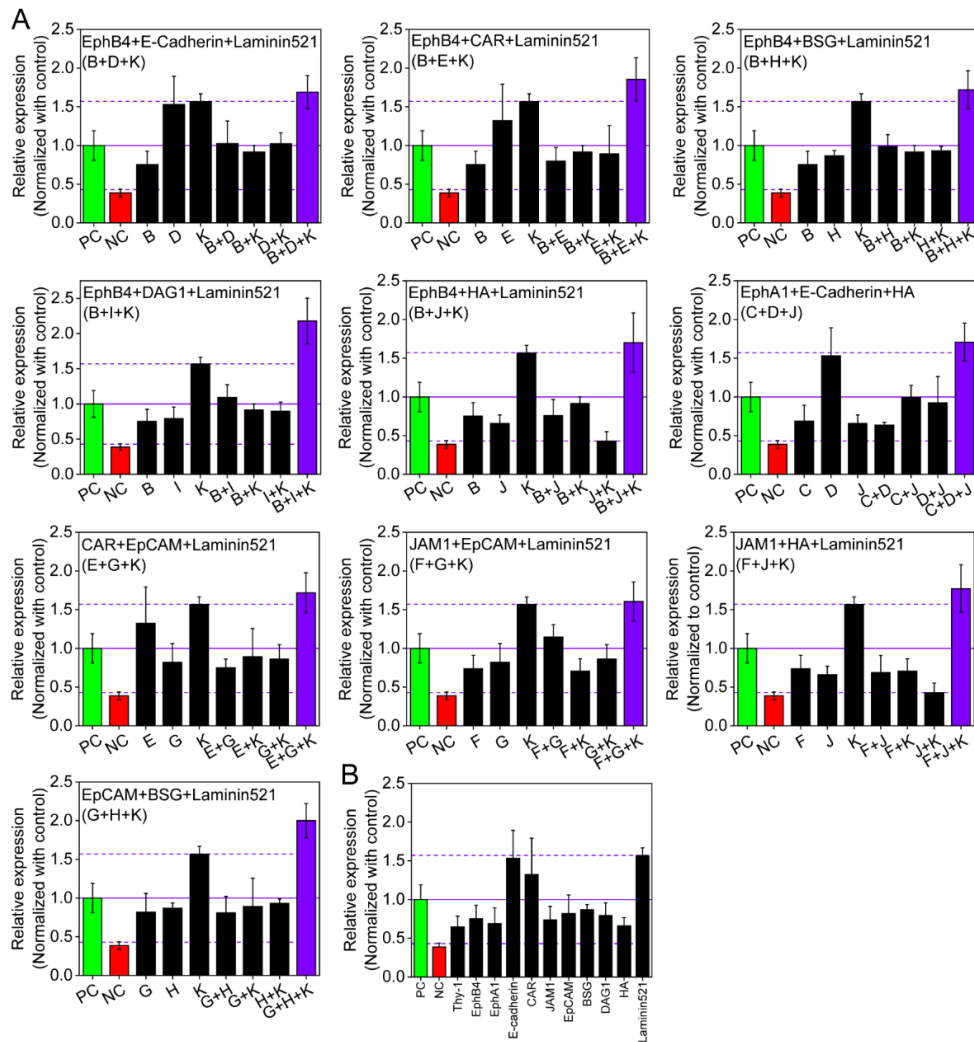
Figure A 22. Primary screening results. (A) Figure showed results of ten hits from the primary screening. HiPSCs were cultured on DMA in the presence of respective proteins for 24 h, followed by IF staining of pluripotency marker Nanog. Mean fluorescence intensity of each individual spot was analyzed and normalized with positive control. The threshold was set was mean + 3SD. Green column demonstrated positive control, red column demonstrated negative control and violet column demonstrated hits. (B) Relative Nanog expression investigated by IF staining of each single protein. Data represented as mean ± SD.
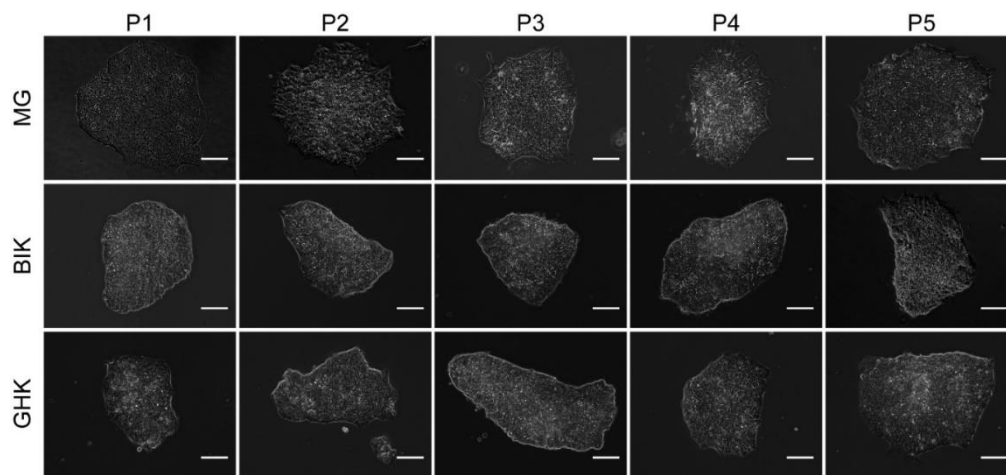
Figure A 23. Representative phase contrast images of hiPSCs colonies through five passages on MG, BIK, and GHK coated well plates. Scale bar: 100 μm.
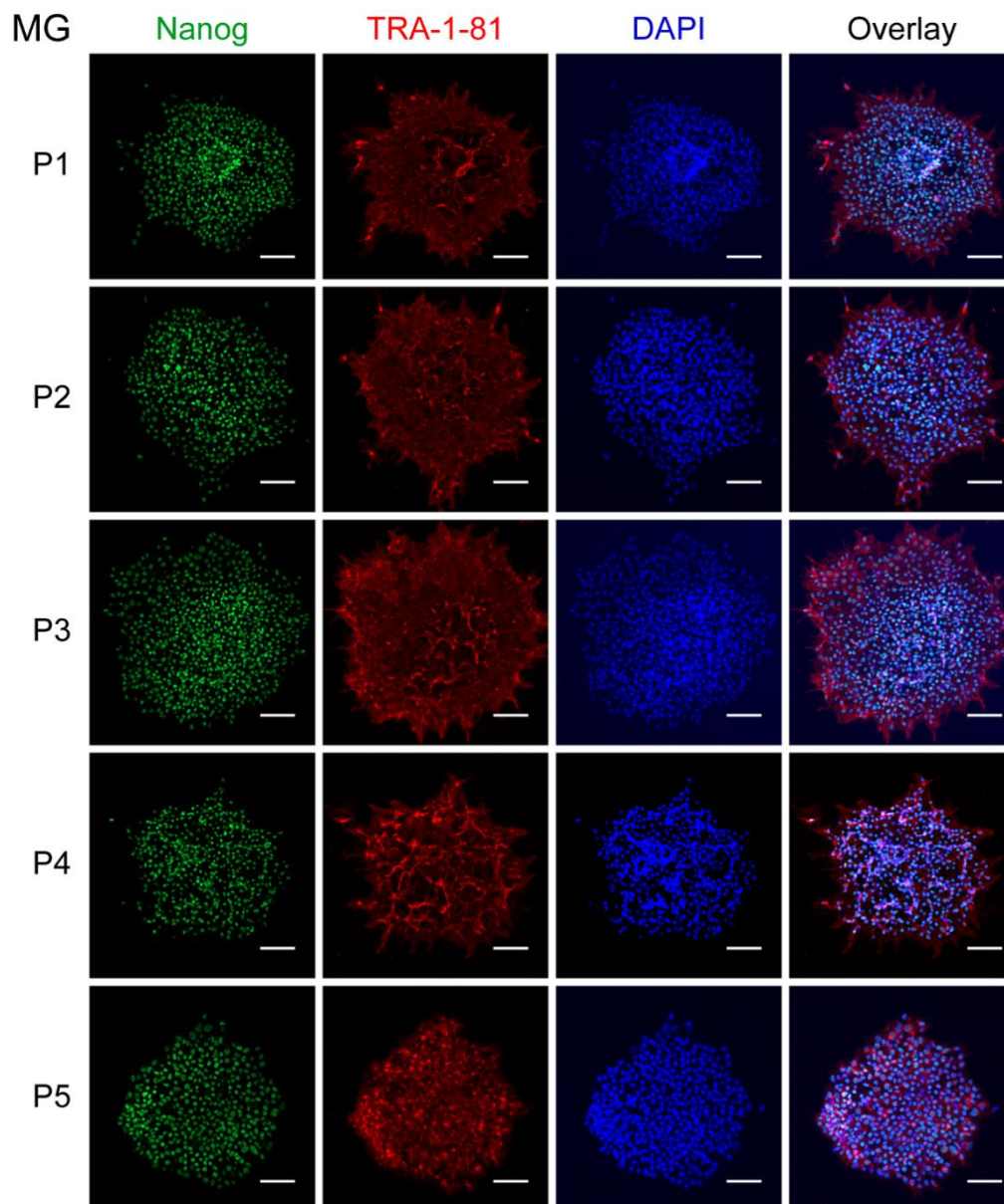
Figure A 24. Positive IF for pluripotency markers Nanog and TRA-1-81 of five passages (P1-P5) of hiPSCs on MG coating. DAPI was used to counterstain cell nuclear. Scale bar: 50 μm.
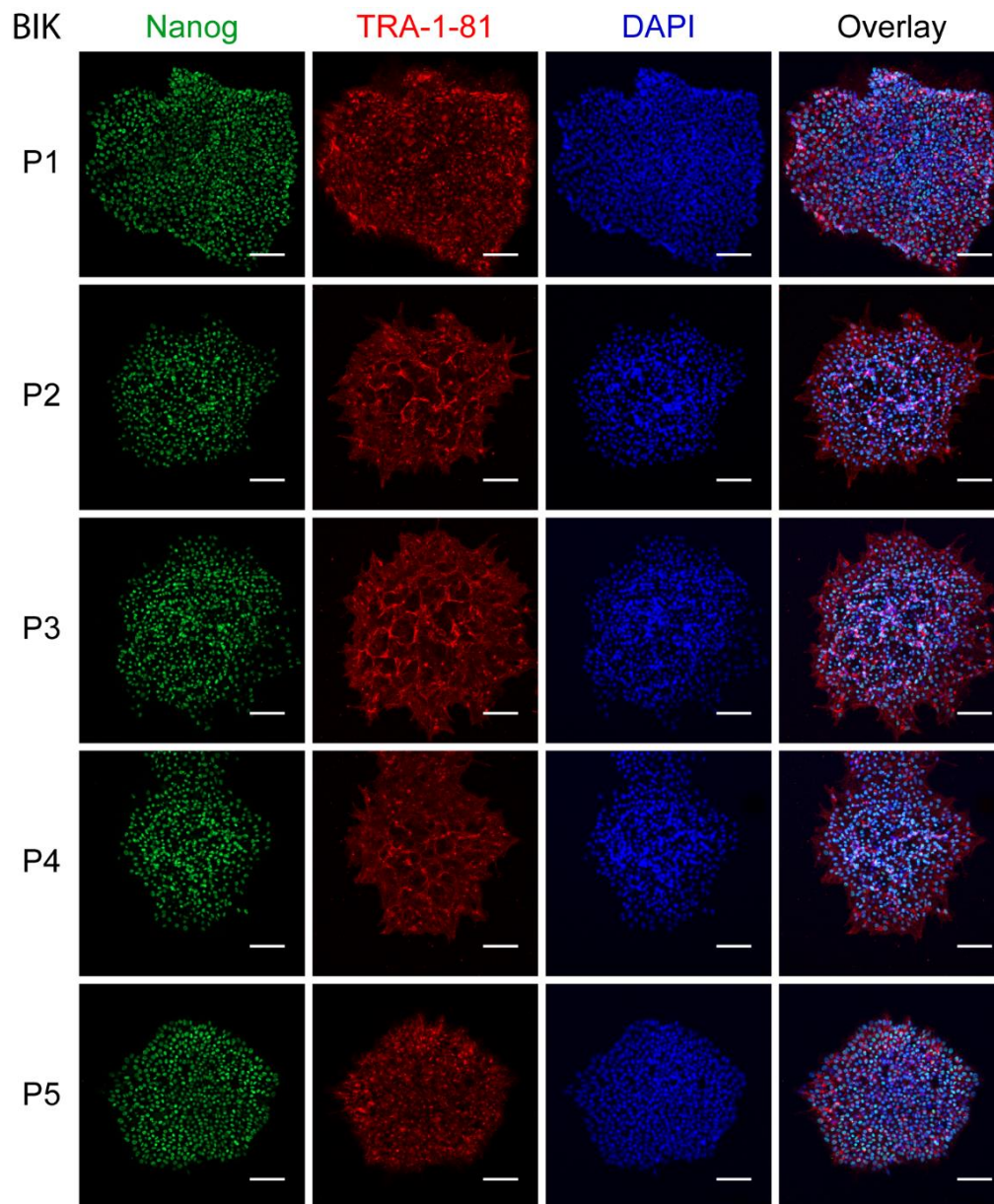
Figure A 25. Positive IF for pluripotency markers Nanog and TRA-1-81 of five passages (P1-P5) of hiPSCs on BIK coating. DAPI was used to counterstain cell nuclear. Scale bar: 50 μm.
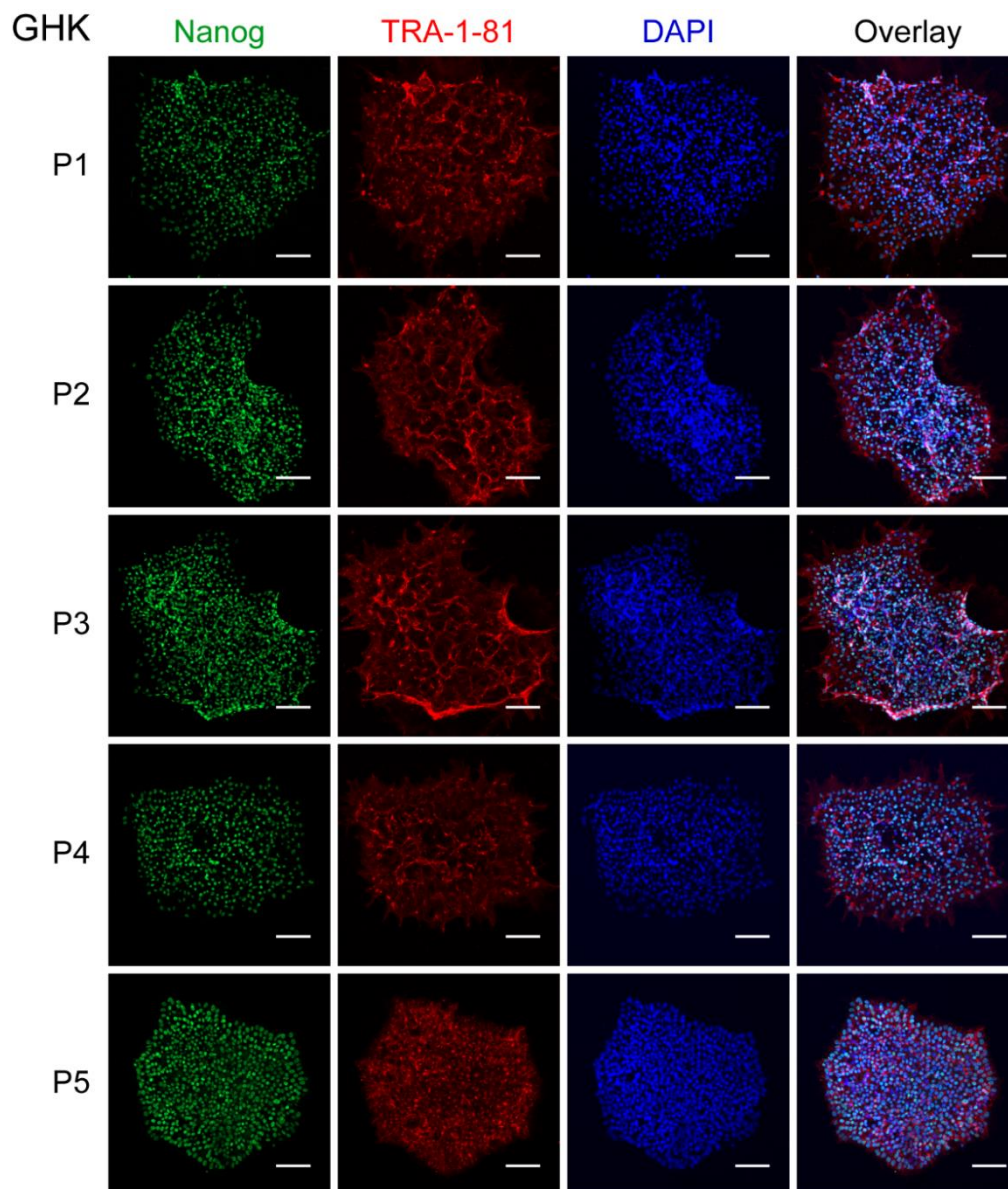
Figure A 26. Positive IF for pluripotency markers Nanog and TRA-1-81 of five passages (P1-P5) of hiPSCs on BIK coating. DAPI was used to counterstain cell nuclear. Scale bar: 50 μm.

References

Abranches, E., Guedes, A.M.V., Moravec, M., Maamar, H., Svoboda, P., Raj, A., & Henrique, D. (2014). Stochastic NANOG fluctuations allow mouse embryonic stem cells to explore pluripotency. *Development* **141**, 2770-2779.

Adams, D., Gonzalez-Duarte, A., O'Riordan, W.D., Yang, C.C., Ueda, M., Kristen, A.V., Tournev, I., Schmidt, H.H., Coelho, T., Berk, J.L., Lin, K.P., Vita, G., Attarian, S., Plante-Bordeneuve, V., Mezei, M.M., Campistol, J.M., Buades, J., Brannagan, T.H., Kim, B.J., Oh, J., Parman, Y., Sekijima, Y., Hawkins, P.N., Solomon, S.D., Polydefkis, M., Dyck, P.J., Gandhi, P.J., Goyal, S., Chen, J., Strahs, A.L., Nochur, S.V., Sweetser, M.T., Garg, P.P., Vaishnaw, A.K., Gollob, J.A., & Suhr, O.B. (2018). Patisiran, an RNAi Therapeutic, for Hereditary Transthyretin Amyloidosis. *New Engl J Med* **379**, 11-21.

Adams, D., Suhr, O.B., Dyck, P.J., Litchy, W.J., Leahy, R.G., Chen, J.H., Gollob, J., & Coelho, T. (2017). Trial design and rationale for APOLLO, a Phase 3, placebo-controlled study of patisiran in patients with hereditary ATTR amyloidosis with polyneuropathy. *Bmc Neurol* **17**, 1-12.

Al-Zaidy, S., Pickard, A.S., Kotha, K., Alfano, L.N., Lowes, L., Paul, G., Church, K., Lehman, K., Sproule, D.M., Dabbous, O., Maru, B., Berry, K., Arnold, W.D., Kissel, J.T., Mendell, J.R., & Shell, R. (2019). Health outcomes in spinal muscular atrophy type 1 following AVXS-101 gene replacement therapy. *Pediatr Pulmonol* **54**, 179-185.

Alisson-Silva, F., Rodrigues, D.D., Vairo, L., Asensi, K.D., Vasconcelos-dos-Santos, A., Mantuano, N.R., Dias, W.B., Rondinelli, E., Goldenberg, R.C.D., Urmenyi, T.P., & Todeschini, A.R. (2014). Evidences for the involvement of cell surface glycans in stem cell pluripotency and differentiation. *Glycobiology* **24**, 458-468.

Amin, H.I., Ai, E., McDonald, H.R., & Johnson, R.N. (2000). Retinal toxic effects associated with intravitreal fomivirsen. *Arch Ophthalmol-Chic* **118**, 426-427.

An, W.F., & Tolliday, N. (2010). Cell-Based Assays for High-Throughput Screening. *Molecular Biotechnology* **45**, 180-186.

Arya, D.P., Coffee, R.L., Willis, B., & Abramovitch, A.I. (2001). Aminoglycoside-nucleic acid interactions: Remarkable stabilization of DNA and RNA triple helices by neomycin. *J Am Chem Soc* **123**, 5385-5395.

Arya, D.P., Xue, L., & Willis, B. (2003). Aminoglycoside (neomycin) preference is for A-form nucleic acids, not just RNA: Results from a competition dialysis study. *J Am Chem Soc* **125**, 10148-10149.

Astriab-Fisher, A., Sergueev, D.S., Fisher, M., Shaw, B.R., & Juliano, R.L. (2000). Antisense inhibition of P-glycoprotein expression using peptide-oligonucleotide conjugates. *Biochem Pharmacol* **60**, 83-90.

Aumailley, M., Bruckner-Tuderman, L., Carter, W.G., Deutzmann, R., Edgar, D., Ekblom, P., Engel, J., Engvall, E., Hohenester, E., Jones, J.C.R., Kleinman, H.K., Marinkovich, M.P., Martin, G.R., Mayer, U., Meneguzzi, G., Miner, J.H., Miyazaki, K., Patarroyo, M., Paulsson, M., Quaranta, V., Sanes, J.R., Sasaki, T., Sekiguchi, K., Sorokin, L.M., Talts, J.F., Tryggvason, K., Uitto, J., Virtanen, I.,

von der Mark, K., Wewer, U.M., Yamada, Y., & Yurchenco, P.D. (2005). A simplified laminin nomenclature. *Matrix Biol* **24**, 326-332.

Barrett, L.E., Sul, J.Y., Takano, H., Van Bockstaele, E.J., Haydon, P.G., & Eberwine, J.H. (2006). Region-directed phototransfection reveals the functional significance of a dendritically synthesized transcription factor. *Nat Methods* **3**, 455-460.

Basiouni, S., Fuhrmann, H., & Schumann, J. (2012). High-efficiency transfection of suspension cell lines. *Biotechniques* **53**, 1-4.

Baxter, M.A., Camarasa, M.V., Bates, N., Small, F., Murray, P., Edgar, D., & Kimber, S.J. (2009). Analysis of the distinct functions of growth factors and tissue culture substrates necessary for the long-term self-renewal of human embryonic stem cell lines. *Stem Cell Res* **3**, 28-38.

Beachley, V.Z., Wolf, M.T., Sadtler, K., Manda, S.S., Jacobs, H., Blatchley, M.R., Bader, J.S., Pandey, A., Pardoll, D., & Elisseeff, J.H. (2015). Tissue matrix arrays for high-throughput screening and systems analysis of cell function. *Nat Methods* **12**, 1197-1204.

Becker, A.K., Erfle, H., Gunkel, M., Beil, N., Kaderali, L., & Starkuviene, V. (2018). Comparison of Cell Arrays and Multi-Well Plates in Microscopy-Based Screening. *High Throughput* **7**, 1-15.

Beers, J., Gulbranson, D.R., George, N., Siniscalchi, L.I., Jones, J., Thomson, J.A., & Chen, G.K. (2012). Passaging and colony expansion of human pluripotent stem cells by enzyme-free dissociation in chemically defined culture conditions. *Nat Protoc* **7**, 2029-2040.

Benz, M., Asperger, A., Hamester, M., Welle, A., Heissler, S., & Levkin, P.A. (2020). A combined high-throughput and high-content platform for unified on-chip synthesis, characterization and biological screening. *Nat Commun* **11**, 1-10.

Benz, M., Molla, M.R., Boser, A., Rosenfeld, A., & Levkin, P.A. (2019). Marrying chemistry with biology by combining on-chip solution-based combinatorial synthesis and cellular screening. *Nat Commun* **10**, 1-10.

Bernasconi, A.G.F., Rebuffat, A.G., Lovati, E., Frey, B.M., Frey, F.J., & Galli, I. (1997). Cortisol increases transfection efficiency of cells. *Febs Lett* **419**, 103-106.

Bleicher, K.H., Bohm, H.J., Muller, K., & Alanine, A.I. (2003). Hit and lead generation: Beyond high-throughput screening. *Nat Rev Drug Discov* **2**, 369-378.

Blinka, S., & Rao, S. (2017). Nanog Expression in Embryonic Stem Cells - An Ideal Model System to Dissect Enhancer Function. *Bioessays* **39**, 1700086.

Borchard, G. (2001). Chitosans for gene delivery. *Adv Drug Deliv Rev* **52**, 145-150.

Boyer, L.A., Lee, T.I., Cole, M.F., Johnstone, S.E., Levine, S.S., Zucker, J.R., Guenther, M.G., Kumar, R.M., Murray, H.L., Jenner, R.G., Gifford, D.K., Melton, D.A., Jaenisch, R., & Young, R.A. (2005). Core transcriptional regulatory circuitry in human embryonic stem cells. *Cell* **122**, 947-956.

Braam, S.R., Zeinstra, L., Litjens, S., Ward-van Oostwaard, D., van den Brink, S., van Laake, L., Lebrin, F., Kats, P., Hochstenbach, R., Passier, R., Sonnenberg, A.,

& Mummery, C.L. (2008). Recombinant vitronectin is a functionally defined substrate that supports human embryonic stem cell self-renewal via alpha V beta 5 integrin. *Stem Cells* **26**, 2257-2265.

Brafman, D.A., Chang, C.W., Fernandez, A., Willert, K., Varghese, S., & Chien, S. (2010). Long-term human pluripotent stem cell self-renewal on synthetic polymer surfaces. *Biomaterials* **31**, 9135-9144.

Brafman, D.A., Chien, S., & Willert, K. (2012). Arrayed cellular microenvironments for identifying culture and differentiation conditions for stem, primary and rare cell populations. *Nat Protoc* **7**, 703-717.

Brafman, D.A., Shah, K.D., Fellner, T., Chien, S., & Willert, K. (2009). Defining Long-Term Maintenance Conditions of Human Embryonic Stem Cells With Arrayed Cellular Microenvironment Technology. *Stem Cells Dev* **18**, 1141-1154.

Braun, S., Jenny, C., Thioudellet, C., Perraud, F., Claudepierre, M.C., Langle-Rouault, F., Ali-Hadji, D., Schughart, K., & Pavirani, A. (1999). In vitro and in vivo effects of glucocorticoids on gene transfer to skeletal muscle. *Febs Lett* **454**, 277-282.

Brehm, M., Heissler, S., Afonin, S., & Levkin, P.A. (2020). Nanomolar Synthesis in Droplet Microarrays with UV-Triggered On-Chip Cell Screening. *Small* **16**, 1905971.

Broach, J.R., & Thorner, J. (1996). High-throughput screening for drug discovery. *Nature* **384**, 14-16.

Brouzes, E., Medkova, M., Savenelli, N., Marran, D., Twardowski, M., Hutchison, J.B., Rothberg, J.M., Link, D.R., Perrimon, N., & Samuels, M.L. (2009). Droplet microfluidic technology for single-cell high-throughput screening. *Proc Natl Acad Sci USA* **106**, 14195-14200.

Bruchmann, J., Pini, I., Gill, T.S., Schwartz, T., & Levkin, P.A. (2017). Patterned SLIPS for the Formation of Arrays of Biofilm Microclusters with Defined Geometries. *Adv Healthc Mater* **6**, 1601082.

Brustikova, K., Sedlak, D., Kubikova, J., Skuta, C., Solcova, K., Malik, R., Bartunek, P., & Svoboda, P. (2018). Cell-Based Reporter System for High-Throughput Screening of MicroRNA Pathway Inhibitors and Its Limitations. *Front Genet* **9**, 45.

Bryant, L.M., Christopher, D.M., Giles, A.R., Hinderer, C., Rodriguez, J.L., Smith, J.B., Traxler, E.A., Tycko, J., Wojno, A.P., & Wilson, J.M. (2013). Lessons Learned from the Clinical Development and Market Authorization of Glybera. *Hum Gene Ther Cl Dev* **24**, 55-64.

Bulaklak, K., & Gersbach, C.A. (2020). The once and future gene therapy. *Nat Commun* **11**, 1-4.

Burkhardt, M.F., Martinez, F.J., Wright, S., Ramos, C., Volfson, D., Mason, M., Garnes, J., Dang, V., Lievers, J., Shoukat-Mumtaz, U., Martinez, R., Gai, H., Blake, R., Vaisberg, E., Grskovic, M., Johnson, C., Irion, S., Bright, J., Cooper, B., Nguyen, L., Griswold-Prenner, I., & Javaherian, A. (2013). A cellular model for sporadic ALS using patient-derived induced pluripotent stem cells. *Mol Cell Neurosci* **56**, 355-364.

Burns, S., Travers, J., Collins, I., Rowlands, M.G., Newbatt, Y., Thompson, N., Garrett, M.D., Workman, P., & Aherne, W. (2006). Identification of small-molecule inhibitors of protein kinase B (PKB/AKT) in an AlphaScreen (TM) high-throughput screen. *J Biomol Screen* **11**, 822-827.

Caiazzo, M., Okawa, Y., Ranga, A., Piersigilli, A., Tabata, Y., & Lutolf, M.P. (2016). Defined three-dimensional microenvironments boost induction of pluripotency. *Nat Mater* **15**, 344-352.

Carvajal-Vergara, X., Sevilla, A., D'Souza, S.L., Ang, Y.S., Schaniel, C., Lee, D.F., Yang, L., Kaplan, A.D., Adler, E.D., Rozov, R., Ge, Y.C., Cohen, N., Edelmann, L.J., Chang, B., Waghray, A., Su, J., Pardo, S., Lichtenbelt, K.D., Tartaglia, M., Gelb, B.D., & Lemischka, I.R. (2010). Patient-specific induced pluripotent stem-cell-derived models of LEOPARD syndrome. *Nature* **465**, 808-812.

Celiz, A.D., Smith, J.G.W., Patel, A.K., Hook, A.L., Rajamohan, D., George, V.T., Flatt, L., Patel, M.J., Epa, V.C., Singh, T., Langer, R., Anderson, D.G., Allen, N.D., Hay, D.C., Winkler, D.A., Barrett, D.A., Davies, M.C., Young, L.E., Denning, C., & Alexander, M.R. (2015). Discovery of a Novel Polymer for Human Pluripotent Stem Cell Expansion and Multilineage Differentiation. *Adv Mater* **27**, 4006-4012.

Chan, H.C.S., Shan, H., Dahoun, T., Vogel, H., & Yuan, S. (2019). Advancing Drug Discovery via Artificial Intelligence. *Trends Pharmacol Sci* **40**, 592-604.

Chang, C.W., Hwang, Y.S., Brafman, D., Hagan, T., Phung, C., & Varghese, S. (2013). Engineering cell-material interfaces for long-term expansion of human pluripotent stem cells. *Biomaterials* **34**, 912-921.

Chang, J., Chen, X., Wang, R., Shi, R., Wang, X., Lu, W., Ma, S., & Xia, Q. (2020). High-Throughput Screening Identifies Two Novel Small Molecule Enhancers of Recombinant Protein Expression. *Molecules* **25**, 353.

Chawla, S.P., Chua, V.S., Fernandez, L., Quon, D., Blackwelder, W.C., Gordon, E.M., & Hall, F.L. (2010). Advanced Phase I/II Studies of Targeted Gene Delivery In Vivo: Intravenous Rexin-G for Gemcitabine-resistant Metastatic Pancreatic Cancer. *Mol Ther* **18**, 435-441.

Chen, G.K., Gulbranson, D.R., Hou, Z.G., Bolin, J.M., Ruotti, V., Probasco, M.D., Smuga-Otto, K., Howden, S.E., Diol, N.R., Propson, N.E., Wagner, R., Lee, G.O., Antosiewicz-Bourget, J., Teng, J.M.C., & Thomson, J.A. (2011a). Chemically defined conditions for human iPSC derivation and culture. *Nat Methods* **8**, 424-429.

Chen, L., Liu, X.L., Su, B., Li, J., Jiang, L., Han, D., & Wang, S.T. (2011b). Aptamer-Mediated Efficient Capture and Release of T Lymphocytes on Nanostructured Surfaces. *Adv Mater* **23**, 4376-4380.

Cheng, J.J., Zeidan, R., Mishra, S., Liu, A., Pun, S.H., Kulkarni, R.P., Jensen, G.S., Bellocq, N.C., & Davis, M.E. (2006). Structure - Function correlation of chloroquine and analogues as transgene expression enhancers in nonviral gene delivery. *J Med Chem* **49**, 6522-6531.

Cherng, J.Y., van de Wetering, P., Talsma, H., Crommelin, D.J., & Hennink, W.E. (1996). Effect of size and serum proteins on transfection efficiency of poly ((2-dimethylamino)ethyl methacrylate)-plasmid nanoparticles. *Pharm Res* **13**, 1038-1042.

Chung, K.H., Rivet, C.A., Kemp, M.L., & Lu, H. (2011). Imaging Single-Cell Signaling Dynamics with a Deterministic High-Density Single-Cell Trap Array. *Anal Chem* **83**, 7044-7052.

Cockrell, A.S., & Kafri, T. (2007). Gene delivery by lentivirus vectors. *Mol Biotechnol* **36**, 184-204.

Colin, B., Rocq, N., Deprez, B., & Couturier, C. (2019). High-Throughput DNA Plasmid Multiplexing and Transfection Using Acoustic Nanodispensing Technology. *Jove-J Vis Exp* **150**, e59570.

Cong, L., Ran, F.A., Cox, D., Lin, S.L., Barretto, R., Habib, N., Hsu, P.D., Wu, X.B., Jiang, W.Y., Marraffini, L.A., & Zhang, F. (2013). Multiplex Genome Engineering Using CRISPR/Cas Systems. *Science* **339**, 819-823.

Cota-Coronado, A., Ramirez-Rodriguez, P.B., Padilla-Camberosl, E., Diaz, E.F., Flores-Fernandez, J.M., Avila-Gonzalez, D., & Diaz-Martinez, N.E. (2019). Implications of human induced pluripotent stem cells in metabolic disorders: from drug discovery toward precision medicine. *Drug Discov Today* **24**, 334-341.

Courtney, M., Chen, X.M., Chan, S., Mohamed, T., Rao, P.P.N., & Ren, C.L. (2017). Droplet Microfluidic System with On-Demand Trapping and Releasing of Droplet for Drug Screening Applications. *Anal Chem* **89**, 910-915.

Courtot, A.M., Magniez, A., Oudrhiri, N., Feraud, O., Bacci, J., Gobbo, E., Proust, S., Turhan, A.G., & Bennaceur-Griscelli, A. (2014). Morphological analysis of human induced pluripotent stem cells during induced differentiation and reverse programming. *Biores Open Access* **3**, 206-216.

Covaceuszach, S., Bozzi, M., Bigotti, M.G., Sciandra, F., Konarev, P.V., Brancaccio, A., & Cassetta, A. (2017). Structural flexibility of human alpha-dystroglycan. *Febs Open Bio* **7**, 1064-1077.

Cui, H.J., Wang, W.S., Shi, L.X., Song, W.L., & Wang, S.T. (2020). Superwettable Surface Engineering in Controlling Cell Adhesion for Emerging Bioapplications. *Small Methods* **4**, 2000573.

Cui, H.J., Wang, X.X., Wesslowski, J., Tronser, T., Rosenbauer, J., Schug, A., Davidson, G., Popova, A.A., & Levkin, P.A. (2021). Assembly of Multi-Spheroid Cellular Architectures by Programmable Droplet Merging. *Adv Mater* **33**, 2006434.

Dabbous, O., Sproule, D.M., Feltner, D.E., Ogrinc, F.G., Menier, M., Droege, M., Maru, B., Khan, F., & Arjunji, R. (2019). Event-Free Survival and Motor Milestone Achievement Following AVXS-101 and Nusinersen Interventions Contrasted to Natural History for Type I Spinal Muscular Atrophy Patients. *Neurology* **92**, S25. 005.

Dakhore, S., Nayer, B., & Hasegawa, K. (2018). Human Pluripotent Stem Cell Culture: Current Status, Challenges, and Advancement. *Stem Cells Int* **2018**, 7396905.

Dash, P.R., Read, M.L., Barrett, L.B., Wolfert, M., & Seymour, L.W. (1999). Factors affecting blood clearance and in vivo distribution of polyelectrolyte complexes for gene delivery. *Gene Ther* **6**, 643-650.

Davie, C.A. (2008). A review of Parkinson's disease. *Brit Med Bull* **86**, 109-127.

Daya, S., & Berns, K.I. (2008). Gene Therapy Using Adeno-Associated Virus Vectors. *Clin Microbiol Rev* **21**, 583-593.

de la Loza, M.C.D., Diaz-Torres, A., Zurita, F., Rosales-Nieves, A.E., Moeendarbary, E., Franze, K., Martin-Bermudo, M.D., & Gonzalez-Reyes, A. (2017). Laminin Levels Regulate Tissue Migration and Anterior-Posterior Polarity during Egg Morphogenesis in Drosophila. *Cell Rep* **20**, 211-223.

Deev, R., Plaksa, I., Bozo, I., & Isaev, A. (2017). Results of an International Postmarketing Surveillance Study of pl-VEGF165 Safety and Efficacy in 210 Patients with Peripheral Arterial Disease. *Am J Cardiovasc Drug* **17**, 235-242.

Deev, R.V., Bozo, I.Y., Mzhavanadze, N.D., Voronov, D.A., Gavrilenko, A.V., Chervyakov, Y.V., Staroverov, I.N., Kalinin, R.E., Shvalb, P.G., & Isaev, A.A. (2015). pCMV-vegf165 Intramuscular Gene Transfer is an Effective Method of Treatment for Patients With Chronic Lower Limb Ischemia. *J Cardiovasc Pharm T* **20**, 473-482.

Deng, Y., Zhang, X., Zhao, X., Li, Q., Ye, Z., Li, Z., Liu, Y., Zhou, Y., Ma, H., Pan, G., Pei, D., Fang, J., & Wei, S. (2013). Long-term self-renewal of human pluripotent stem cells on peptide-decorated poly(OEGMA-co-HEMA) brushes under fully defined conditions. *Acta Biomater* **9**, 8840-8850.

Dimos, J.T., Rodolfa, K.T., Niakan, K.K., Weisenthal, L.M., Mitsumoto, H., Chung, W., Croft, G.F., Saphier, G., Leibel, R., Goland, R., Wichterle, H., Henderson, C.E., & Eggan, K. (2008). Induced pluripotent stem cells generated from patients with ALS can be differentiated into motor neurons. *Science* **321**, 1218-1221.

Ding, X., Wang, W., Wang, Y., Bao, X., Wang, Y., Wang, C., Chen, J., Zhang, F., & Zhou, J. (2014). Versatile reticular polyethylenimine derivative-mediated targeted drug and gene codelivery for tumor therapy. *Mol Pharm* **11**, 3307-3321.

Domogatskaya, A., Rodin, S., & Tryggvason, K. (2012). Functional Diversity of Laminins. *Annu Rev Cell Dev Bi* **28**, 523-553.

Dufes, C., Uchegbu, I.F., & Schatzlein, A.G. (2005). Dendrimers in gene delivery. *Adv Drug Deliv Rev* **57**, 2177-2202.

Dunbar, C.E., High, K.A., Joung, J.K., Kohn, D.B., Ozawa, K., & Sadelain, M. (2018). Gene therapy comes of age. *Science* **359**, eaan4672.

Egashira, T., Yuasa, S., Suzuki, T., Aizawa, Y., Yamakawa, H., Matsuhashi, T., Ohno, Y., Tohyama, S., Okata, S., Seki, T., Kuroda, Y., Yae, K., Hashimoto, H., Tanaka, T., Hattori, F., Sato, T., Miyoshi, S., Takatsuki, S., Murata, M., Kurokawa, J., Furukawa, T., Makita, N., Aiba, T., Shimizu, W., Horie, M., Kamiya, K., Kodama, I., Ogawa, S., & Fukuda, K. (2012). Disease characterization using LQTS-specific induced pluripotent stem cells. *Cardiovasc Res* **95**, 419-429.

Eiselleova, L., Peterkova, I., Neradil, J., Slaninova, I., Hampl, A., & Dvorak, P. (2008). Comparative study of mouse and human feeder cells for human embryonic stem cells. *Int J Dev Biol* **52**, 353-363.

Encabo-Berzosa, M.M., Sancho-Albero, M., Sebastian, V., Irusta, S., Arruebo, M., Santamaria, J., & Duque, P.M. (2017). Polymer functionalized gold nanoparticles as nonviral gene delivery reagents. *J Gene Med* **19**, e2964.

Erfle, H., Neumann, B., Liebel, U., Rogers, P., Held, M., Walter, T., Ellenberg, J., & Pepperkok, R. (2007). Reverse transfection on cell arrays for high content screening microscopy. *Nat Protoc* **2**, 392-399.

Evans, M.J., & Kaufman, M.H. (1981). Establishment in Culture of Pluripotential Cells from Mouse Embryos. *Nature* **292**, 154-156.

Fang, Y. (2012). Ligand-receptor interaction platforms and their applications for drug discovery. *Expert Opin Drug Dis* **7**, 969-988.

Felgner, P.L., Gadek, T.R., Holm, M., Roman, R., Chan, H.W., Wenz, M., Northrop, J.P., Ringold, G.M., & Danielsen, M. (1987). Lipofection: a highly efficient, lipid-mediated DNA-transfection procedure. *Proc Natl Acad Sci U S A* **84**, 7413-7417.

Feng, W.Q., Li, L.X., Ueda, E., Li, J.S., Heissler, S., Welle, A., Trapp, O., & Levkin, P.A. (2014). Surface Patterning via Thiol-Yne Click Chemistry: An Extremely Fast and Versatile Approach to Superhydrophilic-Superhydrophobic Micropatterns. *Adv Mater Interfaces* **1**, 1400269.

Ferraris, G.M.S., Schulte, C., Buttiglione, V., De Lorenzi, V., Piontini, A., Galluzzi, M., Podesta, A., Madsen, C.D., & Sidenius, N. (2014). The interaction between uPAR and vitronectin triggers ligand-independent adhesion signalling by integrins. *Embo J* **33**, 2458-2472.

Ferreira, V., Petry, H., & Salmon, F. (2014). Immune Responses to AAV-Vectors, the Glybera Example from Bench to Bedside. *Front Immunol* **5**, 82.

Filipczyk, A., Marr, C., Hastreiter, S., Feigelman, J., Schwarzfischee, M., Hoppe, P.S., Loeffler, D., Kokkaliaris, K.D., Endele, M., Schauberger, B., Hilsenbeck, O., Skylaki, S., Hasenauer, J., Anastassiadis, K., Theis, F.J., & Schroeder, T. (2015). Network plasticity of pluripotency transcription factors in embryonic stem cells. *Nat Cell Biol* **17**, 1235-1246.

Finkel, R.S., Chiriboga, C.A., Vajsar, J., Day, J.W., Montes, J., De Vivo, D.C., Yamashita, M., Rigo, F., Hung, G., Schneider, E., Norris, D.A., Xia, S.T., Bennett, C.F., & Bishop, K.M. (2016). Treatment of infantile-onset spinal muscular atrophy with nusinersen: a phase 2, open-label, dose-escalation study. *Lancet* **388**, 3017-3026.

Fridman, R., Benton, G., Aranoutova, I., Kleinman, H.K., & Bonfil, R.D. (2012). Increased initiation and growth of tumor cell lines, cancer stem cells and biopsy material in mice using basement membrane matrix protein (Cultrex or Matrigel) co-injection. *Nat Protoc* **7**, 1138-1144.

Gandre-Babbe, S., Paluru, P., Aribeana, C., Chou, S.T., Bresolin, S., Lu, L., Sullivan, S.K., Tasian, S.K., Weng, J.L., Favre, H., Choi, J.K., French, D.L., Loh, M.L., & Weiss, M.J. (2013). Patient-derived induced pluripotent stem cells recapitulate hematopoietic abnormalities of juvenile myelomonocytic leukemia. *Blood* **121**, 4925-4929.

Gao, Y.G., Alam, U., Ding, A.X., Tang, Q., Tan, Z.L., Shi, Y.D., Lu, Z.L., & Qian, A.R. (2018). [12]aneN(3)-based lipid with naphthalimide moiety for enhanced gene transfection efficiency. *Bioorg Chem* **79**, 334-340.

Gao, Y.G., Alam, U., Tang, Q., Shi, Y.D., Zhang, Y., Wang, R.B., & Lu, Z.L. (2016). Functional lipids based on [12]aneN(3) and naphthalimide as efficient non-viral gene vectors. *Org Biomol Chem* **14**, 6346-6354.

Geary, R.S., Norris, D., Yu, R., & Bennett, C.F. (2015). Pharmacokinetics, biodistribution and cell uptake of antisense oligonucleotides. *Adv Drug Deliver Rev* **87**, 46-51.

Gerecht, S., Burdick, J.A., Ferreira, L.S., Townsend, S.A., Langer, R., & Vunjak-Novakovic, G. (2007). Hyaluronic acid hydrogel for controlled self-renewal and differentiation of human embryonic stem cells. *Proc Natl Acad Sci U S A* **104**, 11298-11303.

Geyer, F.L., Ueda, E., Liebel, U., Grau, N., & Levkin, P.A. (2011). Superhydrophobic-Superhydrophilic Micropatterning: Towards Genome-on-a-Chip Cell Microarrays. *Angew Chem Int Edit* **50**, 8424-8427.

Gillette, K.M., Forbes, K., & Sehgal, I. (2003). Detection of matrix metalloproteinases (MMP), tissue inhibitor of metalloproteinase-2, urokinase and plasminogen activator inhibitor-1 within matrigel and growth factor-reduced matrigel basement membrane. *Tumori* **89**, 421-425.

Goetzke, R., Sechi, A., De Laporte, L., Neuss, S., & Wagner, W. (2018). Why the impact of mechanical stimuli on stem cells remains a challenge. *Cell Mol Life Sci* **75**, 3297-3312.

Goldberg, D.E., Smithen, L.M., Angelilli, A., & Freeman, W.R. (2005). HIV-associated retinopathy in the HAART era. *Retina-J Ret Vit Dis* **25**, 633-649.

Gordon, E.M., & Hall, F.L. (2010). Rexin-G, a targeted genetic medicine for cancer. *Expert Opin Biol Th* **10**, 819-832.

Gragoudas, E.S., Adamis, A.P., Cunningham, E.T., Feinsod, M., Guyer, D.R., & Neova, V.I.S.O. (2004). Pegaptanib for neovascular age-related macular degeneration. *New Engl J Med* **351**, 2805-2816.

Graham, F.L., & van der Eb, A.J. (1973). A new technique for the assay of infectivity of human adenovirus 5 DNA. *Virology* **52**, 456-467.

Green, J.J., Shi, J., Chiu, E., Leshchiner, E.S., Langer, R., & Anderson, D.G. (2006). Biodegradable polymeric vectors for gene delivery to human endothelial cells. *Bioconjugate Chem* **17**, 1162-1169.

Gross, B., Sgodda, M., Rasche, M., Schambach, A., Gohring, G., Schlegelberger, B., Greber, B., Linden, T., Reinhardt, D., Cantz, T., & Klusmann, J.H. (2013). Improved Generation of Patient-Specific Induced Pluripotent Stem Cells Using a Chemically-Defined and Matrigel-Based Approach. *Curr Mol Med* **13**, 765-776.

Guo, L., Coyle, L., Abrams, R.M.C., Kemper, R., Chiao, E.T., & Kolaja, K.L. (2013). Refining the Human iPSC-Cardiomyocyte Arrhythmic Risk Assessment Model. *Toxicol Sci* **136**, 581-594.

Hacker, D.L., & Balasubramanian, S. (2016). Recombinant protein production from stable mammalian cell lines and pools. *Curr Opin Struc Biol* **38**, 129-136.

Haensler, J., & Szoka, F.C., Jr. (1993). Polyamidoamine cascade polymers mediate efficient transfection of cells in culture. *Bioconjug Chem* **4**, 372-379.

Haidet-Phillips, A.M., Hester, M.E., Miranda, C.J., Meyer, K., Braun, L., Frakes, A., Song, S.W., Likhite, S., Murtha, M.J., Foust, K.D., Rao, M.H., Eagle, A., Kammesheidt, A., Christensen, A., Mendell, J.R., Burghes, A.H.M., & Kaspar, B.K. (2011). Astrocytes from familial and sporadic ALS patients are toxic to motor neurons. *Nat Biotechnol* **29**, 824-828.

Han, L., Li, Y., Tchao, J., Kaplan, A.D., Lin, B., Li, Y., Mich-Basso, J., Lis, A., Hassan, N., London, B., Bett, G.C.L., Tobita, K., Rasmusson, R.L., & Yang, L. (2014). Study familial hypertrophic cardiomyopathy using patient-specific induced pluripotent stem cells. *Cardiovasc Res* **104**, 258-269.

Hanna, J., Wernig, M., Markoulaki, S., Sun, C.W., Meissner, A., Cassady, J.P., Beard, C., Brambrink, T., Wu, L.C., Townes, T.M., & Jaenisch, R. (2007). Treatment of sickle cell anemia mouse model with iPS cells generated from autologous skin. *Science* **318**, 1920-1923.

Hasegawa, S., Hirashima, N., & Nakanishi, M. (2001). Microtubule involvement in the intracellular dynamics for gene transfection mediated by cationic liposomes. *Gene Ther* **8**, 1669-1673.

Hayashi, Y., & Furue, M.K. (2016). Biological Effects of Culture Substrates on Human Pluripotent Stem Cells. *Stem Cells Int* **2016**, 5380560.

He, L., Kulesskiy, E., Saarela, J., Turunen, L., Wennerberg, K., Aittokallio, T., & Tang, J. (2018). Methods for High-throughput Drug Combination Screening and Synergy Scoring. *Methods Mol Biol* **1711**, 351-398.

Hertzberg, R.P., & Pope, A.J. (2000). High-throughput screening: new technology for the 21st century. *Curr Opin Chem Biol* **4**, 445-451.

Higuchi, A., Kao, S.H., Ling, Q.D., Chen, Y.M., Li, H.F., Alarfaj, A.A., Munusamy, M.A., Murugan, K., Chang, S.C., Lee, H.C., Hsu, S.T., Kumar, S.S., & Umezawa, A. (2015). Long-term xeno-free culture of human pluripotent stem cells on hydrogels with optimal elasticity. *Sci Rep* **5**, 1-16.

Hino, K., Horigome, K., Nishio, M., Komura, S., Nagata, S., Zhao, C., Jin, Y., Kawakami, K., Yamada, Y., Ohta, A., Toguchida, J., & Ikeya, M. (2017). Activin-A enhances mTOR signaling to promote aberrant chondrogenesis in fibrodysplasia ossificans progressiva. *J Clin Invest* **127**, 3345-3358.

Hino, K., Ikeya, M., Horigome, K., Matsumoto, Y., Ebise, H., Nishio, M., Sekiguchi, K., Shibata, M., Nagata, S., Matsuda, S., & Toguchida, J. (2015). Neofunction of ACVR1 in fibrodysplasia ossificans progressiva. *Proc Natl Acad Sci USA* **112**, 15438-15443.

Hockemeyer, D., Soldner, F., Beard, C., Gao, Q., Mitalipova, M., DeKelver, R.C., Katibah, G.E., Amora, R., Boydston, E.A., Zeitler, B., Meng, X.D., Miller, J.C., Zhang, L., Rebar, E.J., Gregory, P.D., Urnov, F.D., & Jaenisch, R. (2009). Efficient

targeting of expressed and silent genes in human ESCs and iPSCs using zinc-finger nucleases. *Nat Biotechnol* **27**, 851-857.

Hockemeyer, D., Wang, H.Y., Kiani, S., Lai, C.S., Gao, Q., Cassady, J.P., Cost, G.J., Zhang, L., Santiago, Y., Miller, J.C., Zeitler, B., Cherone, J.M., Meng, X.D., Hinkley, S.J., Rebar, E.J., Gregory, P.D., Urnov, F.D., & Jaenisch, R. (2011). Genetic engineering of human pluripotent cells using TALE nucleases. *Nat Biotechnol* **29**, 731-734.

Hoepfner, J., Kleinsorge, M., Papp, O., Alfken, S., Heiringhoff, R., Pich, A., Sauer, V., Zibert, A., Gohring, G., Schmidt, H., Sgodda, M., & Cantz, T. (2017). In vitro modelling of familial amyloidotic polyneuropathy allows quantitative detection of transthyretin amyloid fibril-like structures in hepatic derivatives of patient-specific induced pluripotent stem cells. *Biol Chem* **398**, 939-954.

Hu, J.C., Coffin, R.S., Davis, C.J., Graham, N.J., Groves, N., Guest, P.J., Harrington, K.J., James, N.D., Love, C.A., McNeish, I., Medley, L.C., Michael, A., Nutting, C.M., Pandha, H.S., Shorrock, C.A., Simpson, J., Steiner, J., Steven, N.M., Wright, D., & Coombes, R.C. (2006). A phase I study of OncoVEXGM-CSF, a second-generation oncolytic herpes simplex virus expressing granulocyte macrophage colony-stimulating factor. *Clin Cancer Res* **12**, 6737-6747.

Huang, R.Q., Yang, W.L., Jiang, C., & Pei, Y.Y. (2006). Gene delivery into brain capillary endothelial cells using Antp-modified DNA-loaded nanoparticles. *Chem Pharm Bull* **54**, 1254-1258.

Hughes, C.S., Radan, L., Betts, D., Postovit, L.M., & Lajoie, G.A. (2011). Proteomic analysis of extracellular matrices used in stem cell culture. *Proteomics* **11**, 3983-3991.

Imamura, K., Izumi, Y., Watanabe, A., Tsukita, K., Woltjen, K., Yamamoto, T., Hotta, A., Kondo, T., Kitaoka, S., Ohta, A., Tanaka, A., Watanabe, D., Morita, M., Takuma, H., Tamaoka, A., Kunath, T., Wray, S., Furuya, H., Era, T., Makioka, K., Okamoto, K., Fujisawa, T., Nishitoh, H., Homma, K., Ichijo, H., Julien, J.P., Obata, N., Hosokawa, M., Akiyama, H., Kaneko, S., Ayaki, T., Ito, H., Kaji, R., Takahashi, R., Yamanaka, S., & Inoue, H. (2017). The Src/c-Abl pathway is a potential therapeutic target in amyotrophic lateral sclerosis. *Sci Transl Med* **9**, eaaf3962.

Imani, R., Mohabatpour, F., & Mostafavi, F. (2018). Graphene-based Nano-Carrier modifications for gene delivery applications. *Carbon* **140**, 569-591.

Inoue, H., Nagata, N., Kurokawa, H., & Yamanaka, S. (2014). iPS cells: a game changer for future medicine. *Embo J* **33**, 409-417.

Ireland, R.G., Kibschull, M., Audet, J., Ezzo, M., Hinz, B., Lye, S.J., & Simmons, C.A. (2020). Combinatorial extracellular matrix microarray identifies novel bioengineered substrates for xeno-free culture of human pluripotent stem cells. *Biomaterials* **248**, 120017.

Ireland, R.G., & Simmons, C.A. (2015). Human Pluripotent Stem Cell Mechanobiology: Manipulating the Biophysical Microenvironment for Regenerative Medicine and Tissue Engineering Applications. *Stem Cells* **33**, 3187-3196.

Isono, K., Jono, H., Ohya, Y., Shiraki, N., Yamazoe, T., Sugasaki, A., Era, T., Fusaki, N., Tasaki, M., Ueda, M., Shinriki, S., Inomata, Y., Kume, S., & Ando, Y.

(2014). Generation of familial amyloidotic polyneuropathy-specific induced pluripotent stem cells. *Stem Cell Res* **12**, 574-583.

Israel, M.A., Yuan, S.H., Bardy, C., Reyna, S.M., Mu, Y.L., Herrera, C., Hefferan, M.P., Van Gorp, S., Nazor, K.L., Boscolo, F.S., Carson, C.T., Laurent, L.C., Marsala, M., Gage, F.H., Remes, A.M., Koo, E.H., & Goldstein, L.S.B. (2012). Probing sporadic and familial Alzheimer's disease using induced pluripotent stem cells. *Nature* **482**, 216-220.

Itzhaki, I., Maizels, L., Huber, I., Zwi-Dantsis, L., Caspi, O., Winterstern, A., Feldman, O., Gepstein, A., Arbel, G., Hammerman, H., Boulos, M., & Gepstein, L. (2011). Modelling the long QT syndrome with induced pluripotent stem cells. *Nature* **471**, 225-229.

Jackman, R.J., Duffy, D.C., Ostuni, E., Willmore, N.D., & Whitesides, G.M. (1998). Fabricating large arrays of microwells with arbitrary dimensions and filling them using discontinuous dewetting. *Anal Chem* **70**, 2280-2287.

Jager, V., Bussow, K., Wagner, A., Weber, S., Hust, M., Frenzel, A., & Schirrmann, T. (2013). High level transient production of recombinant antibodies and antibody fusion proteins in HEK293 cells. *Bmc Biotechnol* **13**, 1-20.

Jin, L., Zeng, X., Liu, M., Deng, Y., & He, N.Y. (2014). Current Progress in Gene Delivery Technology Based on Chemical Methods and Nano-carriers. *Theranostics* **4**, 240-255.

Jogia, G.E., Tronser, T., Popova, A.A., & Levkin, P.A. (2016). Droplet Microarray Based on Superhydrophobic-Superhydrophilic Patterns for Single Cell Analysis. *Microarrays* **5**, 28.

Joliot, A., Pernelle, C., Deagostinibazin, H., & Prochiantz, A. (1991). Antennapedia Homeobox Peptide Regulates Neural Morphogenesis. *Proc Natl Acad Sci USA* **88**, 1864-1868.

Kabashi, E., Lin, L., Tradewell, M.L., Dion, P.A., Bercier, V., Bourgouin, P., Rochefort, D., Hadj, S.B., Durham, H.D., Velde, C.V., Rouleau, G.A., & Drapeau, P. (2010). Gain and loss of function of ALS-related mutations of TARDBP (TDP-43) cause motor deficits in vivo. *Hum Mol Genet* **19**, 3102-3102.

Kadlecova, Z., Rajendra, Y., Matasci, M., Hacker, D., Baldi, L., Wurm, F.M., & Klok, H.A. (2012). Hyperbranched Polylysine: A Versatile, Biodegradable Transfection Agent for the Production of Recombinant Proteins by Transient Gene Expression and the Transfection of Primary Cells. *Macromol Biosci* **12**, 794-804.

Kaji, E.H., & Leiden, J.M. (2001). Gene and stem cell therapies. *JAMA* **285**, 545-550.

Karagiannis, P., Takahashi, K., Saito, M., Yoshida, Y., Okita, K., Watanabe, A., Inoue, H., Yamashita, J.K., Todani, M., Nakagawa, M., Osawa, M., Yashiro, Y., Yamanaka, S., & Osafune, K. (2019). Induced Pluripotent Stem Cells and Their Use in Human Models of Disease and Development. *Physiol Rev* **99**, 79-114.

Kato, R., Matsumoto, M., Sasaki, H., Joto, R., Okada, M., Ikeda, Y., Kanie, K., Suga, M., Kinehara, M., Yanagihara, K., Liu, Y.J., Uchio-Yamada, K., Fukuda, T., Kii, H., Uozumi, T., Honda, H., Kiyota, Y., & Furue, M.K. (2016). Parametric

analysis of colony morphology of non-labelled live human pluripotent stem cells for cell quality control. *Sci Rep* **6**, 1-12.

Kazuki, Y., Hiratsuka, M., Takiguchi, M., Osaki, M., Kajitani, N., Hoshiya, H., Hiramatsu, K., Yoshino, T., Kazuki, K., Ishihara, C., Takehara, S., Higaki, K., Nakagawa, M., Takahashi, K., Yamanaka, S., & Oshimura, M. (2010). Complete genetic correction of ips cells from Duchenne muscular dystrophy. *Mol Ther* **18**, 386-393.

Kelly, A.M., Plautz, S.A., Zempleni, J., & Pannier, A.K. (2016). Glucocorticoid Cell Priming Enhances Transfection Outcomes in Adult Human Mesenchymal Stem Cells. *Mol Ther* **24**, 331-341.

Keung, A.J., Kumar, S., & Schaffer, D.V. (2010). Presentation Counts: Microenvironmental Regulation of Stem Cells by Biophysical and Material Cues. *Annu Rev Cell Dev Bi* **26**, 533-556.

Kilk, K., El-Andaloussi, S., Jarver, P., Meikas, A., Valkna, A., Bartfai, T., Kogerman, P., Metsis, M., & Langel, U. (2005). Evaluation. of transportan 10 in PEI mediated plasmid delivery assay. *J Control Release* **103**, 511-523.

Kim, B.K., Bae, Y.U., Doh, K.O., Hwang, G.B., Lee, S.H., Kang, H., & Seu, Y.B. (2011). The synthesis of cholesterol-based cationic lipids with trimethylamine head and the effect of spacer structures on transfection efficiency. *Bioorg Med Chem Lett* **21**, 3734-3737.

Kim, T.K., & Eberwine, J.H. (2010). Mammalian cell transfection: the present and the future. *Anal Bioanal Chem* **397**, 3173-3178.

Kim, Y., Choi, J.Y., Lee, S.H., Lee, B.H., Yoo, H.W., & Han, Y.M. (2016). Malfunction in Mitochondrial beta-Oxidation Contributes to Lipid Accumulation in Hepatocyte-Like Cells Derived from Citrin Deficiency-Induced Pluripotent Stem Cells. *Stem Cells Dev* **25**, 636-647.

Kimbrel, E.A., & Lanza, R. (2015). Current status of pluripotent stem cells: moving the first therapies to the clinic. *Nat Rev Drug Discov* **14**, 681-692.

Kinali, M., Arechavala-Gomeza, V., & Feng, L. (2009). Local restoration of dystrophin expression with the morpholino oligomer AVI-4658 in Duchenne muscular dystrophy: a single-blind, placebo-controlled, dose-escalation, proof-of-concept study. (vol 8, pg 918, 2009). *Lancet Neurol* **8**, 1083-1083.

Kingston, R.E., Chen, C.A., & Rose, J.K. (2003). Calcium phosphate transfection. *Curr Protoc Mol Biol* **Chapter 9**, Unit 9 1.

Klim, J.R., Li, L.Y., Wrighton, P.J., Piekarczyk, M.S., & Kiessling, L.L. (2010). A defined glycosaminoglycan-binding substratum for human pluripotent stem cells. *Nat Methods* **7**, 989-994.

Klumpp, C., Kostarelos, K., Prato, M., & Bianco, A. (2006). Functionalized carbon nanotubes as emerging nanovectors for the delivery of therapeutics. *Bba-Biomembranes* **1758**, 404-412.

Kneuer, C., Sameti, M., Haltner, E.G., Schiestel, T., Schirra, H., Schmidt, H., & Lehr, C.M. (2000). Silica nanoparticles modified with aminosilanes as carriers for plasmid DNA. *Int J Pharm* **196**, 257-261.

Koch, L., Kuhn, S., Sorg, H., Gruene, M., Schlie, S., Gaebel, R., Polchow, B., Reimers, K., Stoelting, S., Ma, N., Vogt, P.M., Steinhoff, G., & Chichkov, B. (2010). Laser Printing of Skin Cells and Human Stem Cells. *Tissue Eng Part C-Me* **16**, 847-854.

Kozisek, T., Hamann, A., Nguyen, A., Miller, M., Plautz, S.A., & Pannier, A.K. (2020). High-throughput screening of clinically approved drugs that prime nonviral gene delivery to human Mesenchymal stem cells. *J Biol Eng* **14**, 1-13.

Krewski, D., Andersen, M.E., Tyshenko, M.G., Krishnan, K., Hartung, T., Boekelheide, K., Wambaugh, J.F., Jones, D., Whelan, M., Thomas, R., Yauk, C., Barton-Maclaren, T., & Cote, I. (2020). Toxicity testing in the 21st century: progress in the past decade and future perspectives. *Arch Toxicol* **94**, 1-58.

Kurosawa, H. (2007). Methods for inducing embryoid body formation: In vitro differentiation system of embryonic stem cells. *J Biosci Bioeng* **103**, 389-398.

Kwon, C.H., Wheeldon, I., Kachouie, N.N., Lee, S.H., Bae, H., Sant, S., Fukuda, J., Kang, J.W., & Khademhosseini, A. (2011). Drug-Eluting Microarrays for Cell-Based Screening of Chemical-Induced Apoptosis. *Anal Chem* **83**, 4118-4125.

Lai, E., & van Zanten, J.H. (2001). Monitoring DNA/poly-L-lysine polyplex formation with time-resolved multiangle laser light scattering. *Biophys J* **80**, 864-873.

Lambshead, J.W., Meagher, L., Goodwin, J., Labonne, T., Ng, E., Elefanty, A., Stanley, E., O'Brien, C.M., & Laslett, A.L. (2018). Long-Term Maintenance of Human Pluripotent Stem Cells on cRGDfK-Presenting Synthetic Surfaces. *Sci Rep* **8**, 1-16.

Lan, F., Lee, A.S., Liang, P., Sanchez-Freire, V., Nguyen, P.K., Wang, L., Han, L., Yen, M., Wang, Y.M., Sun, N., Abilez, O.J., Hu, S.J., Ebert, A.D., Navarrete, E.G., Simmons, C.S., Wheeler, M., Pruitt, B., Lewis, R., Yamaguchi, Y., Ashley, E.A., Bers, D.M., Robbins, R.C., Longaker, M.T., & Wu, J.C. (2013). Abnormal Calcium Handling Properties Underlie Familial Hypertrophic Cardiomyopathy Pathology in Patient-Specific Induced Pluripotent Stem Cells. *Cell Stem Cell* **12**, 101-113.

Lander, E.S., Consortium, I.H.G.S., Linton, L.M., Birren, B., Nusbaum, C., Zody, M.C., Baldwin, J., Devon, K., Dewar, K., Doyle, M., FitzHugh, W., Funke, R., Gage, D., Harris, K., Heaford, A., Howland, J., Kann, L., Lehoczky, J., LeVine, R., McEwan, P., McKernan, K., Meldrim, J., Mesirov, J.P., Miranda, C., Morris, W., Naylor, J., Raymond, C., Rosetti, M., Santos, R., Sheridan, A., Sougnez, C., Stange-Thomann, N., Stojanovic, N., Subramanian, A., Wyman, D., Rogers, J., Sulston, J., Ainscough, R., Beck, S., Bentley, D., Burton, J., Clee, C., Carter, N., Coulson, A., Deadman, R., Deloukas, P., Dunham, A., Dunham, I., Durbin, R., French, L., Grafham, D., Gregory, S., Hubbard, T., Humphray, S., Hunt, A., Jones, M., Lloyd, C., McMurray, A., Matthews, L., Mercer, S., Milne, S., Mullikin, J.C., Mungall, A., Plumb, R., Ross, M., Shownkeen, R., Sims, S., Waterston, R.H., Wilson, R.K., Hillier, L.W., McPherson, J.D., Marra, M.A., Mardis, E.R., Fulton, L.A., Chinwalla, A.T., Pepin, K.H., Gish, W.R., Chissoe, S.L., Wendl, M.C.,

Delehaunty, K.D., Miner, T.L., Delehaunty, A., Kramer, J.B., Cook, L.L., Fulton, R.S., Johnson, D.L., Minx, P.J., Clifton, S.W., Hawkins, T., Branscomb, E., Predki, P., Richardson, P., Wenning, S., Slezak, T., Doggett, N., Cheng, J.F., Olsen, A., Lucas, S., Elkin, C., Uberbacher, E., Frazier, M., Gibbs, R.A., Muzny, D.M., Scherer, S.E., Bouck, J.B., Sodergren, E.J., Worley, K.C., Rives, C.M., Gorrell, J.H., Metzker, M.L., Naylor, S.L., Kucherlapati, R.S., Nelson, D.L., Weinstock, G.M., Sakaki, Y., Fujiyama, A., Hattori, M., Yada, T., Toyoda, A., Itoh, T., Kawagoe, C., Watanabe, H., Totoki, Y., Taylor, T., Weissenbach, J., Heilig, R., Saurin, W., Artiguenave, F., Brottier, P., Bruls, T., Pelletier, E., Robert, C., Wincker, P., Rosenthal, A., Platzer, M., Nyakatura, G., Taudien, S., Rump, A., Yang, H.M., Yu, J., Wang, J., Huang, G.Y., Gu, J., Hood, L., Rowen, L., Madan, A., Qin, S.Z., Davis, R.W., Federspiel, N.A., Abola, A.P., Proctor, M.J., Myers, R.M., Schmutz, J., Dickson, M., Grimwood, J., Cox, D.R., Olson, M.V., Kaul, R., Raymond, C., Shimizu, N., Kawasaki, K., Minoshima, S., Evans, G.A., Athanasiou, M., Schultz, R., Roe, B.A., Chen, F., Pan, H.Q., Ramser, J., Lehrach, H., Reinhardt, R., McCombie, W.R., de la Bastide, M., Dedhia, N., Blocker, H., Hornischer, K., Nordsiek, G., Agarwala, R., Aravind, L., Bailey, J.A., Bateman, A., Batzoglou, S., Birney, E., Bork, P., Brown, D.G., Burge, C.B., Cerutti, L., Chen, H.C., Church, D., Clamp, M., Copley, R.R., Doerks, T., Eddy, S.R., Eichler, E.E., Furey, T.S., Galagan, J., Gilbert, J.G.R., Harmon, C., Hayashizaki, Y., Haussler, D., Hermjakob, H., Hokamp, K., Jang, W.H., Johnson, L.S., Jones, T.A., Kasif, S., Kaspryzk, A., Kennedy, S., Kent, W.J., Kitts, P., Koonin, E.V., Korf, I., Kulp, D., Lancet, D., Lowe, T.M., McLysaght, A., Mikkelsen, T., Moran, J.V., Mulder, N., Pollara, V.J., Ponting, C.P., Schuler, G., Schultz, J.R., Slater, G., Smit, A.F.A., Stupka, E., Szustakowki, J., Thierry-Mieg, D., Thierry-Mieg, J., Wagner, L., Wallis, J., Wheeler, R., Williams, A., Wolf, Y.I., Wolfe, K.H., Yang, S.P., Yeh, R.F., Collins, F., Guyer, M.S., Peterson, J., Felsenfeld, A., Wetterstrand, K.A., Patrinos, A., Morgan, M.J., & Conso, I.H.G.S. (2001). Initial sequencing and analysis of the human genome. *Nature* **409**, 860-921.

Lanigan, T.M., Kopera, H.C., & Saunders, T.L. (2020). Principles of Genetic Engineering. *Genes* **11**, 291.

Laperle, A., Hsiao, C., Lampe, M., Mortier, J., Saha, K., Palecek, S.P., & Masters, K.S. (2015). alpha-5 Laminin Synthesized by Human Pluripotent Stem Cells Promotes Self-Renewal. *Stem Cell Rep* **5**, 195-206.

Lee, C.S., Bishop, E.S., Zhang, R.Y., Yu, X.Y., Farina, E.M., Yan, S.J., Zhao, C., Zeng, Z.Y., Shu, Y., Wu, X.Y., Lei, J.Y., Li, Y.S., Zhang, W.W., Yang, C., Wu, K., Wu, Y., Ho, S., Athiviraham, A., Lee, M.J., Wolf, J.M., Reid, R.R., & He, T.C. (2017). Adenovirus-mediated gene delivery: Potential applications for gene and cell-based therapies in the new era of personalized medicine. *Genes Dis* **4**, 43-63.

Lee, G., Ramirez, C.N., Kim, H., Zeltner, N., Liu, B., Radu, C., Bhinder, B., Kim, Y.J., Choi, I.Y., Mukherjee-Clavin, B., Djaballah, H., & Studer, L. (2012). Large-scale screening using familial dysautonomia induced pluripotent stem cells identifies compounds that rescue IKBKAP expression. *Nat Biotechnol* **30**, 1244-1248.

Lee, M., Kim, Y., Ryu, J.H., Kim, K., Han, Y.M., & Lee, H. (2016). Long-term, feeder-free maintenance of human embryonic stem cells by mussel-inspired adhesive heparin and collagen type I. *Acta Biomater* **32**, 138-148.

Lee, M.Y., Kumar, R.A., Sukumaran, S.M., Hogg, M.G., Clark, D.S., & Dordick, J.S. (2008). Three-dimensional cellular microarray for high-throughput toxicology assays. *Proc Natl Acad Sci USA* **105**, 59-63.

Lehmann, J.M., Lenhard, J.M., Oliver, B.B., Ringold, G.M., & Kliewer, S.A. (1997). Peroxisome proliferator-activated receptors alpha and gamma are activated by indomethacin and other non-steroidal anti-inflammatory drugs. *Journal of Biological Chemistry* **272**, 3406-3410.

Lehner, B., & Fraser, A.G. (2004). 5,000 RNAi experiments on a chip. *Nat Methods* **1**, 103-104.

Lei, W.X., Bruchmann, J., Ruping, J.L., Levkin, P.A., & Schwartz, T. (2019). Biofilm Bridges Forming Structural Networks on Patterned Lubricant-Infused Surfaces. *Adv Sci* **6**, 1900519.

Lei, W.X., Demir, K., Overhage, J., Grunze, M., Schwartz, T., & Levkin, P.A. (2020a). Droplet-Microarray: Miniaturized Platform for High-Throughput Screening of Antimicrobial Compounds. *Adv Biosyst* **4**, 2000073.

Lei, W.X., Krolla, P., Schwartz, T., & Levkin, P.A. (2020b). Controlling Geometry and Flow Through Bacterial Bridges on Patterned Lubricant-Infused Surfaces (pLIS). *Small* **16**, 2004575.

Lei, Y.G., & Schaffer, D.V. (2013). A fully defined and scalable 3D culture system for human pluripotent stem cell expansion and differentiation. *Proc Natl Acad Sci USA* **110**, E5039-E5048.

Li, D., Li, P.C., Li, G.P., Wang, J., & Wang, E.K. (2009). The effect of nocodazole on the transfection efficiency of lipid-bilayer coated gold nanoparticles. *Biomaterials* **30**, 1382-1388.

Li, W., & Szoka, F.C., Jr. (2007). Lipid-based nanoparticles for nucleic acid delivery. *Pharm Res* **24**, 438-449.

Li, Y., Li, B., Li, C.J., & Li, L.J. (2015). Key points of basic theories and clinical practice in rAd-p53 (Gendicine (TM)) gene therapy for solid malignant tumors. *Expert Opin Biol Th* **15**, 437-454.

Lim, W.F., Inoue-Yokoo, T., Tan, K.S., Lai, M.I., & Sugiyama, D. (2013). Hematopoietic cell differentiation from embryonic and induced pluripotent stem cells. *Stem Cell Res Ther* **4**, 71.

Lim, Y.B., Choi, Y.H., & Park, J.S. (1999). A self-destroying polycationic polymer: Biodegradable poly(4-hydroxy-L-proline ester). *J Am Chem Soc* **121**, 5633-5639.

Lipinski, C.A., Lombardo, F., Dominy, B.W., & Feeney, P.J. (1997). Experimental and computational approaches to estimate solubility and permeability in drug discovery and development settings. *Adv Drug Deliver Rev* **23**, 3-25.

Liu, G.H., Qu, J., Suzuki, K., Nivet, E., Li, M., Montserrat, N., Yi, F., Xu, X.L., Ruiz, S., Zhang, W.Q., Wagner, U., Kim, A., Ren, B., Li, Y., Goebl, A., Kim, J., Soligalla, R.D., Dubova, I, Thompson, J., Yates, J., Esteban, C.R., Sancho-Martinez, I., & Belmonte, J.C.I. (2012). Progressive degeneration of human neural stem cells caused by pathogenic LRRK2. *Nature* **491**, 603-607.

Liu, H., Kim, Y., Sharkis, S., Marchionni, L., & Jang, Y.Y. (2011). In vivo liver regeneration potential of human induced pluripotent stem cells from diverse origins. *Sci Transl Med* **3**, 82ra39.

Liu, T.T., Zeng, X.W., Sun, F.L., Hou, H.L., Guan, Y.Q., Guo, D.Y., Ai, H.X., Zhang, G.J., & Wang, W. (2017). EphB4 Regulates Self-Renewal, Proliferation and Neuronal Differentiation of Human Embryonic Neural Stem Cells in Vitro. *Cell Physiol Biochem* **41**, 819-834.

Liu, W., Deng, C., Godoy-Parejo, C., Zhang, Y., & Chen, G. (2019). Developments in cell culture systems for human pluripotent stem cells. *World J Stem Cells* **11**, 968-981.

Liu, Y.M., Wenning, L., Lynch, M., & Reineke, T.M. (2004). New poly(D-glucaramidoamine)s induce DNA nanoparticle formation and efficient gene delivery into mammalian cells. *J Am Chem Soc* **126**, 7422-7423.

Liu, Y.X., Tronser, T., Peravali, R., Reischl, M., & Levkin, P.A. (2020). High-Throughput Screening of Cell Transfection Enhancers Using Miniaturized Droplet Microarrays. *Adv Biosyst* **4**, 1900257.

Llames, S., Garcia-Perez, E., Meana, A., Larcher, F., & del Rio, M. (2015). Feeder Layer Cell Actions and Applications. *Tissue Eng Part B-Re* **21**, 345-353.

Luten, J., van Steenis, J.H., Schuurmans-Nieuwenbroek, N.M.E., van Nostrum, C.F., & Hennink, W.E. (2003). Polyphosphazenes as biodegradable non-viral vector systems. *J Control Release* **87**, 277-279.

Luthman, H., & Magnusson, G. (1983). High-Efficiency Polyoma DNA Transfection of Chloroquine Treated-Cells. *Nucleic Acids Res* **11**, 1295-1308.

Macdonald, P.R., Lustig, A., Steinmetz, M.O., & Kammerer, R.A. (2010). Laminin chain assembly is regulated by specific coiled-coil interactions. *J Struct Biol* **170**, 398-405.

Madkhali, O., Mekhail, G., & Wettig, S.D. (2019). Modified gelatin nanoparticles for gene delivery. *Int J Pharm* **554**, 224-234.

Majidi, A., Nikkhah, M., Sadeghian, F., & Hosseinkhani, S. (2016). Development of novel recombinant biomimetic chimeric MPG-based peptide as nanocarriers for gene delivery: Imitation of a real cargo. *Eur J Pharm Biopharm* **107**, 191-204.

Malo, N., Hanley, J.A., Cerquozzi, S., Pelletier, J., & Nadon, R. (2006). Statistical practice in high-throughput screening data analysis. *Nat Biotechnol* **24**, 167-175.

Mata, M., Glorioso, J.C., & Fink, D.J. (2002). Targeted gene delivery to the nervous system using herpes simplex virus vectors. *Physiol Behav* **77**, 483-488.

Matsui, K., Sasaki, Y., Komatsu, T., Mukai, M., Kikuchi, J., & Aoyama, Y. (2007). RNAi gene silencing using cerasome as a viral-size siRNA-carrier free from fusion and cross-linking. *Bioorg Med Chem Lett* **17**, 3935-3938.

Matsusaki, M., Sakaue, K., Kadowaki, K., & Akashi, M. (2013). Three-Dimensional Human Tissue Chips Fabricated by Rapid and Automatic Inkjet Cell Printing. *Adv Healthc Mater* **2**, 534-539.

McNeish, J., Gardner, J.P., Wainger, B.J., Woolf, C.J., & Eggan, K. (2015). From Dish to Bedside: Lessons Learned While Translating Findings from a Stem Cell Model of Disease to a Clinical Trial. *Cell Stem Cell* **17**, 8-10.

Mei, Y., Saha, K., Bogatyrev, S.R., Yang, J., Hook, A.L., Kalcioglu, Z.I., Cho, S.W., Mitalipova, M., Pyzocha, N., Rojas, F., Van Vliet, K.J., Davies, M.C., Alexander, M.R., Langer, R., Jaenisch, R., & Anderson, D.G. (2010). Combinatorial development of biomaterials for clonal growth of human pluripotent stem cells. *Nat Mater* **9**, 768-778.

Meyer, H.J., Turincio, R., Ng, S., Li, J., Wilson, B., Chan, P., Zak, M., Reilly, D., Beresini, M.H., & Wong, A.W. (2017). High throughput screening identifies novel, cell cycle-arresting small molecule enhancers of transient protein expression. *Biotechnol Progr* **33**, 1579-1588.

Miller, D.L., Pislaru, S.V., & Greenleaf, J.E. (2002). Sonoporation: mechanical DNA delivery by ultrasonic cavitation. *Somat Cell Mol Genet* **27**, 115-134.

Mintzer, M.A., & Simanek, E.E. (2009). Nonviral vectors for gene delivery. *Chem Rev* **109**, 259-302.

Mislick, K.A., & Baldeschwieler, J.D. (1996). Evidence for the role of proteoglycans in cation-mediated gene transfer. *Proc Natl Acad Sci USA* **93**, 12349-12354.

Mitne-Neto, M., Machado-Costa, M., Marchetto, M.C.N., Bengtson, M.H., Joazeiro, C.A., Tsuda, H., Bellen, H.J., Silva, H.C.A., Oliveira, A.S.B., Lazar, M., Muotri, A.R., & Zatz, M. (2011). Downregulation of VAPB expression in motor neurons derived from induced pluripotent stem cells of ALS8 patients. *Hum Mol Genet* **20**, 3642-3652.

Miyazaki, T., Futaki, S., Suemori, H., Taniguchi, Y., Yamada, M., Kawasaki, M., Hayashi, M., Kumagai, H., Nakatsuji, N., Sekiguchi, K., & Kawase, E. (2012). Laminin E8 fragments support efficient adhesion and expansion of dissociated human pluripotent stem cells. *Nat Commun* **3**, 1-11.

Miyazaki, T., Futaki, S., Suemori, H., Taniguchi, Y., Yamada, M., Kawasaki, M., Hayashi, M., Kumagai, H., Nakatsuji, N., Sekiguchi, K., & Kawase, E. (2013). Laminin E8 fragments support efficient adhesion and expansion of dissociated human pluripotent stem cells (vol 3, pg 1236, 2012). *Nat Commun* **4**.

Miyazaki, T., Isobe, T., Nakatsuji, N., & Suemori, H. (2017). Efficient Adhesion Culture of Human Pluripotent Stem Cells Using Laminin Fragments in an Uncoated Manner. *Sci Rep* **7**, 1-8.

Mizu, M., Koumoto, K., Anada, T., Matsumoto, T., Numata, M., Shinkai, S., Nagasaki, T., & Sakurai, K. (2004). A polysaccharide carrier for immunostimulatory CpG DNAs to enhance cytokine secretion. *J Am Chem Soc* **126**, 8372-8373.

Mok, H., & Park, T.G. (2006). PEG-assisted DNA solubilization in organic solvents for preparing cytosol specifically degradable PEG/DNA nanogels. *Bioconjugate Chem* **17**, 1369-1372.

Molas, M., Gomez-Valades, A.G., Vidal-Alabro, A., Miguel-Turu, M., Bermudez, J., Bartrons, R., & Perales, J.C. (2003). Receptor-mediated gene transfer vectors: progress towards genetic pharmaceuticals. *Curr Gene Ther* **3**, 468-485.

Mondal, G., Barui, S., & Chaudhuri, A. (2013). The relationship between the cyclic-RGDfK ligand and alpha v beta 3 integrin receptor. *Biomaterials* **34**, 6249-6260.

Montana, G., Bondi, M.L., Carrotta, R., Picone, P., Craparo, E.F., San Biagio, P.L., Giammona, G., & Di Carlo, M. (2007). Employment of cationic solid-lipid nanoparticles as RNA carriers. *Bioconjugate Chem* **18**, 302-308.

Moore, S., Evans, L.D.B., Andersson, T., Portelius, E., Smith, J., Dias, T.B., Saurat, N., McGlade, A., Kirwan, P., Blennow, K., Hardy, J., Zetterberg, H., & Livesey, F.J. (2015). APP Metabolism Regulates Tau Proteostasis in Human Cerebral Cortex Neurons. *Cell Rep* **11**, 689-696.

Moroziewicz, D., & Kaufman, H.L. (2005). Gene therapy with poxvirus vectors. *Curr Opin Mol Ther* **7**, 317-325.

Morris, M.C., Chaloin, L., Mery, J., Heitz, F., & Divita, G. (1999). A novel potent strategy for gene delivery using a single peptide vector as a carrier. *Nucleic Acids Res* **27**, 3510-3517.

Muramatsu, T., & Miyauchi, T. (2003). Basigin (CD147): a multifunctional transmembrane protein involved in reproduction, neural function, inflammation and tumor invasion. *Histol Histopathol* **18**, 981-987.

Musah, S., Morin, S.A., Wrighton, P.J., Zwick, D.B., Jin, S., & Kiessling, L.L. (2012). Glycosaminoglycan-Binding Hydrogels Enable Mechanical Control of Human Pluripotent Stem Cell Self-Renewal. *Acs Nano* **6**, 10168-10177.

Nagaoka, M., Si-Tayeb, K., Akaike, T., & Duncan, S.A. (2010). Culture of human pluripotent stem cells using completely defined conditions on a recombinant E-cadherin substratum. *Bmc Dev Biol* **10**, 1-12.

Napoli, S., Carbone, G.M., Catapano, C.V., Shaw, N., & Arya, D.P. (2005). Neomycin improves cationic lipid-mediated transfection of DNA in human cells. *Bioorg Med Chem Lett* **15**, 3467-3469.

Narsinh, K.H., Sun, N., Sanchez-Freire, V., Lee, A.S., Almeida, P., Hu, S.J., Jan, T., Wilson, K.D., Leong, D., Rosenberg, J., Yao, M., Robbins, R.C., & Wu, J.C. (2011). Single cell transcriptional profiling reveals heterogeneity of human induced pluripotent stem cells. *J Clin Invest* **121**, 1217-1221.

Narva, E., Stubb, A., Guzman, C., Blomqvist, M., Balboa, D., Lerche, M., Saari, M., Otonkoski, T., & Ivaska, J. (2017). A Strong Contractile Actin Fence and Large Adhesions Direct Human Pluripotent Colony Morphology and Adhesion. *Stem Cell Rep* **9**, 67-76.

Navarro, P., Festuccia, N., Colby, D., Gagliardi, A., Mullin, N.P., Zhang, W., Karwacki-Neisius, V., Osorno, R., Kelly, D., Robertson, M., & Chambers, I. (2012a). OCT4/SOX2-independent Nanog autorepression modulates heterogeneous Nanog gene expression in mouse ES cells. *Embo J* **31**, 4547-4562.

Nelson, T.J., Martinez-Fernandez, A., & Terzic, A. (2010). Induced pluripotent stem cells: developmental biology to regenerative medicine. *Nat Rev Cardiol* **7**, 700-710.

Nemunaitis, J., Ganly, I., Khuri, F., Arseneau, J., Kuhn, J., McCarty, T., Landers, S., Maples, P., Romel, L., Randlev, B., Reid, T., Kaye, S., & Kirn, D. (2000). Selective replication and oncolysis in p53 mutant tumors with ONYX-015, an E1B-55kD gene-deleted adenovirus, in patients with advanced head and neck cancer: A Phase II trial. *Cancer Res* **60**, 6359-6366.

Neto, A.I., Demir, K., Popova, A.A., Oliveira, M.B., Mano, J.F., & Levkin, P.A. (2016). Fabrication of Hydrogel Particles of Defined Shapes Using Superhydrophobic-Hydrophilic Micropatterns. *Adv Mater* **28**, 7613-7619.

Ng, V.Y., Ang, S.N., Chan, J.X., & Choo, A.B.H. (2010). Characterization of Epithelial Cell Adhesion Molecule as a Surface Marker on Undifferentiated Human Embryonic Stem Cells. *Stem Cells* **28**, 29-35.

Nguyen, A., Beyersdorf, J., Riethoven, J.J., & Pannier, A.K. (2016). High-throughput screening of clinically approved drugs that prime polyethylenimine transfection reveals modulation of mitochondria dysfunction response improves gene transfer efficiencies. *Bioeng Transl Med* **1**, 123-135.

Nguyen, E.H., Daly, W.T., Le, N.N.T., Farnoodian, M., Belair, D.G., Schwartz, M.P., Lebakken, C.S., Ananiev, G.E., Saghiri, M.A., Knudsen, T.B., Sheibani, N., & Murphy, W.L. (2017). Versatile synthetic alternatives to Matrigel for vascular toxicity screening and stem cell expansion. *Nat Biomed Eng* **1**, 1-14.

Nichols, J., & Smith, A. (2009). Naive and Primed Pluripotent States. *Cell Stem Cell* **4**, 487-492.

Niculescu-Duvaz, D., Heyes, J., & Springer, C.J. (2003). Structure-activity relationship in cationic lipid mediated gene transfection. *Curr Med Chem* **10**, 1233-1261.

Nishikawa, S., Goldstein, R.A., & Nierras, C.R. (2008). The promise of human induced pluripotent stem cells for research and therapy. *Nat Rev Mol Cell Bio* **9**, 725-729.

Nori, S., Okada, Y., Yasuda, A., Tsuji, O., Takahashi, Y., Kobayashi, Y., Fujiyoshi, K., Koike, M., Uchiyama, Y., Ikeda, E., Toyama, Y., Yamanaka, S., Nakamura, M., & Okano, H. (2011). Grafted human-induced pluripotent stem-cell-derived neurospheres promote motor functional recovery after spinal cord injury in mice. *Proc Natl Acad Sci U S A* **108**, 16825-16830.

O'Brien, J.A., & Lummis, S.C.R. (2006). Biolistic transfection of neuronal cultures using a hand-held gene gun. *Nat Protoc* **1**, 977-981.

Ogawa, M., Ogawa, S., Bear, C.E., Ahmadi, S., Chin, S., Li, B., Grompe, M., Keller, G., Kamath, B.M., & Ghanekar, A. (2015). Directed differentiation of cholangiocytes from human pluripotent stem cells. *Nat Biotechnol* **33**, 853-861.

Ohgushi, M., Matsumura, M., Eiraku, M., Murakami, K., Aramaki, T., Nishiyama, A., Muguruma, K., Nakano, T., Suga, H., Ueno, M., Ishizaki, T., Suemori, H., Narumiya, S., Niwa, H., & Sasai, Y. (2010). Molecular Pathway and Cell State

Responsible for Dissociation-Induced Apoptosis in Human Pluripotent Stem Cells. *Cell Stem Cell* **7**, 225-239.

Okita, K., Nakagawa, M., Hong, H.J., Ichisaka, T., & Yamanaka, S. (2008). Generation of Mouse Induced Pluripotent Stem Cells Without Viral Vectors. *Science* **322**, 949-953.

Omole, A.E., & Fakoya, A.O.J. (2018). Ten years of progress and promise of induced pluripotent stem cells: historical origins, characteristics, mechanisms, limitations, and potential applications. *Peerj* **6**, e4370.

Oudeng, G., Benz, M., Popova, A.A., Zhang, Y., Yi, C.Q., Levkin, P.A., & Yang, M. (2020). Droplet Microarray Based on Nanosensing Probe Patterns for Simultaneous Detection of Multiple HIV Retroviral Nucleic Acids. *Acs Appl Mater Inter* **12**, 55614-55623.

Ovadia, E.M., Colby, D.W., & Kloxin, A.M. (2018). Designing well-defined photopolymerized synthetic matrices for three-dimensional culture and differentiation of induced pluripotent stem cells. *Biomater Sci* **6**, 1358-1370.

Ozbolat, I.T., & Hospodiuk, M. (2016). Current advances and future perspectives in extrusion-based bioprinting. *Biomaterials* **76**, 321-343.

Pack, D.W., Hoffman, A.S., Pun, S., & Stayton, P.S. (2005). Design and development of polymers for gene delivery. *Nat Rev Drug Discov* **4**, 581-593.

Palchetti, S., Pozzi, D., Marchini, C., Amici, A., Andreani, C., Bartolacci, C., Digiacomo, L., Gambini, V., Cardarelli, F., Di Rienzo, C., Peruzzi, G., Amenitsch, H., Palermo, R., Screpanti, I., & Caracciolo, G. (2017). Manipulation of lipoplex concentration at the cell surface boosts transfection efficiency in hard-to-transfect cells. *Nanomed-Nanotechnol* **13**, 681-691.

Pan, C.Y., Hicks, A., Guan, X., Chen, H., & Bishop, C.E. (2010). SNL fibroblast feeder layers support derivation and maintenance of human induced pluripotent stem cells. *J Genet Genomics* **37**, 241-248.

Pankov, R., & Yamada, K.M. (2002). Fibronectin at a glance. *J Cell Sci* **115**, 3861-3863.

Parisini, E., Higgins, J.M.G., Liu, J.H., Brenner, M.B., & Wang, J.H. (2007). The crystal structure of human E-cadherin domains 1 and 2, and comparison with other cadherins in the context of adhesion mechanism. *J Mol Biol* **373**, 401-411.

Park, D., Son, K., Hwang, Y., Ko, J., Lee, Y., Doh, J., & Jeon, N.L. (2019). High-Throughput Microfluidic 3D Cytotoxicity Assay for Cancer Immunotherapy (CACI-IMPACT Platform). *Front Immunol* **10**, 1133.

Parodi, M.B., Di Bartolo, E., Brue, C., Cappello, E., Furino, C., Giuffrida, S., Imparato, M., & Reibaldi, M. (2018). Pegaptanib: choroidal neovascularization in patients with age-related macular degeneration and previous arterial thromboembolic events. *Eur J Ophthalmol* **28**, 58-62.

Patil, S., Gao, Y.G., Lin, X., Li, Y., Dang, K., Tian, Y., Zhang, W.J., Jiang, S.F., Qadir, A., & Qian, A.R. (2019). The Development of Functional Non-Viral Vectors for Gene Delivery. *Int J Mol Sci* **20**, 5491.

Pavsic, M., Guncar, G., Djinovic-Carugo, K., & Lenarcic, B. (2014). Crystal structure and its bearing towards an understanding of key biological functions of EpCAM. *Nat Commun* **5**, 1-10.

Payne, N.L., Sylvaini, A., O'Brien, C., Herszfeld, D., Sun, G., & Bernard, C.C.A. (2015). Application of human induced pluripotent stem cells for modeling and treating neurodegenerative diseases. *New Biotechnol* **32**, 212-228.

Pereira, D.A., & Williams, J.A. (2007). Origin and evolution of high throughput screening. *Brit J Pharmacol* **152**, 53-61.

Petridou, N.I., & Skourides, P.A. (2016). A ligand-independent integrin beta 1 mechanosensory complex guides spindle orientation. *Nat Commun* **7**, 1-15.

Pfaffl, M.W. (2001). A new mathematical model for relative quantification in real-time RT-PCR. *Nucleic Acids Res* **29**, e45.

Pfeifer, A., & Verma, I.M. (2001). Gene therapy: Promises and problems. *Annu Rev Genom Hum G* **2**, 177-211.

Popova, A.A., Demir, K., Hartanto, T.G., Schmitt, E., & Levkin, P.A. (2016). Droplet-microarray on superhydrophobic-superhydrophilic patterns for high-throughput live cell screenings. *Rsc Adv* **6**, 38263-38276.

Popova, A.A., Marcato, D., Peravali, R., Wehl, I., Schepers, U., & Levkin, P.A. (2018). Fish-Microarray: A Miniaturized Platform for Single-Embryo High-Throughput Screenings. *Adv Funct Mater* **28**, 1703486.

Popova, A.A., Tronser, T., Demir, K., Haitz, P., Kuodyte, K., Starkuviene, V., Wajda, P., & Levkin, P.A. (2019). Facile One Step Formation and Screening of Tumor Spheroids Using Droplet-Microarray Platform. *Small* **15**, 1901299.

Priola, J.J., Calzadilla, N., Baumann, M., Borth, N., Tate, C.G., & Betenbaugh, M.J. (2016). High-throughput screening and selection of mammalian cells for enhanced protein production. *Biotechnol J* **11**, 853-865.

Pripuzova, N.S., Getie-Kebtie, M., Grunseich, C., Sweeney, C., Malech, H., & Alterman, M.A. (2015). Development of a protein marker panel for characterization of human induced pluripotent stem cells (hiPSCs) using global quantitative proteome analysis. *Stem Cell Res* **14**, 323-338.

Prota, A.E., Campbell, J.A., Schelling, P., Forrest, J.C., Watson, M.J., Peters, T.R., Aurrand-Lions, M., Imhof, B.A., Dermody, T.S., & Stehle, T. (2003). Crystal structure of human junctional adhesion molecule 1: Implications for reovirus binding. *Proc Natl Acad Sci USA* **100**, 5366-5371.

Putnam, D. (2006). Polymers for gene delivery across length scales. *Nat Mater* **5**, 439-451.

Putnam, D., & Langer, R. (1999). Poly(4-hydroxy-L-proline ester): Low-temperature polycondensation and plasmid DNA complexation. *Macromolecules* **32**, 3658-3662.

Qian, X., Villa-Diaz, L.G., Kumar, R., Lahann, J., & Krebsbach, P.H. (2014). Enhancement of the propagation of human embryonic stem cells by modifications in the gel architecture of PMEDSAH polymer coatings. *Biomaterials* **35**, 9581-9590.

Rashid, S.T., Corbineau, S., Hannan, N., Marciniak, S.J., Miranda, E., Alexander, G., Huang-Doran, I., Griffin, J., Ahrlund-Richter, L., Skepper, J., Semple, R., Weber, A., Lomas, D.A., & Vallier, L. (2010). Modeling inherited metabolic disorders of the liver using human induced pluripotent stem cells. *J Clin Invest* **120**, 3127-3136.

Raya, A., Rodriguez-Piza, I., Guenechea, G., Vassena, R., Navarro, S., Barrero, M.J., Consiglio, A., Castella, M., Rio, P., Sleep, E., Gonzalez, F., Tiscornia, G., Garreta, E., Aasen, T., Veiga, A., Verma, I.M., Surralles, J., Bueren, J., & Belmonte, J.C.I. (2009). Disease-corrected haematopoietic progenitors from Fanconi anaemia induced pluripotent stem cells. *Nature* **460**, 53-59.

Recillas-Targa, F. (2006). Multiple strategies for gene transfer, expression, knockdown, and chromatin influence in mammalian cell lines and transgenic animals. *Mol Biotechnol* **34**, 337-354.

Regelin, A.E., Fernholz, E., Krug, H.F., & Massing, U. (2001). High throughput screening method for identification of new lipofection reagents. *J Biomol Screen* **6**, 245-254.

Richardson, P.G., Elias, A.D., Krishnan, A., Wheeler, C., Nath, R., Hoppensteadt, D., Kinchla, N.M., Neuberg, D., Waller, E.K., Antin, J.H., Soiffer, R., Vredenburgh, J., Lill, M., Woolfrey, A.E., Bearman, S.I., Iacobelli, M., Fareed, J., & Guinan, E.C. (1998). Treatment of severe veno-occlusive disease with defibrotide: Compassionate use results in response without significant toxicity in a high-risk population. *Blood* **92**, 737-744.

Richardson, P.G., Riches, M.L., Kernan, N.A., Brochstein, J.A., Mineishi, S., Termuhlen, A.M., Arai, S., Grupp, S.A., Guinan, E.C., Martin, P.L., Steinbach, G., Krishnan, A., Nemecek, E.R., Giralt, S., Rodriguez, T., Duerst, R., Doyle, J., Antin, J.H., Smith, A., Lehmann, L., Champlin, R., Gillio, A., Bajwa, R., D'Agostino, R.B., Massaro, J., Warren, D., Miloslavsky, M., Hume, R.L., Iacobelli, M., Nejadnik, B., Hannah, A.L., & Soiffer, R.J. (2016). Phase 3 trial of defibrotide for the treatment of severe veno-occlusive disease and multi-organ failure. *Blood* **127**, 1656-1665.

Richardson, P.G., Soiffer, R.J., Antin, J.H., Uno, H., Jin, Z.Z., Kurtzberg, J., Martin, P.L., Steinbach, G., Murray, K.F., Vogelsang, G.B., Chen, A.R., Krishnan, A., Kernan, N.A., Avigan, D.E., Spitzer, T.R., Shulman, H.M., Di Salvo, D.N., Revta, C., Warren, D., Momtaz, P., Bradwin, G., Wei, L.J., Iacobelli, M., McDonald, G.B., & Guinan, E.C. (2010). Defibrotide for the Treatment of Severe Hepatic Veno-Occlusive Disease and Multiorgan Failure after Stem Cell Transplantation: A Multicenter, Randomized, Dose-Finding Trial. *Biol Blood Marrow Tr* **16**, 1005-1017.

Richardson, S.C.W., Pattrick, N.G., Man, Y.K.S., Ferruti, P., & Duncan, R. (2001). Poly(amidoamine)s as potential nonviral vectors: Ability to form interpolyelectrolyte complexes and to mediate transfection in vitro. *Biomacromolecules* **2**, 1023-1028.

Riedl, S.A.B., Kaiser, P., Raup, A., Synatschke, C.V., Jerome, V., & Freitag, R. (2018). Non-Viral Transfection of Human T Lymphocytes. *Processes* **6**, 118.

Rigby, P.G. (1969). Prolongation of Survival of Tumour-Bearing Animals by Transfer of Immune Rna with Deae Dextran. *Nature* **221**, 968-969.

Rodin, S., Antonsson, L., Niaudet, C., Simonson, O.E., Salmela, E., Hansson, E.M., Domogatskaya, A., Xiao, Z.J., Damdimopoulou, P., Sheikhi, M., Inzunza, J., Nilsson, A.S., Baker, D., Kuiper, R., Sun, Y., Blennow, E., Nordenskjold, M., Grinnemo, K.H., Kere, J., Betsholtz, C., Hovatta, O., & Tryggvason, K. (2014). Clonal culturing of human embryonic stem cells on laminin-521/E-cadherin matrix in defined and xeno-free environment. *Nat Commun* **5**, 1-13.

Rodin, S., Domogatskaya, A., Strom, S., Hansson, E.M., Chien, K.R., Inzunza, J., Hovatta, O., & Tryggvason, K. (2010). Long-term self-renewal of human pluripotent stem cells on human recombinant laminin-511. *Nat Biotechnol* **28**, 611-617.

Rosenfeld, A., Brehm, M., Welle, A., Trouillet, V., Heissler, S., Benz, M., & Levkin, P.A. (2019). Solid-phase combinatorial synthesis using microarrays of microcompartments with light-induced on-chip cell screening. *Mater Today Bio* **3**, 100022.

Rosenfeld, A., Oelschlaeger, C., Thelen, R., Heissler, S., & Levkin, P.A. (2020). Miniaturized high-throughput synthesis and screening of responsive hydrogels using nanoliter compartments. *Mater Today Bio* **6**, 100053.

Ross, A.M., Jiang, Z.X., Bastmeyer, M., & Lahann, J. (2012). Physical Aspects of Cell Culture Substrates: Topography, Roughness, and Elasticity. *Small* **8**, 336-355.

Rowland, T.J., Miller, L.M., Blaschke, A.J., Doss, E.L., Bonham, A.J., Hikita, S.T., Johnson, L.V., & Clegg, D.O. (2010). Roles of Integrins in Human Induced Pluripotent Stem Cell Growth on Matrigel and Vitronectin. *Stem Cells Dev* **19**, 1231-1240.

Russell, S., Bennett, J., Wellman, J.A., Chung, D.C., Yu, Z.F., Tillman, A., Wittes, J., Pappas, J., Elci, O., McCague, S., Cross, D., Marshall, K.A., Walshire, J., Kehoe, T.L., Reichert, H., Davis, M., Raffini, L., George, L.A., Hudson, F.P., Dingfield, L., Zhu, X.S., Haller, J.A., Sohn, E.H., Mahajan, V.B., Pfeifer, W., Weckmann, M., Johnson, C., Gewaily, D., Drack, A., Stone, E., Wachtel, K., Simonelli, F., Leroy, B.P., Wright, J.F., High, K.A., & Maguire, A.M. (2017). Efficacy and safety of voretigene neparvovec (AAV2-hRPE65v2) in patients with RPE65-mediated inherited retinal dystrophy: a randomised, controlled, open-label, phase 3 trial. *Lancet* **390**, 849-860.

Ryan, S.D., Dolatabadi, N., Chan, S.F., Zhang, X.F., Akhtar, M.W., Parker, J., Soldner, F., Sunico, C.R., Nagar, S., Talantova, M., Lee, B., Lopez, K., Nutter, A., Shan, B., Molokanova, E., Zhang, Y.Y., Han, X.M., Nakamura, T., Masliah, E., Yates, J.R., Nakanishi, N., Andreyev, A.Y., Okamoto, S., Jaenisch, R., Ambasudhan, R., & Lipton, S.A. (2013). Isogenic Human iPSC Parkinson's Model Shows Nitrosative Stress-Induced Dysfunction in MEF2-PGC1 alpha Transcription. *Cell* **155**, 1351-1364.

Sakthivel, K., Kumar, H., Mohamed, M.G.A., Talebjedi, B., Shim, J., Najjaran, H., Hoorfar, M., & Kim, K. (2020). High Throughput Screening of Cell Mechanical Response Using a Stretchable 3D Cellular Microarray Platform. *Small* **16**, 2000941.

Sampaziotis, F., de Brito, M.C., Madrigal, P., Bertero, A., Saeb-Parsy, K., Soares, F.A.C., Schrumpf, E., Melum, E., Karlsen, T.H., Bradley, J.A., Gelson, W.T.H., Davies, S., Baker, A., Kaser, A., Alexander, G.J., Hannan, N.R.F., & Vallier, L. (2015). Cholangiocytes derived from human induced pluripotent stem cells for disease modeling and drug validation. *Nat Biotechnol* **33**, 845-852.

Santos, R.D., Raal, F.J., Catapano, A.L., Witztum, J.L., Steinhagen-Thiessen, E., & Tsimikas, S. (2015). Mipomersen, an Antisense Oligonucleotide to Apolipoprotein B-100, Reduces Lipoprotein(a) in Various Populations With Hypercholesterolemia Results of 4 Phase III Trials. *Arterioscl Throm Vas* **35**, 689-699.

Schenborn, E.T., & Goiffon, V. (2000). DEAE-dextran transfection of mammalian cultured cells. *Methods Mol Biol* **130**, 147-153.

Scherer, F., Anton, M., Schillinger, U., Henkel, J., Bergemann, C., Kruger, A., Gansbacher, B., & Plank, C. (2002). Magnetofection: enhancing and targeting gene delivery by magnetic force in vitro and in vivo. *Gene Ther* **9**, 102-109.

Schvartz, I., Seger, D., & Shaltiel, S. (1999). Vitronectin. *Int J Biochem Cell Biol* **31**, 539-544.

Seibler, P., Graziotto, J., Jeong, H., Simunovic, F., Klein, C., & Krainc, D. (2011). Mitochondrial Parkin Recruitment Is Impaired in Neurons Derived from Mutant PINK1 Induced Pluripotent Stem Cells. *J Neurosci* **31**, 5970-5976.

Senzer, N.N., Kaufman, H.L., Amatruda, T., Nemunaitis, M., Reid, T., Daniels, G., Gonzalez, R., Glaspy, J., Whitman, E., Harrington, K., Goldsweig, H., Marshall, T., Love, C., Coffin, R., & Nemunaitis, J.J. (2009). Phase II Clinical Trial of a Granulocyte-Macrophage Colony-Stimulating Factor-Encoding, Second-Generation Oncolytic Herpesvirus in Patients With Unresectable Metastatic Melanoma. *J Clin Oncol* **27**, 5763-5771.

Setten, R.L., Rossi, J.J., & Han, S.P. (2019). The current state and future directions of RNAi-based therapeutics. *Nat Rev Drug Discov* **18**, 421-446.

Shahryari, A., Saghaeian Jazi, M., Mohammadi, S., Razavi Nikoo, H., Nazari, Z., Hosseini, E.S., Burtscher, I., Mowla, S.J., & Lickert, H. (2019). Development and Clinical Translation of Approved Gene Therapy Products for Genetic Disorders. *Front Genet* **10**, 868.

Shi, J.F., Ma, Y.F., Zhu, J., Chen, Y.X., Sun, Y.T., Yao, Y.C., Yang, Z.G., & Xie, J. (2018). A Review on Electroporation-Based Intracellular Delivery. *Molecules* **23**, 3044.

Shi, Y., Inoue, H., Wu, J.C., & Yamanaka, S. (2017). Induced pluripotent stem cell technology: a decade of progress. *Nat Rev Drug Discov* **16**, 115-130.

Silva, G., Poirot, L., Galetto, R., Smith, J., Montoya, G., Duchateau, P., & Paques, F. (2011). Meganucleases and Other Tools for Targeted Genome Engineering: Perspectives and Challenges for Gene Therapy. *Curr Gene Ther* **11**, 11-27.

Singh, A., Suri, S., Lee, T., Chilton, J.M., Cooke, M.T., Chen, W., Fu, J., Stice, S.L., Lu, H., McDevitt, T.C., & Garcia, A.J. (2013). Adhesion strength-based, label-free isolation of human pluripotent stem cells. *Nat Methods* **10**, 438-444.

Soga, M., Ishitsuka, Y., Hamasaki, M., Yoneda, K., Furuya, H., Matsuo, M., Ihn, H., Fusaki, N., Nakamura, K., Nakagata, N., Endo, F., Irie, T., & Era, T. (2015). HPGCD Outperforms HPBCD as a Potential Treatment for Niemann-Pick Disease Type C During Disease Modeling with iPS Cells. *Stem Cells* **33**, 1075-1088.

Spitalieri, P., Talarico, R.V., Caioli, S., Murdocca, M., Serafino, A., Girasole, M., Dinarelli, S., Longo, G., Pucci, S., Botta, A., Novelli, G., Zona, C., Mango, R., & Sangiuolo, F. (2018). Modelling the pathogenesis of Myotonic Dystrophy type 1 cardiac phenotype through human iPSC-derived cardiomyocytes. *J Mol Cell Cardiol* **118**, 95-109.

Srinivasan, C., Lee, J., Papadimitrakopoulos, F., Silbart, L.K., Zhao, M.H., & Burgess, D.J. (2006). Labeling and intracellular tracking of functionally active plasmid DNA with semiconductor quantum dots. *Mol Ther* **14**, 192-201.

Stepanenko, A.A., & Heng, H.H. (2017). Transient and stable vector transfection: Pitfalls, off-target effects, artifacts. *Mutat Res* **773**, 91-103.

Sugawara, Y., Hamada, K., Yamada, Y., Kumai, J., Kanagawa, M., Kobayashi, K., Toda, T., Negishi, Y., Katagiri, F., Hozumi, K., Nomizu, M., & Kikkawa, Y. (2019). Characterization of dystroglycan binding in adhesion of human induced pluripotent stem cells to laminin-511 E8 fragment. *Sci Rep* **9**, 1-12.

Sun, N., Yazawa, M., Liu, J.W., Han, L., Sanchez-Freire, V., Abilez, O.J., Navarrete, E.G., Hu, S.J., Wang, L., Lee, A., Pavlovic, A., Lin, S., Chen, R., Hajjar, R.J., Snyder, M.P., Dolmetsch, R.E., Butte, M.J., Ashley, E.A., Longaker, M.T., Robbins, R.C., & Wu, J.C. (2012a). Patient-Specific Induced Pluripotent Stem Cells as a Model for Familial Dilated Cardiomyopathy. *Sci Transl Med* **4**, 130ra147.

Sun, Y.B., Chen, C.S., & Fu, J.P. (2012b). Forcing Stem Cells to Behave: A Biophysical Perspective of the Cellular Microenvironment. *Annu Rev Biophys* **41**, 519-542.

Suntivich, R., Drachuk, I., Calabrese, R., Kaplan, D.L., & Tsukruk, V.V. (2014). Inkjet Printing of Silk Nest Arrays for Cell Hosting. *Biomacromolecules* **15**, 1428-1435.

Szejtli, J. (1998). Introduction and General Overview of Cyclodextrin Chemistry. *Chem Rev* **98**, 1743-1754.

Takahashi, K., Tanabe, K., Ohnuki, M., Narita, M., Ichisaka, T., Tomoda, K., & Yamanaka, S. (2007). Induction of pluripotent stem cells from adult human fibroblasts by defined factors. *Cell* **131**, 861-872.

Takahashi, K., & Yamanaka, S. (2006). Induction of pluripotent stem cells from mouse embryonic and adult fibroblast cultures by defined factors. *Cell* **126**, 663-676.

Takayama, K., Inamura, M., Kawabata, K., Katayama, K., Higuchi, M., Tashiro, K., Nonaka, A., Sakurai, F., Hayakawa, T., Furue, M.K., & Mizuguchi, H. (2012). Efficient Generation of Functional Hepatocytes From Human Embryonic Stem Cells and Induced Pluripotent Stem Cells by HNF4 alpha Transduction. *Mol Ther* **20**, 127-137.

Takizawa, M., Arimori, T., Taniguchi, Y., Kitago, Y., Yamashita, E., Takagi, J., & Sekiguchi, K. (2017). Mechanistic basis for the recognition of laminin-511 by alpha 6 beta 1 integrin. *Sci Adv* **3**, e1701497.

Tan, Q., Lui, P.P.Y., Rui, Y.F., & Wong, Y.M. (2012). Comparison of Potentials of Stem Cells Isolated from Tendon and Bone Marrow for Musculoskeletal Tissue Engineering. *Tissue Eng Pt A* **18**, 840-851.

Tanaka, T., Takahashi, K., Yamane, M., Tomida, S., Nakamura, S., Oshima, K., Niwa, A., Nishikomori, R., Kambe, N., Hara, H., Mitsuyama, M., Morone, N., Heuser, J.E., Yamamoto, T., Watanabe, A., Sato-Otsubo, A., Ogawa, S., Asaka, I., Heike, T., Yamanaka, S., Nakahata, T., & Saito, M.K. (2012). Induced pluripotent stem cells from CINCA syndrome patients as a model for dissecting somatic mosaicism and drug discovery. *Blood* **120**, 1299-1308.

Teriete, P., Banerji, S., Noble, M., Blundell, C.D., Wright, A.J., Pickford, A.R., Lowe, E., Mahoney, D.J., Tammi, M.I., Kahmann, J.D., Campbell, I.D., Day, A.J., & Jackson, D.G. (2004). Structure of the regulatory hyaluronan binding domain in the inflammatory leukocyte homing receptor CD44. *Mol Cell* **13**, 483-496.

Thomas, C.E., Ehrhardt, A., & Kay, M.A. (2003). Progress and problems with the use of viral vectors for gene therapy. *Nat Rev Genet* **4**, 346-358.

Tong, L.M., Fong, H., & Huang, Y.D. (2015). Stem cell therapy for Alzheimer's disease and related disorders: current status and future perspectives. *Exp Mol Med* **47**, e151.

Torchilin, V.P., Levchenko, T.S., Rammohan, R., Volodina, N., Papahadjopoulos-Sternberg, B., & D'Souza, G.G.M. (2003). Cell transfection in vitro and in vivo with nontoxic TAT peptide-liposome-DNA complexes. *Proc Natl Acad Sci USA* **100**, 1972-1977.

Tronser, T., Demir, K., Reischl, M., Bastmeyer, M., & Levkin, P.A. (2018). Droplet microarray: miniaturized platform for rapid formation and high-throughput screening of embryoid bodies. *Lab Chip* **18**, 2257-2269.

Tronser, T., Popova, A.A., Jaggy, M., Bastmeyer, M., & Levkin, P.A. (2017). Droplet Microarray Based on Patterned Superhydrophobic Surfaces Prevents Stem Cell Differentiation and Enables High-Throughput Stem Cell Screening. *Adv Healthc Mater* **6**, 1700622.

Troster, A., Heinzlmeir, S., Berger, B.T., Gande, S.L., Saxena, K., Sreeramulu, S., Linhard, V., Nasiri, A.H., Bolte, M., Muller, S., Kuster, B., Medard, G., Kudlinzki, D., & Schwalbe, H. (2018). NVP-BHG712: Effects of Regioisomers on the Affinity and Selectivity toward the EPHrin Family. *Chemmedchem* **13**, 1629-1633.

Tulpule, A., Kelley, J.M., Lensch, M.W., McPherson, J., Park, I.H., Hartung, O., Nakamura, T., Schlaeger, T.M., Shimamura, A., & Daley, G.Q. (2013). Pluripotent Stem Cell Models of Shwachman-Diamond Syndrome Reveal a Common Mechanism for Pancreatic and Hematopoietic Dysfunction. *Cell Stem Cell* **12**, 727-736.

Ueda, E., Feng, W.Q., & Levkin, P.A. (2016). Superhydrophilic-Superhydrophobic Patterned Surfaces as High-Density Cell Microarrays: Optimization of Reverse Transfection. *Adv Healthc Mater* **5**, 2646-2654.

Ueda, E., Geyer, F.L., Nedashkivska, V., & Levkin, P.A. (2012). Droplet Microarray: facile formation of arrays of microdroplets and hydrogel micropads for cell screening applications. *Lab Chip* **12**, 5218-5224.

Ullah, I., Busch, J.F., Rabien, A., Ergun, B., Stamm, C., Knosalla, C., Hippenstiel, S., Reinke, P., & Kurtz, A. (2020). Adult Tissue Extracellular Matrix Determines Tissue Specification of Human iPSC-Derived Embryonic Stage Mesodermal Precursor Cells. *Adv Sci* **7**, 1901198.

Utz, V.M., Coussa, R.G., Antaki, F., & Traboulsi, E.I. (2018). Gene therapy for RPE65-related retinal disease. *Ophthalmic Genet* **39**, 671-677.

Vallier, L., Touboul, T., Brown, S., Cho, C., Bilican, B., Alexander, M., Cedervall, J., Chandran, S., Ahrlund-Richter, L., Weber, A., & Pedersen, R.A. (2009). Signaling Pathways Controlling Pluripotency and Early Cell Fate Decisions of Human Induced Pluripotent Stem Cells. *Stem Cells* **27**, 2655-2666.

van den Pol, A.N., Mocarski, E., Saederup, N., Vieira, J., & Meier, T.J. (1999). Cytomegalovirus cell tropism, replication, and gene transfer in brain. *J Neurosci* **19**, 10948-10965.

van Raaij, M.J., Chouin, E., van der Zandt, H., Bergelson, J.M., & Cusack, S. (2001). Dimeric structure of the coxsackievirus and adenovirus receptor D1 domain at 1.7 angstrom resolution (vol 8, pg 1147, 2000). *Structure* **9**, U5-U5.

Vasquez, R.J., Howell, B., Yvon, A.M.C., Wadsworth, P., & Cassimeris, L. (1997). Nanomolar concentrations of nocodazole alter microtubule dynamic instability in vivo and in vitro. *Mol Biol Cell* **8**, 973-985.

Villa-Diaz, L.G., Ross, A.M., Lahann, J., & Krebsbach, P.H. (2013). Concise Review: The Evolution of Human Pluripotent Stem Cell Culture: From Feeder Cells to Synthetic Coatings. *Stem Cells* **31**, 1-7.

Vitillo, L., & Kimber, S.J. (2017). Integrin and FAK Regulation of Human Pluripotent Stem Cells. *Curr Stem Cell Rep* **3**, 358-365.

Voter, A.F., Manthei, K.A., & Keck, J.L. (2016). A High-Throughput Screening Strategy to Identify Protein-Protein Interaction Inhibitors That Block the Fanconi Anemia DNA Repair Pathway. *J Biomol Screen* **21**, 626-633.

Waldrop, M.A., & Kolb, S.J. (2019). Current Treatment Options in Neurology-SMA Therapeutics. *Curr Treat Options Neurol* **21**, 25.

Walker, J.R., Yermekbayeva, L., Butler-Cole, C., Weigelt, J., Bountra, C., Arrowsmith, C.H., Edwards, A.M., Bochkarev, A., Dhe-Paganon, S. (2009). SAM Domain of Human Ephrin Type-A Receptor 1 (EphA1).

Wang, D., & Gao, G. (2014). State-of-the-art human gene therapy: part II. Gene therapy strategies and clinical applications. *Discov Med* **18**, 151-161.

Wang, J., Zhang, P.C., Lu, H.F., Ma, N., Wang, S., Mao, H.Q., & Leong, K.W. (2002). New polyphosphoramidate with a spermidine side chain as a gene carrier. *J Control Release* **83**, 157-168.

Wang, J.L., Rao, S., Chu, J.L., Shen, X.H., Levasseur, D.N., Theunissen, T.W., & Orkin, S.H. (2006). A protein interaction network for pluripotency of embryonic stem cells. *Nature* **444**, 364-368.

Wang, L., & MacDonald, R.C. (2004). Effects of microtubule-depolymerizing agents on the transfection of cultured vascular smooth muscle cells: Enhanced expression with free drug and especially with drug-gene lipoplexes. *Mol Ther* **9**, 729-737.

Wang, Y., Chou, B.K., Dowey, S., He, C.X., Gerecht, S., & Cheng, L.Z. (2013). Scalable expansion of human induced pluripotent stem cells in the defined xeno-free E8 medium under adherent and suspension culture conditions. *Stem Cell Res* **11**, 1103-1116.

Wang, Y.X., Zheng, C.G., Jiang, Y.H., Zhang, J.Q., Chen, J.Y., Yao, C., Zhao, Q.G., Liu, S., Chen, K., Du, J., Yang, Z., & Gao, S.R. (2012). Genetic correction of beta-thalassemia patient-specific iPS cells and its use in improving hemoglobin production in irradiated SCID mice. *Cell Res* **22**, 637-648.

Wang, Z.H., Kim, M.C., Marquez, M., & Thorsen, T. (2007). High-density microfluidic arrays for cell cytotoxicity analysis. *Lab Chip* **7**, 740-745.

Watanabe, K., Ueno, M., Kamiya, D., Nishiyama, A., Matsumura, M., Wataya, T., Takahashi, J.B., Nishikawa, S., Nishikawa, S., Muguruma, K., & Sasai, Y. (2007). A ROCK inhibitor permits survival of dissociated human embryonic stem cells. *Nat Biotechnol* **25**, 681-686.

Wiethoff, C.M., & Middaugh, C.R. (2003). Barriers to nonviral gene delivery. *J Pharm Sci* **92**, 203-217.

Wildey, M.J., Haunso, A., Tudor, M., Webb, M., & Connick, J.H. (2017). High-Throughput Screening. *Annu Rep Med Chem* **50**, 149-195.

Williams, R.S., Johnston, S.A., Riedy, M., Devit, M.J., Mcelligott, S.G., & Sanford, J.C. (1991). Introduction of Foreign Genes into Tissues of Living Mice by DNA-Coated Microprojectiles. *Proc Natl Acad Sci USA* **88**, 2726-2730.

Wirth, T., Parker, N., & Yla-Herttuala, S. (2013). History of gene therapy. *Gene* **525**, 162-169.

Woodruff, G., Young, J.E., Martinez, F.J., Buen, F., Gore, A., Kinaga, J., Li, Z., Yuan, S.H., Zhang, K., & Goldstein, L.S.B. (2013). The Presenilin-1 Delta E9 Mutation Results in Reduced gamma-Secretase Activity, but Not Total Loss of PS1 Function, in Isogenic Human Stem Cells. *Cell Rep* **5**, 974-985.

Woodruff, K., & Maerkl, S.J. (2016). A High-Throughput Microfluidic Platform for Mammalian Cell Transfection and Culturing. *Sci Rep* **6**, 1-12.

Woods, N.B., Muessig, A., Schmidt, M., Flygare, J., Olsson, K., Salmon, P., Trono, D., von Kalle, C., & Karlsson, S. (2003). Lentiviral vector transduction of NOD/SCID repopulating cells results in multiple vector integrations per transduced cell: risk of insertional mutagenesis. *Blood* **101**, 1284-1289.

Wu, G.Y., & Wu, C.H. (1987). Receptor-mediated in vitro gene transformation by a soluble DNA carrier system. *J Biol Chem* **262**, 4429-4432.

Wu, G.Y., & Wu, C.H. (1988). Receptor-mediated gene delivery and expression in vivo. *J Biol Chem* **263**, 14621-14624.

Wu, R.Z., Bailey, S.N., & Sabatini, D.M. (2002). Cell-biological applications of transfected-cell microarrays. *Trends Cell Biol* **12**, 485-488.

Xia, Z.J., Chang, J.H., Zhang, L., Jiang, W.Q., Guan, Z.Z., Liu, J.W., Zhang, Y., Hu, X.H., Wu, G.H., Wang, H.Q., Chen, Z.C., Chen, J.C., Zhou, Q.H., Lu, J.W., Fan, Q.X., Huang, J.J., & Zheng, X. (2004). [Phase III randomized clinical trial of intratumoral injection of E1B gene-deleted adenovirus (H101) combined with cisplatin-based chemotherapy in treating squamous cell cancer of head and neck or esophagus]. *Ai Zheng* **23**, 1666-1670.

Xiang, S.N., Tong, H.J., Shi, Q., Fernandes, J.C., Jin, T., Dai, K.R., & Zhang, X.L. (2012). Uptake mechanisms of non-viral gene delivery. *J Control Release* **158**, 371-378.

Xu, C.H., Inokuma, M.S., Denham, J., Golds, K., Kundu, P., Gold, J.D., & Carpenter, M.K. (2001). Feeder-free growth of undifferentiated human embryonic stem cells. *Nat Biotechnol* **19**, 971-974.

Xu, F., Celli, J., Rizvi, I., Moon, S., Hasan, T., & Demirci, U. (2011). A three-dimensional in vitro ovarian cancer coculture model using a high-throughput cell patterning platform. *Biotechnol J* **6**, 204-212.

Xu, F., Moon, S.J., Emre, A.E., Turali, E.S., Song, Y.S., Hacking, S.A., Nagatomi, J., & Demirci, U. (2010). A droplet-based building block approach for bladder smooth muscle cell (SMC) proliferation. *Biofabrication* **2**, 014105.

Xue, Y.P., Yang, Y.K., Lv, S.Z., Liu, Z.Q., & Zheng, Y.G. (2016). High-throughput screening methods for nitrilases. *Appl Microbiol Biot* **100**, 3421-3432.

Yagi, T., Ito, D., Okada, Y., Akamatsu, W., Nihei, Y., Yoshizaki, T., Yamanaka, S., Okano, H., & Suzuki, N. (2011). Modeling familial Alzheimer's disease with induced pluripotent stem cells. *Hum Mol Genet* **20**, 4530-4539.

Yamada, T., Yoshikawa, M., Kanda, S., Kato, Y., Nakajima, Y., Ishizaka, S., & Tsunoda, Y. (2002). In vitro differentiation of embryonic stem cells into hepatocyte-like cells identified by cellular uptake of indocyanine green. *Stem Cells* **20**, 146-154.

Yamashita, A., Morioka, M., Kishi, H., Kimura, T., Yahara, Y., Okada, M., Fujita, K., Sawai, H., Ikegawa, S., & Tsumaki, N. (2014). Statin treatment rescues FGFR3 skeletal dysplasia phenotypes. *Nature* **513**, 507-511.

Yang, X., Huang, B., Deng, L.L., & Hu, Z.G. (2018). Progress in gene therapy using oncolytic vaccinia virus as vectors. *J Cancer Res Clin* **144**, 2433-2440.

Yao, H., Wang, K.Y., Wang, Y., Wang, S.S., Li, J.F., Lou, J.N., Ye, L.Y., Yan, X.Y., Lu, W.Y., & Huang, R.Q. (2015). Enhanced blood-brain barrier penetration and glioma therapy mediated by a new peptide modified gene delivery system. *Biomaterials* **37**, 345-352.

Yazawa, M., Hsueh, B., Jia, X.L., Pasca, A.M., Bernstein, J.A., Hallmayer, J., & Dolmetsch, R.E. (2011). Using induced pluripotent stem cells to investigate cardiac phenotypes in Timothy syndrome. *Nature* **471**, 230-234.

Ye, J.X., Alvin, K., Latif, H., Hsu, A., Parikh, V., Whitmer, T., Tellers, M., Edmonds, M.C.D., Ly, J., Salmon, P., & Markusen, J.F. (2010). Rapid Protein Production Using CHO Stable Transfection Pools. *Biotechnol Progr* **26**, 1431-1437.

Ye, L., Chang, Y.H., Xiong, Q., Zhang, P., Zhang, L., Somasundaram, P., Lepley, M., Swingen, C., Su, L., Wendel, J.S., Guo, J., Jang, A., Rosenbush, D., Greder, L., Dutton, J.R., Zhang, J., Kamp, T.J., Kaufman, D.S., Ge, Y., & Zhang, J. (2014). Cardiac repair in a porcine model of acute myocardial infarction with human induced pluripotent stem cell-derived cardiovascular cells. *Cell Stem Cell* **15**, 750-761.

Yi, Y., Noh, M.J., & Lee, K.H. (2011). Current Advances in Retroviral Gene Therapy. *Curr Gene Ther* **11**, 218-228.

Yla-Herttuala, S. (2012). Endgame: Glybera Finally Recommended for Approval as the First Gene Therapy Drug in the European Union. *Mol Ther* **20**, 1831-1832.

Yoshida, Y., Takahashi, K., Okita, K., Ichisaka, T., & Yamanaka, S. (2009). Hypoxia Enhances the Generation of Induced Pluripotent Stem Cells. *Cell Stem Cell* **5**, 237-241.

Yoshimura, M., & Oka, T. (1990). Transfection of beta-casein chimeric gene and hormonal induction of its expression in primary murine mammary epithelial cells. *Proc Natl Acad Sci U S A* **87**, 3670-3674.

Yoshitoshi-Uebayashi, E.Y., Toyoda, T., Yasuda, K., Kotaka, M., Nomoto, K., Okita, K., Yasuchika, K., Okamoto, S., Takubo, N., Nishikubo, T., Soga, T., Uemoto, S., & Osafune, K. (2017). Modelling urea-cycle disorder citrullinemia type 1 with disease-specific iPSCs (vol 486, pg 613, 2017). *Biochem Bioph Res Co* **488**, 570-571.

Young, J.E., Boulanger-Weill, J., Williams, D.A., Woodruff, G., Buen, F., Revilla, A.C., Herrera, C., Israel, M.A., Yuan, S.H., Edland, S.D., & Goldstein, L.S.B. (2015). Elucidating Molecular Phenotypes Caused by the SORL1 Alzheimer's Disease Genetic Risk Factor Using Human Induced Pluripotent Stem Cells. *Cell Stem Cell* **16**, 373-385.

Yu, H.B., Li, M., Wang, W.P., & Wang, X.L. (2016). High throughput screening technologies for ion channels. *Acta Pharmacol Sin* **37**, 34-43.

Yu, J., Hu, K., Smuga-Otto, K., Tian, S., Stewart, R., Slukvin, I.I., & Thomson, J.A. (2009). Human induced pluripotent stem cells free of vector and transgene sequences. *Science* **324**, 1266-1266.

Yu, J.Y., Vodyanik, M.A., Smuga-Otto, K., Antosiewicz-Bourget, J., Frane, J.L., Tian, S., Nie, J., Jonsdottir, G.A., Ruotti, V., Stewart, R., Slukvin, I.I., & Thomson, J.A. (2007). Induced pluripotent stem cell lines derived from human somatic cells. *Science* **318**, 1917-1920.

Yu, X.L., Hu, T., Du, J.M., Ding, J.P., Yang, X.M., Zhang, J., Yang, B., Shen, X., Zhang, Z., Zhong, W.D., Wen, N., Jiang, H.L., Zhu, P., & Chen, Z.N. (2008). Crystal structure of HAb18g/CD147 - Implications for immunoglobulin superfamily homophilic adhesion. *Journal of Biological Chemistry* **283**, 18056-18065.

Yurchenco, P.D. (2011). Basement Membranes: Cell Scaffoldings and Signaling Platforms. *Csh Perspect Biol* **3**, a004911.

Zhang, J.H., Chung, T.D.Y., & Oldenburg, K.R. (1999). A simple statistical parameter for use in evaluation and validation of high throughput screening assays. *J Biomol Screen* **4**, 67-73.

Zhang, W.W., Li, L.J., Li, D.G., Liu, J.L., Li, X.Q., Li, W., Xu, X.L., Zhang, M.J., Chandler, L.A., Lin, H., Hu, A.G., Xu, W., & Lam, D.M.K. (2018). The First Approved Gene Therapy Product for Cancer Ad-p53 (Gendicine): 12 Years in the Clinic. *Hum Gene Ther* **29**, 160-179.

Zhang, Y., & Yu, L.C. (2008). Microinjection as a tool of mechanical delivery. *Curr Opin Biotech* **19**, 506-510.

Zhao, N.X., Qi, J.J., Zeng, Z.H., Parekh, P., Chang, C.C., Tung, C.H., & Zu, Y.L. (2012). Transfecting the hard-to-transfect lymphoma/leukemia cells using a simple cationic polymer nanocomplex. *J Control Release* **159**, 104-110.

Zweigerdt, R., Olmer, R., Singh, H., Haverich, A., & Martin, U. (2011). Scalable expansion of human pluripotent stem cells in suspension culture. *Nat Protoc* **6**, 689-700.

Acknowledgements

Upon the completion of the dissertation, I am grateful to those who have offered encouragement and support during my Ph.D.

First of all, I am very thankful to my Ph.D. supervisor, Prof. Dr. Pavel Levkin (Institute of Biological and Chemical Systems - Functional Molecular Systems (IBCS-FMS), KIT), for giving me the opportunity to perform research work in his lovely group, for consistent attention and full support in the progress of my Ph.D. work, for providing critical feedback through our discussions, and also for his guidance and great support for the accomplishment of the work presented in this dissertation. Besides, I am also very grateful to his encouragement in my academic and personal life, making me on my way of being an independent scientific researcher and living in the moment.

I would like to thank Prof. Dr. Martin Bastmeyer (Zoological Institute of Cell and Neurobiology, KIT) for taking his time to be my Korreferent. I am grateful to Prof. Dr. Ute Schepers (Institute of Functional Interfaces, KIT) and Prof. Dr. Rainer Suntz (Institute of Chemical Technology and Polymer Chemistry, KIT) to be the Prüfer of my Ph.D. defense.

I would like to thank Prof. Dr. Andrew Cato (Institute of Biological and Chemical Systems - Biological Information Processing (IBCS-BIP), KIT) and Dr. Gary Davidson (IBCS-FMS, KIT) for being my TAC members and for all the valuable scientific suggestions and advises.

Thanks to Dr. Markus Reischl (Institute of Automation and Applied Informatics (IAI), KIT), Dr. Sarah Bertels (Zoological Institute of Cell and Neurobiology, KIT), Dr. Ravindra Peravali (IBCS-BIP) for their collaborative work, support, suggestions and expertise.

Thanks to Prof. Dr. Pavel Levkin and Prof. Dr. Mo Yang (Faculty of Engineering, The Hong Kong Polytechnic University) for providing me the opportunity to visit research group of Prof. Dr. Mo Yang and conduct some experiments there.

I am grateful to Dr. Anna Popova, for her support in both academic research and daily life. I thank Johannes Scheiger for the measurements of Scanning electron microscope (SEM), Energy-dispersive X-ray spectroscopy (EDX), and Atomic force